MASTER

RLO-1040-T1

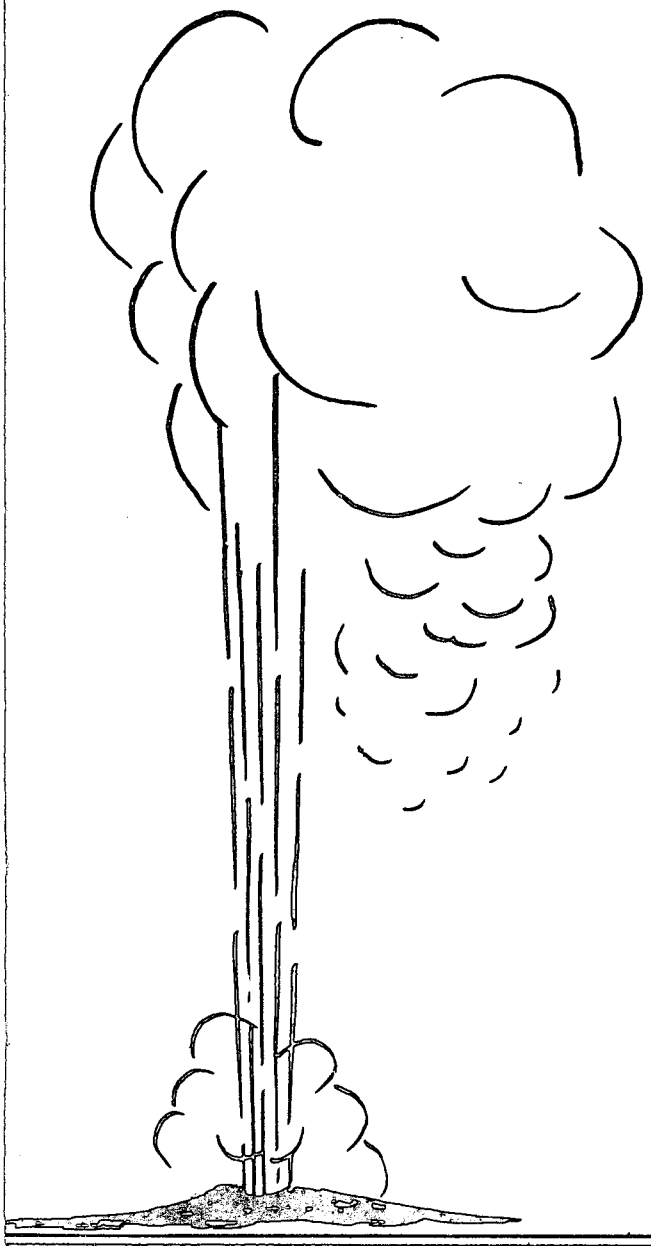

GEOTHERMAL RESOURCE ASSESSMENT OF MOUNT HOOD

Final Report

By
Donald A. Hull

July 1979

Work Performed Under Contract No. EG-77-C-06-1040

State of Oregon
Department of Geology and Mineral Industries
Portland, Oregon

U. S. DEPARTMENT OF ENERGY

Geothermal Energy

DISTRIBUTION OF THIS DOCUMENT IS UNLIMITED

DISCLAIMER

This report was prepared as an account of work sponsored by an agency of the United States Government. Neither the United States Government nor any agency Thereof, nor any of their employees, makes any warranty, express or implied, or assumes any legal liability or responsibility for the accuracy, completeness, or usefulness of any information, apparatus, product, or process disclosed, or represents that its use would not infringe privately owned rights. Reference herein to any specific commercial product, process, or service by trade name, trademark, manufacturer, or otherwise does not necessarily constitute or imply its endorsement, recommendation, or favoring by the United States Government or any agency thereof. The views and opinions of authors expressed herein do not necessarily state or reflect those of the United States Government or any agency thereof.

DISCLAIMER

Portions of this document may be illegible in electronic image products. Images are produced from the best available original document.

RLO-1040-T1
Distribution Category UC-66a

DISCLAIMER

This book was prepared as an account of work sponsored by an agency of the United States Government. Neither the United States Government nor any agency thereof, nor any of their employees, makes any warranty, express or implied, or assumes any legal liability or responsibility for the accuracy, completeness, or usefulness of any information, apparatus, product, or process disclosed, or represents that its use would not infringe privately owned rights. Reference herein to any specific commercial product, process, or service by trade name, trademark, manufacturer, or otherwise, does not necessarily constitute or imply its endorsement, recommendation, or favoring by the United States Government or any agency thereof. The views and opinions of authors expressed herein do not necessarily state or reflect those of the United States Government or any agency thereof.

GEOTHERMAL RESOURCE ASSESSMENT OF MOUNT HOOD

FINAL REPORT

U. S. DEPARTMENT OF ENERGY

CONTRACT NO. AC06-77-ET-28369

Principal Investigator: Donald A. Hull
Department of Geology and Mineral Industries
State of Oregon

Editor: Joseph F. Riccio
Department of Geology and Mineral Industries
State of Oregon

July 1979

DISTRIBUTION OF THIS DOCUMENT IS UNLIMITED

TABLE OF CONTENTS

	Page
INTRODUCTION	1
STRATIGRAPHY AND STRUCTURE OF THE COLUMBIA RIVER BASALT GROUP IN THE CASCADE RANGE, OREGON	5
GEOLOGY AND GEOCHEMISTRY OF MT. HOOD VOLCANO	79
GRAVITY MEASUREMENTS IN THE AREA OF MOUNT HOOD, OREGON	137
HEAT FLOW MODELING OF THE MOUNT HOOD VOLCANO, OREGON	191
OVERVIEW	265
CONCLUSIONS	272
GEOCHEMICAL STUDIES OF ROCKS, WATER, AND GASES AT MT. HOOD, OREGON	273

INTRODUCTION

On July 1, 1977, the Oregon Department of Geology and Mineral Industries began research on two geothermal resource projects with funds provided by the U. S. Energy Research and Development Administration (ERDA) (now U. S. Department of Energy) under Contract No. EG-77-C-06-1040. The projects are: (a) geothermal resource assessment of Mt. Hood Volcano in the Cascade Range; and (b) statewide inventory of low temperature geothermal resources. An application for an extension and additional funding of these projects was submitted to ERDA (DOE) on September 14, 1977, funded on December 28, 1977, and later extended to December 31, 1978. A no-cost extension to the contract was issued by DOE on January 1, 1979, with the original completion date as specified in Article II of the contract changed to June 15, 1979. Further, the contract number was changed from EG-77-C-06-1040 to AC06-77-ET-28369 as of the above date.

The Mt. Hood geothermal resource assessment project was a joint undertaking by the Department of Energy (DOE), U. S. Geological Survey (USGS), U. S. Forest Service (USFS), and Oregon Department of Geology and Mineral Industries (DOGAMI). The role each major participant of the project played in the study is set down in the signed ERDA-USGS-USFS-DOGAMI agreement under letter dated February 11, 1977, from Dr. David L. Williams, Program Manager, DGE, ERDA.

The primary objective of the project was the assessment and characterization of the geothermal resource potential of Mt. Hood. Mt. Hood was selected because: (a) it is one of the largest stratovolcanoes in the Cascade Range; (b) it has been active in the past 250 years; and (c) it is readily accessible for research. Furthermore, the volcano is approximately 50 airline miles east-southeast of the City of Portland and any substantial geothermal resource, whether low to high temperature, could be utilized by Metropolitan Portland.

Dr. Donald A. Hull, Oregon State Geologist, was the principal investigator for DOGAMI. This final report was edited and written, in part, by Dr. Joseph F. Riccio. A portion of the field studies administered by DOGAMI have been managed by its staff personnel and/or consultants, whereas other phases have been conducted by university researchers under subcontract to DOGAMI as noted below:

(1) Stratigraphy and structure of the Columbia River Basalt Group in the Cascade Range, Oregon: By Marvin H. Beeson and Michael R. Moran, Earth Science Department, Portland State University (PSU Grant No. 90-262-8126).

(2) Geology and geochemistry of Mt. Hood Volcano: By Craig M. White, Department of Geology, University of Oregon (UO Grant No. 50-262-8902).

(3) Gravity measurements in the area of Mount Hood, Oregon: By Richard W. Couch and Michael Gemperle, Geophysics Group, School of Oceanography, Oregon State University (OSU Grant No. 30-262-917).

(4) Heat flow modelling of the Mount Hood Volcano, Oregon: By David D. Blackwell and John L. Steele, Department of Geological Science, Southern Methodist University (SMU #86-09).

A geochemical study by DOGAMI and Lawrence Berkeley Laboratory (LBL), University of California (DOE Contract No.

W-7405-ENG-48) resulted in a joint publication (LBL-7092 - DOGAMI 0-79-2) entitled Geochemical studies of rocks, water, and gases at Mt. Hood, Oregon. DOGAMI's portion of the project was funded under its Contract No. EG-77-C-06-1040. A copy of the publication is enclosed.

The first technical progress report by DOGAMI for the Mt. Hood assessment was submitted in October 1977; technical progress report No. 2 was submitted in May 1978. This final report only involves DOGAMI's portion of the Mt. Hood assessment project. The final report on the Statewide Inventory of Low Temperature Geothermal Resources (AC06-77-ET-28369) was submitted to DOE under separate cover.

The geoscience researchers engaged in the joint geothermal assessment project met in Portland on January 9-10, 1979, at which time preliminary results of various aspects of the assessment effort were informally presented. This final report, including those by the university researchers under subcontract to DOGAMI, does not include any substantial input as to conclusions or recommendations presented informally or formally by the USGS.

Besides the supervision of the studies undertaken by the university researchers, DOGAMI was also charged with the drilling of temperature gradient holes on or near Mt. Hood. DOGAMI also undertook the temperature logging of available "free" holes that were within the scope of the Mt. Hood project. These data were made available to David Blackwell for heat flow determinations and for the heat flow modelling of Mt. Hood. Further, DOGAMI provided for the technical supervision

of the drilling of Old Maid Flat No. 1/2. This entailed, in part, providing for the litho-logging and preservation of cuttings (which were made available to David Blackwell for rock conductivity tests and to Marvin Beeson for trace element geochemistry) from this exploratory hole; temperature logging of the hole; well-site interpretation of the several geophysical logs taken by others in this hole; and coordination and logistics between the interested parties of the assessment group relative to the drilling and logging of this hole.

Further, DOGAMI provided personnel to the USGS for the siting and staking of seismic shot holes.

DOGAMI also provided for litho-logging and cuttings preservation of Timberline No. 2. Limited drilling supervision was also provided on this hole.

Temperature gradient logging of Old Maid Flat No. 3 (Clear Fork) drilled by Northwest Geothermal Corporation was done by DOGAMI. Cuttings and temperature gradient data were submitted to David Blackwell for the heat flow studies noted above.

Water analyses from samples obtained from several of the temperature gradient holes were made available to the interested assessment parties.

STRATIGRAPHY AND STRUCTURE OF THE COLUMBIA RIVER BASALT GROUP IN THE CASCADE RANGE, OREGON

By

Marvin H. Beeson and Michael R. Moran
Earth Sciences Department,
Portland State University

Final report of work carried out under PSU Grant No. 90-262-8126 From the Oregon Department of Geology and Mineral Industries; June 1977 through March, 1978.

CONTENTS

		Page
	ABSTRACT	9
I.	COLUMBIA RIVER BASALT STRATIGRAPHY IN WESTERN OREGON	12
II.	STRATIGRAPHY AND STRUCTURE OF THE COLUMBIA RIVER BASALT IN REGIONS WITHIN THE CASCADE RANGE	21
	A. Hood River Area	21
	Structure and Stratigraphy	21
	Geologic History	25
	B. Bull Run Watershed Area	28
	Introduction	28
	Structure and Stratigraphy	30
	C. Salmon River Area	39
	Introduction	39
	Structure and Stratigraphy	39
	Geologic History	41
	D. Clackamas River Area	42
	Introduction	42
	Structure and Stratigraphy	43
	Geologic History	50
	E. Old Maid Flat Exploratory Hole	51
III.	GENERALIZED STRUCTURAL MODEL FOR COLUMBIA RIVER BASALT IN THE CASCADE RANGE	57
	A. Introduction	57
	B. NE Trending Folds and Thrust Faults	57
	C. Wrench Fault Zone	62
	D. NW Trending Faults and Fractures	62
	E. Cascade Upwarp and Subsidence	63

Page

IV. GEOLOGIC HISTORY..... 69

A. Pre-Columbia River Basalt..... 69

B. Columbia River Basalt..... 69

C. Post-Columbia River Basalt..... 71

FIGURES

Figure		Page
I-1	LOCATION MAP	11
II-1	DISTRIBUTION OF COLUMBIA RIVER BASALT GROUP IN OREGON, WASHINGTON, AND IDAHO	13
II-2	COLUMBIA RIVER BASALT GROUP STRATIGRAPHY	14
II-3	STRATIGRAPHY OF THE COLUMBIA RIVER BASALT GROUP IN WESTERN OREGON	16
II-4	DISTINCTIVE CHARACTERISTICS OF WESTERN OREGON COLUMBIA RIVER BASALT GROUP STRATIGRAPHIC UNITS	17
III-1	TECTONIC MAP OF THE CLACKAMAS RIVER AREA	44
III-2	GENERALIZED STRATIGRAPHIC COLUMN FOR COLUMBIA RIVER BASALT IN THE CLACKAMAS RIVER AREA	47
III-3	GEOCHEMICAL DATA ON SAMPLES FROM OLD MAID FLAT EXPLORATORY HOLE	53
III-4	COLUMBIA RIVER BASALT STRATIGRAPHY IN OLD MAID FLAT HOLE	54
IV-1	DEVELOPMENT OF BULL RUN THRUST FAULT	61
IV-2	PATTERN OF FAULTING	64
IV-3	FRACTURE PATTERN CONTROLLING STREAM TREND	65
	GEOLOGIC AND REGIONAL STRUCTURE MAPS (6) (Maps not conducive to printing)	

ABSTRACT

The Columbia River Basalt Group lava flows identified in the Mt. Hood area of the Oregon Cascade Range are assigned to the Grande Ronde Basalt and Wanapum Basalt formations of the Yakima Basalt Subgroup, except for three intercalated flows of Prineville chemical type. The composite section has a stratigraphic thickness of approximately 550 m and consists of 26 flows that can be separated into eight distinct geochemical and/or magnetic polarity subdivisions.

Deformation began during the incursion of the Grande Ronde Basalt and is represented by NE trending folds traversing the Cascade Range which have structural relief of approximately 300 m and by an echelon NNW to NW trending folds and faults that occur from the Clackamas River area to Portland along the Portland Hills - Brothers fault trend. During this stage of deformation, thrust faults developed parallel to some of the anticlinal axes in patterns similar to those of the Columbia Plateau. Later deformation includes vertical N10W to N55W strike slip faulting, which, when considered with the fold trends, indicates a right lateral wrench system of regional magnitude. The Columbia Plateau style of deformation clearly crosses the axis of the Cascades with several of the larger folds being present in both provinces. A N30W trending fault located just west of the Salmon River separates the NE trending folds through the Cascades from the Portland Hills - Brothers wrench fault trend.

Distribution of the Columbia River Basalt in the area surrounding Mt. Hood and its deeper occurrences in the exploratory hole at Old Maid Flat indicates that the basalt may have been downdropped along much of the axial region of the range.

The major exposures of CRB utilized in this study are (Figure I-1):

Clackamas River Area (mapped by James L. Anderson, unpublished Master's thesis, Portland State University).

Bull Run Watershed (mapped by Beverly Vogt, unpublished Master's thesis, Portland State University).

Hood River Drainage and Hood River fault zone (mapped by Susan Timm, unpublished Master's thesis, Portland State University).

The Salmon River Area (mapped by M. H. Beeson and M. R. Moran).

The Columbia River Gorge which consists of one large exposure of CRB through the Cascade Range was not mapped for this report although some data were available from both published literature and isolated sections studied by Mr. M. R. Moran (unpublished Master's thesis, Portland State University).

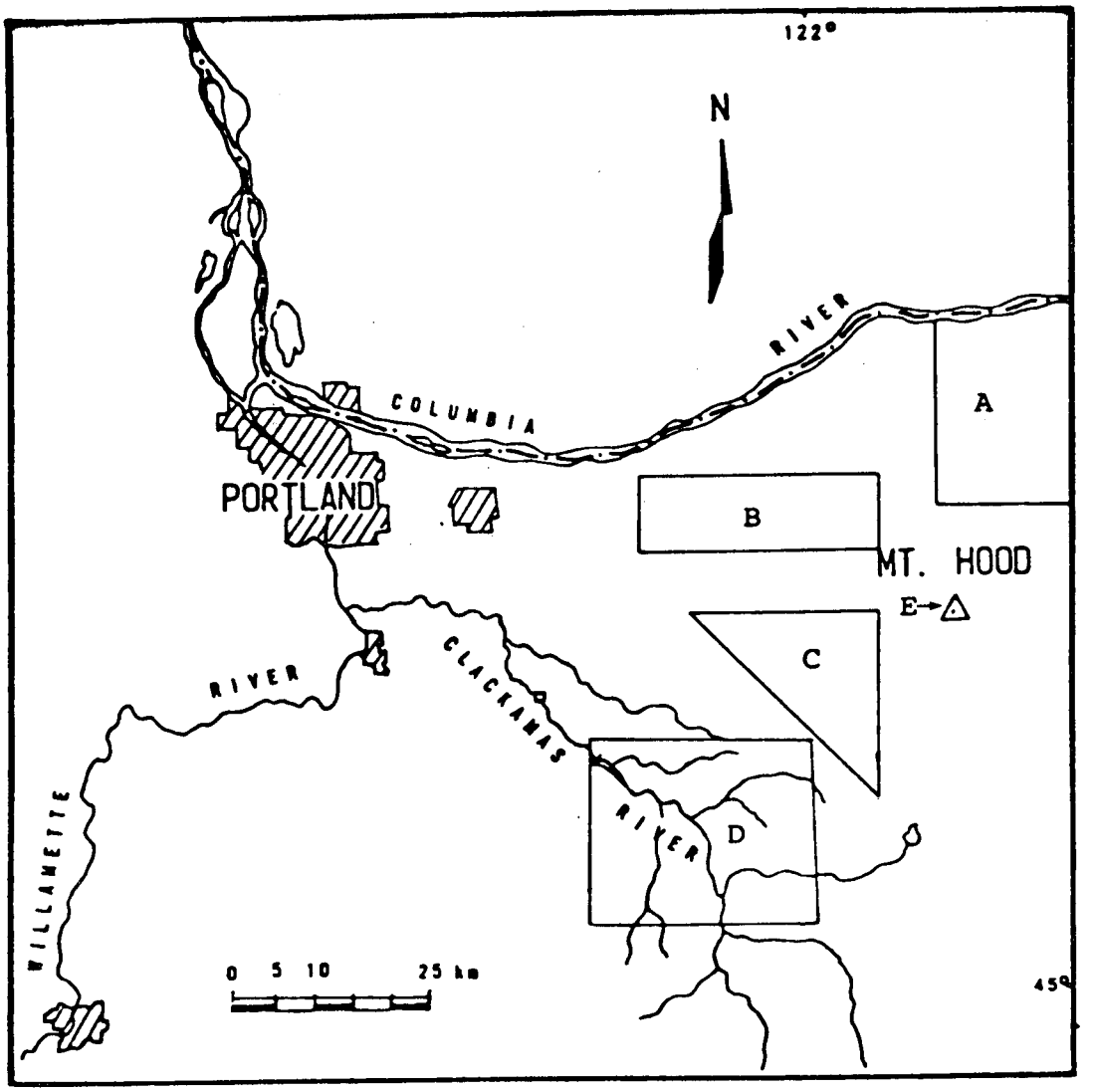

Figure I-1. Location Map

A - Hood River Area
B - Bull Run Watershed Area
C - Salmon River Area
D - Clackamas River Area
E - Old Maid Flat Exploratory Hole

II. COLUMBIA RIVER BASALT GROUP STRATIGRAPHY IN WESTERN OREGON

The Miocene Columbia River Basalt Group in Oregon, Washington, and Idaho is an accumulation of tholeiitic flood basalt flows covering approximately $2x10^5$ km^2 (Figure II-1; Waters, 1962). These fluid flows spread over this region, the Columbia Plateau, as nearly horizontal sheets, attaining a total thickness of at least 1,500 m near Pasco, Washington (Asaro and others, 1978). The flows were extruded from large N to NW trending fissure systems in the eastern half of the plateau (Waters, 1961; Taubeneck, 1970; Swanson and others, 1975) between approximately 16 and 6 million years ago (Watkins and Baksi, 1974; McKee and others, 1977).

The stratigraphic subdivisions and nomenclature have undergone a number of revisions and refinements as mapping has progressed and as modern geochemical and paleomagnetic data have accumulated. Many contributions have been made to the Columbia River Basalt Group stratigraphy, some of the more noteworthy being Waters (1961, 1962); Mackin (1961); Schmincke (1967); Wright and others (1973); and Nathan and Fruchter (1974). The Group is divided into five formations (Figure II-2). Two of these, the Imnaha Basalt and the Picture Gorge Basalt, are restricted to the southeastern and southern portions of the province, respectively; the remaining three, the Grande Ronde Basalt, the Wanapum Basalt, and the Saddle Mountains Basalt, are grouped together as the Yakima Basalt Subgroup. All of the Columbia River Basalt Group flows identified west of the axis of the Cascade

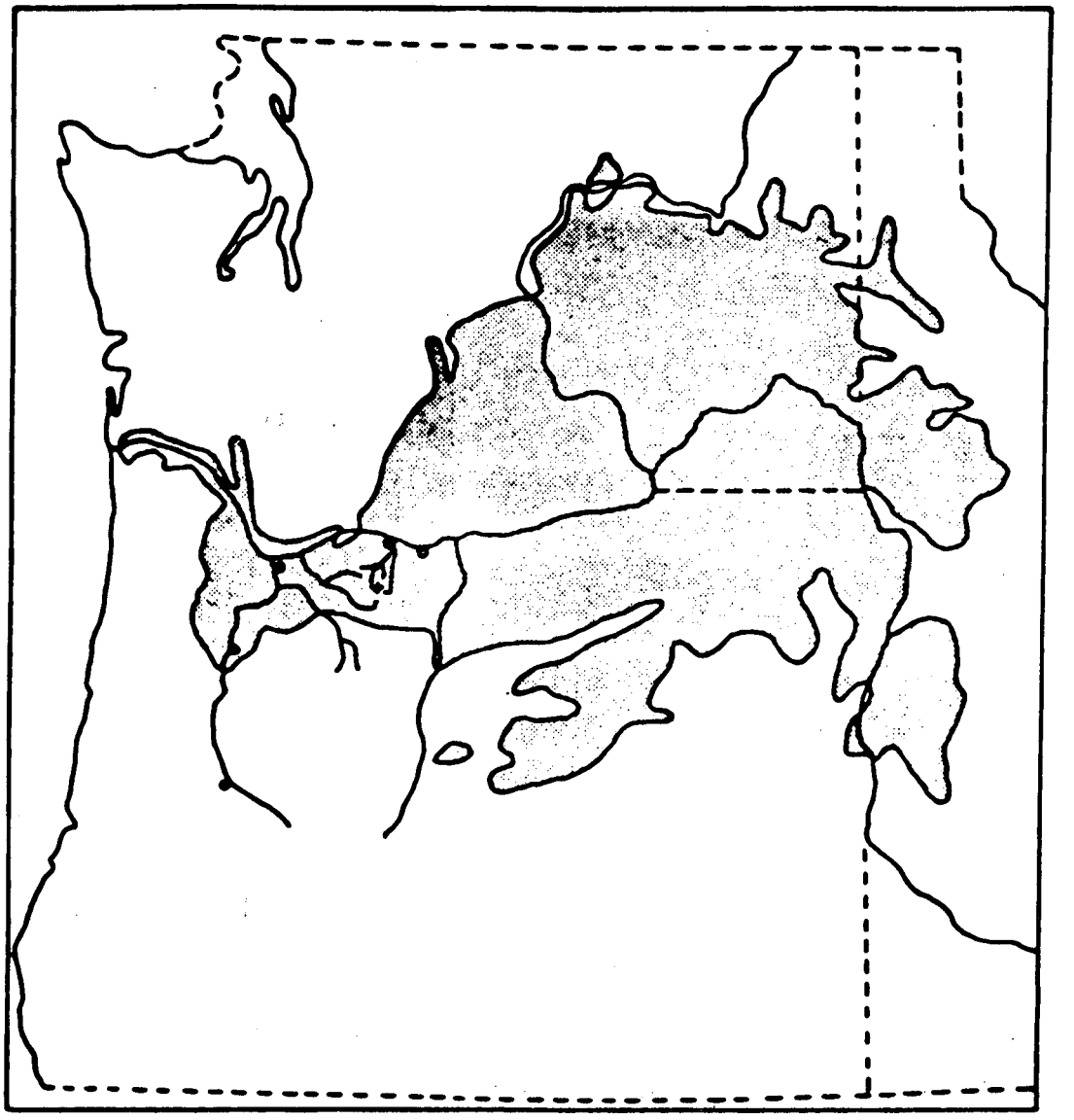

Figure II-1. Distribution of Columbia River Basalt Group in Oregon, Washington, and Idaho; + Mt. Hood.

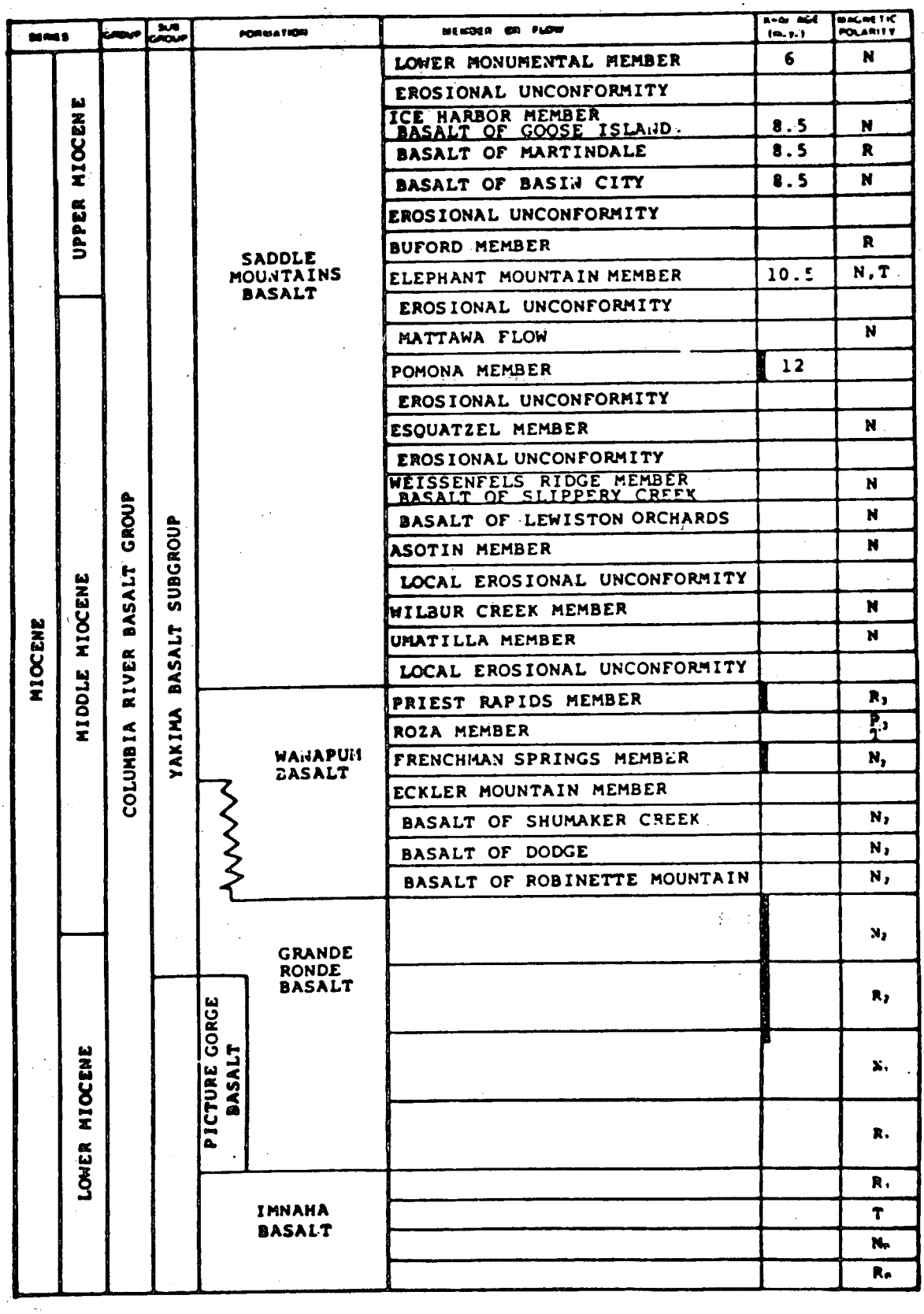

Figure II-2. Columbia River Basalt Group Stratigraphy

Mountains belong to this subgroup, with the exception of flows of the Prineville chemical type, discussed below. The coastal Miocene basalts of Oregon and Washington form three distinct stratigraphic units that are consanguineous with the three formations of the Yakima Basalt Subgroup (Snavely and others, 1973).

Some of the basalt flows originating in the eastern part of the Columbia Plateau flowed into western Oregon through a topographic low in the ancestral Cascade Mountains. This low extended from the Clackamas River drainage on the south to the present Columbia River Gorge on the north. The Yakima Basalt Subgroup, about 1,500 m thick in the Pasco Basin of Washington, thins to approximately 550 m in the Cascade Range. Many stratigraphic members recognized on the plateau are not present or comprise fewer flows in western Oregon. The Saddle Mountains Basalt, which ranges from 150 to 275 m thick in the Pasco Basin, has not been found in the Cascade Range, even though the Pomona Member is present near the Columbia River in the Coast Range of Oregon and Washington (Snavely and others, 1973; Kienle, 1971). The members of the Yakima Basalt Subgroup that occur in western Oregon are indicated in Figure II-2.

In western Oregon, the Columbia River Basalt Group comprises approximately 29 basalt flows which may be divided into three formations of the Yakima Basalt Subgroup (Figure II-3). Distinctive characteristics of each member and of other informal subdivisions are given in Figure II-4. These units are tentatively identifiable in the field on the basis

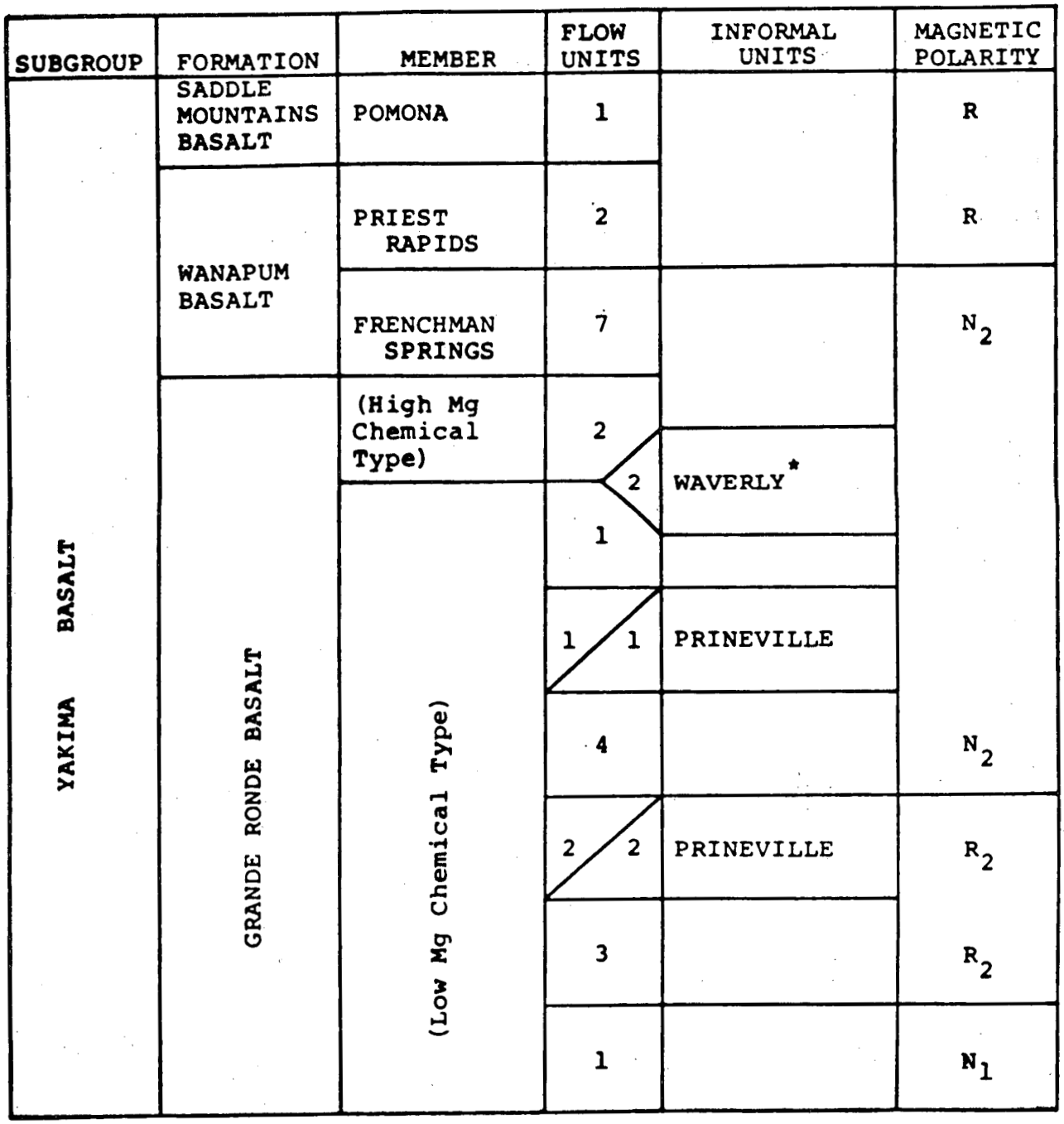

Figure II-3. Stratigraphy of the Columbia River Basalt Group in western Oregon

STRATIGRAPHIC UNIT	FIELD CRITERIA Jointing, polarity & lithology	LABORATORY CRITERIA Geochemistry** & petrography
Pomona Member	Blocky to columnar jointing Reversed polarity Clear plagioclase phenocrysts (3-4 mm) Clots of plagioclase and pyroxene	Sm <5 La <20 Fe <8%
Priest Rapids Member	Reversed polarity Coarse sugary texture	Sm >7 La 25-30 Sc 35-40 Eu ≥2.5
Frenchman Springs Member	Well-formed colonnade Normal polarity Texture often coarse Large (1-cm) plagioclase phenocrysts	Sm >7 La 25-30 Sc 35-40 Eu ≤2.5
*High Mg Grande Ronde Basalt	Blocky and platy jointing Normal polarity Coarse texture	Sm <6 La 20-24 Sc 35-40
*Waverly flows	Upper flow - very poorly jointed Lower flow - large columns with platy jointing Normal polarity	Sm <6 La 15-18 Upper flow - clots of plagioclase and pyroxene Lower flow - pilotaxitic
*Low Mg Grande Ronde Basalt	Well-formed entablature Fine texture	Sm <7 La 25-30 Sc 30-35
*Prineville flows	Well-formed blocky to wavy colonnade Fine texture	Ba~2,000 Eu >4 Co <35 Abundant apatite laths

Figure II-4. Distinctive characteristics of western Oregon Columbia River Basalt Group stratigraphic units

* Informal units.

** Geochemical data obtained by neutron activation analysis. All data in parts per million except where specified.

of jointing characteristics, magnetic polarity, grain size, and the presence or absence of large plagioclase phenocrysts. Laboratory data, especially major or trace element chemistry, are necessary for more accurate determinations.

Grande Ronde Basalt is the most widespread of all the Columbia River Basalt Group formations in western Oregon; occurring almost everywhere the CRB has been mapped. Of the four magnetic polarity intervals formally recognized within the Grande Ronde Basalt, only the oldest, a reversed interval (R_1), has not been found in western Oregon. The oldest normal interval (N_1) is represented by a single flow that occurs at the bottoms of the sections in Multnomah Creek and in the Clackamas River (Anderson, 1978).

Grande Ronde Basalt may also be divided chemically on the basis of magnesium content into "Low Mg" and "High Mg" flows (Figure II-3). In western Oregon, two High Mg flows occur as the top two flows of the Grande Ronde Basalt. Because of their distinctive jointing patterns and textures, the two High Mg flows are generally distinguishable in the field from the Low Mg flows, and this informal subdivision is therefore useful for geologic mapping in western Oregon. In the Columbia Plateau, however, the High Mg flows may also occur lower in the Grande Ronde Basalt section (D. A. Swanson, personal communication).

The Grande Ronde Basalt section in western Oregon also contains localized units that do not occur extensively in the plateau and are not formally recognized. In the Clackamas River area, two flows of the chemically distinctive Prineville

chemical type (Uppuluri, 1974) occur at the top of the second reversed (R_2) section (Anderson, 1978). One Prineville flow, probably an N_2 flow, occurring near the top of the Low Mg Grande Ronde Basalt, has been found in the exploratory hole at Old Maid Flat. The Prineville chemical-type flows probably originated near Prineville, where 13 flows are exposed (Uppuluri, 1974), and spread northward and westward, onlapping and interfingering with flows of Low Mg Grande Ronde Basalt. Prineville flows have not been found in the Willamette Valley, but the lower part of the Grande Ronde section is not exposed in the Portland area, and few chemical analyses have been made on CRB from other parts of the valley. Prineville flows are not known to occur in the Bull Run Watershed (B. F. Vogt, personal communication) or in the Columbia River Gorge (Beeson and others, 1976).

In the Waverly Heights area near Milwaukie, Oregon, two flows which have been informally designated the Waverly flows (Beeson and others, 1976) occur between the High Mg and the Low Mg Grande Ronde Basalt flows. They are localized by structural and/or erosional lows which existed at that time. Chemically, they are very similar to the Low K_2O Grande Ronde Flows that occur at or very near this same stratigraphic horizon in the Pasco Basin (Ledgerwood, 1978) and along the Snake River in Washington. The Waverly flows are also similar chemically to the older Imnaha Basalts.

The Frenchman Springs Member of the Wanapum Basalt is widespread in the CRB occurrences in western Oregon. It is not present along some structural highs such as the Portland

Hills anticline, either because it was excluded by developing structures or because it has since been eroded. In the Columbia Plateau, Grande Ronde and Wanapum Basalts are separated by the Vantage interbed; in western Oregon, this same contact is marked by a distinctive weathering surface and an interbed of carbonaceous material. Interbeds occur between other CRB flows in western Oregon, but because the Vantage interbed is characterized by deep weathering, structural deformation, and sedimentary deposits, it must represent a longer time interval. Tree molds and carbonaceous material are common at this boundary. The first two Frenchman Springs flows above the interbed contain plagioclase megaphenocrysts which aid in positive stratigraphic determination.

The Priest Rapids Member occurs in the Bull Run Watershed (B. F. Vogt, personal communication) and at Crown Point on the Columbia River as one or possibly two intracanyon flows. Priest Rapids flows have not been found in any other location in western Oregon.

The Pomona Member of the Saddle Mountains Basalt occurs along the lower Columbia River of Oregon and Washington. This flow probably traversed the Cascade Range as an intracanyon flow whose course is yet to be determined. Pomona flows have not been found in the Cascade Range or in the Portland area.

III. STRATIGRAPHY AND STRUCTURE OF THE COLUMBIA RIVER BASALT IN REGIONS WITHIN THE CASCADE RANGE

A. Hood River Area

The Hood River Valley is located 100 km east of Portland and extends north about 26 km from the northern flank of Mount Hood to the City of Hood River on the Columbia River (Figure I-1). The valley floor is nearly flat, sloping less than one degree to the north, and is overlain by glacial outwash and stream deposits at least three meters thick. The valley is flanked on the east and west by steep-sided ridges.

The entire valley and surrounding hills are underlain by CRB; however, exposures are limited to stream channels and steep hillsides. The CRB basalts have undergone weathering and a thick soil covers all but the steepest slopes. Hillside exposures are usually the result of excavations.

The valley is interrupted in its approximate center by Middle Mountain, an asymmetric hill of northeast dipping basalt.

The Hood River flows northeast along the west border of the valley with a gradient of 1 degree, providing the only outcrops of CRB from north to south within the valley. Two levels of terraces border the Hood River; the lower terraces often mark the end of an exposure of the basalts, though CRB may be found further up slope. The higher terrace consists entirely of stream-deposited glacial outwash.

Stratigraphy and structure

The Yakima Basalt Subgroup of the Columbia River Basalt Group exposed in the Hood River Valley consists of two low Mg R_2 flows, five Low Mg N_2 flows, and four High MgO flows of the

Grande Ronde Basalt formation and six Frenchman Springs flows and one Priest Rapids flow of the Wanapum Basalt formation. One complete section of the Wanapum Basalt underlain by two (?) High Mg flows and one Low Mg flow was sampled along Snakehead Creek in the Neal Creek drainage and analyzed for trace elements. Four High Mg flows overlain by a thin ($\leq$ 3 m) eroded section of a Frenchman Springs flow and a thin ($\sim$ 10 m) cap of Priest Rapids at the junction of Lake Branch Creek and the West Fork Hood River was measured and analyzed. Stratigraphic sections of more than three flows in contact elsewhere in the valley were not analyzed.

The Grande Ronde Basalt is exposed along the Hood River and its tributaries west of Middle Moutain. Frenchman Springs basalt is exposed directly north of Middle Mountain along Hood River.

The entire section of Yakima Basalt in the Hood River Valley is exposed on Middle Mountain except for the Priest Rapids Member. In the southwest corner of the valley the Priest Rapids flow probably occurs as an intracanyon flow.

The Hood River area is gently folded with a general dip to the east. Frenchman Springs flows crop out at an elevation of 1600 ft in the southwest corner of the valley and at 400 ft north of Middle Mountain. Younger Pliocene (?) basalts overlie the Frenchman Springs basalt from Tucker Bridge (2N/10E-5) to the Columbia River. Frenchman Springs basalt is exposed at the mouth of Hood River.

An anticline trends north through the southwest corner of the Hood River Valley between Lake Branch Creek and the West

Fork Hood River. Another anticline trends east across the southern part of Middle Mountain and plunges to the east. No dip in the Yakima Basalt is evident along Green Point Creek.

Two main structural trends occur within the area - NE to E trending normal (?) faults and folds and NW trending faults and dikes. Two NE trending faults were mapped, one in the structurally complex Neal Creek drainage and one in the southwest corner of the Hood River Valley. South of Snakehead Creek, a breccia zone approximately 100 m wide marks a fault zone with a throw of about 150 m up to the south. Several small faults occur just north of and parallel to this breccia zone. The NE trending fault in the southwest corner is not manifest but is indicated by a stratigraphic offset in the Yakima Basalt with a throw of about 70 m down to the south.

Along the West Fork Hood River, Frenchman Springs flows are exposed at an elevation of 1350 ft (1N/9E-28); the base of the Frenchman Springs Member is not exposed. Less than one km to the north, the Vantage horizon at the base of the Frenchman Springs Member is exposed along Lake Branch Creek at an elevation of 1550 ft (1N/9E-28b).

Three small olivine basalt dikes (~1 m wide) were mapped in the High Mg Grande Ronde Basalt (1N/9E-22 & 28). They trend N10W, N15W, and N45W. A series of small faults trending N10W to N55W occur along the Hood River north of Green Point Creek. The faults have about one m wide breccia zones. The faults all occur within the Low Mg Grande Ronde Basalt section. Because Low Mg Grande Ronde flows are indistinguishable from one another, determination of direction and magnitude

of movement was not possible. Due to the narrow width of the breccia zones and the generally small amount of shearing in adjacent flows, the offset was probably only a few m. One fault near Ditch Creek clearly displaced a flow 2 m down to the south.

The Hood River displays two prominent bends which are fault associated, one in (2N/9E-36d) and the other in (2N/10E-31b). In Sec. 36 displacement is visible along the fault on the east side of the river but not on the west. The dip is to the north. Not enough faulted flows were exposed to determine throw or direction of movement; however, a two m thick breccia zone occurs along the fault in Sec. 31. Direction of movement was difficult to determine but a slickenside trending N10W and dipping 52S was measured.

Between Dee (1N/10E-7) and the dam on the Hood River (2N/10E-31) a repeated exposure of two Low Mg R_2 Grande Ronde flows and three overlying Low Mg N_2 Grande Ronde flows necessitates a fault down to the southeast through Middle Mountain. The Vantage horizon is exposed on Middle Mountain at about 1600 ft elevation (1N/10E-18) and to the northeast at about elevation 2400 ft (1N/10E-8) indicating a displacement of 280 m. The fault passes between the two prominent fault-controlled river bends discussed above. The Low Mg N_2 Grande Ronde flows exposed northeast of the fault are about 230 m thick; the Low Mg N_2 Grande Ronde section to the southwest is about 130 m. thick. The increased thickness and extensive palagonite breccia on at least two Low Mg N_2 Grande Ronde flows northeast of the fault suggest that the area may have been a topographic and/or structural

low when these lavas entered the Hood River Valley.

On the east side of Hood River Valley a breccia zone about 150 m wide marks the location of the Hood River fault which trends N5-15W. The throw is at least 270 m down to the southwest. The valley is cut by several NW trending faults, all down to the southwest. Hood River Valley does not appear to be a graben. A cross-section through Middle Mountain shows several tilted blocks, dipping to the east and separated by faults. The Frenchman Springs flows crop out at approximately the same elevation on the west side of Middle Mountain as they do on the east side of the Hood River fault. Although unmapped, it is believed that a fault trends approximately east-west along the south edge of Middle Mountain and is down to the south. Highly fractured basalt is exposed along the south side of Middle Mountain. Another fault may pass under Blue Ridge on the west side of the upper Hood River Valley. Either, at least 300 m of Yakima Basalt has been eroded from the upper valley, or, it has been down-faulted with respect to Middle Mountain.

Geologic History

The area which is now the Hood River Valley was a topographic low for most or all of the time the Grande Ronde flows were deposited. The lowest basalt member exposed, Low Mg (R_2) Grande Ronde, has a thick palagonite flow top, indicating contact with deep water while the flow was molten. Palagonite breccia is mixed with the flow. Beneath the palagonite, large vesicles ($\sim$10 cm in diameter) and vesicle columns fill the top 3 m of the flow. The flow may have been invasive--one

which dives under loose sediments carrying water and sediments on top.

The Low Mg (N_2) and High Mg (N_2) Grande Ronde flows also have flow top palagonite exposed along the Hood River. The area was probably a closed basin without exterior drainage or at least with disrupted drainage.

The thicker section of Low Mg (N_2) Grande Ronde Basalts found north of the major fault through Middle Mountain likely were ponded in a confining topographic low. Because of poor exposures, it is difficult to determine if the individual flows are thicker or if there is a greater number of Low Mg (N_2) Grande Ronde flows in this area. The probability that valleys existed at the time the Low Mg flows were being extruded is supported by the existence of an intracanyon flow exposed at the junction of West and Middle Forks Hood River.

The High Mg flows have a fairly constant thickness indicating low relief at the time of extrusion except in the southwest corner of the area. Along Lake Branch Creek four High Mg Grande Ronde flows are mapped. Because only the top two m of the lowest exposed High MgO Grande Ronde flows are visible, the High Mg Grande Ronde thickness is unknown. Palagonite flow-top breccia covers the entire exposure of the lowest High Mg flow from Lake Branch Creek to Mohr Park on the West Fork Hood River. The palagonite and increased number of High Mg flows indicates the area was a structural low during the extrusion of the High Mg Grande Ronde flows.

After the High Mg Grande Ronde flows transgressed the area, a period of non-deposition ensued at around 15 my BP

as indicated by the Vantage horizon.

Folding began during the accumulation of the Grande Ronde Basalt and continued, accompanied by faulting, during the deposition of Frenchman Springs flows. The NE-SW trending fault which passes between Lake Branch Creek and the West Fork Hood River occurred after the Frenchman Springs basalt had been deposited. The Frenchman Springs flows were eroded from the structural high created by the fault in the area north of Lake Branch Creek. The Priest Rapids Basalt flowed into the area filling the structural low to the south of the fault and lapped onto the up-faulted eroded Frenchman Springs basalt to the north. The Priest Rapids flow attains a thickness of about 60 m south of the fault. Further west along Lake Branch Creek the Priest Rapids flow overlies about 3 m of pillow basalt.

The NE trending fault in the Neal Creek drainage displays ~10 m thick ridges of cemented breccia which are subparallel to the trend of the Hood River fault. This fault may have been associated with deep shearing which allowed hydrothermal fluids to escape upward into and cement the breccia.

Lake Branch Creek and the West Fork Hood River are separated by a late Pliocene to early Pleistocene andesite flow (Wise, 1969). The andesite laps against High Mg Grande Ronde Basalts on the northeast and against Frenchman Springs and Priest Rapids flows on the east at about the same elevation. This indicates that the NE trending fault through Lake Branch Creek-West Fork Hood River occurred prior to the andesite flow.

The NW trending faults occurred after the Priest Rapids flows were extruded and therefore are younger than the NE trending faults. Some faults appear to be contemporaneous with folding because the faults parallel the strike.

B. Bull Run Watershed Area

Introduction

The Bull Run Watershed lies within the eastern portions of Multnomah and Clackamas Counties and covers more than 390 km^2 (Figure I-1).

Lolo Pass and Mount Hood are to the east; the Columbia River Gorge, Larch Mountain, and the Benson Plateau are to the north; the town of Sandy and the Sandy River are to the west; and the communities of Alder Creek, Brightwood, Wemme, and Zigzag lie to the south. Interstate 80N passes the area on the north, U. S. Highway 26 to the south.

Access to the watershed is by permit only, and locked gates are at each of the entrances. Major approaches are from Sandy on Forest Service Road S-10, from Brightwood on Road S-224, and from Zigzag and Lolo Pass on Road N-12.

The maximum elevation of 4,600 ft is on Hiyu Mountain at the eastern boundary of the watershed. The elevation decreases toward the west; the lowest elevation, less than 500 ft is at the Sandy entrance.

The major stream in the area is the Bull Run River, which flows to the north and then to the southwest from its headwaters at Bull Run Lake. Several smaller streams in the southeast portion of the watershed join and flow into Blazed Alder, which, in turn, flows north into Bull Run River; other streams

flow into this river from the east, north and south. Reservoirs No. 1 and 2 are formed by dams on the Bull Run River.

Basalt of the Columbia River Group undoubtedly underlies all of the watershed but is covered by younger geologic units and unconsolidated surficial deposits. Because stream erosion has cut through the younger material, all basalt exposures occur in proximity to rivers and streams. The highest exposure of CRB occurs at an elevation of 3100 ft northwest of Nanny Creek. Lowest exposure is at an elevation of 500 ft along the Bull Run River.

Basalt occurs along at least 80 km of the major streams, but reservoir water covers at least 10 percent of these exposures. In steep-gradient bedrock streams, exposure is often nearly continuous, but in low-gradient streams, percentage of exposure is often much less. Along roads, exposure is generally less than 10 percent.

The base of the CRB is not exposed in the watershed. The deepest part of the basalt section is exposed in Blazed Alder Creek. About 18 km to the north, outside of the watershed, CRB unconformably overlies rocks of the Eagle Creek formation.

Beaulieu (1974) maps overlying units as the Rhododendron formation in the western portion of the watershed and as Pliocene and Quaternary volcanic rocks in the eastern section. During this study, isolated patches of Rhododendron were noted but not mapped further to the east along the Bull Run River.

CRB was mapped along the Bull Run River and Blazed Alder Creek by Wells and Peck (1961) and Peck and others (1964);

more detailed mapping was done by Beaulieu (1974). Engineering studies include those by Dames and Moore (1972a, b; 1973), Patterson (1973), Ruff (1957), Schlicker (1961), Shannon and Wilson, Inc., (1958a, b; 1961, 1963, 1965, 1973), and Stevens and Thompson, Inc. (1957, 1965). A soils survey of the area was conducted by Stevens (1964).

Structure and stratigraphy

Grande Ronde Basalt flows, with a total thickness of about 150 m and Wanapum Basalt flows, with a total thickness of 137 m occur within the watershed. The basal exposed flow is a Log Mg (R_2) flow found in Blazed Alder Creek. Above it lies approximately 95 m of Low Mg (N_2) basalt comprising at least four and possibly more separate flows. These flows are difficult to differentiate either in the field or by trace element geochemistry. Rocks from these flows have extremely fine-grained textures; one of the N_2 flows is characterized by small, clear, glassy plagioclase phenocrysts. All of the flows in this group have the same kind of distinctive jointing: a small colonnade and a proportionally much larger entablature.

Two High Mg Grande Ronde flows with a total thickness of about 43 m lie above the Low Mg flows. These rocks are coarser in texture than the Low Mg flows. Rocks from the top flow are also quite open in texture. The tops of both of these flows, but particularly the upper flow, are deeply weathered. The lowest flow of the two is characterized by a blocky colonnade and multiple layers of sheet vesicles. The upper flow is characterized by well-developed columns,

sections of which display, platy jointing. A thin soil zone, and, in one place, a 9 m thick interbed separates the two flows.

The Vantage interbed lies between the Grande Ronde and overlying Wanapum Basalt flows. In the Bull Run syncline, the Vantage is composed of sandy and silty sediments with local soil zones and carbonized wood. The maximum thickness is 1.5 m at Log Creek. In the Bull Run syncline, the base of the Wanapum flow above the Vantage often has up to 9 m of pillow basalt; in the anticline, the contact is flow-on-flow with no evidence of pillows, soil or carbonized wood.

Above the Vantage horizon are the Wanapum flows: six N_2 Frenchman Springs flows and one (or possibly two) R_3 Priest Rapids intracanyon flows totaling at least 137 m. The Frenchman Springs rocks are coarse in texture; three of the six flows, the first, second and fourth, have large, glassy, plagioclase phenocrysts (phyric). The third flow has occasional plagioclase phenocrysts (rarely phyric); the fifth and sixth flows are aphyric. All of these flows display well-developed colonnades and no entablatures. A red clay zone occurs locally between the two upper aphyric Frenchman Springs flows.

The Priest Rapids intracanyon flow displays reversed polarity and, where exposed along the Bull Run River, is characterized by at least 100 m of bedded palagonite, an 8 m thick colonnade and a 60 m thick entablature. Where it overflowed the canyon, the Priest Rapids flow is 12 m thick and forms massive blocky columns. This thinner part of the flow may in fact be a separate Priest Rapids flow, but poor exposures make

it impossible to locate a contact.

The dominant structure is a NE trending (roughly N60E) syncline and anticline. A N60E trending, 12 degree SE dipping, thrust fault with at least 180 m of vertical offset occurs on the north limb of the anticline. The entire area displays fractures that trend in sundry directions, but particularly with trends of N10-20W, and N55-65W. The entire structure has a slight regional dip of about 2 degrees to the west-southwest.

The most northerly fold is a N60E trending syncline in which the Bull Run River flows to the southwest. The axis of the syncline lies slightly to the south of the river. The development and persistence of this syncline during the Miocene are shown by pillows that occur locally at the base of the highest High Mg Grande Ronde flow; a 9 m interbed between the two High Mg Grande Ronde flows near the main dam; a less than 30 cm thick interbed between the two High Mg Grande Ronde flows at North Fork; a soil zone of the Vantage horizon; and pillows at the lowest Wanapum flow. The intracanyon Priest Rapids flow has been found only in the syncline and its periphery.

The NE trending, thrust-faulted anticline parallels the syncline and lies south-southeast of it. It is defined by elevations and attitudes of various CRB flows, and is characterized by the absence of pillows, interbeds, and the Priest Rapids intracanyon flow. A Wanapum flow-top near the county line on Road S-154 is deeply weathered -- more than the corresponding flow-top in the syncline -- indicating a Miocene

topographic high corresponding to the upper portions of the anticline. The syncline and anticline are believed to extend northeastward through Hood River Valley, where they are now broken by N-NW trending faults, to the Columbia River Gorge where they appear as the Mosier syncline and Ortley anticline.

The complete High and Low Mg Grande Ronde section does not occur in the upper reaches of Blazed Alder Creek. In the northern portion of this creek, at least four N_2 Low Mg flows overlie the R_2 Low Mg reversed flow; upstream in the southern part, High Mg flows are missing. Apparently a structure was developing in Bull Run during early CRB time. After the reverse flow entered the area, a topographic high began to develop where the present-day abbreviated section occurs. A slight relative subsidence both north and south of the high developed. The N_2 Low Mg basalt flowed around the high which was eventually covered by later High Mg flows. Gravity and magnetic maps show anomalies roughly corresponding to this abbreviated section.

The ancient high delineated by the abbreviated section in Blazed Alder Creek was evidently a zone of weakness, because as folds developed, the anticline failed at the margin of the high, producing the thrust fault with vertical offset of 180 m and net slip of at least 900 m.

The best exposure of the thrust fault is just downstream from the confluence of Boulder and Blazed Alder Creeks, where the fault plane is exposed at stream level. Below the thrust plane about 2 m of the underlying basalt flow is coarsely brecciated. Extremely finely-ground tectonic breccia occurs

for about 10 m above the thrust plane.

Because of this thrust fault, CRB occurs at higher elevations and more extensively in the southeastern section of Bull Run than has been previously mapped. Highest exposure is at an elevation of 3100 ft. All the CRB in the forward section of the thrust has been disturbed, even if not actually brecciated, and therefore does not produce good outcrops in these areas. Although dense and coherent, a very minor amount of silicification was observed in the breccia of the upper thrust plate.

Linear ridges of tectonic breccia with trends of about N10-20W were observed in Blazed Alder Creek in the lower plate over which thrusting occurred. A smaller ridge also lies within the thrust zone along Boulder Creek. The linear ridges may represent an older, pre-thrust zone of weakness that brecciated during the thrusting, or both zones may be due to later fracturing which cut across the thrusted area.

A vertical fault occurs at North Fork quarry on Road S-10. The fault trends roughly N20W, but horizontal slickensides within the foot-wide fault zone trend in two directions; N30E and N30W. This fault, because of poor exposures, could not be traced for any significant distance.

Numerous fractures occur in the CRB in Bull Run. Although no attempt was made to do a statistical analysis of fracture trends, certain dominant fracture trends are apparent throughout the area. Some fractures are merely breaks in the basalt that cut through regular jointing, and in some cases, several flows; while other fractures are brecciated or contain

brecciated zones.

A major fracture trend is N10-20W. Fractures with this trend are found throughout the watershed, but notable concentrations occur along the north-flowing sections of Blazed Alder Creek and Bull Run River and their tributaries. Brecciated zones with this trend also occur near the thrust fault. Along the Bull Run River just upstream from Log Creek, a large brecciated zone with this trend crops out. Aerial photographs and SLAR imagery show a linear with this identical trend that extends north along Blazed Alder Creek and Bull Run River, cuts through the glacial cirque on Falls Creek, and continues up Tanner Creek to the Columbia Gorge and into Washington State. A dike of Boring basalt with this same trend crops out along Blazed Alder Creek before curving slightly and disappearing in a side stream. At one point in Blazed Alder Creek, this dike cuts an older N55W trending breccia zone, another frequently occurring fracture trend in Bull Run.

The N55W trend is found throughout the area but seems to occur most frequently near the thrust fault. Upstream from the thrust fault, N20-55W fractures often contain breccia; these fractures, however, decrease in frequency with distance from the fault.

Other less common fracture trends include N-S, N20E and N80W. Fractures frequently affect patterns of mass wasting and erosion. For example, at the base of the falls at Falls Creek and along Road S-10 on the east side of Falls Creek, massive failure of extremely large blocks of Wanapum Basalt has occurred along N15W trends.

Fractures often control the directions in which streams flow in Bull Run. At one point Blazed Alder Creek flows in a N20W trend and then makes an abrupt turn and follows a N55W fracture. These fractures seem to be most influential in controlling stream direction when the stream is flowing across the regional anticline-syncline structure.

The path of an intracanyon flow of reversed Priest Rapids basalt has been traced from east to west through the watershed. The greatest measured thickness at any one place is 177 m but that thickness was not measured from the absolute bottom of the ancestral channel. The most easterly exposure occurs in the eastern portion of the watershed between Log and Otter Creeks. The intracanyon flow forms a mound on the bench west of Otter Creek and then is exposed by the Bull Run River at the point where the river changes directions from north to west. Again, on the north bench overlooking the river, the intracanyon flow forms large mounds of basalt. The next mapped exposure to the west is in a quarry on the south side of the Bull Run River. Further west, the flow is again cut by the Bull Run River; it then forms a ridge in a clearcut north of the river. It is last exposed in North Fork. From there, it is presumed to have flowed to Crown Point in the Columbia Gorge. It is correlated with the Crown Point intracanyon flow by similar chemistry, magnetic polarity, morphology and flow characteristics, and large amounts of bedded palagonite. Crown Point is on trend and geographically close to the intracanyon flow in Bull Run.

The intracanyon flow in Bull Run is characterized by a

100 m thick palagonite sequence which in places has been waterworked. Foreset beds indicate flow directions to the west and southwest. In other places, the palagonite is unsorted and contains large blocks of basalt up to 3 m in diameter. The flow has a relatively thin colonnade whose thickness varies from area to area but which was measured at 7.6 m along the Bull Run River. The entablature forms distinctive, flat-topped mounds which contrast with the CRB benches surrounding it.

Another distinguishing characteristic of this flow is its somewhat ambiguous remnant magnetic polarity. At some places, the flow produces a normal reading on the fluxgate magnetometer, elsewhere it is reversed. Always, however, a reversed polarity is shown at the top of the section.

The present-day river does not exactly follow the course of the ancestral river through which the intracanyon flow moved. Where the present-day river breaks into the old channel, it reveals an almost vertical, smooth, basaltic canyon wall with a U-shaped valley floor. A very small section of the ancestral valley floor is exposed in the Bull Run River and contains relatively poorly sorted, rounded to subangular basaltic pebbles, cobbles, and occasional boulders ranging in diameter from less than 1 cm to over 1.5 m.

The Bull Run Watershed region was being deformed in earliest CRB time as shown by the abbreviated section in Blazed Alder Creek. The base of the CRB is not exposed in this area to record possible earlier deformation. By High Mg Grande Ronde time, the NE trending syncline and anticline were already

developing, as evidenced by the local interbed and pillows between the two High Mg flows in the syncline.

During Vantage time, as elsewhere on the Columbia Plateau, no basalt flows occurred. Instead, saprolite and soil zones developed and drainage systems evolved. When the Frenchman Springs flows entered the area, pillows formed in the syncline at the base of the earliest Frenchman flow.

Between Frenchman Springs and Priest Rapids time, a major east-west river drainage system formed. It was through this 180 m deep canyon that the Priest Rapids intracanyon flow entered the area from the east and flowed west-northwest to Crown Point in the present-day Columbia River Gorge.

Sometime during Wanapum time, and probably before Priest Rapids time, thrusting occurred on the northwest limb of the anticline. Phyric Frenchman Springs flows but not Priest Rapids flows have yet been found on the upper thrust plate. Vertical fracturing accompanied the thrusting, with most intense fracturing nearest the thrust zone.

The CRB surface was eventually covered by younger volcanic and volcaniclastic rocks. Fracturing undoubtedly continued to occur, and erosion along these fractures eventually re-exposed CRB. The most recent fracturing appears to be the N10-20W trend that is visible on SLAR imagery and air photos. Boring dikes with this same trend indicate that east-west extension accompanied or occurred after the north-south compression of the region.

C. Salmon River Area

Introduction

Located between the Bull Run River and the Clackamas River drainages is a series of small isolated outcrops of CRB which cover approximately 25 km^2 within a map area of about 250 km^2. Relationships between these exposures are difficult to determine because of structural complexities within some of the areas and because of rather extensive areas of intervening younger Rhododendron Formation and sedimentary valley fill.

Structure and stratigraphy

Like other areas previously discussed, the Columbia River Basalt Group exposed in this area is assigned to the Yakima Basalt Subgroup. As in nearly all exposures of CRB in western Oregon, the basalts in this region are mapped as Grande Ronde Basalt and Wanapum Basalt. The base of the basalt is not exposed in this region while the upper contact is unconformable with the Rhododendron Formation. The Wanapum Basalt is represented by two to four flows with an approximate total thickness of 75 m. Although a combination of intricate structure, poor accessability, and discontinuous outcrops precludes ascertaining the number of flows in the Grande Ronde Basalt, certain relationships can be determined. Two High Mg chemical type flows occupy the upper part of the formation and attain a thickness of about 70 m. The low Mg chemical type possesses an unknown number of flows but can be subdivided into the CRB N_2 and R_2 paleomagnetic intervals that are about 160 m and at least 50 m thick, respectively.

Traversing the area is the N30W trending Salmon River fault that separates the Columbia Plateau type structural trends from those of the Portland Hills-Brothers fault zone. This N30W trending fault displays a vertical displacement of about 145 m down to the west with a moderate amount of associated tectonic breccia near Arrah Wanna. However, it is believed that this apparent displacement is the result of offset of some pre-existing structure by right lateral movement because (a) near the Salmon River opposite sides of the fault lack significant vertical displacement, and (b) along this trend in the Upper Salmon River the fault displays right lateral displacement. Folds to the east of this fault trend generally N60E with the Bull Run-Ortley anticline terminating at the Salmon River fault in the vicinity of Brightwood. The upper Salmon River area is a broad asymmetric anticline with the same trend and a possible connection with the outcrops at Robinhood quarry. West of the Salmon River fault a small segment of a minor anticline occurs in the Alder Creek-Sandy River area that strikes N75W similar to the folds of the Portland Hills and is the only fold mapped in the Clackamas River drainage.

The intervening synclines are not exposed except for a small area of hyaloclastic material that may mark the axis of a syncline near the confluence of the South Fork and Salmon River. The location of other synclinal axes are based on other lines of evidence and are discussed below.

Faulting has severely complicated stratigraphic relationships in all areas except Alder Creek and the upper Salmon

River. The Salmon River anticline is, however, down faulted about 75 m on the north by a NE trending normal fault.

The region between Arrah Wanna and the U. S. Highway 26 bridge crossing of the Salmon River has been deformed by several faults, all in close proximity to one another, but with different trends. A short segment of a thrust fault southwest of Arrah Wanna has displaced the basalt stratigraphically about 180 m. Associated tectonic breccias exceed 100 m in thickness; however, the thrust plane is not exposed. This fault has roughly the same trend and displacement as the Promontory Park fault in the Clackamas River and may well connect with it. The Salmon River fault is exposed an elevation of 2400 ft on Arrah Wanna trail and is responsible for the disappearance of the basalt section to the west at this locality. Displacement along this fault is not known. A N5-10W trending fault has been mapped passing near three quarries in the basalt. It is represented in the quarry in the Salmon River by a 30 m wide breccia zone and at the two quarries north of the Sandy River, near North Boulder Creek, as a much broader, less easily defined structure that has displaced the western quarry down with respect to the upper quarry.

Geologic History

The history of this region is not easily interpreted because of the lack of continuity between outcrops and the lack of exposed synclinal areas; however, certain events can be deduced. The NE trending folds are known to have formed during the incursion of the basalts because of the on-lap against anticlines of some flows and the hyaloclastic and pillow

deposits found only in structurally depressed areas. These features are not observed in this area but occur in the eastward extension of the folds. Similarly the Arrah Wanna thrust fault probably formed during the later stages of the deformational episode that produced the folds as is the case with the Bull Run thrust and some of the thrusts on the Columbia Plateau.

The youngest tectonic event to have occurred is the Salmon River Fault. When projected to the south, the fault apparently has displaced Pliestocene glacial features as seen on air photos and SLAR imagery near Tumbling Creek, a tributary of the upper Salmon River.

D. Clackamas River Area

Introduction

Columbia River Basalt is exposed in the Clackamas River area within deeply cut canyons of an extensive drainage system that covers more than 700 km^2. The basalt flows form impressive cliffs with occasional waterfalls within this area some 73 km southwest of Mt. Hood (Figure I-1). The eastern part of the area is characterized by the constructional volcanic terrain of the high Cascade Range while the west is dominated by more maturely dissected western Cascade topography.

The basalts of the Columbia River Group are overlain, underlain and interfingered with volcanic and volcaniclastic rocks of local Cascadian origin. The Clackamas River valley in the vicinity of Ripplebrook Ranger Station is the approximate southern limit of these basalts, where they lap against

a pre-existing topographic high formed by the Little Butte Volcanic Series. Successive flows of CRB filled relatively smooth terrain to the north of the highland and encroached progressively deeper into the foothill valleys. Sediment and distal volcanic facies in turn covered the southern perimeter of the basalt during the interflow periods to form a number of interbeds up to 46 m thick. Similarly, deposits of the Sardine Formation rapidly buried the basalt after the last flow entered the area.

Deep incision by the Clackamas River and its tributaries has exposed more than 550 m of CRB in this area. The complete basalt sequence can be seen in the cliffs forming the canyon walls in the vicinity of Three Lynx.

Structure and stratigraphy

The general geometry of the CRB in the Clackamas River area is a broad slab that is gently inclined toward the northwest. Dips over most of the area are less than 10 degrees, in part accounting for the extensive exposures that occur between Lake Harriet on the east and North Fork Reservoir on the west.

The structure of the area consists predominantly of northwest-trending faults that cut the gently tilted basalt in an en echelon pattern (Figure III-1), as is reflected in the drainage pattern of the northwest flowing Clackamas River. NE and N-S trending faults also occur, but are in the minority. Some faults are predominantly strike-slip and others are predominantly dip-slip; however, all fault planes are vertical or near-vertical. Moreover, there is an absence of

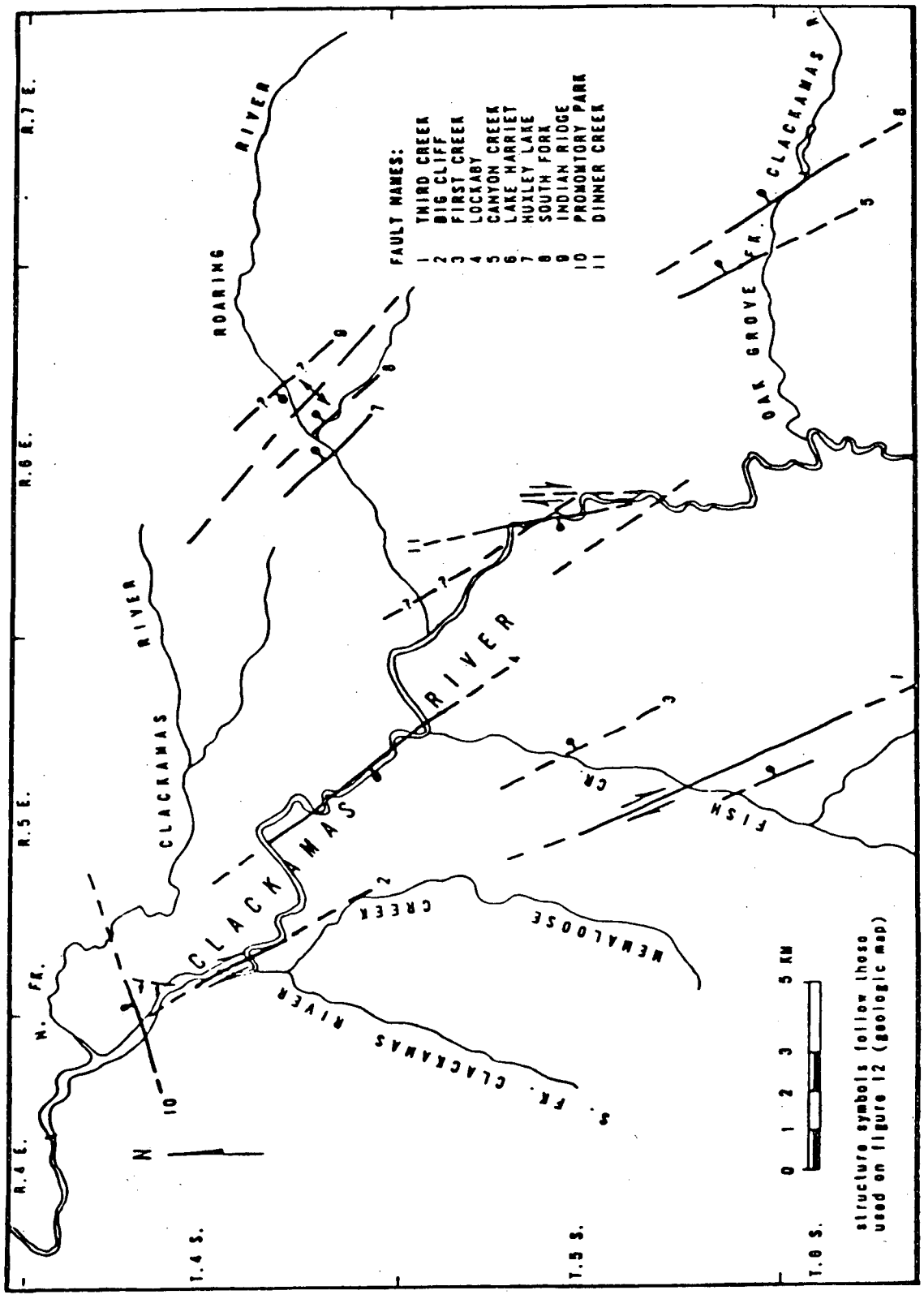

Figure III-1. Tectonic Map of the Clackamas River Area

drag-folds associated with these faults.

The faults in the northeast part of the area constitute the deformed boundary of an otherwise relatively unwarped body of basalt. Dips in the Roaring River and Lake Harriet areas range between 20 and 40 degrees adjacent to faults with offsets of 200 m or more. The attitudes of flows observed within the Roaring River drainage define a northwest trending anticline with a crest that appears to be down-dropped as a block or blocks along the Huxley Lake, South Fork and the Indian Ridge faults. The Lake Harriet attitudes appear to reflect the asymmetrical east limb of the "Clackamas Anticline" of Peck and others (1964), or possibly a monoclinal fold down to the east. Faults over the rest of the area are not associated with steeply dipping flows, in distinct contrast with those on the northeast perimeter of the area. The Lockaby fault, for example, has more than 100 m of vertical offset along a very narrowly defined vertical fault plane. Flows adjacent to it are relatively undisturbed by this movement between NW trending en echelon faults. However, this simple picture is complicated by strike-slip movement along at least two of these faults.

Right lateral faults occur at Big Cliff and near Third Creek, a tributary of Fish Creek. Both of these faults define prominent air photo linears that are clearly evident within rocks of the overlying Sardine Formation. An apparent normal displacement of 15 to 30 m occurs across the Third Creek fault, but no detectible displacement can be seen at Big Cliff. The amount of horizontal offset on either of

these faults cannot be deduced based upon existing data. However, many lesser fractures with horizontal slickensides can be seen throughout the area, suggesting that the collective offset on all such fractures and faults could be substantial.

The shallow dips exposed in the Clackamas River canyon are only slightly greater than the gradient of the river itself, so that abrupt changes in the stratigraphy along the river are nearly always the result of faulting rather than folding. Both the disappearance of the top of the CRB at North Fork Reservoir and the appearance of the base of the section near Three Lynx are, in part, the result of dip-slip movements on normal faults rather than dip alone. The net effect of this faulting and particularly that at North Fork Reservoir is that one does not traverse the entire CRB sequence from northwest to southeast through the Clackamas River canyon. Less than half of the 17 flows are exposed at highway level across the area due to faulting. Thus, an excursion through the Clackamas River canyon is an experience limited to the lower half of the section.

The stratigraphy of the Clackamas River area consists of Wanapum and Grande Ronde Basalt. Only the Frenchman Springs Member has thus far been identified within the former of these two formations. The Grande Ronde stratigraphy is very similar to that observed elsewhere, except that interbedded sedimentary units are more common and the distinctive Prineville chemical type is present.

The Grande Ronde Basalt in the Clackamas River area consists of at least eleven flows and five or more interbeds with a combined thickness of more than 425 m (Figure III-2). Two

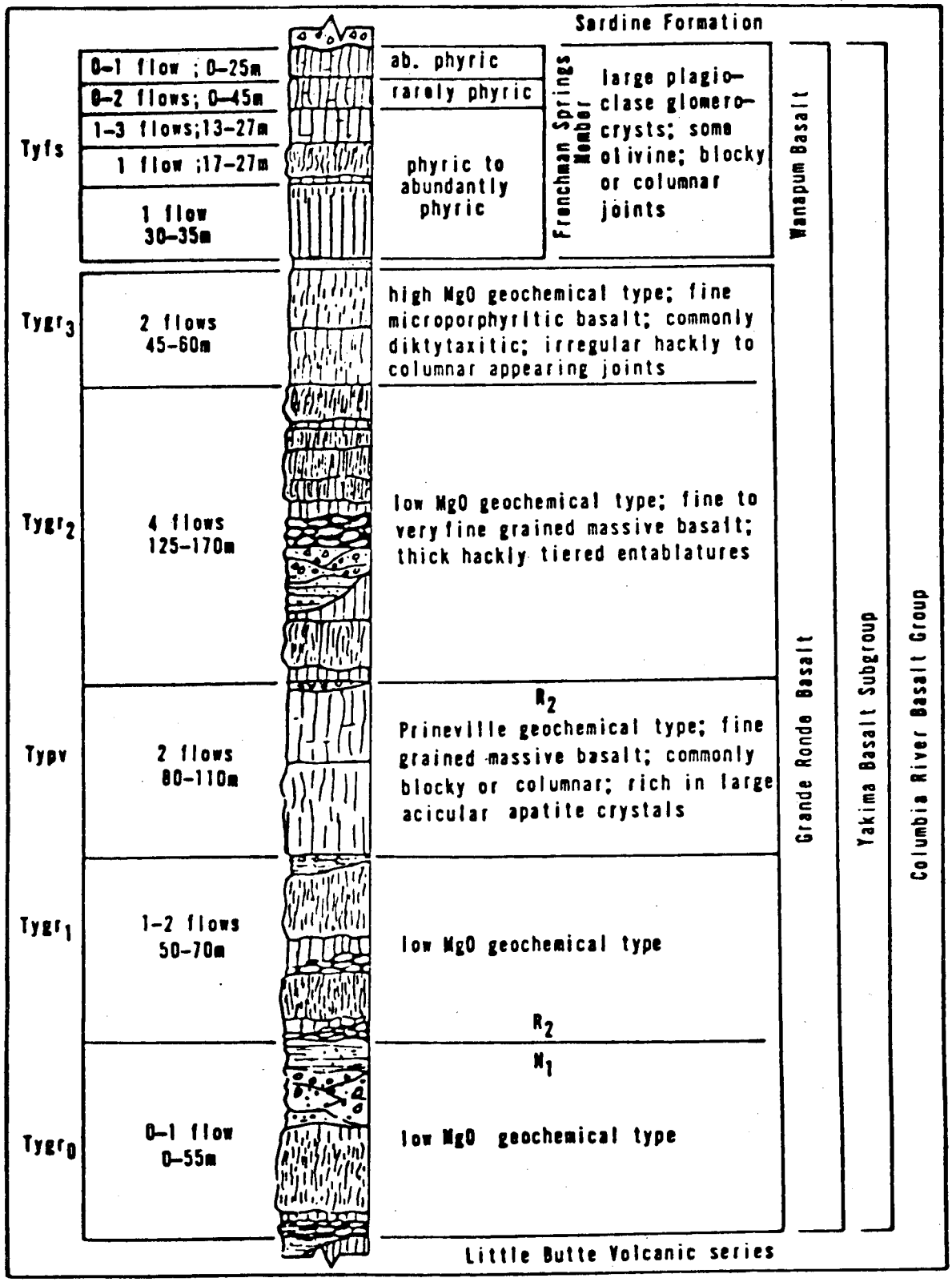

Figure III-2. Generalized Stratigraphic Column for Columbia River Basalt in the Clackamas River Area

High Mg flows occur at the top of the formation. The remainder of the Grande Ronde Basalt consists of flows of the Low Mg geochemical type separated into two approximately equal parts by two intercalated flows of Prineville chemical type. There are two paleomagnetic reversal events within the Clackamas River section that divide it into three plarity intervals. These are considered to be equivalent to the R_2/N_1 and N_2/R_2 paleomagnetic horizons recognized by previous workers elsewhere in the Columbia Plateau (Figure II-2). The N_2/R_2 paleomagnetic break coincides with the Low Mg/Prineville geochemical break, making this a well-defined stratigraphic horizon.

The Prineville flows are distinctive from the standpoint of both trace element and major oxide geochemistry. They also differ from other flows within the Grande Ronde section from the standpoint of petrography and certain physical characteristics.

The Prineville basalt type was first recognized and described by Uppuluri (1973, 1974) from exposures near Prineville Dam in central Oregon. Other flows of this chemical type were also observed by Nathan and Fruchter (1974) at Buck Creek and Tygh Ridge about 47 km north-northeast of the type locality, where they are intercalated with flows of the Low Mg Grande Ronde geochemical type. Wright, and others (1973) and Brock and Grolier (1973) noted the anomalously high P_2O_5 concentrations in these flows, as did Uppuluri at the type locality.

The Prineville chemical type flows in the Clackamas River drainage are easily distinguishable from other Grande Ronde flows by both major oxide and trace element data. Four trace

elements, Sm, Eu, Ba and Co, are particularly striking as differentiators. Ba concentrations in the Clackamas River flows are higher by a factor of two to three than any of the other flows in the section. The only comparable value anywhere in the Columbia River Basalt Group is that of the Umatilla Member of the Saddle Mountains Basalt, which has Ba concentrations that are slightly higher. Conversely, Co abundances in the Clackamas River flows are 30 to 37 percent lower than all other flows in the section. It is in fact lower than in any other chemical type in the entire Columbia River Basalt Group. Eu, like Ba, has concentrations that are greater than the other flows by a factor of two to three, which is approximately equal to the Umatilla and slightly exceeded by the youngest of the two Ice Harbor flows of the Saddle Mountains Basalt. Sm concentrations are 30 to 60 percent higher than Low Mg flows and 80 to 85 percent higher than High Mg Grande Ronde flows. Major oxide distinctions include P_2O_5 concentrations that are three to four times greater, SiO_2 that is 2 to 4 percent lower, and TiO_2 that is up to 40 percent higher than other Grande Ronde types.

The Prineville flows, as their unusual chemistry would suggest, are petrographically distinguishable from other Grande Ronde flows. Their most distinctive characteristic is the anomalously long, acicular apatite crystals that occur in great abundance in all thin sections. Acicular apatite also occurs in other flows in the section but is relatively finer-grained by a factor of three to four. The presence of these crystals is a direct reflection of the anomalously high

P_2O_5 content.

The Prineville flows can also be distinguished from the rest of the Grande Ronde section on the basis of jointing characteristics. They rarely have hackly entablatures and consist almost entirely of fair-to-well-developed blocky colonnades. This contrasts dramatically with the entablature-dominant, Low Mg Grande Ronde flows above and below them.

The stratigraphy of the basalts along the Clackamas River is also characterized by interbeds, as previously noted. These units increase in number and thickness from north to south across the area. They are useful stratigraphic markers on a local basis. Although the composition of the interbeds is varied, the presence of stratified, fine-grained deposits clearly indicates that bodies of water covered much of the area. Pillow complexes up to 25 m thick commonly occur above these deposits indicating ponded water. This condition prevailed throughout CRB time in the Clackamas River area and was also the case in other peripheral areas of the Columbia Plateau as well (Swanson, 1978).

Geologic History

Very little contemporaneous structural activity is indicated during CRB time. Minor pre-reversal folding is indicated by dips that are steeper within the Prineville flows than in overlying flows in some localities. The magnitude of this folding is considered minor since the number of flows and their collective thickness within the Grande Ronde subunits is nearly constant across the Clackamas River area (Anderson, 1978). Broad basining and possible faulting is indicated by the

exclusion of the upper two to three flows of the Frenchman Springs sequence from the area immediately adjacent to the southern edge of the basalt. This occurs over a distance of 1.8 to 3.7 km and involves about 67 m of section.

The major offsets observed on faults cutting CRB in the Clackamas River area are mostly post-Sardine in age.

E. Old Maid Flat Exploratory Hole

The exploratory hole at Old Maid Flat (2S/8E-15cd) on the western flank of Mt. Hood was drilled to a depth of 4,003 ft at an elevation of 2,750 ft. The hole was drilled with rotary bits and all samples collected were cuttings brought up with the circulating mud. Most samples from any given depth contained much less than 100 percent of any one rock type indicating a significant amount of uphole contamination, becoming a more serious problem with depth. From a complete set of samples split from those collected at the time of drilling, we chose samples for analysis that seemed most likely to contain a high percentage of basalt. We were guided in this choice by the lithologic log and various downhole geophysical logs. From these samples we chose seven that appeared to represent seven individual flows, most of which were greater than 30 m thick, and one sample consisting of large chips of gabbro brought up on the bit from a depth near 3500 ft. Each sample selected was thoroughly washed and sieved to obtain larger fragments which were then hand picked with the aid of a binocular microscope. The most abundant group of basaltic chips in each sample with similar physical characteristics were selected for analysis. Approximately one gram of each

sample was selected and then further cleaned in an ultrasonic vibrator to remove any traces of drilling mud and other clay-sized particles. The eight prepared samples were then analyzed by instrumental neutron activation analysis (INAA) in the standard manner.

The geochemical data generated are presented in Figure III-3 and a summarized evaluation of this data in terms of identification and correlation is presented in Figure III-4. The results are summarized as follows:

1. All basalt samples analyzed are CRB and each was identified with considerable confidence as to individual chemical type.

2. Basalt occurs beneath the Old Maid Flat site at a depth interval from 2028 to 3850 ft, a total interval of 1822 ft. This composite thickness is very similar to the CRB in the Clackamas River area. We originally predicted that the thickness of CRB beneath Mt. Hood would be between 1500 and 2000 ft based on a composite thickness of all units of CRB known to occur from the Columbia River Gorge to the Clackamas River.

3. The bottom 1045 ft of this interval is bracketed by Low Mg Grande Ronde Basalt flows which is comparable in thickness to sections at Multnomah Creek (1100 ft) and in Clackamas River Area (1500 ft).

4. Sample OMF 3140 is from a Prineville chemical type flow. The position of this flow, below a Low Mg Grande Ronde flow is similar to that of the uppermost Prineville flow at Tygh Ridge (Nathan and Ruchter, 1974). No other Prineville flows are known in the Cascade Range other than those recently

SAMPLE	NA		LA		SM		CE		EU	
OMF 2072	2.05	0.04	25.7	1.80	7.52	0.14	57.00	3.00	2.18	0.09
OMF 2900	1.94	0.04	22.8	1.60	6.01	0.12	49.00	3.00	1.90	0.08
OMF 3140	2.43	0.04	23.4	1.80	8.69	0.14	53.00	3.00	3.57	0.13
OMF 3290	2.20	0.04	23.5	1.60	6.63	0.12	50.00	3.00	2.32	0.09
OMF 3518	2.02	0.04	11.1	1.20	3.12	0.08	30.00	2.00	1.10	0.06
OMF 3530	2.33	0.04	23.6	1.80	7.58	0.14	51.00	3.00	2.69	0.11
OMF 3680	2.00	0.04	26.7	1.80	6.82	0.12	58.00	3.00	1.81	0.08
OMF 3850	2.25	0.04	26.5	2.00	7.23	0.14	60.00	3.00	2.17	0.09

SAMPLE	LU		TH		HF		CO		FE	
OMF 2072	0.60	0.09	4.10	0.40	3.80	0.60	38.40	1.10	10.62	0.12
OMF 2900	0.54	0.08	5.20	0.40	3.60	0.60	38.30	1.10	8.74	0.11
OMF 3140	0.62	0.09	3.90	0.40	3.10	0.60	27.40	0.90	8.69	0.11
OMF 3290	0.62	0.09	4.40	0.40	3.40	0.60	33.00	1.00	8.44	0.10
OMF 3518	0.35	0.06	1.50	0.30	2.40	0.40	42.70	1.00	6.91	0.09
OMF 3530	0.51	0.09	4.40	0.40	3.60	0.60	30.90	1.00	8.59	0.11
OMF 3680	0.44	0.08	6.20	0.40	4.30	0.60	35.90	1.00	8.67	0.11
OMF 3850	0.58	0.09	6.60	0.50	6.00	0.70	35.30	1.10	9.34	0.12

SAMPLE	SC		CR		BA		
OMF 2072	36.60	0.20	31.00	10.00	490.00	150.00	Frenchman Springs Member
OMF 2900	33.99	0.19	17.00	8.00	550.00	140.00	Low Mg Grande Ronde Basalt
OMF 3140	36.40	0.20	8.00	7.00	2400.00	300.00	Prineville Basalt
OMF 3290	33.33	0.19	20.00	8.00	1030.00	170.00	Log Mg Grande Ronde Basalt (Contaminated)
OMF 3518	26.02	0.15	340.00	80.00	170.00	100.00	Gabbro - Not CRB
OMF 3530	35.28	0.20	31.00	10.00	1290.00	180.00	Low Mg Grande Ronde Basalt (Contaminated)
OMF 3680	31.95	0.18	17.00	8.00	590.00	140.00	Low Mg Grande Ronde Basalt
OMF 3850	33.48	0.20	21.00	9.00	630.00	140.00	Low Mg Grande Ronde Basalt

Figure III-3. Geochemical data on Old Maid Flat drill hole samples.

Elevation	Depth	Thickness	Sample	Geochemical Identification & Comments
2750'	0	2028'		Post CRB Mudflow Deposits, alluvium and volcanic sediments
722'	2028'	60'	OMF2072	Frenchman Springs Member
662'	2088'	727'		(Local volcanic episode)
-65'	2815'	167'	OMF2900	Low Mg Grande Ronde Basalt (2253-Age dated Sample - 12.2 ± 2 m.y.) #3070' Sidewall sample Normal Polarity)
-232'	2982'	208'	OMF3140	Prineville Basalt
-440'	3190'	150'	OMF3290	Low Mg Grande Ronde Basalt (contaminated w/Prineville)
-590'	3340'	170'	OMF3518	(Interbed & small intrusion) Gabbro - dike or sill
-760'	3510'	120'	OMF3530	Low Mg Grande Ronde Basalt (contamined w/Prineville)
-880'	3630'	110'	OMF3680	Low Mg Grande Ronde Basalt
-990'	3740'	110'	OMF3850	Low Mg Grande Ronde Basalt
-1100'	3850'	150'		Volcanic sediments (XLTuff - age dated 8 m.y.)
-1250'	3970'			

Total Thickness of CRB interval - 1822'; 1045' of Low Mg Grande Ronde

Figure III-4. Columbia River Basalt stratigraphy in Old Maid Flat Exploratory Hole

found in the Clackamas River area (Beeson and others, 1976; Anderson, 1978).

5. Samples OMF 3290 and OMF 3530 are Low Mg Grande Ronde contaminated with approximately 40 percent Prineville basalt from uphole. This is indicated by the Low Mg Grande Ronde chemistry except for Ba, Sm, Sc, Co and Eu which have values between those of Prineville and Low Mg Grande Ronde.

These preliminary conclusions indicate that, except for local interbeds, a normal thickness of CRB occurs under Mt. Hood and that the 3850 ft sample is probably the lowest (or near to the lowest) CRB flow in this area. This suggests that the rocks below this sample are older than the CRB. It is possible that the lower 153 ft of the hole represents an interbed, but it is doubted that the CRB extends much below this level. Further study of the geophysical logs and the cuttings should be carried out to refine the thickness of basalt flows and detect possible interbeds, although interbeds beds of significant thickness are known to occur between depths of 3340 and 3510 ft and 2088 and 2815 ft. The lower interval is complicated by a gabbroic intrusive (OMF 3518) not related to CRB. The upper interval is much thicker than any known interbed in the Cascade Range (even the Clackamas River area which is marginal to an older highland) which indicates a contemporaneous local center of andesitic volcanic activity. This local volcanic activity effectively produced a topographic high which prevented CRB flows from covering this area until the Frenchman Springs flow which occurs in the hole from 2028 to 2088 ft. It should be noted that the

only volcanic interbed within the CRB in the nearby Bull Run River area is a synclinally localized, 30 ft thick, light tuffaceous sediment which occurs between two High Mg Grande Ronde flows and is within the same time interval as this major interbed at Mt. Hood. The same stratigraphic horizon in the Salmon River and Brightwood areas show no interbed.

The CRB at Old Maid Flat occurs between an elevation of 772 ft above and 1100 ft below sea level. Therefore, it is likely that considerable down faulting occurred about Mt. Hood in addition to earlier folding of CRB. The presence of a Prineville basalt flow locally suggests that the area was structurally low, although not the lowest point in the structure as no hyaloclasitic materials were noted in the cuttings from the Old Maid Flat hole.

A sample of the uppermost Grande Ronde flow from 2953 ft was dated by 40K/40Ar with the resulting age determined to be 12.2 $\pm$ 2 my which seems to conflict with the relative age from stratigraphic criteria. It is believed that the data is compatible because the age may be within the limits of analytical error and the possibility of Argon loss at elevated geothermal temperatures which probably existed in the geologic past is exceedingly great. Atlantic Richfield Hanford Company (p. 49, 1976) dated approximately 300 samples of Yakima Basalt by the 40K/40Ar method. They state:

> "The apparent ages of the samples below Rosa range in erratic fashion from about 11 to 15 million years B.P. Investigations as to the cause for the erratic relationship between potassium-40 and argon-40 revealed that the variation in apparent age increased as the glass content increased and was highly erratic in those samples in which glass had altered to palagonite."

Low Mg Grande Ronde flows, as a group, are finer grained and contain more glass than other units.

IV. GENERALIZED STRUCTURAL MODEL OF THE CRB IN THE CASCADE RANGE

A. Introduction

Although the exposures of CRB are somewhat limited in the general Mt. Hood area, certain consistencies lead the authors to believe that a generalized structural model can be presented that is at least a first order approximation of the actual geologic structure.

The structural model which is proposed consists of 1) several NE trending folds passing through the Cascade Range and merging with folds of the Columbia Plateau (at least one of the anticlines is faulted and thrust in places); 2) a wrench fault zone exposed in the Clackamas River area which is aligned with the Brothers fault zone and the Portland Hills fault zone and along which NW trending en echelon faults and a few NW trending folds occur; and 3) N-NW trending fractures and faults some of which display right lateral movement, the more northerly oriented often being the locus of dike injection; 4) Cascade upwarp and cauldron-type faulting around Mt. Mood.

B. NE Trending Folds and Thrust Faults

The most dominant and consistent structural trend in the CRB is the NE trending folds. Most strike from N40 to 65E which is similar to those along the Columbia River from Hood River to The Dalles. Because the structure began to develop during the time that the CRB was still spreading over the area, it is assumed that fold trends project across the present Cascade Range and merge with those of the plateau. The

mapping of CRB in the Hood River Valley area tends to confirm this premise.

The characteristics of the NE-trending folds are generalized as follows:

1. They are asymmetrical with gentle dips (5-15 degrees) on the SE limbs of the anticlines and steep dips (25-35 degrees) on the NW limbs.

2. The anticlines are occasionally thrust faulted on the NW limb with thrusting from SE to NW.

3. Folding began by High Mg Grande Ronde time. Pillow lavas and interbeds often occur in synclines; abbreviated sections occur in crests of anticlines.

4. Folding continued to build structural relief long after the last CRB flow (Priest Rapids) entered the area. Total structural relief on the folds in the Bull Run Watershed is on the order of 300 m.

5. These folds seem to change trend and/or terminate near the N30W trending Salmon River fault.

6. Near the anticline hingeline, zones of brecciation which parallel flow layers are common.

These folds are similar in trend, age, and physical characteristics to those in CRB on the western margin of the Columbia Plateau (Kienle and others, 1978) which strongly suggests that they belong to the same episode of deformation.

An extrapolation of Columbia Plateau folds southwestward across the Cascade Range, provides the following structural correlations:

1. The Mosier syncline extends up the West Fork Hood

River and becomes the Bull Run syncline.

2. The Ortley anticline extends into the Bull Run anticline which then curves southward to Brightwood where it terminates against the N30W trending Salmon River fault. This anticline is known to be faulted on the NW limb where it crosses the Columbia River. The NW limb is also thrust-faulted in the Bull Run Watershed area.

3. The Dalles syncline has no equivalent fold exposed west of the Cascades, but it should project under Mt. Hood. It is suspected that this is the major syncline through the Cascades in this area, and possibly contains western Oregon CRB flows not found in other exposures of the Cascades, such as the Waverly flows and the Pomona flow.

4. The south limb of this syncline may be the north limb of the anticline that is mapped in the upper Salmon River. No thrust fault has been observed in this anticline, but tectonic breccias occur just northwest of this anticline near the south Fork Salmon River.

Thrust zones parallel to the NE fold structures have not been previously noted. A major thrust on the NW limb of the Bull Run anticline and fragments of thrust zones on the South Fork Salmon River (?) and in the vicinity of Arrah Wanna have been mapped. The characteristics of these thrust faults are as follows:

1. Thick (100-200 m) massive fine to coarse breccia zone above thrust plane.

2. Thin (1-3 m) coarse breccia zone below the thrust plane.

3. Low angle (~12 degrees SE) thrust plane.

4. Magnitude of thrusting is approximately one km with approximately 200 m of throw.

5. Within the breccia zone flow contacts and attitudes are obscured.

6. Dip of the thrust faults changes along strike and may become faults which appear to have mostly vertical movement in the same sense as the thrust movement.

7. Thrust faults are associated with pre-existing zones of weakness in the basalt such as thinned CRB sections or vertical faults.

8. NW trending fractures (N20W) appear to cut thrust zone breccias which have resulted in cemented zones which now stand out as resistant ridges as a result of differential weathering.

9. Breccias of thrust zones are massive and show coherent but little hydrothermal alteration or cementation except for the N20W trending ridges.

Detailed stratigraphy in the Bull Run Watershed area reveals an abbreviated section of CRB adjacent to the thrust fault. It is believed that this thinned section is directly related to the development of the thrust fault in this area (Figure IV-1).

It is concluded that the thrust faults represent fairly shallow, thin-skinned deformation of the brittle, competent basaltic flows in response to N-NW to S-SE compression. These faults may not extend to a great depth below the basaltic layer because the underlying less competent rocks may have

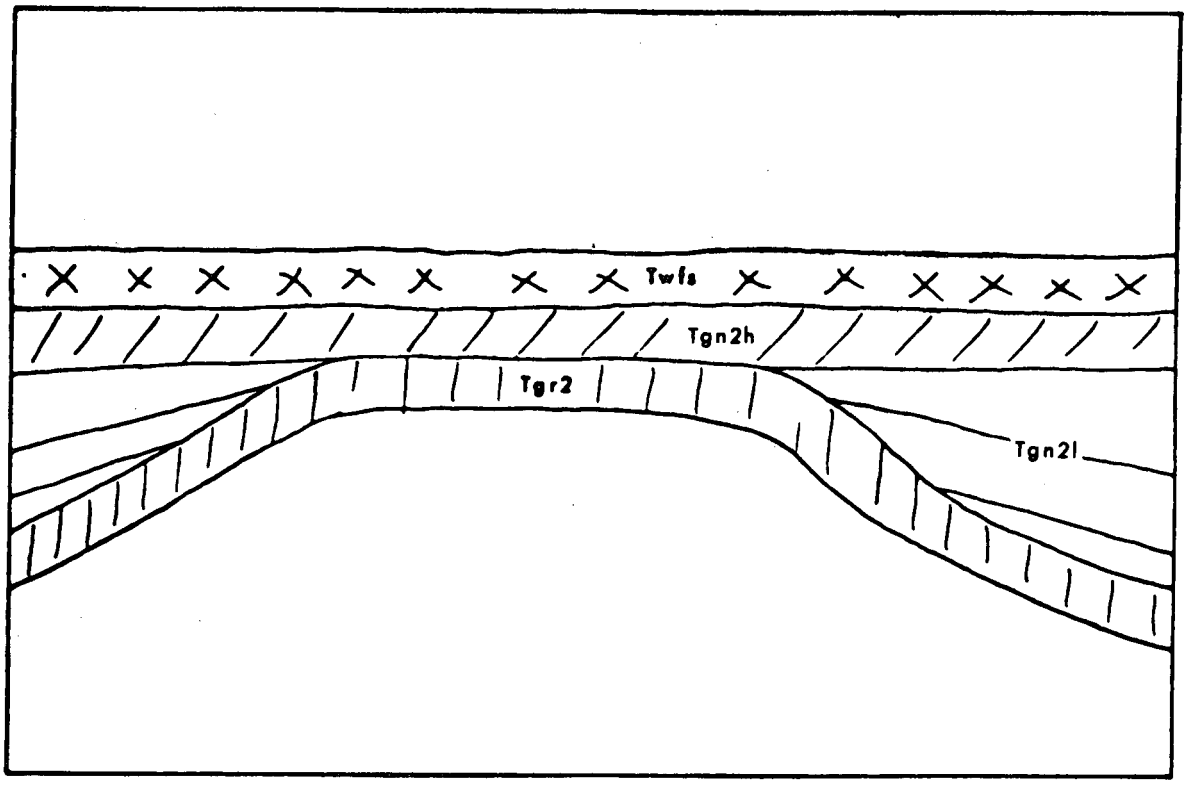

a)

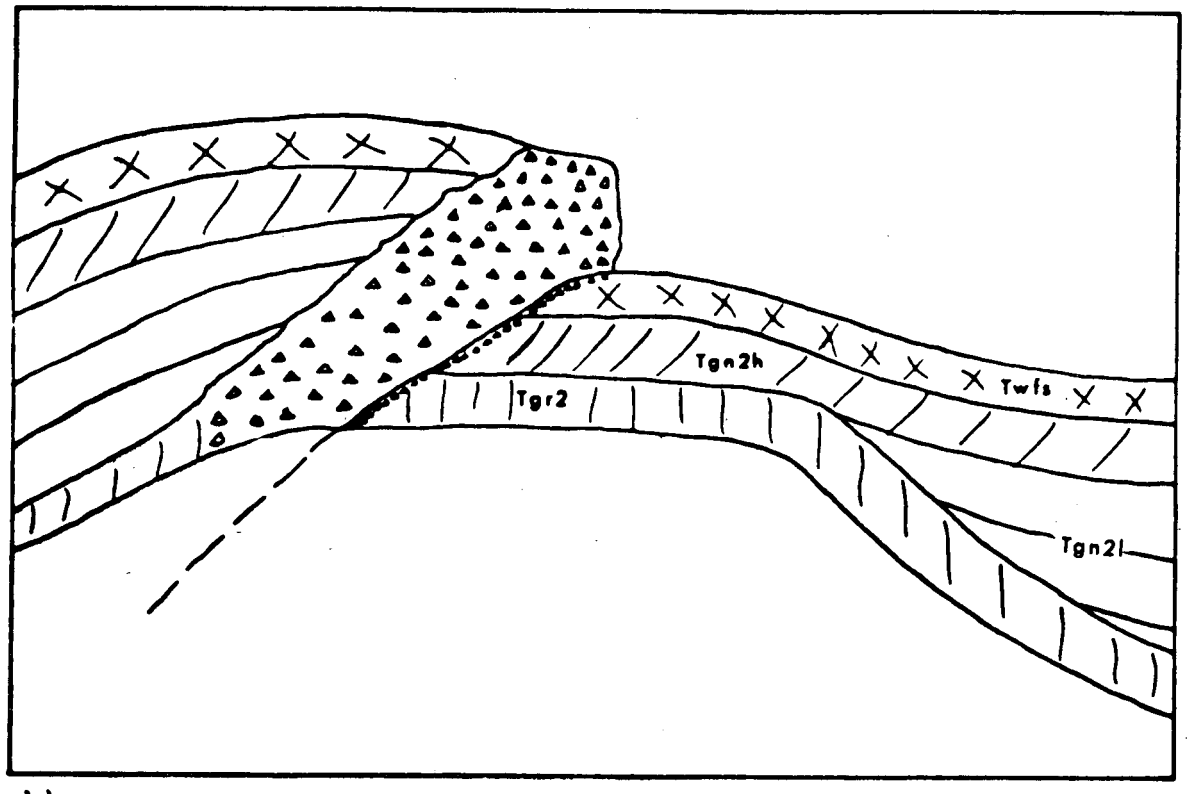

b)

Figure IV-1. Development of Bull Run thrust fault. Sketches show cross-sections (a) pre-thrust and (b) post-thrust

failed more by folding. There is no evidence to indicate that these zones extended through the lithosphere to provide paths for magmas to migrate to the surface.

C. Wrench Fault Zone

The second major feature of this structural model is a wrench fault zone exposed in the Clackamas River area. This wrench zone which is on trend with the Brother's fault zone - Portland Hills fault zone has the following characteristics:

1. En echelon faults, both right lateral and normal, which are oriented about N30W, slightly different than the trend of the wrench zone itself ($\sim$ N45W).

2. A few NW trending folds occur such as the one in Roaring River and the Portland Hills. The trend of these folds is slightly more westerly than that of the wrench itself. Fold of this trend seem to be restricted to the southwest of the N30W trending Salmon River fault. The wrench zone seems to be more convergent (more folds) near Portland and more divergent (more faulting) in the Clackamas River area.

D. NW Trending Faults and Fractures

Another structural feature that appears to occur throughout the entire area is a system of N-NW trending fractures and faults. Some of these faults display slickensides which indicate that right lateral movement has occurred. These fractures and faults may be subdivided roughly into three dominant trends:

1. N10-20W - Have little if any vertical offset; fault zones are narrow ($\sim$ 5 m), brecciated and cemented; cavity

fillings are common; Boring-type (Plio-Pleistocene) basaltic dikes usually occur in fractures having this orientation; fractures with this orientation cut across the flows and breccia zone.

2. N30W - Have wide breccia zone (10-30 m); some cavity fillings; no dikes; occasional considerable vertical offset.

3. N55W - Trends occur most commonly near the thrust zone in the Bull Run Watershed Area; no vertical offset observed; little breccia in a narrow ($\sim$1 m) zone.

These fractures seem to vary considerably in length, but the N30W and the N10-20W are more extensive than the N55W fractures. Individual fractures seem to connect to those of another trend which gives the impression that the lithosphere has rifted along an irregular line bounded by fractures of different orientations (Figure IV-2). Detailed observations along streams show that stream trends are often the result of two trends which intersect one another (Figure IV-3). We interpret these trends to indicate predominantly extension along N10-20W zones and right lateral movement along N30W zones. The N55W zones show little evidence of movement and may be a secondary effect concentrated near existing thrust faults.

E. Cascade Upwarp and Subsidence

The CRB dips gently away from the High Cascades on both the west and east flanks of the Cascades in the vicinity of Mt. Hood. This broad feature is probably related more to the nature of subduction beneath the Cascades than to coupled

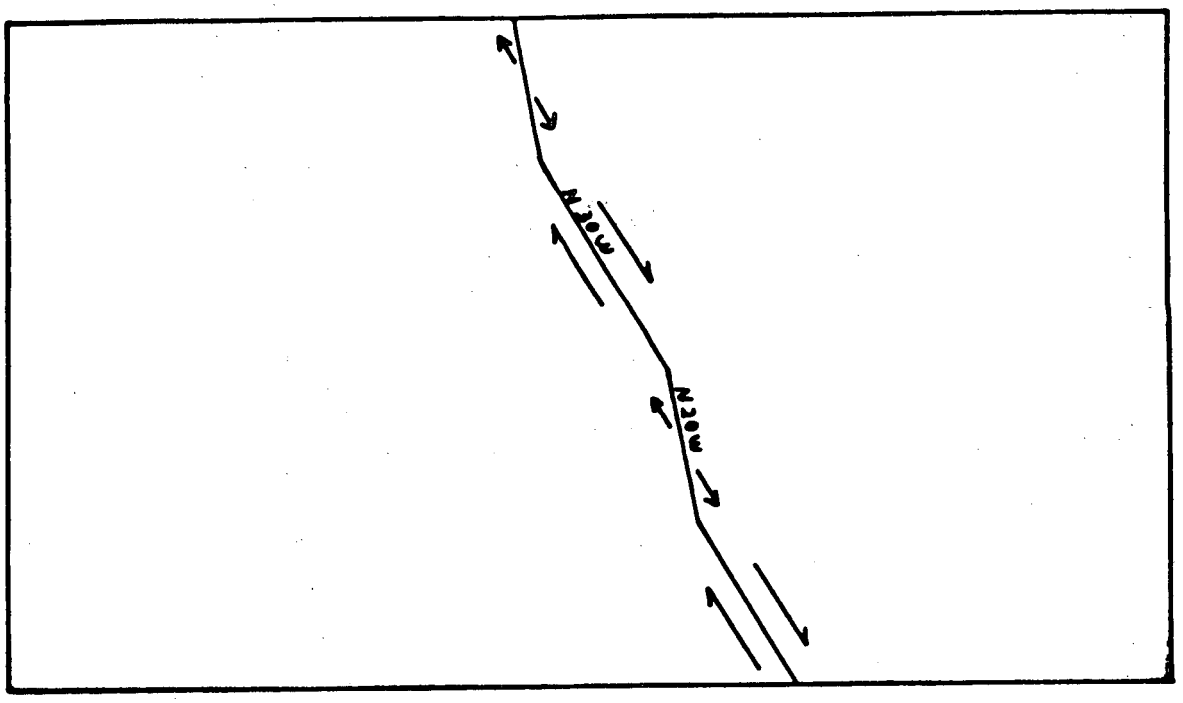

Figure IV-2. Pattern of faulting. N20W trend is zone of extension and dike emplacement.

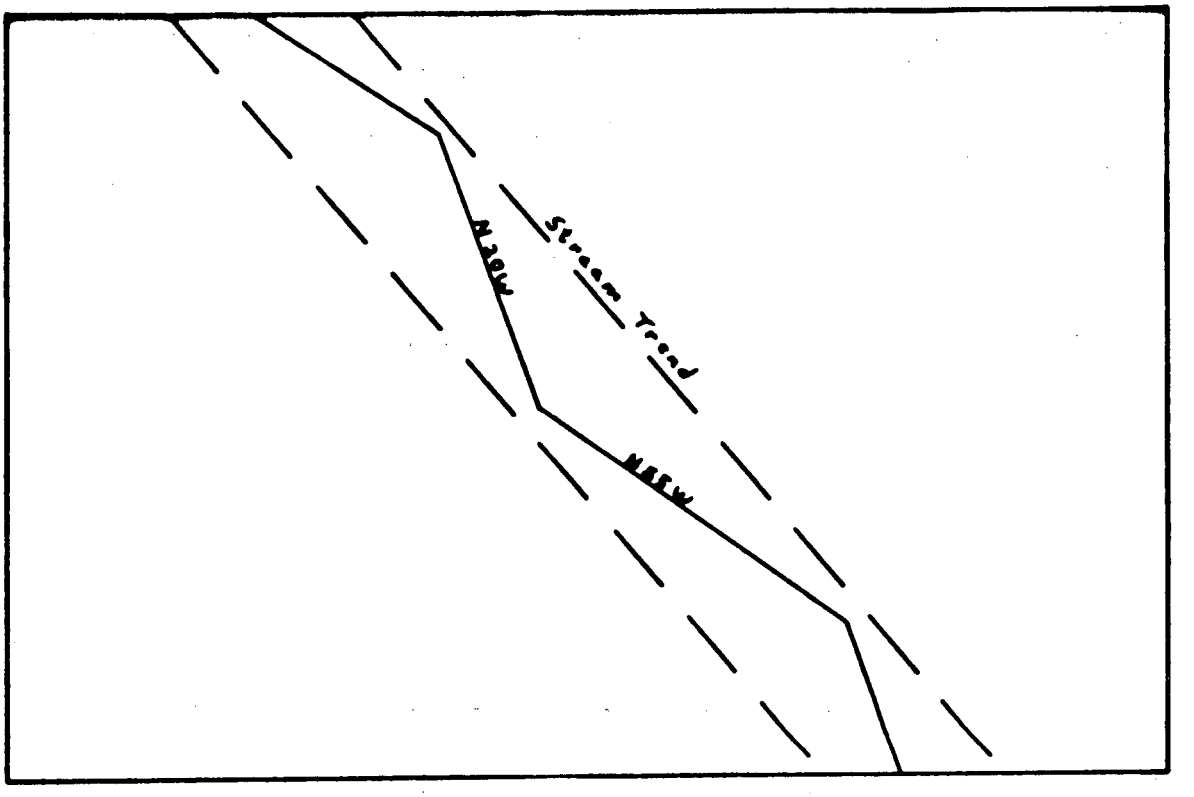

Figure IV-3. Fracture pattern controlling stream trend in upper Blazed Alder Creek.

wrenching of the continental lithospheric plate. We assume that active subduction occurred during most of the Cascade volcanism which resulted in intrusion and extrusion of intermediate composition melts which heated and swelled the crust producing upwarping. Lack of present day seismicity argues against an active subduction zone and subsidence of the crest of the range may indicate recent extension.

North-trending faults within the Hood River fault zone contain slickensides which indicate right lateral movement with a vertical component. We believe that the Cascade Range, due possibly to its higher than normal heat flow, has behaved anomalously to the regional stresses resulting in a right lateral wrenching along this zone. Deeper rocks along the Cascade Range may behave more plastically to wrenching, than the cooler, more brittle rocks near the surface. This wrenching combined with E-W extension may have produced the series of eastward tilted blocks in the Hood River area. It also seems possible that the extension may have caused partial melting at the base of the crust thereby produting magma to supply the High Cascade volcanoes in the absence of an active subduction zone.

The top of the CRB at an elevation of 2028 ft in the Old Maid Flat exploratory hole suggests the possibility that cauldron-type subsidence has occurred. Extension of the Cascade Range and magmatization at depth may both be instrumental in producing the subsidence. The margins of the subsidence are not well known due to extremely sparse data, but the abrupt termination of the CRB south of Middle Mountain and the general

physiography would suggest that subsidence is largely confined between the Hood River fault zone on the east and a NE-trending line from Dee to Zigzag on the west. North of Dee to the Columbia River, tilted blocks towards the Hood River fault zone may reflect the termination of graben-type subsidence. Radiometric ages of andesite near the Hood River fault decrease northward suggesting progression of faulting to the north. The southern margin of subsidence is even more poorly defined, but it does terminate north of the Salmon River.

V. GEOLOGIC HISTORY OF THE MOUNT HOOD AREA

A. Pre-Columbia River Basalt

Geologic evidence as to the nature of the area prior to CRB time (16 my BP) is limited largely to exposures of the Eagle Creek Formation and the in part, time-equivalent, Little Butte Volcanic Series. The Eagle Creek formation is composed mostly of mudflow deposits and conglomerates and ubiquitous basaltic andesite flows derived from volcanoes of the western Cascades, located north of the Columbia River Gorge and south of the Clackamas River. The Little Butte Volcanic Series consists primarily of mudflow deposits and tuffs. The lowland area between the aforementioned highs must have contained one or more westwardly-flowing streams. Perhaps the John Day Formation - correlative in part to the Eagle Creek and Little Butte Formations - may have extended as a wedge into this low area or gap. The lowest section from the Old Maid Flat exploratory hole is similar to rocks of the John Day Formation which crops out near Warm Springs, 50 km to the southeast.

The Portland Hills fault - Clackamas River wrench zone was probably already active and expressed topographically, judging from the distribution of the CRB northwest of Portland (Beeson and others, 1976) and its abrupt termination in the Clackamas River area.

B. Columbia River Basalt

During the middle Miocene (16-14 my BP) approximately 29 different flows of the Columbia River Basalt Group entered the area. The maximum number of flows in any one section is about 20 flows which means that approximately one flow entered

the area every 100,000 years; however, there apparently was variation in time between successive flows. Flows present represent the N_1, R_2, N_2, and R_3 magnetic polarity intervals and longer than normal intervals exist between flows at the Vantage horizon and between the Frenchman Springs and Priest Rapids Members of the Wanapum Basalt. At least one N_1 flow occurs in the Columbia River Gorge and in the Clackamas River indicating that some of the earliest flows to pass through the Cascades covered the entire gap. This same distribution generally characterizes most succeeding units up through the Frenchman Springs flows.

After Frenchman Springs time, either uplift in the Cascade Range, subsidence in the Columbia Plateau, or NE trending folds prevented later flows from covering extensive areas across the Cascades. The Rosa flows apparently did not extend into the area because they are not present in any of the CRB sections; and Priest Rapids flows have only been found locally along the Mosier syncline in the Bull Run Watershed area where they are partly confined as intracanyon flows.

During the time that the CRB flowed through the Cascade Range several geologic events took place which are detailed as follows:

1. Invasion of the Prineville Basalt flows - While the Low Mg Grande Ronde Basalt flows were flowing through the Cascades from the east, eruptions of basalt in the vicinity of the Prineville, Oregon, produced approximately 13 flows (Uppuluri, 1974), three of which flowed northwestward into the Cascade region to interfinger with the Grande Ronde Basalt. Two Prineville flows (stratigraphically at the top

of R_2) extended into the Clackamas River area and northward to Tygh Ridge. Later (near top of Low Mg Grande Ronde N_2), one flowed northward to Tygh Ridge and by an unknown route into the Mt. Hood area.

2. Local andesitic volcanic center near Old Maid Flat - Eruption began during the interval between High Mg and Low Mg Grande Ronde time and probably continued throughout CRB time even though one Frenchman Springs flow finally covered at least part of this andesitic center.

3. NE trending folds - The Waverly flows near Milwaukie seem to be localized flows that were probably channeled by a syncline or stream canyon developed within a structural depression or zone of weakness. Waverly flows have not been discovered as yet in the Cascades. A possible path for these two flows is The Dalles - Mt. Hood syncline. In the Bull Run watershed area the omission of all Low Mg N_2 flows in the Blazed Alder Creek exposures indicate structural development during CRB time.

4. Priest Rapids Intracanyon Flow - Priest Rapids lava flowed through the Mosier syncline and into canyons cut into CRB as deep as Low Mg Grande Ronde. The former stream valley extended from the West Fork Hood River through the Bull Run Watershed to Crown Point. The Priest Rapids flows overfilled the canyons and completely obliterated the former drainage, probably defeating the stream and shifting it to another location.

5. Pomona flow (12 my BP) - After Priest Rapids time,

structural development of the NE trending folds continued and volcanism in the Cascades filled structural valleys to the east with volcanic debris which was partially water deposited. An example of the latter is the Selah Member of the Ellensburg formation (Kent, 1978). The Pomona flow passed through the Cascade Range, probably channeled by structural and erosional valleys, in a yet to be determined location.

C. Post-Columbia River Basalt

Volcanism and plutonism continued in the Cascades area in post-CRB time. Larger volcanic centers were probably concentrated on The Dalles - Mt. Hood syncline. The Still Creek (11.6 my BP) and Laurel Hill (8 my BP) plutons must have been emplaced in The Dalles - Mt. Hood syncline which probably defeated any stream which might have flowed within the structure. Perhaps it was during this time interval that the Columbia River was shifted to its present course. In post-CRB time several geologic events occurred:

1. Continued development of NE trending folds and thrust faulting in places. At least 300 m of structural amplitude exists along north-south cross-sections in the Bull Run Watershed, most of which developed after the last Frenchman Springs flow (approximately 14-15 mp BP). Even more relief may be present on the extension of The Dalles syncline, buried under Mount Hood.

2. Rhododendron volcanism - Most Rhododendron deposits were produced as a result of eruption from andesitic volcanic centers. Much of the products preserved occur as sedimentary

deposits that accumulated in synclinal depressions in the CRB.

3. Development of NW trending faults and fractures - NW trending faults appear to have been active after most of the NE trending events occurred. The N30W trending Salmon River fault cuts off the NE trending folds. Considerable displacement occurs on N30W trending faults at Arrah Wanna and on Middle Mountain. A N15W fracture in Blazed Alder Creek and Tanner Creek is extremely linear across the Bull Run syncline. N10-20W fractures also cut the thrust zone breccias.

4. Uplift of the Cascade Arch - Uparching of the Cascade Range occurred sometime subsequent to the CRB eruptions (14-15 my BP). Insufficient data are available to determine when the major uplift occurred. Perhaps uplift was most active during subduction which resulted in thickening of the crust, emplacement of plutons and heating and possible hydration of the lithosphere. Most plutons and extrusions in the Mt. Hood Area range in age from 11.6 to 4 my BP.

5. Boring Lava volcanism - Boring lava was erupted from centers and widely scattered N-N20W trending dikes which are common from Hood River to Portland (Allen, 1977). Boring volcanism seems to be associated with E-W extension throughout the area.

6. Subsidence along the High Cascades - The Hood River fault probably resulted from right lateral wrenching and subsequent subsidence after the earlier erupted Boring-type lavas (reversed polarity, perhaps 3 my BP). Some of these flows are tilted about 10 degrees to the east towards the

Hood River fault.

7. High Cascade volcanism - This was perhaps the last major event and may have been associated with subsidence around Mt. Hood.

REFERENCES CITES

Allen, J. E., 1975, Volcanoes of the Portland Area, Oregon: Ore Bin, V. 37, No. 9, p. 145-157.

Anderson, J. L., 1978, The structure and stratigraphy of the Columbia River Basalt in the Clackamas River drainage: Portland State University master's thesis, 136 p.

Atlantic Richfield Hanford Company, 1976, Preliminary Feasibility Study of Radioactive Wastes in Columbia River Basalts: ERDA Rept. ARH-ST-137, (text, 168 p.) and v. 2 (appendixes, 264 p.).

Beaulieu, J. D., 1974, Geologic hazards of the Bull Run Watershed, Multnomah and Clackamas Counties, Oregon: Oregon Dept. of Geology and Mineral Industries Bulletin 82, 77 p.

Beeson, M. H., Johnson, A. G., and Moran, M. R., 1976, Portland environmental geology - fault identification: Menlo Park, Calif., Final technical report (Sept. 1, 1974, to Dec. 31, 1975) to the U. S. Geological Survey, 107 p.

Beeson, M. H., Moran, M. R., and Olson, F. L., 1976, Geochemical data on Columbia River Basalt stratigraphy in western Oregon: Geol. Soc. America Abs. with programs, v. 8, no. 3, p. 354.

Bikerman, M., 1970, K-A ages of Laurel Hill pluton and dike, Oregon: Ore Bin, v. 32, no. 11, p. 211-215.

Brock, M. R., and Groiler, M. H., 1973, Chemical analyses of basalt samples from the Columbia Plateau, Washington, Oregon and Idaho: U. S. Geol. Survey open file report.

Dames and Moore, 1972a, Progress report, consultations and inspections, earth slide, North Fork of the Bull Run River: Portland, Oregon, report for the City of Portland, 8 p., unpublished.

_____, 1972b, Progress report no. 2, consultations and inspections, earth slide, North Fork of the Bull Run River: Portland, Oregon, report for the City of Portland, 4 p., unpublished.

_____, 1973, Summary report, consultations and inspections, earth slide, North Fork, Bull Run River: Portland, Oregon, report for the City of Portland, 7 p., unpublished.

Kent, M. H., 1978, Stratigraphy and petrography of the Selah Member of the Ellensburg Formation in south-central Washington and north-central Oregon: Portland State University Master's thesis, 118 p.

Kienle, C. F., Jr., Newcomb, R. C., Deacon, R. J., Faroqui, S. M., Bentley, R. D., Anderson, J. L., and Thoms, R. E., 1978, Western Columbia Plateau's Tectonic Structures and their Age of Deformation: in Tectonics and Seismicity of the Columbia Plateau Workshop, Basalt Waste Isolation Program, Battelle Conference, Seattle, Washington, 17 p.

Kienle, C. F., Jr., 1971, The Yakima Basalt in western Oregon and Washington: University of California, Santa Barbara, doctoral dissertation, 171 p.

Ledgerwood, R. K., 1978, Subsurface stratigraphic correlation, in Basalt Waste Isolation Program annual report - fiscal year 1978: Richland, Wash., Rockwell Hanford Operations, p. 82-87.

Mackin, J. H., 1961, A stratigraphic section in the Yakima Basalt and Ellensburg Formation in south-central Washington: Olympia, Wash., State of Washington Division of Mines and Geology Report of Investigations 19, 45 p.

McKee, E. H., Swanson, D. A., and Wright, T. L., 1977, Duration and volume of Columbia River Basalt volcanism, Washington, Oregon, and Idaho: Geological Society of America Abstract with Programs, v. 9, no. 4, p. 463-464.

Nathan, Simon, and Fruchter, J. R., 1974, Geochemical and paleomagnetic stratigraphy of the Picture Gorge and Yakima Basalts (Columbia River Group) in central Oregon: Geological Society of America Bulletin, v. 85, p. 63-76.

Patterson, P. V., 1973, North Fork Bull Run River landslide - post-construction engineering geology report: Portland, Oregon, Mount Hood National Forest, Materials Engineering Section, 32 p.

Peck, D. L., Griggs, A. B., Schlicker, H. G., Wells, F. G., and Dole, H. M., 1964, Geology of the central and northern part of the western Cascades: U. S. Geological Survey Professional Paper 449, 56 p.

Ruff, L. L., 1957, Bull Run Dam No. 2 - geology and foundations: Report for the City of Portland Bureau of Water Works, 11 p., unpublished.

Schlicker, H. G., 1961, Geological Reconnaissance of Bull Run damsite No. 2: Portland, Oregon, report to the City of Portland Bureau of Water Works, unpublished.

Schmincke, H. U., 1967, Stratigraphy and petrography of four upper Yakima Basalt flows in south-central Washington: Geological Society of America Bulletin, v. 78, p. 1385-1422.

Shannon and Wilson, Inc., 1958a, Test embankment Bull Run Dam No. 2: Portland, Oregon, report to the City of Portland, 8 p., unpublished.

_____, 1958b, Report of soil tests for the design of proposed Bull Run Dam No. 2: Portland, Oregon, report to Stevens and Thompson, Inc., 10 p., unpublished.

_____, 1961, Report on geology and engineering feasibility of increased storage at Bull Run Lake, Oregon: Portland, Oregon, report for the City of Portland, 22 p., unpublished.

_____, 1963, Design and performance memorandum, Bull Run Dam No. 2, Oregon: Portland, Oregon, unpublished.

_____, 1965, Preliminary site explorations and studies, Ditch Camp slide, Bull Run, Oregon: Portland, Oregon, report to Stevens and Thompson, Inc., 29 p., unpublished.

_____, 1973, Geologic reconnaissance and preliminary engineering studies for a water tunnel - Bull Run Dam No. 2 to Dodge Park area: Portland, Oregon, report to the City of Portland, 15 p., unpublished.

Snavely, P. D., Macleod, N. S., Wagner, H. C., 1973, Miocene tholeiitic basalts of coastal Oregon and Washington and their relations to coeval basalts of the Columbia Plateau: Geological Society of America Bulletin, v. 84, no. 2, p.387-424.

Stevens, F. R., 1964, Soil Survey, Bull Run-Sandy area, Oregon: Portland, Oregon, Mount Hood National Forest Administrative Report, 477 p., unpublished.

Stevens and Thompson, Inc., 1957, Bull Run Storage Dam No. 2 and hydroelectric power facilities, Bull Run River: Portland, Oregon, report for the City of Portland, 61 p., unpublished.

_____, 1965, Report on water supply conduits through Ditch Camp slide area: Portland, Oregon, report for the City of Portland, 9 p., unpublished.

Swanson, D. A., 1978, Highlights of the regional Columbia River Basalt mapping program, in Basalt Waste Isolation Program: Richland, Wash., Rockwell Hanford Operations RHO-BWI-78-100, p. 47.

Swanson, D. A., Wright, T. L., and Helz, R. T., 1975, Linear vent systems and estimated rates of magma production and eruption for the Yakima Basalt on the Columbia Plateau: American Journal of Science, v. 275, p. 877-905.

Swanson, D. A., Wright, T. L., Hooper, P. R., and Bentley, R. D., in press, Revisions in stratigraphic nomenclature of the Columbia River Basalt Group: U. S. Geological Survey Bulletin.

Taubeneck, W. H., 1970, Dikes of Columbia River Basalt in northeastern Oregon, western Idaho, and southeastern Washington, in Gilmour, E. H., and Stradling, eds., Proceedings of the Second Columbia River Basalt Symposium: Cheney, Wash., Eastern Oregon State College Press, p. 73-96.

Uppuluri, V. R., 1973, A stratigraphic and compositional study of basalts of the Columbia River Group near Prineville, central Oregon: M. S. thesis, University of Oregon, Eugene, 87 p.

_____, 1974, Prineville chemical type: A new basalt type in the Columbia River Group: Geological Society of America Bulletin, v. 85, p. 1315-1318.

Waters, A. C., 1961, Stratigraphic and lithologic variations in the Columbia River Basalt: American Journal of Science, v. 259, p. 583-611.

_____, 1962, Basalt magma types and their tectonic association: Pacific Northwest of the United States: American Geophysical Union Geophysical Monograph 6, p. 158-170.

Watkins, N. D., and Baksi, A. K., 1974, Magnetostratigraphy and oroclinal folding of the Columbia River, Steens, and Owyhee basalts in Oregon, Washington, and Idaho: American Journal of Science, v. 274, p. 148-189.

Wise, W. S., 1969, Geology and petrology of the Mount Hood area - a study of High Cascade volcanism: Geological Society of America Bulletin, v. 80, no. 6, p. 969-1006.

Wright, T. L., Groiler, M. J., and Swanson, D. A., 1973, Chemical variation related to the stratigraphy of the Columbia River Basalt: Geological Society of America Bulletin, v. 84, p. 371-386.

GEOLOGY AND GEOCHEMISTRY OF MT. HOOD VOLCANO

By

CRAIG M. WHITE

Department of Geology

University of Oregon

May 1979

Final report of work carried out under OU Grant No. 50-262-8902 from the Oregon Department of Geology and Mineral Industries; July, 1977 through March, 1979.

TABLE OF CONTENTS

	Page
ABSTRACT	82
INTRODUCTION	84
Scope	86
Analytical Procedures	86
POST-GLACIAL DACITES	88
Petrography	89
Geochemistry	93
Conditions of Equilibration	100
Pyroxene Geothermometer	100
Iron-Titanium Oxide Geothermometer	102
Plagioclase Geothermometer	103
Geobarometry	105
MAIN STAGE LAVAS	107
Petrography	107
Geochemistry	108
Major Elements	108
Trace Elements	114
SUMMARY AND GEOTHERMAL IMPLICATIONS	120
APPENDIX I	123-131
APPENDIX II	132
Radiometric Dating	132
REFERENCES	136

LIST OF FIGURES

		Page
1	SCHEMATIC COLUMN OF THE MT. HOOD SECTION.....	85
2	GEOLOGIC SKETCH MAP OF THE SUMMIT AREA OF MT. HOOD.....	90
3	PLOT OF CONCENTRATIONS OF K_2O, Zr, Th AND La.....	96
4	PLOT OF THE CONCENTRATION OF SiO_2 VERSUS K_2O.....	98
5	PLOT OF THORIUM CONCENTRATION VERSUS SiO_2.....	99
6	ILMENITE-HEMATITE AND MAGNETITE-ULVOSPINEL SOLID SOLUTION AS A FUNCTION OF T AND fO_2.....	104
7	WEIGHT PERCENT SiO_2 IN MAIN-STAGE MT. HOOD LAVAS..	113
8	EXCLUDED TRACE ELEMENTS VERSUS FLOW NUMBER.....	115
9	INCLUDED TRACE ELEMENTS VERSUS FLOW NUMBER.....	116
10	MAJOR ELEMENTS VERSUS FLOW NUMBER.....	117
11	PLOT OF EXCLUDED ELEMENTS VERSUS SiO_2 MAIN-STAGE LAVAS.....	119
12	GRAPH OF THEORETICAL COOLING TIME VERSUS VOLUME FOR MAGMA BODIES.....	122

LIST OF TABLES

		Page
1	MINERAL COMPOSITIONS USED IN EQUILIBRIA CALCULATIONS.....	92
2	MAJOR AND TRACE ELEMENT COMPOSITIONS.....	94-95
3	LEAST SQUARES MIXING MODEL FOR LAVA COMPOSITIONS.....	101
4	MAJOR AND TRACE ELEMENT ANALYSES OF MAIN-STAGE LAVAS.....	109-112
5	RADIOMETRIC DATES.....	133
6	MAJOR ELEMENT COMPOSITION.....	135

ABSTRACT

The lavas that comprise Mt. Hood volcano can be divided on the basis of their age and modal composition into three suites: (1) the sequence of pyroxene and hornblende andesites that was erupted prior to the last glaciation and which comprise about 90 percent of the volcano; (2) the post-glacial hornblende dacites that were erupted primarily as hot avalanche flows from domes near the summit; and (3) the flows of olivine andesite that were erupted from several satellite vents on the flanks of Mt. Hood. This report presents new compositional data for the Main-Stage lavas and the post-glacial dacites.

Samples of Main-Stage lavas were obtained from five subaerial flow sequences and from the Timberline exploratory hole. Major and trace element analyses indicate that the sequentially erupted lavas in any one section are not related as member of a simple fractional crystallization series. The occurrence of siliceous lavas near the base of some sections indicates that Main-Stage magma reservoirs may have been compositionally zoned. When the trace element abundances in all Main-Stage lavas are compared, at least two discrete magma batches can be identified.

Eruption of the post-glacial dacties took place during three eipsodes at approximately 10,000 yrs, 2,000 yrs, and 200 yrs BP. Each eruptive episode produced a geochemically

distinct series of lavas. Within each age group, sequentially erupted lavas appear to be related by small degree of fractionation of the observed phenocryst phases. It is suggested that the contrasting processes of differentiation indicated for the post-glacial versus the Main-Stage magmas (fractional crystallization vs magma zonation) may be related to the considerable differences in volumes and cooling rates inferred for their respective reservoirs.

Estimates of the conditions of equilibration of the post-glacial dacites were made by comparing the phenocryst compositions in a dacite sample with experimental equilibria data. The calculations yielded the following results: temperature = 910 to 920°C; logarithm of oxygen fugacity = -10.5; minimum load pressure = 3.5 to 7 kb (approximately equal to 10 to 20 kilometers depth).

Because of the inferred small volumes and deep residence levels of the post-glacial magma reservoirs, it is unlikely that they would generate a significant geothermal anomaly within or immediately beneath Mt. Hood. Nonetheless, because of the very young age of the most recent eruptions (100 - 200 yrs BP), a local heat source could be provided by magma that is still residing at shallow depths within the volcanic conduit. In addition, deep-seated magma chambers associated with the Main-Stage volcanism could, if of sufficient volume, continue to affect the regional geothermal gradient in the vicinity of Mt. Hood.

INTRODUCTION

Mt. Hood is the northernmost of the large composite volcanoes that form the crest of the Cascade Range in Oregon. The volcano is predominantly andesitic in composition and consists of about 180 cubic kilometers of flows and pyroclastic debris. Although there are no well-documented accounts of historic eruptions at Mt. Hood, the continuous near-summit fumarolic activity indicates that the volcano is still active.

In his major study of the Mt. Hood area, Wise (1969) divided the volcano into three lava groups; a voluminous series of andesitic lavas that was erupted prior to the last glaciation, a post-glacial group of dacitic plug domes and pyroclastic flows, and several post-glacial satellite cones of olivine andesite. Crandall and Rubin (1977) subdivided the dacitic rocks by delineating three age units within the pyroclastic facies. The lowermost block and ash flows are interbedded with glacial till and outwash, and on this basis, their age is estimated to be about 10,000 to 12,000 years BP. These flows are overlain by two younger pyroclastic sequences that contain charcoal which have yielded radiocarbon dates of 1,700 years and 200 years BP.

The schematic column of the Mt. Hood section (Figure 1) summarizes the stratigraphic divisions made by Wise (1969) and Crandall and Rubin (1977). For this report, the pre-glacial

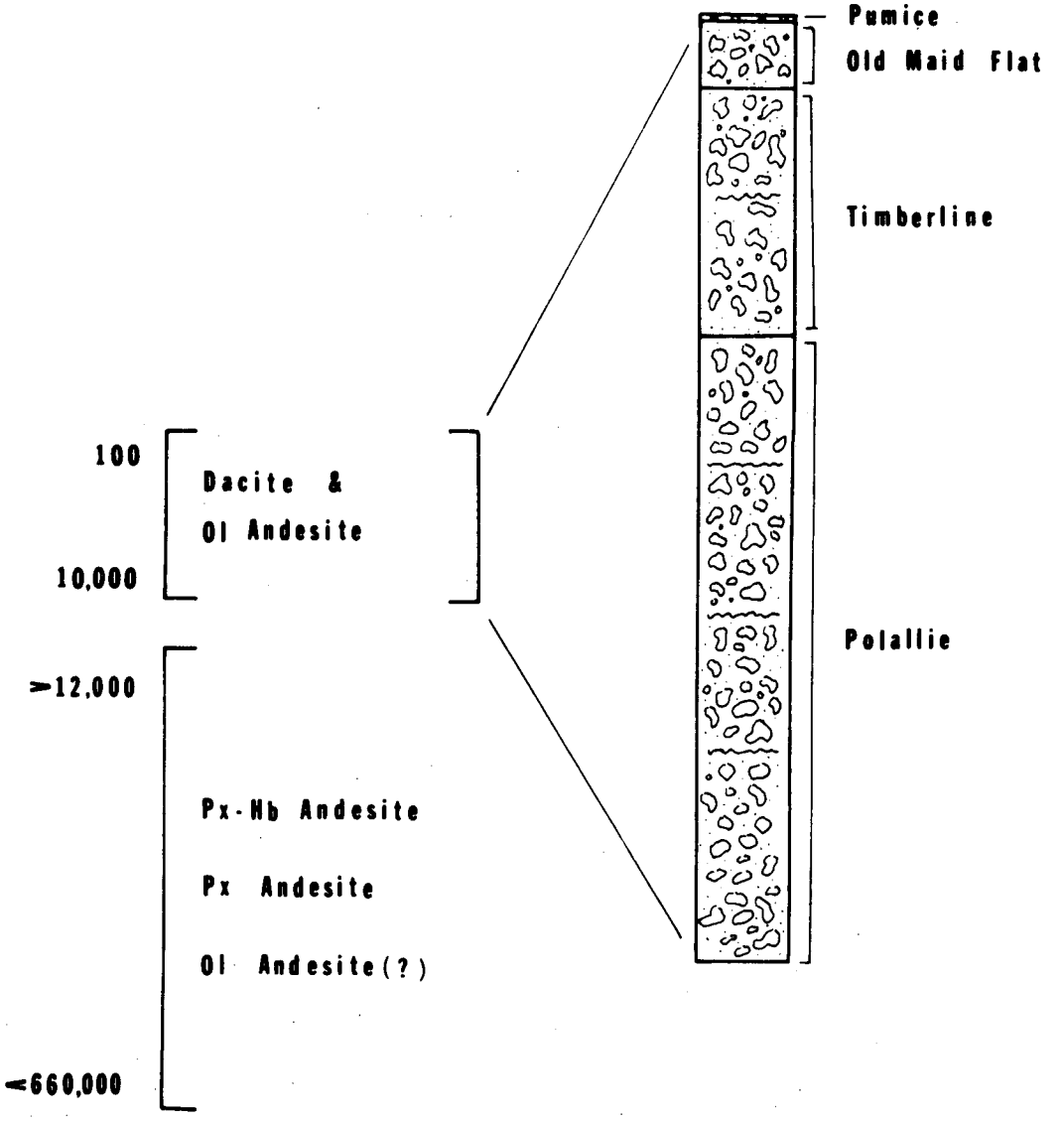

Figure 1. Schematic column of the Mt. Hood Section. The thickness of the post-glacial pyroclastic section is roughly proportional to the volumes of each age group.

Mt. Hood sequence will be called the Main-Stage lavas and the post-glacial silicic rocks will generally be referred to as dacites, although some andesitic rocks do occur in the sequence The names, Polallie, Timberline, and Old Maid Flat have been applied by Crandall (pers. comm.) to the 10,000-12,000 yr, 1,700 yr, and 200 yr-old block and ash flows, respectively, and these names will be used in place of the absolute age designations.

Scope

The present day study was initiated in order to apply recently developed techniques in petrology and geochemistry to the problem of the late-stage magmatic evolution of the Mt. Hood lavas. Because knowledge of the order of eruption of lavas is critical in evaluating competing petrological models, new analyses of rock samples have been made only where the relative ages of flows in a section have been determined by field observation, drilling, or radiometric dating. The goal of the study is to aid in the assessment of Mt. Hood as a potential geothermal resource area and, for this reason, emphasis has been placed on the evolution of the young, silicic rocks at Mt. Hood, even though they are volumetrically less important than the Main-Stage lavas.

Analytical Procedures

Concentrations of eight major elements in all the Mt. Hood samples were determined by X-ray flourescence spectrometry of fused glass discs. Sample splits were analyzed for

Na and Mg by use of a Varian model 175 atomic absorption unit. Zr, Sr, Rb, and Ni concentrations were determined by X-ray flourescence analysis of pressed powders; all other trace element analyses were made by use of instrumental neutron activation. Complete trace element analyses were made by counting irradiated samples for two and six hours on a 4096 channel germanium crystal detector. Less precise analyses were obtained for most of the dacitic rocks by counting samples for two hours on a 2048 channel detector; a procedure that is more rapid and less costly than that used for the complete analyses but which yielded reliable values for Th and La. Mineral analyses were made with an electron microprobe.

POST-GLACIAL DACITES

Post-glacial dacitic lavas at Mt. Hood occur primarily as voluminous pyroclastic debris flows which fill radial drainages and mantle the lower slopes of the volcano. The abundance of prismatically jointed blocks throughout the pyroclastic section and the uniform magnetic orientation of blocks in some flows indicate that most of the debris was deposited at elevated temperature; in some cases at temperatures above the Curie point. The flows probably originated from explosive eruptions at the sides or base of an episodically active dome, the remnants of which cap most of the near-summit ridges.

The Polallie block and ash flows are the oldest and most voluminous of the post-glacial pyroclastic deposits. They occur primarily on the east and northeast sides of the volcano where they are well exposed in sections up to 150 meters thick in the canyons of Polallie and Cold Spring Creeks. Flows of Polallie age have not been identified on the south, west, or northwest slopes of Mt. Hood. A crumble-breccia that occurs at the 9500-foot level on Cooper Spur may represent a portion of the Polallie dome that was undermined by the repeated block and ash eruptions.

In contrast to the Polallie eruptions, the explosive activity that produced the Timberline and Old Maid Flat flows was strongly directed to the south and west. The 1,700-year-old Timberline pyroclastic flows mantle the south slope of Mt. Hood in the vicinity of Timberline Lodge and form thick

sections in the upper reaches of the Zigzag and Sandy Rivers. The 200-year-old flows of the Old Maid Flat group overlie flows of Timberline age in exposures along the Sandy River where a twenty-centimeter-thick ash layer marks the contact. It is likely that rocks of Old Maid Flat age also form the noticeably steeper portion of the south slope between the 8000-foot level and the base of Crater Rock. The large blocks in this area are similar in their mineralological and chemical composition to blocks from other Old Maid Flat sections and they probably were formed by the collapse of a young dome that occupied the Devils Kitchen amphitheater, just south of the present summit (Figure 2).

The hornblende dacite plug dome that forms Crater Rock is the site of the most intense fumarolic activity in the summit region. Its extrusion probably followed the explosive activity that produced the Old Maid Flat flows and caused the collapse of the Devils Kitchen dome. Additional evidence of very young activity was found by Crandall (pers. comm., 1979), who recognized small pumice fragments on the surface of the Old Maid Flat flows in the upper portions of the White River valley. The pumice is unlike that erupted from neighboring volcanoes and was almost certainly produced by a minor eruption of Mt. Hood, possibly during the reported activity in the middle 1800s.

Petrography

All of the post-glacial dacitic rocks at Mt. Hood contain abundant phenocrysts of plagioclase and ferromagnesian minerals

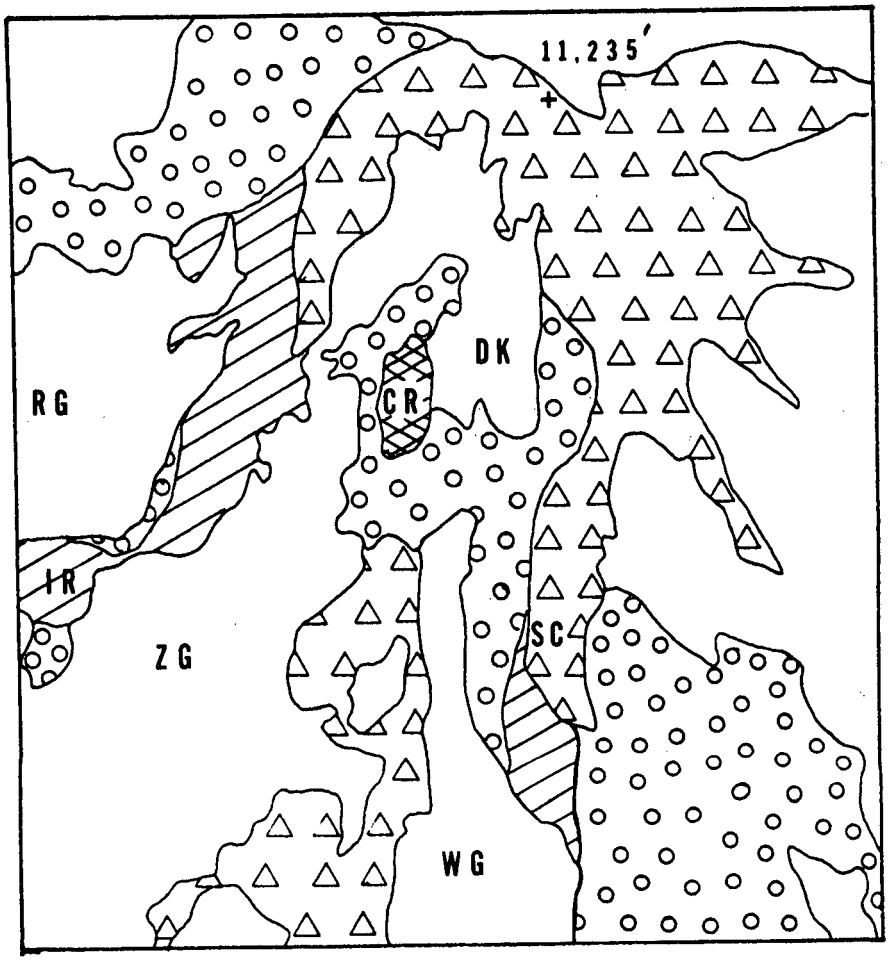

Snow and Ice

Moraine

Plug dome
Hornblende dacite

Flows or crumble breccia
Hornblende dacite

Main-Stage lava flows
Hornblende or pyroxene andesite

CR Crater Rock
DK Devils Kitchen
WG White River Glacier
ZG Zig Zag Glacier
RG Reid Glacier
IR Illumination Rock

scale:
2000 ft.

Figure 2. Geologic sketch map of the summit area of Mt. Hood

in a groundmass of fine-grained crystals, crypto-crystalline material and, rarely, light brown glass. Phenocrysts and microphenocrysts of plagioclase and orthopyroxene ± amphibole ± clinopyroxene form between 30 and 35 percent of the mode in nearly all observed samples.

Although most phenocryst grains are optically zoned, the range of mineral compositions as revealed by the electron microprobe (Table 1) is relatively narrow. Most phenocrysts are fresh and display subhedral or euhedral crystal outlines; however, amphibole grains are commonly rimmed by fine-grained aggregates of opaque minerals and, in some rocks, may be totally replaced by this material. Clinopyroxene is generally the smallest and least abundant of the phenocryst minerals and its occurrence in a given specimen appears to be inversely related to the abundance of hornblende.

It would be impossible to assign a specimen to one of the three age groups on the basis of petrography alone; nonetheless, general petrographic characteristics can be recognized in each of the pyroclastic units. Blocks from the Polallie flows commonly contain much less modal amphibole and greater amounts of modal clinopyroxene than blocks from the two younger units. In addition, amphibole phenocrysts are generally quite fresh in the Old Maid Flat blocks but appear to be progressively more resorbed in the older units. These characteristics may reflect the small but progressive increase in the silica contents of the post-glacial dacitic rocks with time.

TABLE 1

Mineral Compositions Used in Equilibria Calculations

Pyroxenes	core opx A	core cpx A	rim opx A	rim cpx A	gr mass opx B	gr mass cpx B
SiO2	52.62	52.10	52.54	52.45	52.82	51.83
TiO2	.05	.34	.05	.39	.17	.51
Al2O3	.67	1.73	.84	1.45	.96	2.04
FeO	22.66	9.12	21.25	9.15	22.63	8.91
MgO	22.90	14.57	22.64	14.77	22.30	14.33
MnO	.69	.28	.68	.28	.65	.25
CaO	1.11	21.70	1.25	21.70	1.19	21.39
total	100.70	99.85	99.25	100.18	100.71	99.26
EN	65	14	67	14	65	14
FS	35	42	33	42	35	42
WO	--	44	--	44	--	44

Plagioclases	core plag A	rim plag A	core plag B	rim plag B	gr mass plag C	gr mass plag D
SiO2	56.45	54.53	56.39	54.45	54.19	54.34
Al2O3	27.07	28.14	26.96	28.13	28.54	28.13
FeO	.32	.41	.26	.45	.38	.53
MgO	.10	.11	.08	.12	.11	.09
CaO	9.52	10.55	9.55	10.67	11.16	10.89
Na2O	5.79	5.31	5.92	5.22	5.18	5.20
K2O	.19	.18	.23	.20	.16	.20
total	99.44	99.23	99.41	99.29	99.75	99.35
AN	48	52	47	53	54	54

Oxides	ilm A	ilm B	ilm C	mt A	mt B
SiO2	.02	.31	.31	.80	.69
TiO2	39.90	35.95	39.04	4.54	8.21
Al2O3	.29	.50	.45	2.78	2.22
FeO	56.50	60.06	56.04	84.44	82.13
MgO	2.80	2.32	2.88	1.88	2.06
MnO	.10	.06	.08	.14	.14
Cr2O3	.06	.08	.07	.26	.26
V2O3	.71	.87	.68	.39	.39
total	100.39	100.19	99.55	95.30	96.17
HM	27	34	28	--	--
IL	73	66	72	--	--
MT	--	--	--	85	75
ULV	--	--	--	15	25

All analyses were made with an electron microprobe using a 3 micron beam width. All phases are from sample CR-55A; a prismatically jointed block from near the middle of the Polallie Canyon section.

Geochemistry

The major and trace element compositions of 27 post-glacial silicic lavas from Mt. Hood are given in Table 2. Although some overlap in major elements does occur among the three age groups, a general trend can be seen in which rocks from the younger units are slightly richer in SiO_2 and poorer in MgO, CaO, and Fe_2O_3.

In contrast to the major elements, the concentrations of K_2O, Zr, Th, and La bear a more complex relationship to the age of the sampled unit. This behavior is illustrated in Figure 3, in which the abundances of the four excluded elements are plotted versus a schematic scale of decreasing age. Because the Polallie canyon exposure offered the opportunity to sample a thick continuous section, the samples of Polallie age have been plotted in five positions, according to their stratigraphic height. In contrast, the stratigraphic position of the Timberline and Old Maid Flat samples within their respective units cannot be determined in the field, and for this reason, analyses of these rocks are plotted as if they were exactly time-equivalent. Analyses of the Crater Rock plug dome and the post-Old Maid Flat-age pumice are plotted as the youngest samples.

Examination of the lower portion of Figure 3 reveals a general trend of increasing K_2O, Zr, Th and La upward through the Polallie Canyon section. In a similar way, the Old Maid Flat--Crater Rock--pumice samples show an increase in excluded element concentrations with time. This trend is reversed at

TABLE 2

	Blocks in Polallie Pyroclastic Flows							Blocks in Old Maid Flat Pyroclastic Flows					Basal Old Maid Flat Ash
	HD-83	HD-84	CR-55A	HD-85	HD-4	HD-5	HD-6	HD-2	HD-28	HD-29	HD-30	HD-31	HD-48
SiO_2	61.99	61.93	61.26	62.73	62.56	62.82	62.90	63.77	63.26	63.34	63.22	63.49	60.70
TiO_2	.74	.78	.74	.77	.75	.76	.76	.72	.71	.72	.72	.71	.86
Al_2O_3	17.52	17.65	19.17	17.42	17.05	17.13	17.04	16.84	17.27	17.11	17.06	16.95	17.35
M_9O	2.71	2.41	2.28	1.68	2.41	2.30	2.26	2.24	2.21	2.26	2.36	2.28	3.01
Fe_2O_3	5.90	5.68	5.42	5.74	5.50	5.82	5.44	5.26	5.17	5.29	5.26	5.18	6.28
MnO	.09	.09	.07	.09	.07	.07	.07	.07	.07	.07	.08	.07	.09
CaO	5.53	5.67	5.36	5.60	5.46	5.42	5.40	5.16	5.30	5.29	5.25	5.18	5.98
Na_2O	3.97	4.26	3.86	4.21	4.41	4.17	4.36	4.37	4.48	4.35	4.48	4.56	4.21
K_2O	1.39	1.39	1.65	1.55	1.59	1.63	1.59	1.43	1.39	1.42	1.41	1.44	1.34
P_2O_5	.17	.16	.18	.20	.19	.19	.18	.15	.14	.15	.15	.14	.18
Rb	22	21	26	26	27	25	27	22	17	20	20	20	19
Sr	672	626	609	621	600	596	598	552	558	551	555	546	633
Zr	143	144	169	156	179	176	175	137	140	146	145	145	155
Th	3.5	3.3	4.1	4.5	4.3	5.3	n.d.	2.9	2.6	n.d.	2.7	n.d.	n.d.
La	18.3	18.3	20.2	22.2	22.2	22.2	n.d.	15.9	15.6	n.d.	14.0	n.d.	n.d.

CONTINUATION OF TABLE 2

	Blocks in Timberline Pyroclastic Flows					Near-Summit Dacite Flows				Crater Rock	Pumice
	HD-17	HD-18	HD-19	HD-26	HD-27	HD-23	HD-25	HD-8	HD-60	HD-9	HD-10
SiO_2	63.19	63.26	62.91	63.58	63.56	62.40	62.26	62.76	62.93	64.11	62.88
TiO_2	.71	.72	.71	.70	.70	.77	.78	.77	.80	.69	.73
Al_2O_3	17.00	16.99	17.06	16.92	16.89	17.25	17.16	17.11	17.67	16.94	17.71
M_9O	2.40	2.34	2.43	2.29	2.35	2.40	2.45	2.42	2.24	2.11	2.18
Fe_2O_3	5.36	5.34	5.38	5.16	5.13	5.72	5.68	5.59	5.44	5.12	5.36
MnO	.07	.08	.07	.07	.07	.08	.08	.08	.08	.08	.08
CaO	5.45	5.36	5.36	5.22	5.25	5.44	5.41	5.46	5.59	5.10	5.30
Na_2O	4.17	4.24	4.44	4.39	4.42	4.40	4.68	4.19	3.53	4.21	4.08
K_2O	1.49	1.52	1.50	1.53	1.49	1.38	1.32	1.43	1.54	1.49	1.50
P_2O_5	.15	.15	.14	.13	.15	.17	.18	.17	.18	.15	.19
Rb	20	21	21	22	23	18	18	21	24	23	21
Sr	572	579	562	537	557	550	545	555	561	534	545
Zr	146	159	152	152	154	163	151	160	149	148	174
Th	2.9	n.d.	n.d.	3.0	3.5	2.9	n.d.	n.d.	n.d.	3.3	3.8
La	16.8	n.d.	n.d.	15.6	18.2	16.7	n.d.	n.d.	n.d.	15.8	17.7

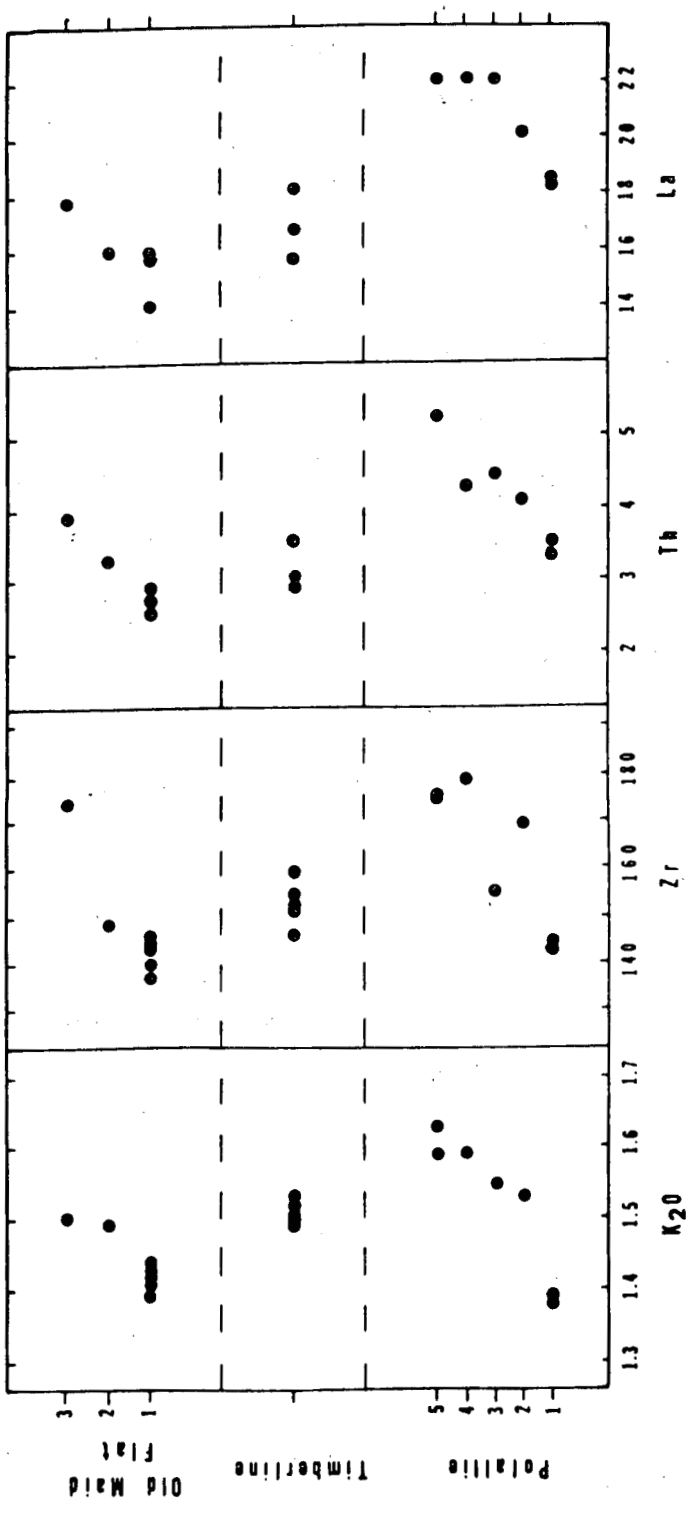

Figure 3. A plot of the concentrations of K_2O (wt. %), zirconium (ppm), thorium (ppm), and Lanthanum (ppm) versus a schematic scale of stratigraphic height. Samples are from prismatically jointed blocks in post-glacial pyroclastic flows.

the major time breaks where the initial products of each eruptive episode are depleted in these elements relative to last-erupted lavas of the preceding episode.

The trends within the Polallie section and the Old Maid Flat-Crater Rock-Pumice lava group are consistent with small degrees of fractional crystallization; however, the occurrence of a geochemical reversal at each of the major time breaks indicates that the Polallie, Timberline and Old Maid Flat lavas are probably not related to one another through a simple Bowen-type fractionation process. Because the younger rocks are neither less siliceous nor more phenocryst rich than the older ones, it is also unlikely that the three eruptive groups are related through progressively deeper tapping of a simply-zoned magma chamber. Although a single, complexly-zoned magma chamber cannot be ruled out as a source of all of the post-glacial dacitic lavas, it is more likely that each of the three major eruptive episodes tapped discrete magma batches. The distinct geochemical character of the lavas of each eruptive episode is emphasized by plotting the excluded elements versus silica. Plots of potash and thorium values are shown in Figures 4 and 5.

In order to further investigate the relationship among the post-glacial dacitic rocks, several least-squares mixing calculations were made in which the major-element compositions of rocks in the Polallie eruptive group were used as end members. These calculations test the possibility that one rock composition could be generated from another by subtraction of the observed phenocryst phases. It can be seen from the results

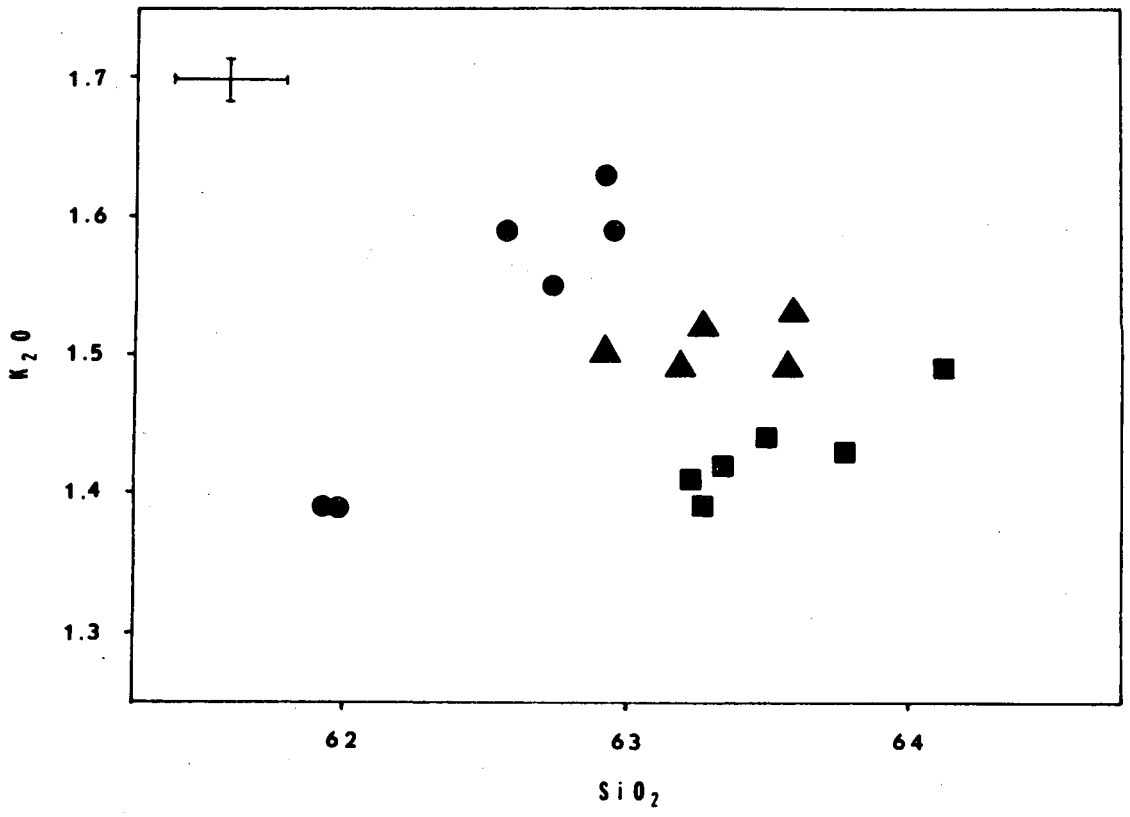

Figure 4. A plot of the concentration of SiO_2 versus K_2O. Circles are analyses of Polallie blocks, triangles are analyses of Timberline blocks, squares are analyses of Old Maid Flat blocks. 1 sigma error bars are given in the upper left of the figure.

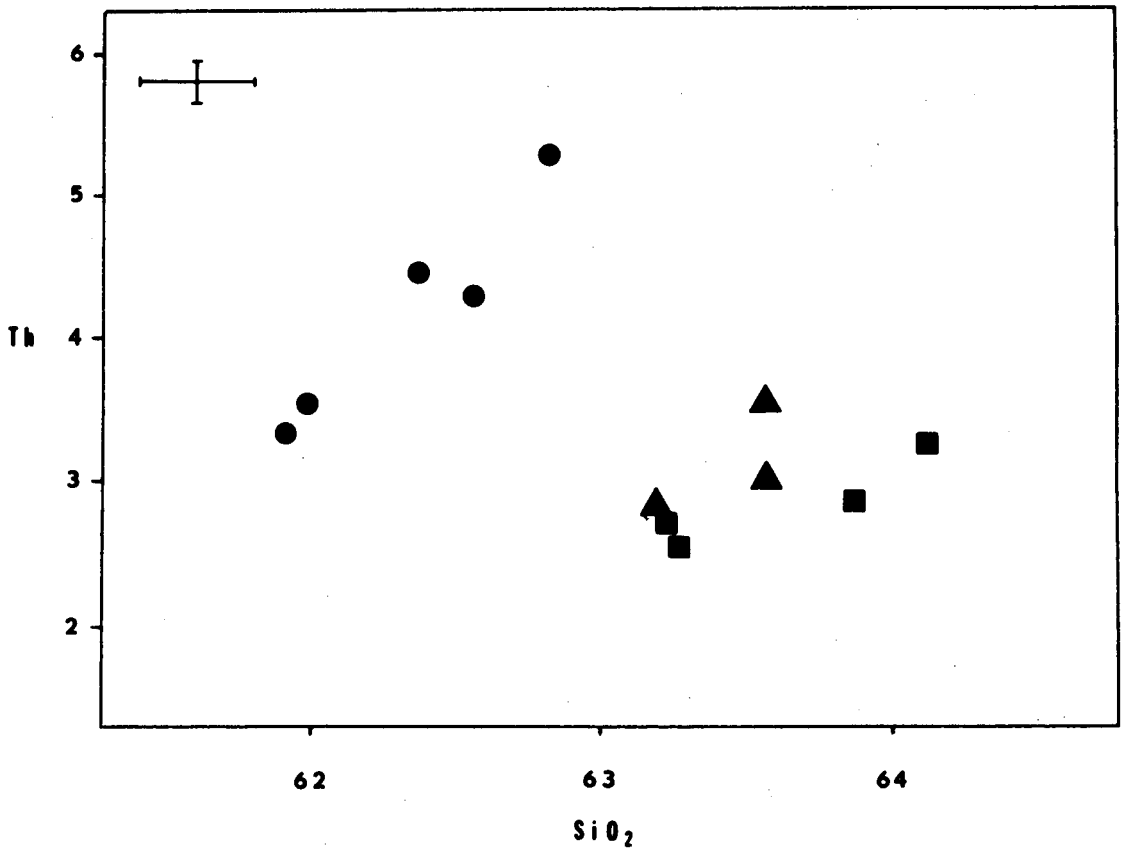

Figure 5. A plot of thorium concentration (ppm) versus SiO_2. Symbols are the same as those in Figure 4.

presented in Table 3 that the range of rock compositions through the Polallie canyon suite could be generated by about 10 percent fractional crystallization of plagioclase and orthopyroxene. When an attempt is made to relate the rocks of the Timberline group to those from the upper portion of the Polallie section a reasonable fractionation model cannot be obtained.

In summary, the geochemical data from the post-glacial silicic lavas indicate that eruptions of discrete magma batches took place at 12,000-10,000 yrs, 1,700 yrs, and 200 yrs BP. Because the lavas are very similar in mineralogical and major-element chemical composition, it is likely that successive magma batches equilibrated under similar conditions. During each eruptive episode the magmas were differentiated to a small degree by the removal of phenocryst minerals from the melt.

Conditions of equilibration

The temperature, pressure, water content, and oxygen fugacity of the dacitic magmas can be estimated by comparing the mineral compositions of the natural rocks with experimental data on crystal-crystal and crystal-liquid equilibria. A sample (CR-55A) from a prismatically jointed block near the middle of the Polallie Canyon section was selected for these calculations and an extensive analysis was made of its phenocryst and groundmass phases.

Pyroxene Geothermometer

Distribution of the component $Mg_2Si_2O_6$ between calcium-

TABLE 3

LEAST SQUARES MIXING MODEL FOR LAVA COMPOSITIONS OF POLALLIE BLOCKS

	F	X PLAG	X OPX	r^2
Parent (HD-83) to:				
HD-4	.041	.021	.020	.081
HD-6	.068	.039	.029	.633

LEASE SQUARES MIXING MODEL FOR LAVA COMPOSITIONS OF OLD MAID FLAT BLOCK, AND DACITE FROM CRATER ROCK

	F	X PLAG	X AMPH	r^2
Parent (HD-30) to:				
HD-9	.034	.013	.021	.647

Least squares mixing calculations are based on major element analyses of whole rocks and microprobe analyses of phenocryst phases. F is the total percent of the crystals removed from the magma. r^2 is the sum of the errors between the calculated daughter composition and the analyzed composition. Note that the Polallie magmas appear to have fractionated plagioclase and orthopyroxene whereas the Old Maid Flat magma differentiated by removal of plagioclase and amphibole.

rich pyroxene and magnesian orthopyroxene has been shown to be temperature dependent. Because they are relatively unaffected by pressure, the compositions of co-existing pyroxenes in the igneous rocks can be used as a geothermometer. From experimental equilibria studies, Wood and Banno (1973) showed that temperature is related to simple pyroxene compositions by

$$T(^{o}K) = \frac{-10202}{\ln(X^{cpx}_{Mg_2Si_2O_6}/X^{opx}_{Mg_2Si_2O_6}) - 7.65\,X^{opx}_{Fe} + 3.88(X^{opx}_{Fe})^2 - 4.6}$$

When the compositions of three pyroxene pairs from sample CR-55A (Table 1) are substituted in the above equation, the calculated temperatures are:

Pyroxene cores.....910° C
Pyroxene rims.....920° C
Groundmass pyroxenes.....918° C

The temperatures fall within a remarkably narrow range and, although they may be somewhat low for low-silica dacites, they are in general agreement with temperature estimates made for dacitic magmas at Mt. Lassen.

Iron-Titanium Oxide Geothermometer

The iron-titanium oxide geothermometer utilizes the co-existing solid-solution phases ulvospinel-magnetite and ilmenite-hematite. When these minerals crystallize under equilibrium conditions, their compositions are uniquely determined by both temperature and the fugacity of oxygen (fO_2). Buddington and Lindsley (1964) published a series of calibration curves from which the temperature and the logarithm of fO_2 of a system can

be estimated from the mole fraction of hematite and ulvospinel in the co-existing oxide phases.

When the compositions of these minerals in sample CR-55A are compared with the curves in Figure 6, it can be seen that the ilmenite solid-solution ratio falls outside the range calibrated by Buddington and Lindsley. Although it is not possible to precisely interpolate the curves, an estimate of fO_2 can be made by using the co-existing magnetite composition and the equilibrium temperature obtained from the two pyroxene geothermometers. These values intersect at point A on Figure 6 and a corresponding value for log fO_2 of -10.5 can be determined from the ordinate. It should be noted that a reasonable interpolation of the ilmenite curves at Hm_{25}-Hm_{30} would pass close to point A and thereby further confirm the pyroxene-based temperature estimates.

Plagioclase Geothermometer

The compositional dependence of plagioclase on both temperature and water pressure has long been established by petrologists. Kudo and Weill (1970) successfully formulated an expression by which this relationship could be used to determine the equilibration temperature of plagioclase-liquid pairs at several different water pressures. If temperature can be estimated by an independent method, then the Kudo-Weill equations can be used to estimate the partial pressure of water in a magma at the time of plagioclase crystallization.

The temperatures obtained by the Kudo-Weill method for sample CR-55A, listed as a function of water pressure, are:

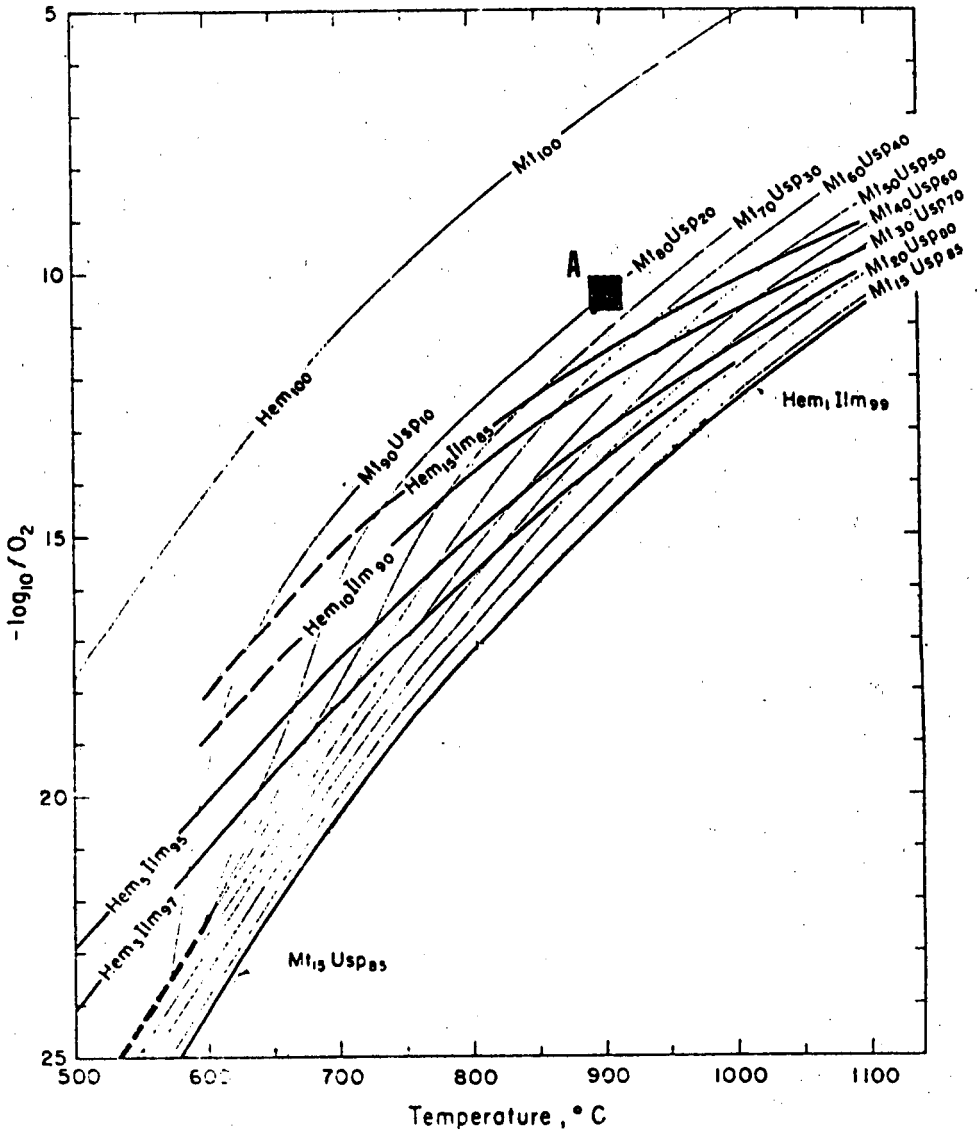

Figure 6. Compositions, in mole percent, of co-existing ilmenite-hematite and magnetite-ulvospinel solid solutions as a function of temperature and oxygen fugacity (after Buddington and Lindsley, 1964). Point A shows the intersection of the magnetite-ulvospinel compositional range in sample CR-55A with the temperature of equilibration of the Polallie magma as calculated from the two pyroxene geothermometer.

P_{H_2O}	Dry	0.5 kb	1.0 kb	5.0 kb
T^oC (pheno)	1148	1095	1057	765
T^oC (gmass)	1178	1129	1091	803

An estimate of P_{H_2O} can be made from these data by interpolating the values at a temperature of 915°C. This procedure yields a P_{H_2O} value of 3.0 kb for the phenocryst temperatures and 3.5 kb when the groundmass plagioclase temperatures are used.

Because the partial pressure of water in a magma cannot normally be greater than the total load pressure, the P_{H_2O} estimates represent the lowest pressures at which the Polallie magma could have equilibrated with plagioclase. If the magma was not water saturated, then P_{total} would, of course, have to be greater than 3-3.5 kb, and the depth of the magma chamber would exceed 10 kilometers.

Geobarometry

An estimate of the minimum load pressure under which the Polallie magma last equilibrated can be made by using equations developed by Carmichael and his co-workers (1971) for the activity of silica in magmatic systems. Because for many reactions the silica activity is dependent on T and fO_2 as well as P_{total}, independent estimates of these variables must be made before Carmichael's equations can be used.

The procedure by which a pressure estimate may be obtained from mineral composition data is well documented elsewhere and a list of the pertinent equations will not be given in this report. For the Polallie lavas, a value for log $a^{liquid}_{SiO_2}$ can be estimated from the reaction

$$1/3\ Fe_3O_4 + SiO_2 = FeSiO_3 + 1/6\ O_2$$

in which $FeSiO_3$ is the ferrosilite component of the orthopyroxene. By substituting the compositional data for magnetic and orthopyroxene (Table 1) and the independent estimates for T and fO_2 into Carmichael's equations, a value of 6.7 kb is obtained as a minimum load pressure for the equilibration of the Polallie magma. This pressure corresponds to a depth of about 20 kilometers for the location of the magma chamber immediately prior to the eruption of the Polallie lavas.

MAIN STAGE LAVAS

More than 90 percent of the volume of Mt. Hood volcano is composed of a preglacial series of flows, breccias, and pyroclastic rocks; the great majority of which are andesitic in composition. Unlike the composite cones of the central Oregon Cascade Range, Mt. Hood is not built on an extensive platform of Pleistocene basaltic flows, but rather rests directly on volcanic rocks of Pliocene and Miocene age. The age of Mt. Hood volcano is not known; however, because lavas having reversed remnant magnetism have not yet been found, an age of 660,000 yrs should be considered as a maximum date for the onset of eruption.

In order to best understand the magmatic evolution of the Main Stage lavas, surface samples were taken for analysis only where four or more flows could be sampled in unambiguous stratigraphic order. In addition, the Timberline drill hole (3S/9E-7aac) offered a unique opportunity to sample eleven flows through a vertical section of about 1,400 feet. A detailed log of this drill hole is attached (Appendix I).

Petrography

All of the observed Main Stage lavas contain phenocrysts of plagioclase, orthopyroxene and, in lesser abundance, clinopyroxene. Amphibole occurs in about 66 percent of the samples and is generally partially or completely replaced by pseudomorphic mats of fine-grained opaque minerals. In contrast to the observation by Wise (1969) that amphibole-bearing andesite flows occur only in the upper portion of the volcano, the present

study indicates that there is no relationship between the stratigraphic height of a flow and its amphibole content. Microprobe analyses were not made of phenocryst phases in the Main Stage lavas; however, mineral analyses and petrographic descriptions are presented by Wise (1969) and a flow-by-flow description of the mineralogy of the cuttings from the Timberline drill hole is given in Appendix I.

Geochemistry

The major and trace element composition of samples from five sections and the Timberline drill hole are given in Table 4. The analyses in each set are presented in order of increasing stratigraphic height. The drill hole samples probably represent a complete flow sequence; however, because of lack of continuous exposure, it is unlikely that all flows in the subaerial sections have been sampled.

Major Elements

In contrast to the post-glacial silicic lavas, the Main-Stage flows show little systematic chemical variation through individual measured sections. The behavior of silica in six sections is given as an Example in Figure 7. Although it is clear from this figure that there is no serial variation of SiO_2 concentrations upward through the sections, there is a general tendency for the flows at the lowest projected stratigraphic elevations (<4900 ft.) to be relatively enriched in silica ($>62\%$ SiO_2).

The occurrence of siliceous rocks at the base of the Mt. Hood section is inconsistent with a Bowen-type model of

TABLE 4

MAJOR AND TRACE ELEMENT ANALYSES OF MAIN STAGE LAVAS

	TIMBERLINE DRILL HOLE										
	TDH-11	TDH-10	TDH-9	TDH-8	TDH-7	TDH-6	TDH-5	TDH-4	TDH-3	TDH-2	TDH-1
SiO_2	64.79	62.03	63.71	62.30	60.73	61.90	61.11	62.33	60.77	59.89	59.73
TiO_2	.66	.78	.74	.73	.85	.81	.74	.80	.82	.76	.85
Al_2O_3	16.61	17.85	17.13	17.81	17.67	17.11	17.86	16.91	17.92	17.90	17.75
MgO	2.16	2.19	1.95	2.50	2.79	2.61	2.74	2.58	2.63	4.07	3.41
Fe_2O_3	5.33	5.72	5.18	6.01	6.35	6.07	6.34	5.92	6.07	6.27	6.36
MnO	.08	.08	.08	.08	.10	.09	.10	.08	.09	.10	.10
CaO	4.69	5.76	5.35	5.24	5.96	5.70	5.74	5.60	6.22	5.65	6.27
Na_2O	3.96	4.06	4.38	4.09	4.20	4.25	4.24	4.19	4.09	4.14	4.15
KaO	1.59	1.38	1.34	1.11	1.18	1.29	.99	1.42	1.22	1.06	1.20
PaO_5	.13	.16	.15	.13	.18	.16	.15	.17	.17	.15	.18
Rb	27	27	21	17	19	20	17	20	17	18	13
Sr	427	471	585	513	507	471	532	538	542	544	505
Zr	151	127	133	157	143	137	135	141	133	132	123
Ni	36	17	27	32	41	42	49	42	41	43	43
Sc	11.2	11.3	11.4	11.9	12.9	12.6	12.9	12.9	12.7	13.4	14.1
Co	14.5	14.9	13.3	16.2	18.4	17.6	18.8	17.6	18.0	19.2	19.5
Hf	4.5	3.7	3.8	3.6	3.9	3.7	3.8	4.2	3.7	4.1	3.8
Ta	1.0	.7	.7	.6	.6	.8	.4	n.d.	n.d.	n.d.	.6
U	1.4	1.4	1.1	n.d.	2.6	.9	n.d.	n.d.	1.2	1.0	1.4
Th	4.8	n.d.	3.4	2.4	2.4	2.6	2.3	3.3	2.7	2.5	2.6
Ba	430	309	360	378	249	308	250	358	335	292	298
La	20.4	16.1	18.6	13.7	15.4	15.1	15.0	17.0	16.3	15.8	15.9
Ce	41.8	33.6	36.9	28.4	30.8	32.4	31.9	37.1	34.3	33.4	33.4
Nd	n.d.	n.d.	20	n.d.	n.d.	n.d.	n.d.	n.d.	n.d.	n.d.	n.d.
Sm	4.1	3.9	4.1	3.5	4.0	3.9	3.9	4.0	3.9	3.8	3.9
Ev	1.0	1.1	1.2	1.0	1.2	1.1	1.1	1.1	1.1	1.2	1.1
Tb	n.d.	.6	.5	.4	.6	.7	.5	n.d.	.5	n.d.	.6
Yb	1.2	1.4	.8	.8	1.6	1.0	1.3	1.3	1.2	1.3	1.3
Lu	.3	.2	.2	.2	.3	.2	.2	.2	.2	.2	.2

TABLE 4 CONTINUED

	ELIOT BRANCH - COOPER SPUR SECTION						YOCUM RIDGE SECTION			
	HD-66	HD-67	HD-68	HD-69	HD-74	HD-72	HD-78	HD-79	HD-80	HD-81
SiO_2	62.71	60.58	60.73	60.67	60.90	60.14	59.89	59.27	59.98	63.30
TiO_2	.74	.91	.90	.85	.87	.93	.93	.98	.80	.77
Al_2O_3	17.70	17.22	17.08	17.68	17.28	17.69	18.10	17.65	18.54	17.12
MgO	1.85	2.77	2.74	2.74	2.67	2.66	2.77	3.19	2.78	1.92
Fe_2O_3	5.91	6.20	6.10	6.10	6.18	6.14	6.67	6.70	6.61	5.46
MnO	.09	.09	.09	.10	.10	.09	.10	.10	.11	.09
CaO	5.55	6.06	6.02	5.86	5.92	6.34	6.16	6.45	6.02	5.31
Na_2O	4.16	4.35	4.47	4.25	4.34	4.23	4.29	4.10	4.14	4.27
K_2O	1.14	1.55	1.58	1.47	1.50	1.49	.98	1.33	.86	1.61
P_2O_5	.16	.27	.31	.28	.25	.28	.18	.24	.15	.15
Rb	18	21	25	23	20	19	12	19	13	29
Sr	593	807	811	908	1040	1116	583	679	582	572
Zr	147	185	209	170	160	152	135	150	114	137
Ni	24	23	27	28	27	25	n.d.	n.d.	n.d.	n.d.
Sc	11.6	11.6	11.6	11.6	13.6	11.6	11.9	n.d.	12.5	10.8
Hf	4.0	4.8	4.8	4.7	4.6	4.3	3.5	4.0	3.4	4.3
Ta	1.4	1.8	1.4	1.6	1.4	1.1	1.0	.9	.9	1.3
U	1.4	4.5	1.9	2.1	1.8	1.6	2.9	n.d.	5.2	2.4
Th	3.1	4.8	5.1	4.9	4.4	4.3	1.9	3.1	1.5	3.9
Ba	300	463	436	476	450	496	235	331	200	240
La	17.5	28.3	28.4	28.6	31.5	32.9	13.2	19.3	n.d.	18.6
Ce	36.3	57.7	59.7	58.4	66.4	69.0	36.1	39.3	25.6	39.5
Nd	n.d.	42	n.d.	31	42	44	18	n.d.	n.d.	n.d.
Sm	4.1	5.8	5.8	5.5	6.6	6.5	4.5	4.6	3.5	4.3
Eu	1.2	1.5	1.6	1.5	1.6	1.7	1.2	1.3	1.1	1.0
Tb	.6	.7	.7	n.d.	.6	.5	.5	.6	.5	.5
Yb	1.1	1.3	1.4	1.5	1.3	1.3	1.2	1.2	1.4	1.6
Lu	.2	.2	.2	.2	.3	.2	.2	.2	.2	.3

TABLE 4 CONTINUED

	ZIGZAG CANYON-MISSISSIPPI HEAD SECTION					MT. HOOD MEADOWS SECTION					
	HD-89	HD-88	HD-87	HD-86	HD-1	HD-16	HD-15	HD-14	HD-13	HD-12	HD-11
SiO_2	61.43	61.16	60.11	61.85	62.98	59.52	59.96	60.07	59.65	60.55	61.75
TiO_2	.78	.85	.88	.77	.76	.94	.95	.92	.93	.87	.77
Al_2O_3	17.26	17.43	17.78	17.74	16.95	17.87	17.55	17.53	17.59	17.47	17.39
MgO	3.03	2.63	3.06	2.12	2.38	2.80	2.84	2.90	3.07	2.82	2.60
Fe_2O_3	6.34	6.27	6.42	6.36	5.56	7.00	6.79	6.64	6.81	5.92	5.80
MnO	.10	.09	.09	.09	.07	.09	.09	.09	.09	.08	.08
CaO	5.55	5.80	6.23	5.52	5.46	5.99	5.96	5.95	6.12	5.99	5.75
Na_2O	4.15	4.25	3.93	4.16	4.21	4.30	4.22	4.27	4.17	4.51	4.27
K_2O	1.19	1.31	1.34	1.22	1.48	1.26	1.40	1.41	1.36	1.55	1.43
P_2O_5	.16	.21	.16	.17	.16	.23	.25	.22	.23	.24	.17
Rb	23	21	22	21	23	15	20	19	18	18	22
Sr	524	571	580	580	568	596	574	589	562	928	603
Zr	167	154	159	161	158	158	183	175	178	152	150
Ni	n.d.	n.d.	n.d.	n.d.	n.d.						
Sc	12.8	11.6	13.6	11.5	11.5						
Hf	4.3	4.5	4.6	4.0	4.3						
Ta	1.4	1.6	1.4	1.4	.9						
U	1.3	1.3	1.8	1.5	n.d.						
Th	3.2	1.8	3.7	3.3	3.8						
Ba	329	333	310	321	327						
La	20.5	19.2	19.8	18.7	18.1						
Ce	40.1	38.3	39.5	37.7	39.3						
Nd	22	20	20	n.d.	n.d.						
Sm	4.4	4.3	4.4	4.3	4.0						
Eu	1.2	1.2	1.2	1.2	1.1						
Tb	.5	.5	.5	.5	.4						
Yb	1.4	1.5	1.4	1.3	1.0						
Lu	.2	.2	.3	.2	.2						

TABLE 4 CONTINUED

	COE BRANCH-BARRETT SPUR SECTION				LANGILLE CRAGS SECTION		
	HD-43	HD-46	HD47	HD-45	HD-75	HD-76	HD-77
SiO_2	63.70	60.19	60.96	62.31	61.95	62.51	60.82
TiO_2	.70	.85	.87	.79	.89	.88	.85
Al_2O_3	17.44	17.77	18.00	17.19	16.98	16.47	17.59
MgO	2.04	2.98	2.61	2.48	2.36	2.35	2.54
Fe_2O_3	4.84	6.44	5.99	5.70	5.70	5.75	6.21
MnO	.07	.09	.07	.08	.08	.09	.09
CaO	5.23	6.05	5.73	5.53	5.81	5.61	5.88
Na_2O	4.33	4.07	4.50	4.23	4.15	4.26	4.30
K_2O	1.50	1.40	1.11	1.53	1.78	1.79	1.46
P_2O_5	.15	.17	.17	.16	.30	.29	.25
RB	21	24	11	20	23	26	23
Sr	550	575	615	636	927	881	909
Zr	152	177	135	157	197	193	177

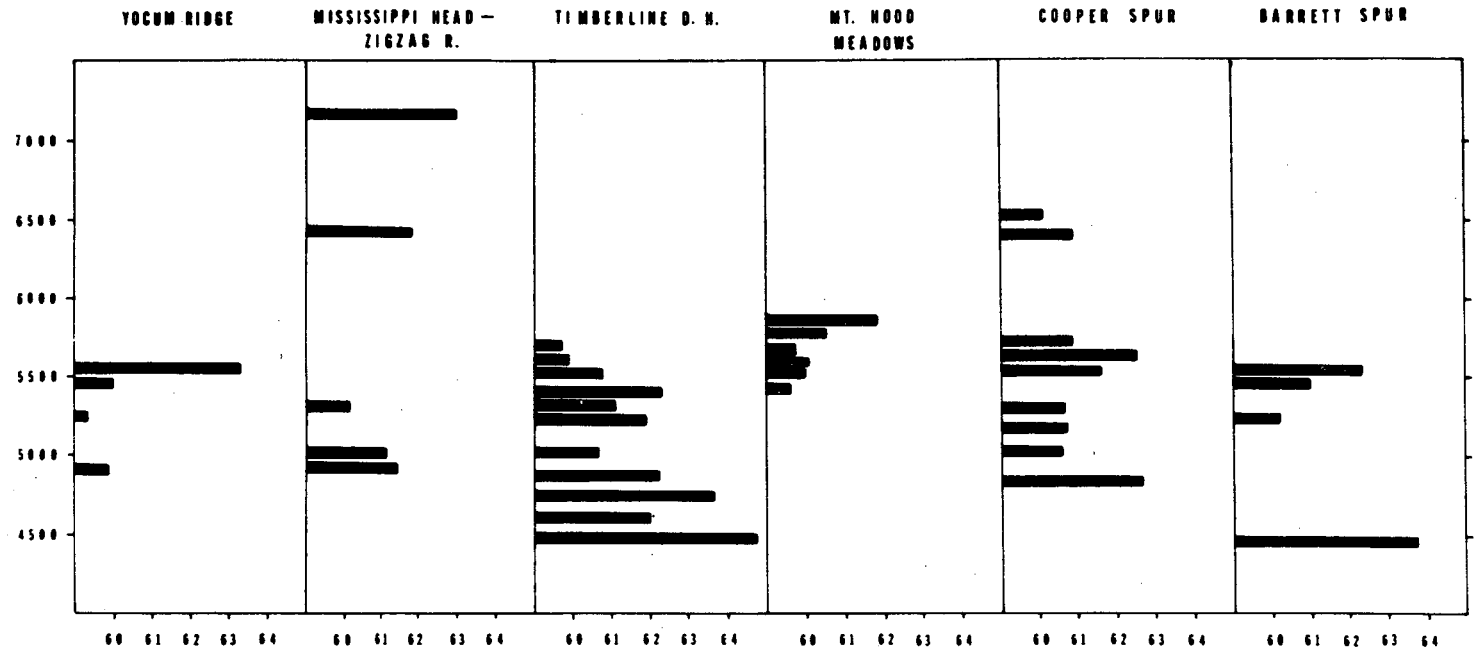

Figure 7. A graph of weight percent SiO_2 in Main Stage Mt. Hood lavas. The surface section has been projected with an initial dip of 10° to a distance from the summit that is equal to that of the Timberline drill hole.

fractional crystallization; however, numerous other examples exist of volcanoes in which the initial eruptions produced the most siliceous lavas in a sequence. At Hekla volcano in Iceland, this cycle has been repeated many times and the silica content of the initial products of each eruptive episode has been shown to be proportional to the length of the quiescent period between eruptions (Thorarinsson, 1954). An analysis of this kind cannot be made for the Main Stage Mt. Hood lavas because the absolute time intervals between eruptions are not known. Nonetheless, the eruption of siliceous lavas during the earliest stages of volcanism indicates that at least the initial magma chamber beneath Mt. Hood was compositionally zoned. The recurrence of rocks of dacitic composition at higher intervals in the Main Stage sequence may mark the initiation of later eruptive episodes.

Trace Elements

In general, the trace element compositions of the Main Stage lavas tend to reflect the major element contents in any one section of the flows. This tendency can be seen by comparing the trace element trends in Figures 8 and 9 with the trends for SiO_2 and MgO given in Figure 10. As might be expected, the excluded elements mimic the silica trend whereas the trends of Ni, Co, and Sc are similar to that of magnesia. The relatively consistent covariation of the major and trace elements in the drill hole section indicates that these flows may be genetically related, perhaps as differentiates of a common parental melt.

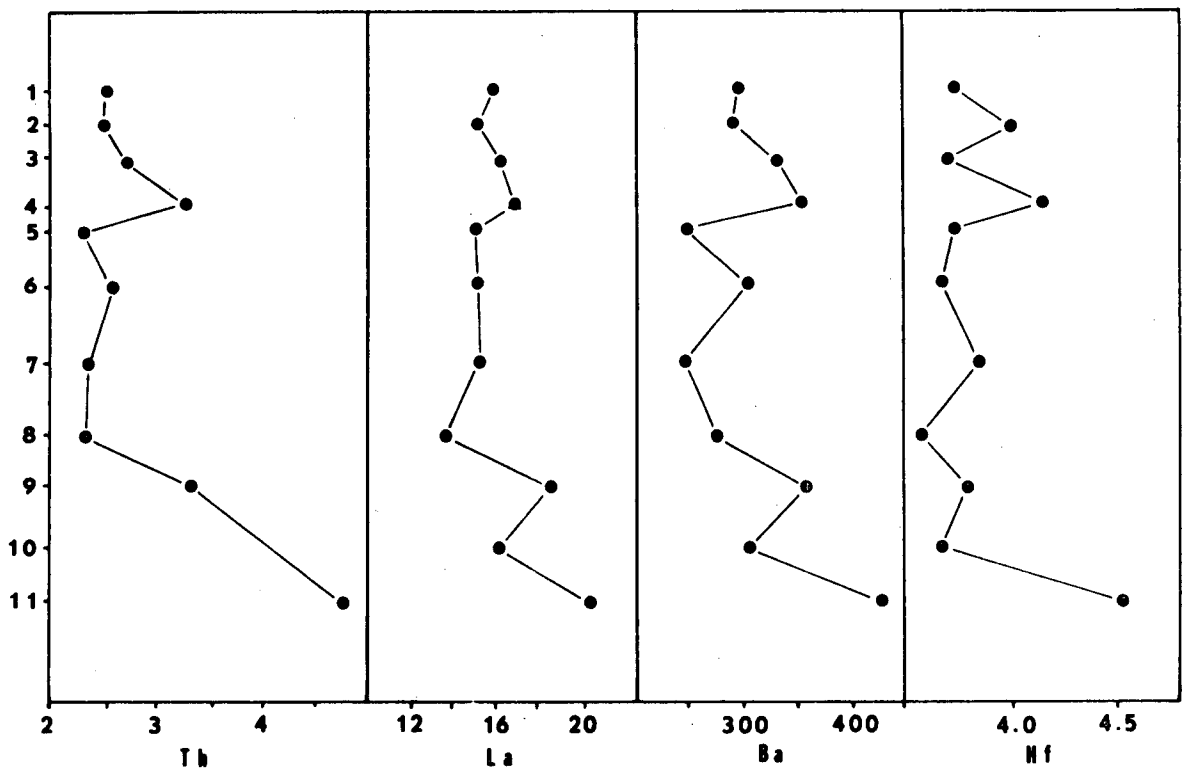

Figure 8. A plot of the concentrations of selected excluded trace elements versus flow number for the Timberline drill hole section.

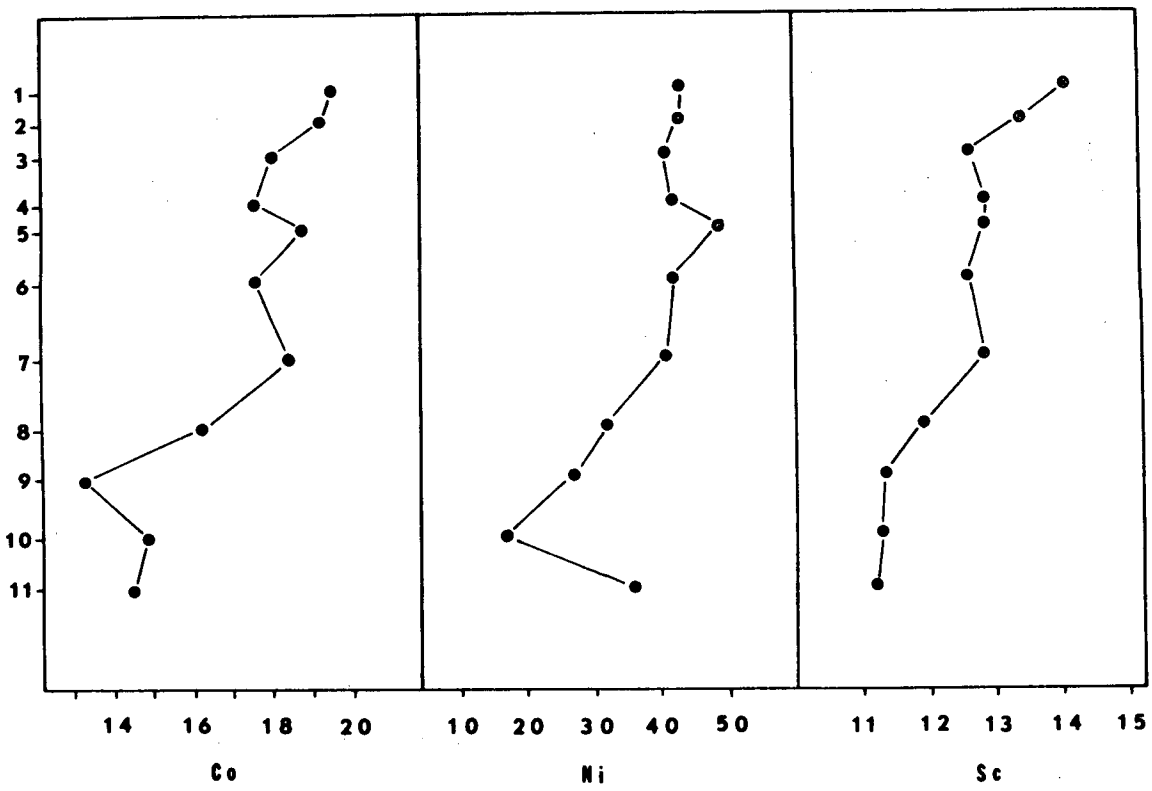

Figure 9. A plot of the concentrations of selected included trace elements versus flow number for the Timberline drill hole.

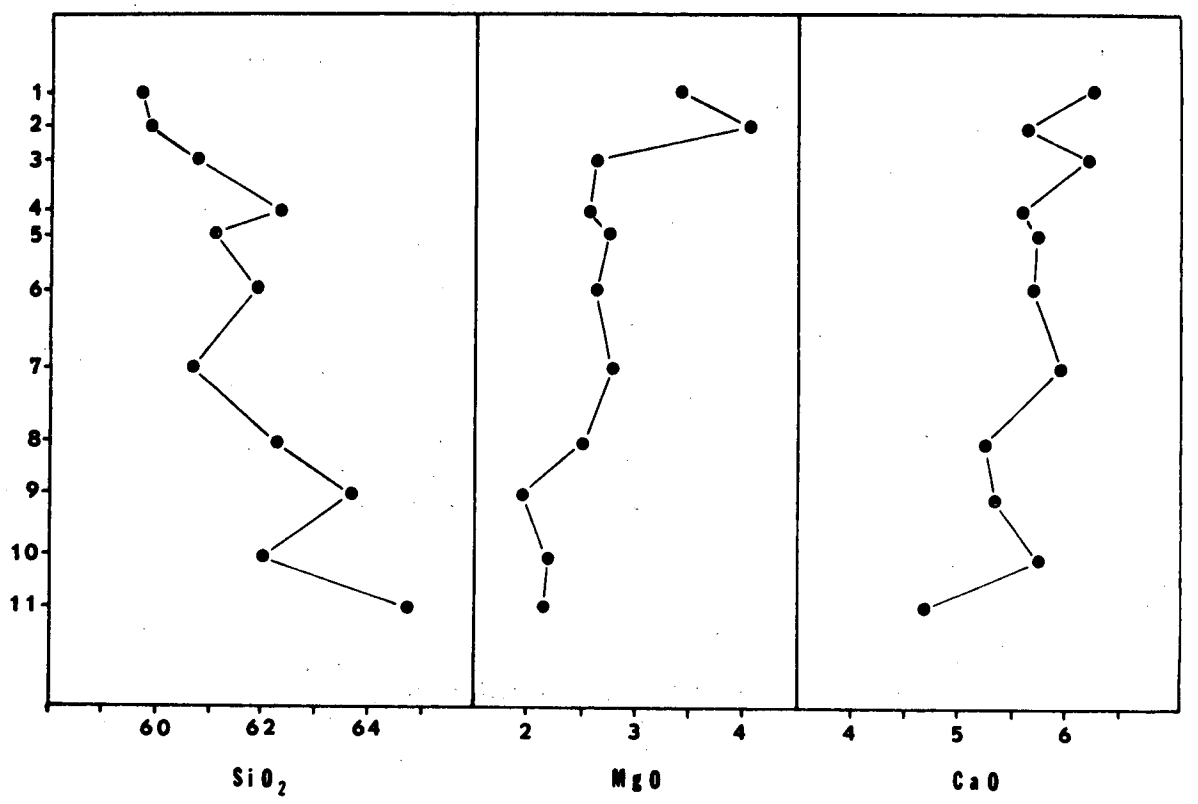

Figure 10. A plot of the concentrations of selected major elements versus flow number for the Timberline drill hole.

When the trace element compositions of flows from different sections are compared, chemical differences appear that cannot be readily explained by late stage differentiation processes. As shown by Figure 11, some flows are noticeably enriched in K_2O and the excluded trace elements compared to other Main-Stage lavas with similar major element compositions. With the exception of the basal flow (HD-66), the lavas in the Eliot Branch-Cooper Spur section have the highest excluded element contents whereas the Timberline drill hole samples contain the lowest concentrations of these elements. Flows from other sections fall within one or the other of these trends or occupy intermediate positions.

The existence of geochemically distinct lava suites in asymmetrical distribution around the volcano indicates that Mt. Hood was probably built by periodic eruptions of discrete magma batches from several different vents. Those flows that have intermediate concentrations of excluded trace elements may represent separate magma batches or may be mixtures of two or more end-member parent compositions. The variability in abundance in trace elements in lavas with similar SiO_2 contents could be caused by differences in the proportion of partial melting that produced each magma batch. Because of the eutectic nature of partial melting, small differences in the amount of melting would not affect the major element composition of the liquid; however, a parental magma that is produced by small degree of melting would have considerably higher abundances of the excluded trace elements than one representing a greater proportion of melt.

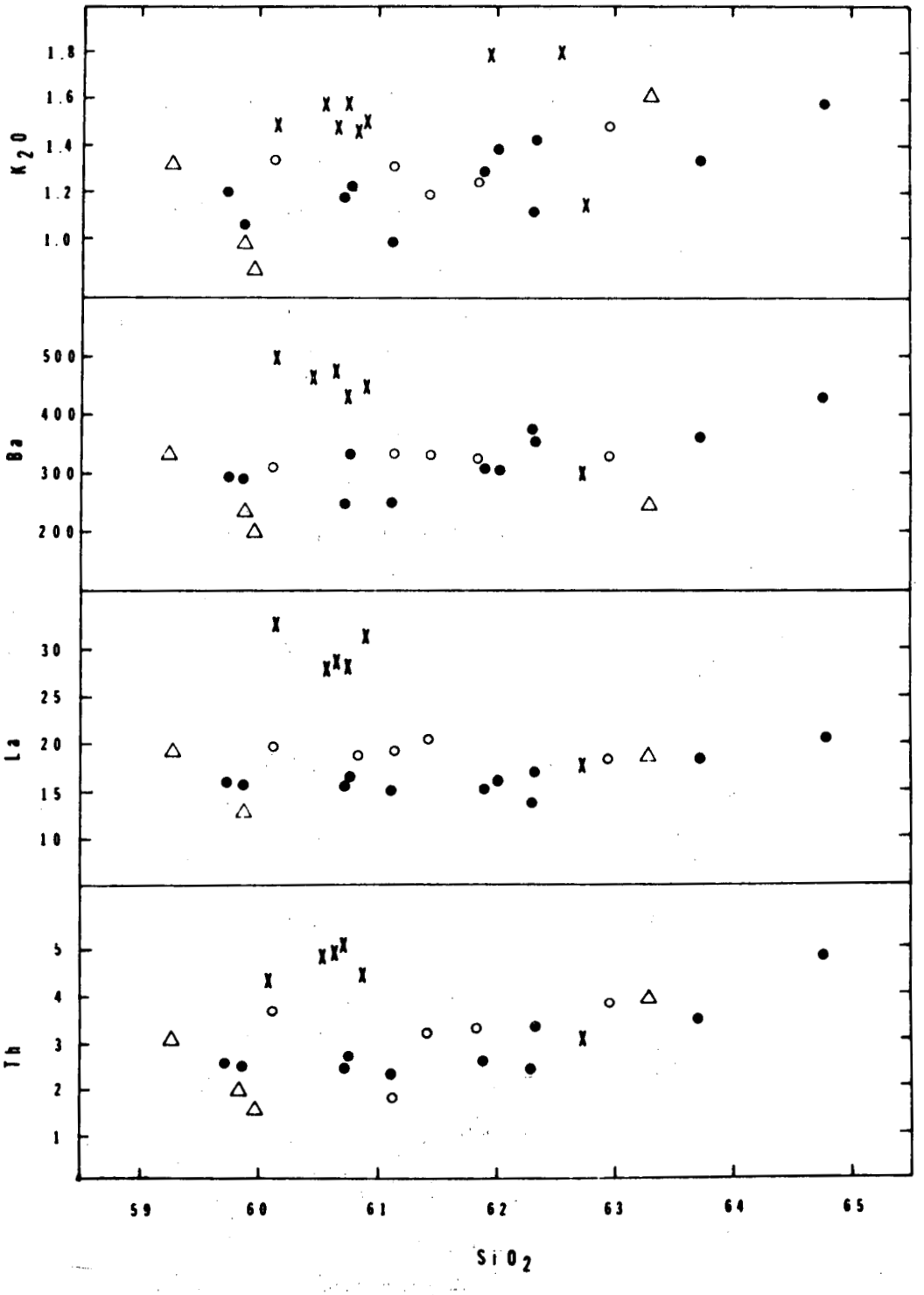

Figure 11. A plot of selected excluded elements versus SiO_2 in Main Stage lavas. Solid circles = Timberline d.h.; open circles = Mississippi Head-Illumination Rock section; triangles = Yocum Ridge section; X = Eliot Branch-Cooper Spur Section.

SUMMARY AND GEOTHERMAL IMPLICATIONS

The post-glacial silicic lavas were erupted during three temporally distinct episodes, each of which tapped a discrete batch of magma that was being differentiated by small amount of fractional crystallization. Equilibria calculations indicate that immediately prior to eruption the dacite magmas were at temperatures of 900 to 920° C, had a maximum water saturation of 30 percent and were at least 20 km beneath Mt. Hood.

The Main Stage lavas comprise about 90 percent of the volume of Mt. Hood and, like the young dacites, represent several geochemically distinct magma batches. In contrast to the post-glacial magmas, the Main-Stage magmas do not appear to have undergone fractional crystallization during the course of an eruptive episode. Instead, the existence of silica-rich lavas near the base of the Mt. Hood sequence indicates that the Main-Stage magma chambers may have been compositionally zoned. It is suggested that processes resulting in zonation of a magma may be more likely to occur in large Main-Stage chambers than in those representing the more rapidly cooled, small, post-glacial magma bodies.

The geothermal evaluation of an igneous system is based on the age, volume and depth of possible magma chambers. Smith and Shaw (1975) suggest 10 km as a maximum depth for magma chambers associated with potential geothermal resources. If the late-stage Mt. Hood magmas last equilibrated at depths greater than 20 km, as suggested by the equilibrium calculations, then residual magma in the chamber would probably have

little influence on near-surface geothermal systems. Because of the young age of the most recent eruptions, a local heat source could be provided by magma that is still residing at shallow depths within the volcanic conduit. Calculations indicate that a cylindrical conduit which has the diameter of Crater Rock plug dome would contain about 0.3 km^3 of magma in the upper 10 km of its length.

The geothermal significance of the Main-Stage volcanism cannot be precisely evaluated because the age and depth of the associated magma chambers is not known. Estimates of the age and volume of the residual magmas indicate that they may still be associated with major geothermal anomalies (Figure 12); however, there is no reason to believe that these magmas are located at shallow depths. Deep-seated magma bodies could have considerable effect on the regional geothermal gradient in the Mt. Hood area, although it is unlikely that they would significantly affect the thermal regime of the volcanic edifice. Potential resources associated with a high regional anomaly would more likely be found along deeply penetrating structures.

In summary, the geological and geochemical evidence indicates that geothermal anomalies may exist at two levels in the Mt. Hood area; a shallow, localized anomaly associated with the young volcanic conduit, and a deep, regional anomaly associated with residual magmas from the Main-Stage volcanism of Mt. Hood.

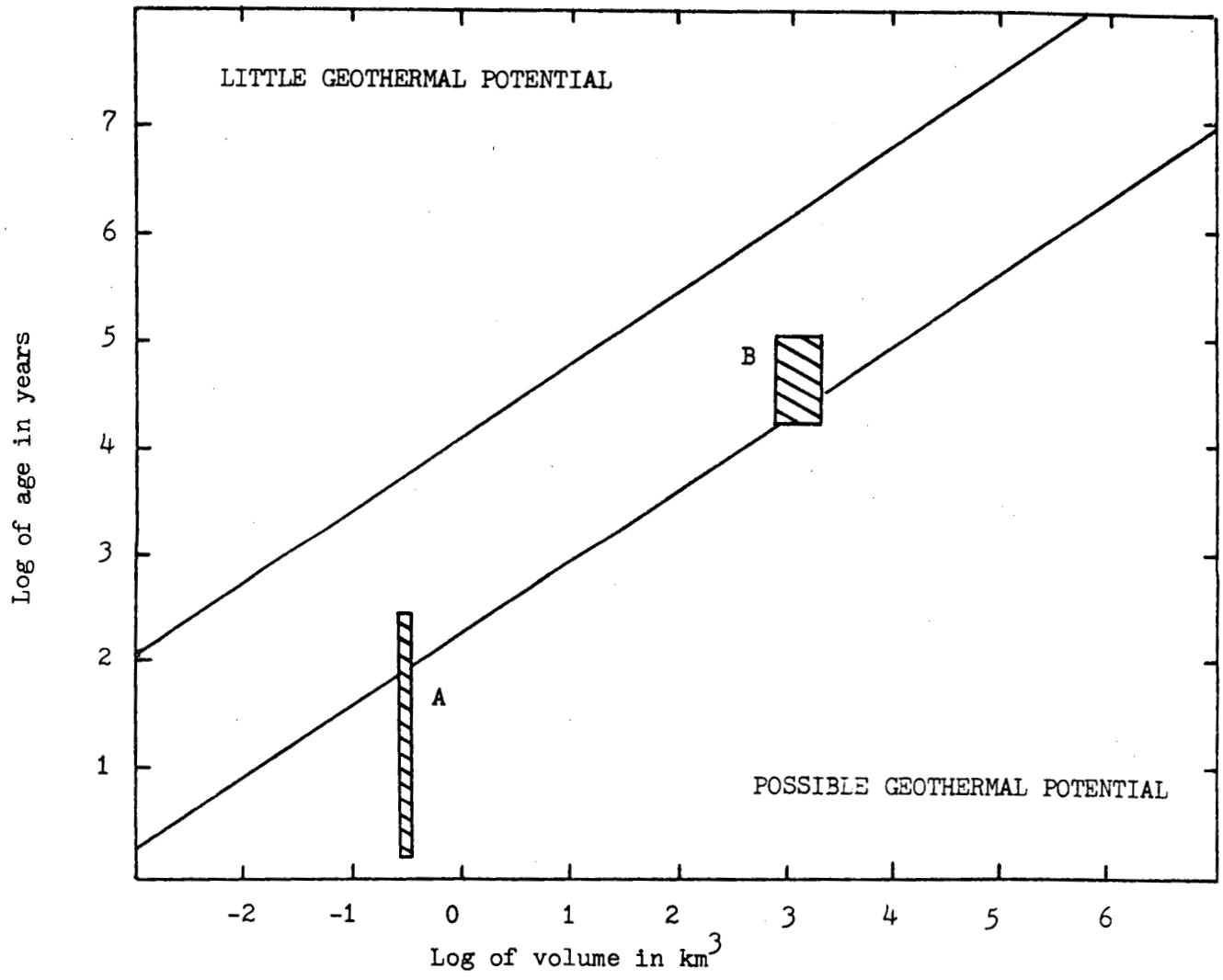

Figure 12. Graph of theoretical cooling time versus volume for magma bodies. Systems having magma chambers with large molten fractions would plot below the diagonal lines; systems that are now approaching ambient temperatures would plot above the diagonal lines; systems that may now be approaching a completely crystallized state would plot between the diagonal lines (after Smith and Shaw, 1975). Field A shows the age and volume range for a shallow volcanic conduit beneath Mt. Hood. Field B shows a range of ages (15,000 yrs - 100,000 yrs) and volumes (assuming that the erupted volume = 10-20% of the total magma reservoir) of a hypothetical Main-Stage magma chamber.

APPENDIX I

LITHOLOGIC LOG TIMBERLINE LODGE DRILL HOLE, 1978

Lithologic Symbols

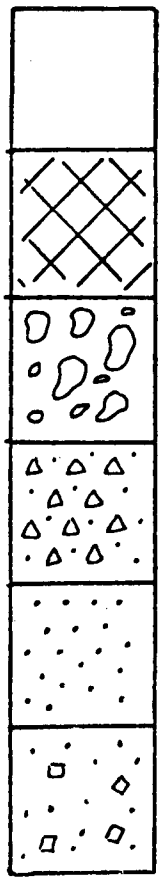

Lava flow

Brecciated lava flow

Mud flow or interflow colluvium

Dacitic block and ash flow

Lapilli

Crystal tuff

Plag Px Am Dacite. Large Am phenocrysts occur in chips from first 10 feet of hole, whereas the remaining 30 feet is composed of dacite with small Am phenocrysts and a higher proportion of Cpx.

Heterogeneous mixture of dacite and andesite. Large fragments in return.

FLOW #1. Light gray andesite with large Pl phenocrysts, abundant small crystals of honey to medium brown Opx, and less abundant phenocrysts of green-brown Cpx. Matrix is sugary in texture and has a salt and pepper appearance.

T. S.* **Plag = Opx >> Opaq > Cpx > Am**
Amphibole is present as small relict grains composed of finely granular opaque minerals.

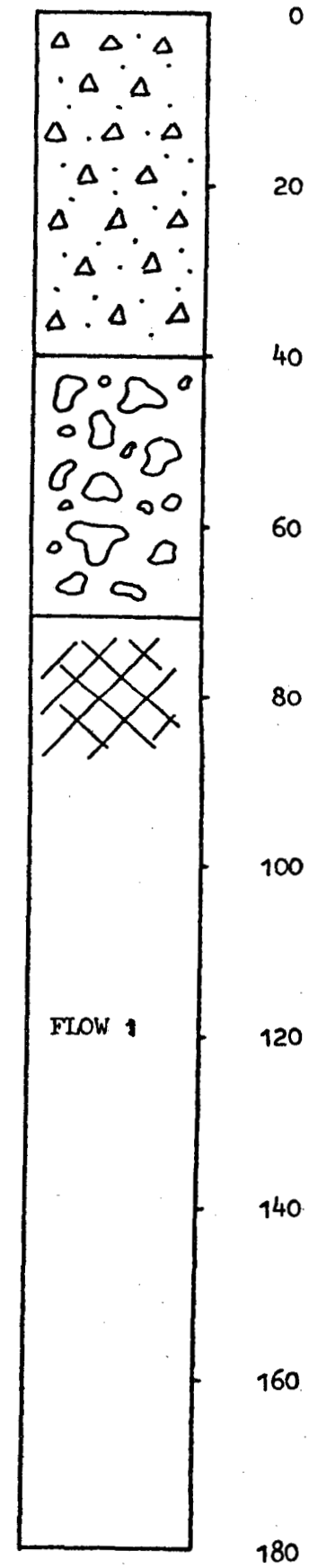

*** Relative modal proportions of phenocryst and microphenocryst minerals were determined by observation of thin sections of drill hole cuttings; description following flow # is from the field log and was made with the aid of a binocular microscope.**

FLOW 2. Brown andesite with large phenocrysts of brown Opx and less abundant Cpx. The matrix has been altered to a light brown color by oxidation.

T. S. Plag > Opx > Cpx >> Opaq > Am
Amphibole present as small relict grains similar to those in flow #1.

FLOW 3. Medium brown andesite with phenocrysts of Pl, medium brown Opx and green Cpx. Matrix is fine-grained and gray-brown in color. A large proportion of the flow is vesicular and has been oxidized to a hematite-red color. Much of the flow has probably been autobrecciated.

T. S. Plag >> Opx = Cpx > Opaq
Plagioclase contains inclusions of brown glass.
No amphibole was observed.

Heterogeneous mixture of highly oxidized andesite and black glassy andesite.

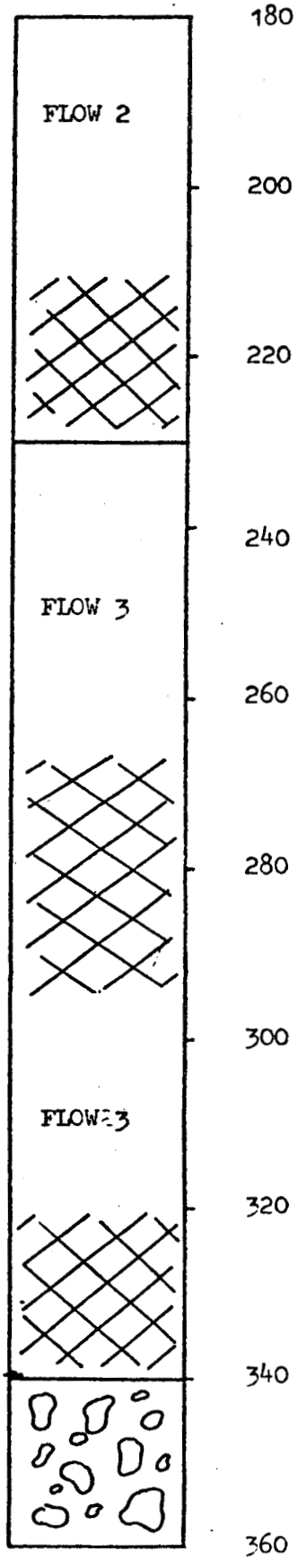

FLOW 4. Dense, light gray andesite with large Pl phenocrysts and smaller phenocrysts of brown pyroxene. Two pyroxene types are not descernible. Matrix is gray with some irregular patches of pink oxidation alteration.

T. S. Plag > Opx >>Cpx >> Am?
Amphibole is present only as indistinct relicts.

Oxidixed heterogeneous mixture of andesites.

FLOW 5. Vesicular, medium gray-pink andesite with phenocrysts of Pl, brown Opx and green Cpx.

T. S. Plag > Opx >> Opaq = Cpx

Highly oxidized, bb-sized, black glassy lapilli.

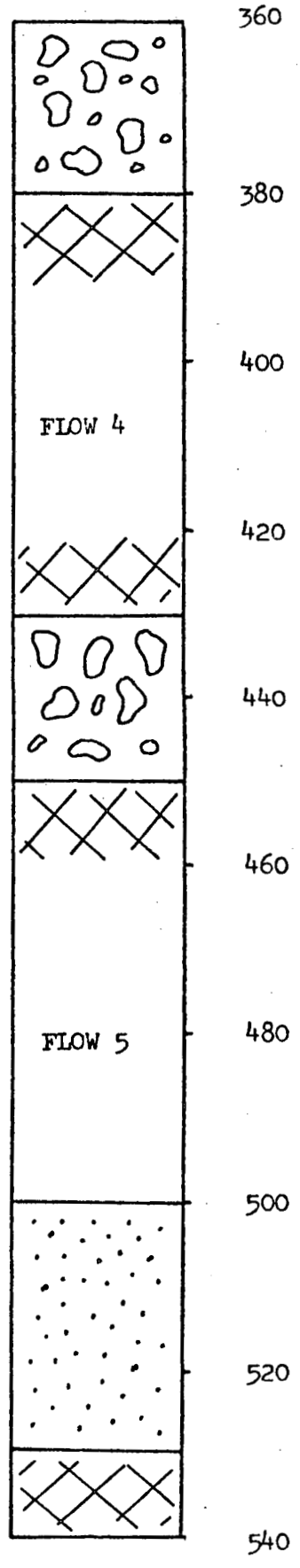

FLOW 6. Dense light gray andesite with large phenocrysts of Pl, euhedral medium brown phenocrysts of Opx, and small honey-colored microphenocrysts of Opx. Matrix is very light gray.

T. S. Plag > Opx > Am > Cpx =Opaq
Amphibole occurs as large phenocryst grains that have been completely converted to granular opaques + px? + plag?

Heterogeneous mixture of gray andesite, brown andesite and highly oxidized glassy fragments.

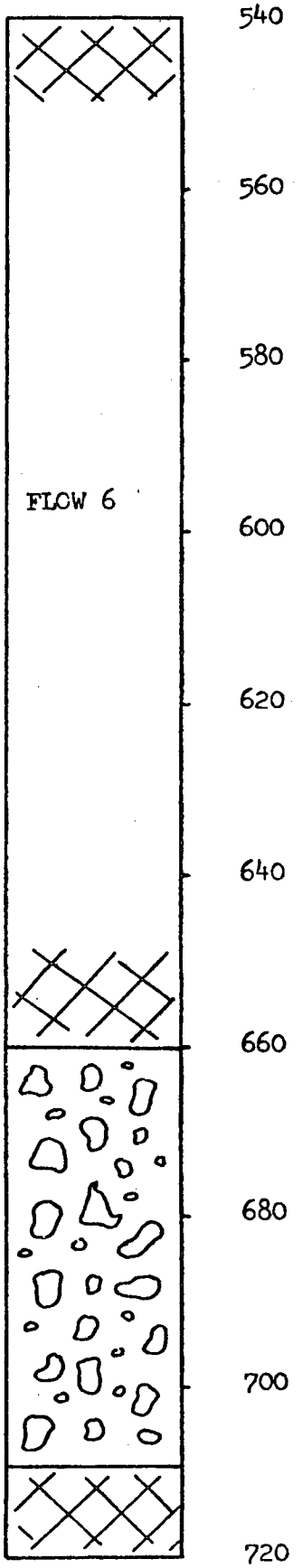

FLOW 7. Dark gray andesite with large Pl phenocrysts and small, dark brown pyroxene phenocrysts. Matrix is dark in color and probably contains a large proportion of glass.

T. S. Plag >Opx >>Cpx = Opaq

Heterogeneous mixture of at least three types of andesite, the most abundant of which has a distinctive limonite-yellow colored groundmass.

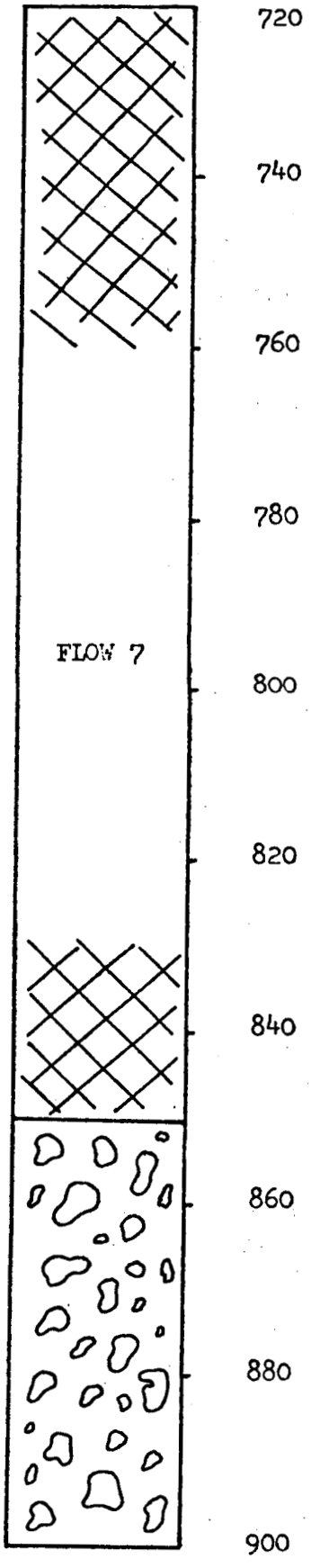

FLOW 8. Black, glassy andesite with large Pl phenocrysts, rare, large, dark brown Opx crystals, and a distinctive dark gray spotted matrix.

T. S. Plag > Opx > Cpx > Opaq
Orthopyroxene grains are rimmed with Cpx.

Crystal tuff with Pl crystals in a matrix of light gray to yellow ash and lapilli. Pyrite is a very abundant alteration mineral in this rock.

FLOW 9. Medium gray andesite with large phenocrysts of Pl and small crystals of red-brown pyroxene. Much of this flow is brecciated and oxidized. Pyrite is present as an alteration mineral but is less abundant than in the crystal tuff just above.

T. S. Plag > Opx = Am
Amphibole occurs as large grains of oxyhornblende that is rimmed with granular opaque minerals. This is the first occurrence of amphibole in the drill hole section that is not totally altered.

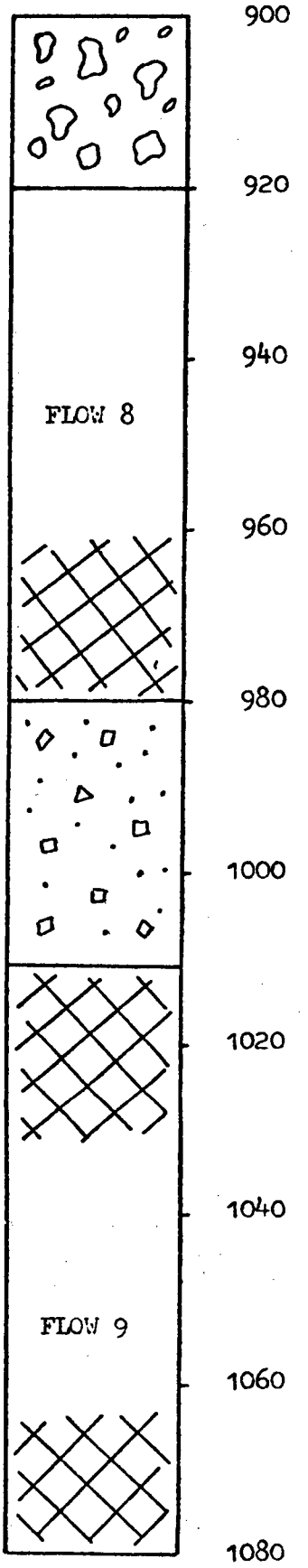

Continued brecciated flow 9.

(Convert to mud circulation at 1140'. Return is very mixed with a large proportion of oxidized lapilli and pyritic crystal tuff similar to units described above. It is likely that down-hole contamination from the more easily eroded units has masked the lithology in this interval. All return below this point probably contains a significant proportion of contamination from above)

FLOW 10. Medium gray andesite with large glassy-looking phenocrysts of Pl and small honey-colored crystals of Opx. Matrix is sugary with a salt and pepper appearance.

No thin section

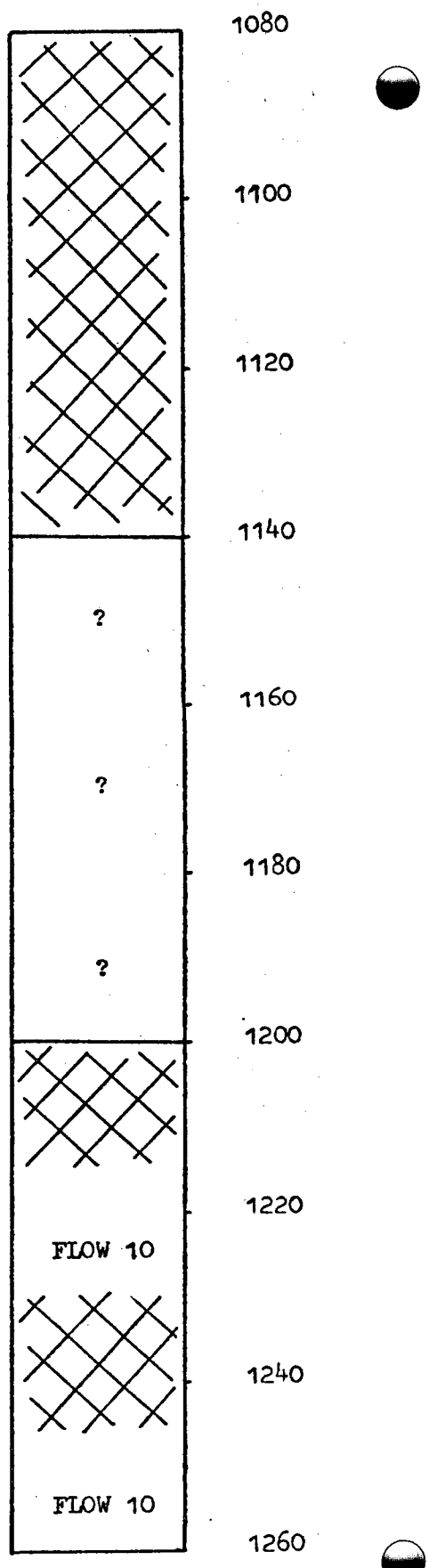

Continued flow 10.

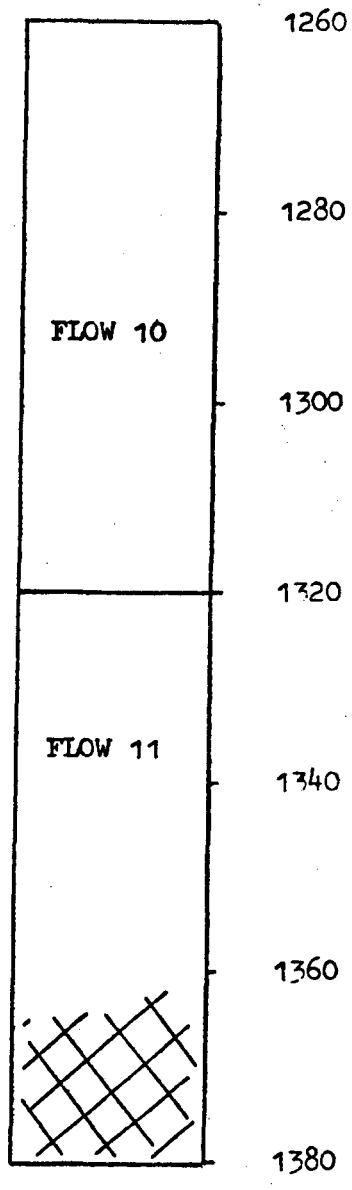

FLOW 11. Light gray andesite with small phenocrysts of Pl and Opx in a holocrystalline light gray matrix. Return contains abundant oxidized rock starting at 1360' which indicates that the base of the flow may be just below the bottom of the drill hole.

No thin section

Bottom of hole at 1380'.

APPENDIX II

Radiometric Dating

Three samples of cuttings from the Old Maid Flat drill hole (2S/8E-15cd) were dated by the potassium/argon method. Samples OMF-2953 and OMF-3530 are from basaltic units that have been identified by optical and geochemical methods as members of the Columbia River Group (Beeson and Moran, 1978). OMF-3970 is from an andesite flow below the Columbia River Basalt. All three dates (Table 5) are anomalously young; the dated units most likely suffered loss of radiogenic argon as a result of one or more post-Miocene thermal events.

Two potassium/argon dates also were obtained from whole rock samples from pre-Mt. Hood units. HD-64 is a sample of hornblende dacite from the northwest peak of Mill Creek Buttes (1S/10E-27d d). Wise (1969) identified two domes and several associated flows at Mill Creek Buttes and, because of their constructional form, believed them to be of Pleistocene age. The K/Ar dates obtained for the present study indicate that these rocks are considerably older than Wise's estimate and were probably erupted toward the end of the episode of volcanism that produced the lower Pliocene Rhododendron and Dalles formations.

Sample HD-62 is from a lava flow that is exposed in a road cut just north of Still Creek (3S/8E-29d). The flow is intruded by the Still Creek granodiorite. Because the sample was taken within 100 yards of the contact, it is likely that the date may reflect the age of the thermal event associated with the

TABLE 5

RADIOMETRIC DATES

Sample No.	% K	Ar (cc/g)	% Ar	A (m.y.)
OMF-2953	1.1577	5.5205×10^{-7}	4.75	12.2 ± 2.0
OMF-3530	1.2935	2.9802×10^{-7}	4.38	5.9 ± 1.1
OMF-3970	0.8711	2.6895×10^{-7}	7.62	7.9 ± 0.8
HD-64	0.7170	2.0786×10^{-7}	13.57	7.5 ± 0.4
HD-62	1.1170	4.0346×10^{-7}	20.76	9.3 ± 0.3

Still Creek - Laurel Hill plutonism. The 9.27 m.y. date does in fact fall within the age range cited by other authors for the Laurel Hill pluton (Bickerman, 1971).

It should be noted that the major element composition of the flow from which sample HD-62 (Table 6) was taken is unlike that of any previously reported lower Pliocene lava. The high ratio of total Fe/Mg and the high TiO_2 content are suggestive of Columbia River Basalt composition; however, the altered nature of the sample precluded a confident geochemical correlation.

TABLE 6

MAJOR ELEMENT COMPOSITION

	HD-64	HD-62
SiO_2	62.89	51.62
TiO_2	.71	1.82
Al_2O_3	17.42	14.43
MgO	2.79	4.77
Fe_2O_3	5.20	13.41
CaO	6.04	8.75
Na_2O	3.87	3.69
K_2O	.85	.99
P_2O_5	.14	.30

REFERENCES

Beeson, M. H., and Moran, M. R., 1978, Columbia River Basalt Stratigraphy in Old Maid Flat Deep Drill Hole: Unpublished Report, p. 1-6.

Bickerman, M., 1970, K-AR Ages of Laurel Hill Pluton and Dike, Oregon: The Ore Bin, v. 32, n. 11, p. 211-215.

Buddington, A. F., and Lindsley, D. H., 1964, Iron-Titanium Oxide Minerals and Synthetic Equivalents, J. Petrol, v. 5, p. 310-357.

Crandall, D. R., and Rubin, M., 1977, Late-Glacial and Post-Glacial Eruptions at Mt. Hood, Oregon: Geol. Soc. Am. Abs. with Programs 9, n. 4.

Kudo, A. M., and Weill, D F., 1970, An Igneous Plagioclase Thermometer: Contrib. Mineral. Petrol., v. 25, p. 52-65.

Nicholls, J., Carmichael, I. S. E., and Stormier, J. C., 1971, Silica activity and P_{total} in Igneous Rocks: Contr. Mineral. Petrol., v. 35, p. 20.

Smith, R. L., and Shaw, H. R., 1975, Igneous-Related Geothermal Systems, in: Assessment of Geothermal Resources of the United States: U. S. Geological Survey Circular 726, p. 58-84.

Thorarinsson, S., 1954, The Tephra Fall from Hekla on March 29, 1947, in: The Eruption of Hekla 1947-48, II: Soc. Scient. Islandica., p. 68.

Wise, W. S., 1969, Geology and Petrology of the Mt. Hood area: a Study of High Cascade Volcanism: Geol. Soc. Am. Bull., v. 80, p. 969-1006.

Wood, B. J., and Banno, S., 1973, Garnet-orthopyroxene and orthopyroxene-clinopyroxene Relationships in Simple and Complex Systems: Contrib. Mineral. Petrol., v. 42, p. 109-124.

GRAVITY MEASUREMENTS IN THE AREA OF MOUNT HOOD, OREGON

By

RICHARD COUCH
MICHAEL GEMPERLE

Geophysics Group

School of Oceanography

Oregon State University

May 1979

Final report of work carried out under OSU Grant No. 30-262-9117 from the Oregon Department of Geology and Mineral Industries; July 1977 through March 1979.

GTR 790517

TABLE OF CONTENTS

Page

ABSTRACT..... 142

GRAVITY ANOMALIES IN THE AREA OF MOUNT HOOD, OREGON..... 143

Gravity Measurements..... 143

Reduction of the Gravity Measurements..... 148

Free-Air Gravity Anomalies..... 150

Bouguer Gravity Anomalies..... 152

Regional Gravity Anomalies..... 161

MODELS OF MOUNT HOOD..... 169

ELEVATION OF THE COLUMBIA RIVER BASALT..... 176

POROSITY ESTIMATES..... 181

TRAVEL TIME RESIDUALS..... 185

ACKNOWLEDGEMENTS..... 187

REFERENCES..... 188

APPENDIX..... 189

LIST OF FIGURES

		Page
1	TOPOGRAPHIC MAP OF MOUNT HOOD	144
2	GRAVITY STATION LOCATION MAP	146
3	FREE-AIR GRAVITY ANOMALY MAP OF MOUNT HOOD	151
4	COMPLETE BOUGUER GRAVITY ANOMALY MAP OF MOUNT HOOD. REDUCTION DENSITY 2.67 gm/cm^3	153
5	GRAPH OF THE STANDARD DIVIATION OF THE COMPLETE BOUGUER ANOMALIES VERSUS THE COMPLETE BOUGUER REDUCTION DENSITY	155
6	COMPLETE BOUGUER GRAVITY ANOMALY MAP OF MOUNT HOOD. REDUCTION DENSITY 2.27 gm/cm^3	156
7a	COMPLETE BOUGUER GRAVITY ANOMALY MAP: TIMBERLINE AREA. REDUCTION DENSITY 2.67 gm/cm^3	160
7b	COMPLETE BOUGUER GRAVITY ANOMALY MAP: TIMBERLINE AREA. REDUCTION DENSITY 2.27 gm/cm^3	160
8	REGIONAL GRAVITY ANOMALY MAP OF THE MOUNT HOOD AREA: > 13 km/cycle	163
9	RESIDUAL GRAVITY ANOMALY MAP OF THE MOUNT HOOD AREA: < 13 km/cycle	164
10	REGIONAL GRAVITY ANOMALY MAP OF THE MOUNT HOOD AREA: > 8.1 km/cycle	165
11	RESIDUAL GRAVITY ANOMALY MAP OF THE MOUNT HOOD AREA: < 8.1 km/cycle	167
12	SPHERE MODEL CONSISTENT WITH MOUNT HOOD GRAVITY ANOMALIES	170
13	CYLINDRICAL CORE MODEL OF MOUNT HOOD	171
14	CYLINDER AND CONE MODEL CONSISTENT WITH MOUNT HOOD GRAVITY ANOMALIES	173
15	DENSITY CONTRAST VERSUS RADIUS FOR CYLINDER AND CONE MODEL	174
16	ESTIMATED ELEVATION OF THE COLUMBIA RIVER BASALTS	178
17	COMPARISON OF MAPPED AND COMPUTED PRE-PLIOCENE TOPOGRAPHIC SURFACE	180
18	ESTIMATED POROSITIES IN MOUNT HOOD AREA	183

LIST OF FIGURES (Con't.) Page

19 ESTIMATED SEISMIC WAVE TRAVEL-TIME RESIDUALS IN MOUNT HOOD AREA..... 186

LIST OF TABLES

Page

1 APPENDIX..... 189

2 ANDESITE DENSITIES AND VELOCITIES..... 181

ABSTRACT

The analysis of gravity measurements at 337 stations on and about Mount Hood indicate lateral and vertical variations in the density of the flows and pyroclastics in and beneath Mount Hood. Complete Bouguer gravity anomalies indicate that the axis of Mount Hood is located on an elongate gravity high, oriented approximately N75E. Mount Hood is superimposed on a gravity low that extends from north of the mountain to the southern extent of the survey area. The gravity low suggests a north-south oriented graben-like structure. Prominent lineations in the gravity anomalies oriented approximately N23W occur both northwest and southwest of Mount Hood. A simple cone-on-a-cylinder model for the core of Mount Hood agrees with the gravity anomalies. Long wavelength anomalies suggest that undulations in the Columbia River Basalts beneath and about Mount Hood range from less than 500 m to over 1400 m above sea level. Porosities of the average rocks which comprise Mount Hood are estimated to be approximately 20 to 30 percent and the density is approximately 2.27 gm/cm^3.

GRAVITY ANOMALIES IN THE AREA OF MT. HOOD, OREGON

Gravity Measurements

Personnel of the Geophysics Group, Oregon State University (OSU) conducted a gravity survey in the High Cascade Mountains of northern Oregon during August and September, 1977 and August and September, 1978. The survey area which extends from 45°10' to 45°35'N lat. and from 121°25' to 122°00'W long. includes the picturesque 3424 m (11235 ft) high Mt. Hood stratovolcano and many surrounding foothills and mountains of the Cascade Range.

Figure 1 shows a topographic map of the area of and about Mt. Hood based on data contained on the U. S. Geological Survey (USGS) 1:250,000 quadrangle map, The Dalles NL 10-9. The map, contoured at an interval of 1000 ft (304.8 m), shows approximately 10,000 ft (3050 m) of topographic relief in the area of Mt. Hood. Mt. Hood, a relatively symmetric volcanic cone of Late Pleistocene to Holocene age, is surrounded by a north-south trending ridge over 6000 ft (1830 m) in elevation on the east and southeast side and isolated mountains and dissected ridges on the south, west, and northwest sides. Mt. Hood is composed almost entirely of pyroxene andesite and rises 8000 ft (2400 m) above a platform of Pliocene andesites and basalts (Wise, 1969). The high relief and few roads make access to the area difficult; consequently to achieve an approximately uniform grid of gravity stations most measurements were made by back-packing the meter to the station sites.

Mr. Kenneth Keeling, with the assistance of Messeurs.

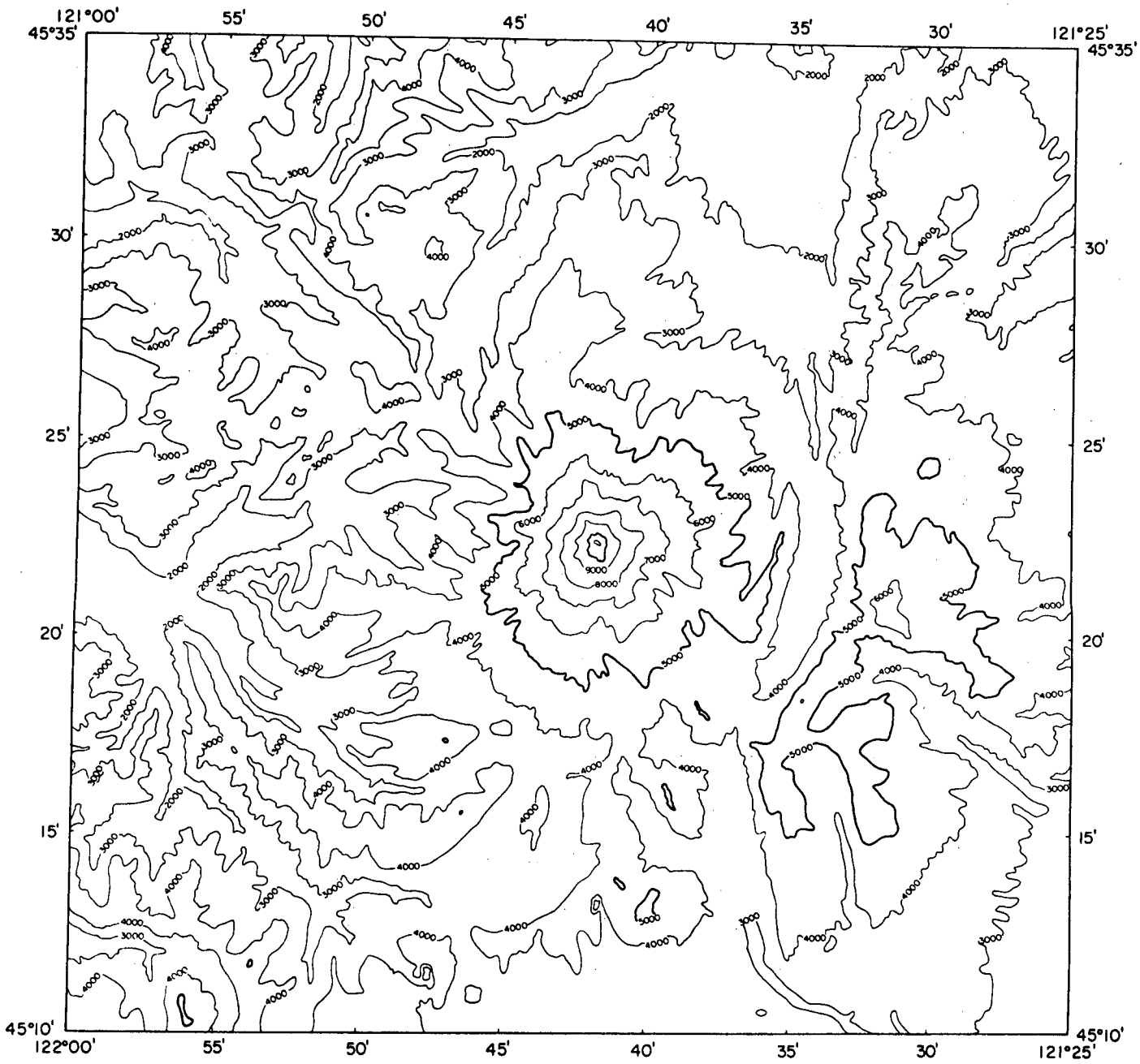

TOPOGRAPHIC MAP
MOUNT HOOD AREA, OREGON

DATA FROM USGS 1 250,000 QUADRANGLE MAP
THE DALLES NL 10-9

KILOMETERS
0 2 4 6 8
0 1 2 3 4 5
MILES

UNIVERSAL TRANSVERSE MERCATOR PROJECTION
CONTOUR INTERVAL 1000 FEET

OREGON STATE UNIVERSITY
DECEMBER, 1977

Figure 1

Terry Jones, William Plank, and Mark Brown obtained gravity measurements at 239 stations in the approximately 2000 km^2 area. Messeurs. Gordon Ness and John Bowers established 51 closely spaced gravity stations in the vicinity of the geothermal test hole south southeast of Timberline Lodge (3S/9E-7ca) on the south slope of Mt. Hood and added an additional 33 stations to the area survey. These stations, combined with station data from the Oregon State University Library (Thiruvathukal, 1968), total 337 and yield an approximate spatial density of one station per 6 km^2.

Figure 2 shows the locations of the 337 gravity stations in the Mt. Hood survey area. In addition to the approximately uniform scatter of stations in the area, a high concentration of stations which form a plus sign near the middle of the map, occur along lines which extend north, south, east and west from a point near the site of the geothermal test hole. Gravity stations are concentrated also toward the south and west along Highway U. S. 26 on the south flank of Mt. Hood. A solitary gravity station is located on the summit of Mt. Hood.

Base stations for the measurements were established at Zigzag Ranger Station, Government Camp, White Bridge Park, Parkdale, and near Cooper Spur. The Zigzag Ranger Station gravity base station (980,489.14 mgl) was tied to the USAF gravity base station WA-142A (Woollard and Rose, 1963) located at Portland International Airport (980,648.3 mgl) by personnel of the USGS (personnel comm. D. G. Barnes, 1969) and by the personnel of the OSU Geophysics Group (unpublished data, OSU Gravity Library, 1975). The detailed survey near Timberline

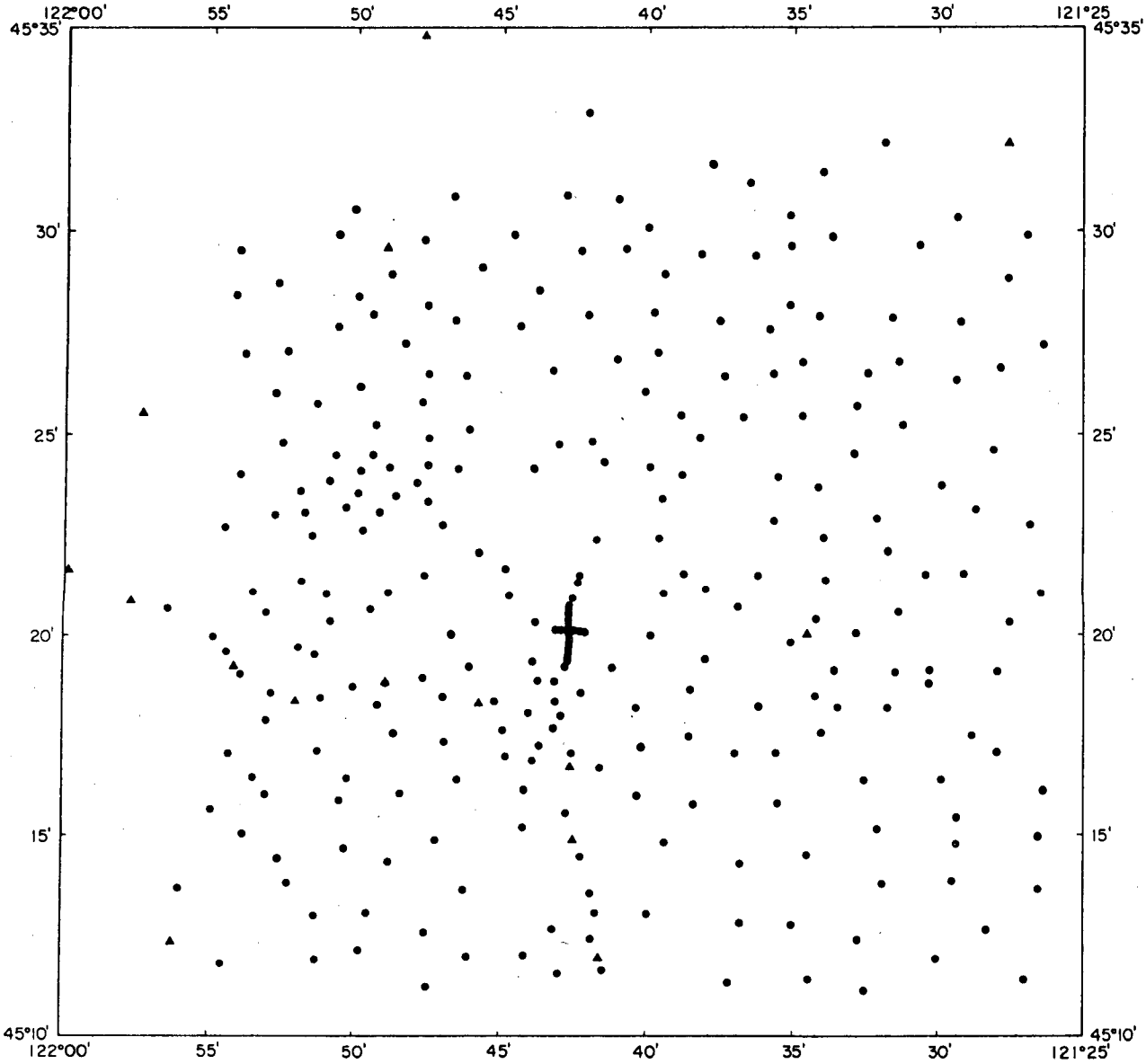

GRAVITY STATIONS
MOUNT HOOD AREA, OREGON

AREA OF THIS MAP

GRAVITY STATIONS
▲ J. THIRUVATHUKAL . 1969 OSU
● K KEELING 1977 OSU
G. NESS & J BOWERS 1978 OSU

KILOMETERS
0 2 4 6 8
0 1 2 3 4 5
MILES

UNIVERSAL TRANSVERSE MERCATOR PROJECTION

OREGON STATE UNIVERSITY
DECEMBER, 1978

Figure 2

Lodge is referenced to the gravity base station at Zigzag Ranger Station. The measurements were made with a LaCoste and Romberg Model G Geodetic Gravity Meter #126.

USGS benchmarks, spot elevations on USGS 7.5 minute and 15 minute topographic maps and barometric altimetry provided vertical control for the gravity stations. The estimated uncertainties in the vertical control associated with these methods of elevation determination are $\pm$ 1, $\pm$ 5, and $\pm$ 10 feet respectively. A recording barometer base station, used to monitor barometric changes during the survey, provided data to ascertain the validity and accuracy of altitudes determined by barometric altimetry.

USGS 7.5 minute and 15 minute topographic maps were used to determine horizontal position. The estimated uncertainty in horizontal position is $\pm$ 0.02 minutes of latitude and longitude. MSS Inc., Corvallis, established reference points for the gravity stations near the geothermal drill site. The positions and elevations of the detailed gravity survey, determined by triangulation and leveling techniques, were established with reference to a USGS benchmark at Timberline Lodge. The estimated uncertainty is less than $\pm$ 0.3 meters in the horizontal position of each station and less than $\pm$ 0.3 meters in the vertical elevation of each station with respect to the USGS benchmark.

The observed gravity was corrected for earth tides using the formulation of Longman (1959) and for meter drift by linear interpolation between values observed at reoccupied base stations. The mean drift of the gravity meter observed during

reoccupation of base stations at the end of a gravity traverse or loop was $\pm$ 0.04 mgl and the standard deviation was 0.09 mgl. The maximum observed drift was 0.47 mgl. The uncertainties in the measurements caused by the drift of the meter is generally much less than caused by the uncertainties in the corresponding station elevations.

Reduction of the Gravity Measurements

The gravity measurements were reduced to free-air and complete Bouguer gravity anomalies with standard techniques. The following equation from Scheibie and Howard (1964) and Oliver (1973), used in this study, yields the free-air gravity anomaly:

$$FAA = OG - THG + (0.09411549 - 0.000137789 \sin^2\theta)h - 0.67 \times 10^{-8} h^2$$

where,

FAA = Free-air anomaly in milligals

OG = Observed gravity in milligals

THG = Theoretical gravity in milligals

θ = Latitude

h = Elevation in feet

The International Gravity Formula (IGF), yields theoretical gravity (THG) values at designated latitudes. The IGF of 1930 (Swick, 1942), used in this study, is:

$$THG = 978049.0 \ (1 + .0052884 \sin^2 \phi - 0.0000059 \sin^2 2\phi)$$

The following equation yields the complete Bouguer gravity anomaly (CBA).

$$CBA = FAA - 2\pi Gph + TCC - CC$$

where,

CBA = Complete Bouguer gravity anomaly in milligals

FAA = Free-air gravity anomaly in milligals

and G = Universal gravitational constant (6.67×10^{-8}cgs)

p = Reduction density in gm/cm^3

h = Elevation in feet

TTC = Total terrain correction in milligals

CC = Curvature correction = $hp\ (1.671 \times 10^{-8} + h[-1.229 \times 10^{-8} + h(4.76 \times 10^{-16})]$ milligals (Oliver, 1973)

Terrain corrections for each station account for the change in gravity caused by topography about the station. Total terrain corrections, (TTC) for each station were computed for topography within a distance of 166.7 km of the station. This distance is equivalent to Hayford-Bowie zone "0" (Swick, 1942). A computer program written by D. L. Plouff (1977a) of the USGS which uses digital terrain data was used to compute terrain corrections. The program also incorporated a modification of the program developed by Plouff (1977b) which permitted the calculation of the terrain correction for the distance interval zero to 0.895 km, Hammer's zone F (Hammer, 1939). The digital terrain data was based on the National Cartographic and Information Center 0.01 inch digitization of 1:250,000 scale topographic maps. These data provide the average elevation in 0.5, 1.0 and 3.0 minute square areas. The gravitational effects of the topography were calculated for radial distances from zero to 2.29 km using topography digitzied at 0.5 minute increments, from 2.29 km to 15 km using 1.0 minute data, and 15 km

to 166.7 km using 3 minute data. The terrain effect calculated for the area between 0 and 2.29 km of the station exceeded 5.0 mgls for 40 stations. Subsequently these stations were recalculated by hand, utilizing a method outlined by Oliver and others (1969).

Table 1 (Appendix) lists the principal facts for each gravity station in the Mount Hood study area. The table heading explains the column designations. The table does not list the parameters or values of special reductions or analyses described in this report, however, these can be calculated from the principal facts and the relations described in the appropriate text of this report.

Free-Air Gravity Anomalies

Figure 3 shows a free-air gravity anomaly map of the Mount Hood area based on measurements at the station locations shown in Figure 2. The map contours are at intervals of 10 mgl and heavy contours occur at 0, 50, 100 and 150 mgl levels. The free-air anomalies reflect the very irregular topography of the area and the 0 mgl contour of the gravity map coincides approximately with the 3000 foot topographic contour in Figure 1. The summit of Mount Hood, approximately in the center of the map, exhibits a free-air anomaly of greater than +150 mgls. Elongate gravity anomaly lows near 45°30'N lat and 121°35' and 121°45'W long are oriented approximately north-south. The easternmost gravity anomaly low extends southward past Mount Hood at least to the southern limit of the survey area. The westernmost gravity low extends to just west of Mount Hood where it appears

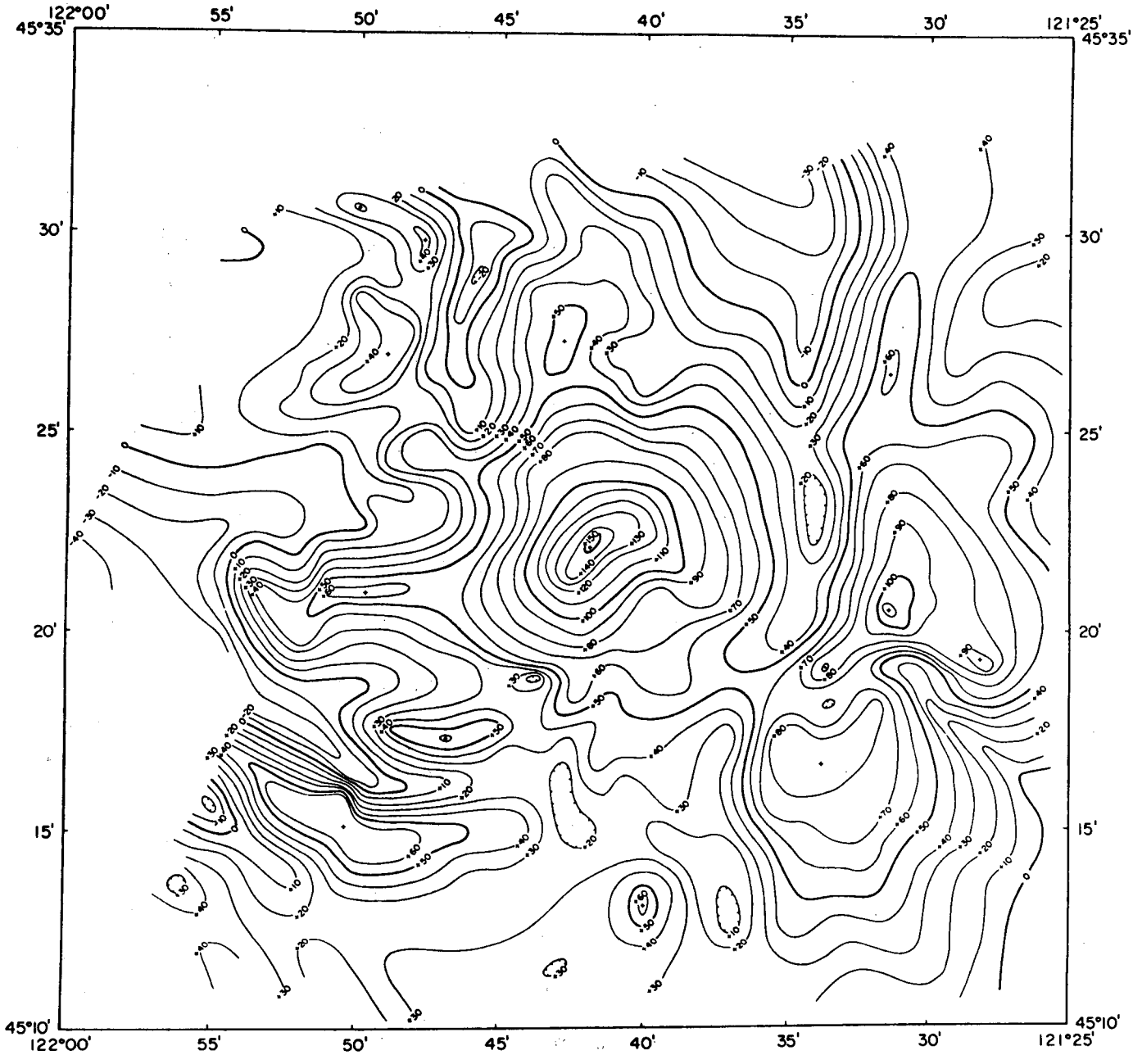

FREE-AIR GRAVITY MAP
MOUNT HOOD AREA, OREGON

GRAVITY DATA FROM
J THIRUVATHUKAL 1969 OSU
K KEELING 1977 OSU

KILOMETERS
0 2 4 6 8
0 1 2 3 4 5
MILES

OREGON STATE UNIVERSITY
DECEMBER, 1977

UNIVERSAL TRANSVERSE MERCATOR PROJECTION
CONTOUR INTERVAL 10 MGALS
ESTIMATED STATION UNCERTAINTY ±2 MGAL

Figure 3

to be interrupted by a series of gravity highs oriented approximately east-west. The two north-south trending lows suggest a major structural offset in the basement rocks beneath the post-Miocene rocks which form Mount Hood. The relatively short wavelength, positive anomalies associated with Mount Hood and the surrounding mountains suggest the mountains are not locally compensated to any significant extent and consequently are interpreted as localized loads imposed on a relatively rigid crust or lithosphere.

Bouguer Gravity Anomalies

Figure 4 shows a complete Bouguer gravity anomaly map of the Mount Hood area. The map, prepared using a standard reduction density of 2.67 gm/cm^3, exhibits contours at intervals of 2 mgls and heavy contours at 10 mgl intervals. A marked gravity low of less than -108 mgls occurs on Mount Hood. This gravity low is the most negative part of a larger gravity low which extends north of Mount Hood to about 45°30' and extends south of Mount Hood at least to the limit of the survey area. The negative anomaly, closed north of Mount Hood, is open to the south and suggests a large geologic feature on which Mount Hood is superimposed that begins in the vicinity of Mount Hood and extends southward. The anomalies east of Mount Hood near 45°20-25'N lat and 121°30-34' W long show only a small correlation with topography; hence, the average density of the near-surface rocks which form the topographic features is near 2.67 gm/cm^3. The negative correlation between the topography and gravity anomaly of Mount Hood and the mountains west and south

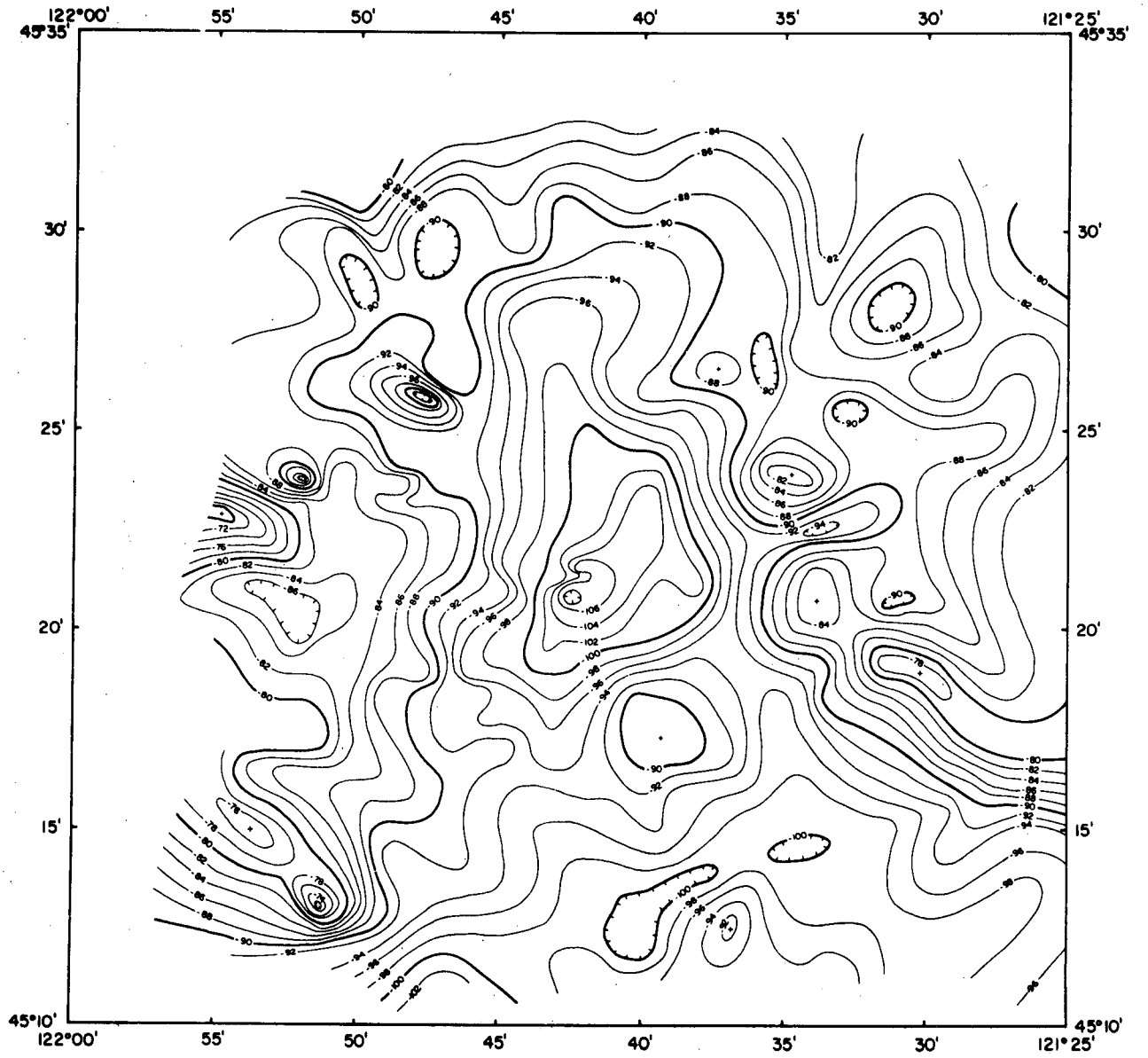

COMPLETE BOUGUER GRAVITY ANOMALY MAP

MOUNT HOOD AREA, OREGON

GRAVITY DATA FROM

J. THIRUVATHUKAL	1969	O.S.U.
K. KEELING	1977	O.S.U.
G. NESS & J. BOWERS	1978	O.S.U.

KILOMETERS
0 2 4 6 8
0 1 2 3 4 5
MILES

OREGON STATE UNIVERSITY
DECEMBER, 1978

UNIVERSAL TRANSVERSE MERCATOR PROJECTION
CONTOUR INTERVAL 2 MGALS
ESTIMATED STATION UNCERTAINTY ±2 MGAL
REDUCTION DENSITY 2.67 gm/cm³

Figure 4

of Mount Hood suggest the standard reduction density (2.67 gm/cm^3) is greater than the average density of the rocks which form the mountains.

Computation of the standard deviation of the complete Bouguer anomalies of a region yields an indication of the correlation of the anomalies and the topography of the region. Figure 5 shows a graph of the standard deviation of the complete Bouguer gravity anomaly as a function of density for the Mount Hood area. The curve shows a minimum when the density equals 2.27 gm/cm^3. To determine a regional density for Mount Hood the gravity station data were separated into a set which included all the stations and a subset which included only the stations located on Mount Hood proper. Both sets of data indicate approximately the same density, 2.27 gm/cm^3, when the standard deviation of the computed anomalies is a minimum. Although the density of 2.27 gm/cm^3 yields anomalies with a minimum correlation with the topography of the area, the curve in Figure 5 is relatively flat near the minimum and suggests the actual densities of the topographic features have a broad range. For example, the Bouguer gravity anomalies in Figure 4 suggest the average density of the mountains immediately east of Mount Hood is greater than 2.27 gm/cm^3 and may be as high as 2.7 gm/cm^3.

Figure 6 shows a complete Bouguer anomaly map of the Mount Hood area based on a reduction density of 2.27 gm/cm^3. The Bouguer anomaly associated with Mount Hood is less than -64 mgls; however, it is actually an anomaly high with respect to the surrounding anomalies. The anomaly high associated with

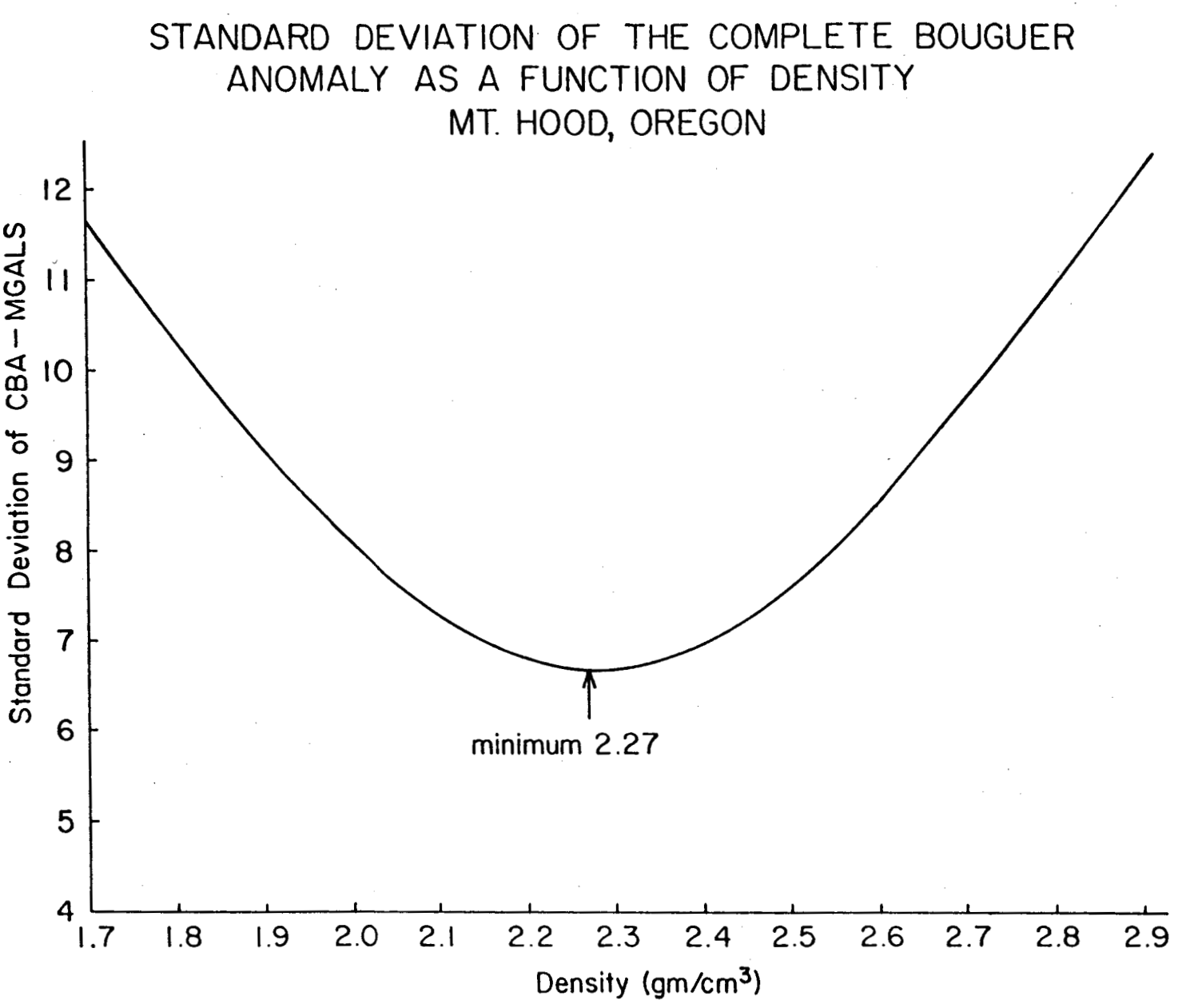
STANDARD DEVIATION OF THE COMPLETE BOUGUER ANOMALY AS A FUNCTION OF DENSITY MT. HOOD, OREGON
Standard Deviation of CBA – MGALS
12
11
10
9
8
7
6
5
4
minimum 2.27
1.7
1.8
1.9
2.0
2.1
2.2
2.3
2.4
2.5
2.6
2.7
2.8
2.9
Density (gm/cm3)

Figure 5

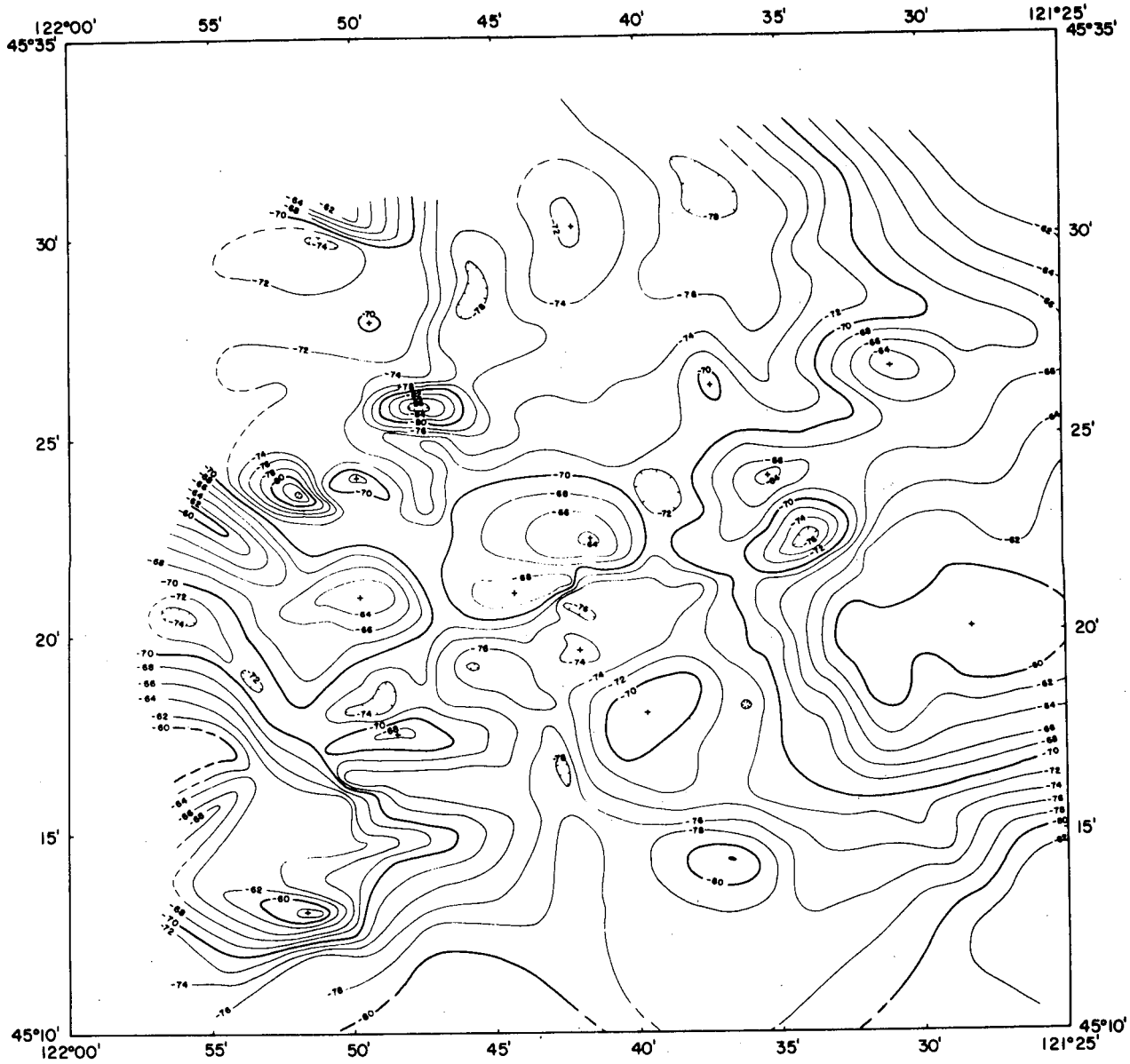

COMPLETE BOUGUER GRAVITY ANOMALY MAP
MOUNT HOOD AREA, OREGON

GRAVITY DATA FROM

J. THIRUVATHUKAL	1969	OSU
K. KEELING	1977	OSU
G. NESS & J. BOWERS	1978	OSU

KILOMETERS
0 2 4 6 8
0 1 2 3 4 5
MILES

OREGON STATE UNIVERSITY
DECEMBER, 1978

UNIVERSAL TRANSVERSE MERCATOR PROJECTION
CONTOUR INTERVAL 2 MGALS
ESTIMATED STATION UNCERTAINTY ±2 MGAL
REDUCTION DENSITY 2.27 gm/cm³

Figure 6

Mount Hood is flanked on the northeast and southwest by Bouguer anomaly highs. Together, these contiguous highs suggest a structural high, oriented approximately N75E, beneath the Plio-Pleistocene rocks which form Mount Hood and the surrounding mountains. The gravity high transects at an angle what appears to be an extensive north-south oriented gravity low. The east side of the gravity low exhibits higher gradients and is generally better delineated than the west side. The low suggests a graben-like structure with the east farther down and/or bounded by more prominent faults than the west side.

This interpretation of the gravity anomalies suggests Mount Hood sets in and covers to some extent a north-south oriented graben. The gravity high near the center of Mount Hood suggests its location may be structurally controlled in that the central vent lies along a structural ridge indicated by the contiguous gravity highs which cross the north-south gravity low. An alternative explanation of the gravity high associated with Mount Hood is that it reflects the internal structure of the mountain and may indicate the main vent or core of the mountain. Because of the sparcity of stations, gravity anomalies are not well delineated near the summit.

South of Mount Hood, near 45°15'N lat., gravity gradients suggest a structural lineation oriented approximately N85 E. The senior author has speculated, on the basis of the alignment of earthquake epicenters and SLAR imagery, that a fault - possibly a thrust fault - may extend along the base of Mount Hood on the south side. The gravity anomalies are consistent

with this hypothesis but do not strongly support it.

Prominent lineations in the gravity anomalies oriented approximately N23°W occur both northeast and southwest of Mount Hood. Two lineations northeast and two southeast of Mount Hood appear to extend completely across the area mapped in the gravity survey and may be complementary to the east northeast-south southwest lineations described above.

Many closed short-wavelength anomalies occur also in the area and are very likely associated with surface or very near surface structural and/or compositional features.

Closely spaced gravity stations occur along lines which extend north, south, east and west from gravity station GS 33 which is located 70 feet west of the geothermal drill hole south of Timberline Lodge. To obtain accurate gravity measurements differential leveling was used to determine the station elevations. The initial elevation, 5936', was stamped in the USDA, Bureau of Public Roads BM 50-1, located in the front steps of Timberline Lodge. A stadia survey connected all gravity stations to an X-Y coordinate system. The initial azimuth, 190°, was scaled from the Pucci chairlift as shown on 7.5 minute USGS Topographic Map, Mount Hood. Poor weather prevented additional ties. Longitudes and Latitudes of the stations were computed based on:

a) The initial station MHL 8 latitude (45° 19.87') and longitude (121° 42.61')

b) The scale 1" of latitude = 101.27 feet at 45°20' N lat. as per Oregon Plane Coordinate Projection Tables SP 270

c) And a scale ratio at 45°20' of 1" long/1" lat = 0.708 and 1" long = 71.699 feet.

Table 1 in the back of this report lists the latitude, longitude and gravity anomaly values for the gravity survey near the Timberline drill site.

Figure 7a shows a complete Bouguer gravity anomaly, based on a reduction density of 2.67 gm/cm^3, around the Timberline geothermal drill site at approximately 45°19.7'N lat, 121°42.6'W long. The map indicates a general east-west trend to the anomaly contours and decreasing anomalies towards the north away from the drill site. The gravity anomalies contoured at an interval of 2 mgls suggest a relatively uniform structure in the vicinity of the drill site and rock layers of a relatively low density.

Figure 7b shows a complete Bouguer anomaly of the same area as Figure 7a but based on a reduction density of 2.27 gm/cm^3. This density as discussed previously, is more representative of the average density of the rocks of Mount Hood. Figure 7b indicates that the drill site is located on a relative gravity high. The Bouguer anomaly high is of low amplitude and closed. The anomaly suggests a thickening of the more dense layers which form this sector of Mount Hood, an intrusive body, or a doming of the layers. A density contrast of 0.6 gm/cm^3 between massive andesite (2.6 gm/cm^3) and andesitic ash containing water (2.0 gm/cm^3) suggests a flow or intrusive thickness of approximately 80 m. A relatively steep gradient in the gravity anomalies which trends approximately east northeast-west southwest occurs north of the drill site near 45°21'N

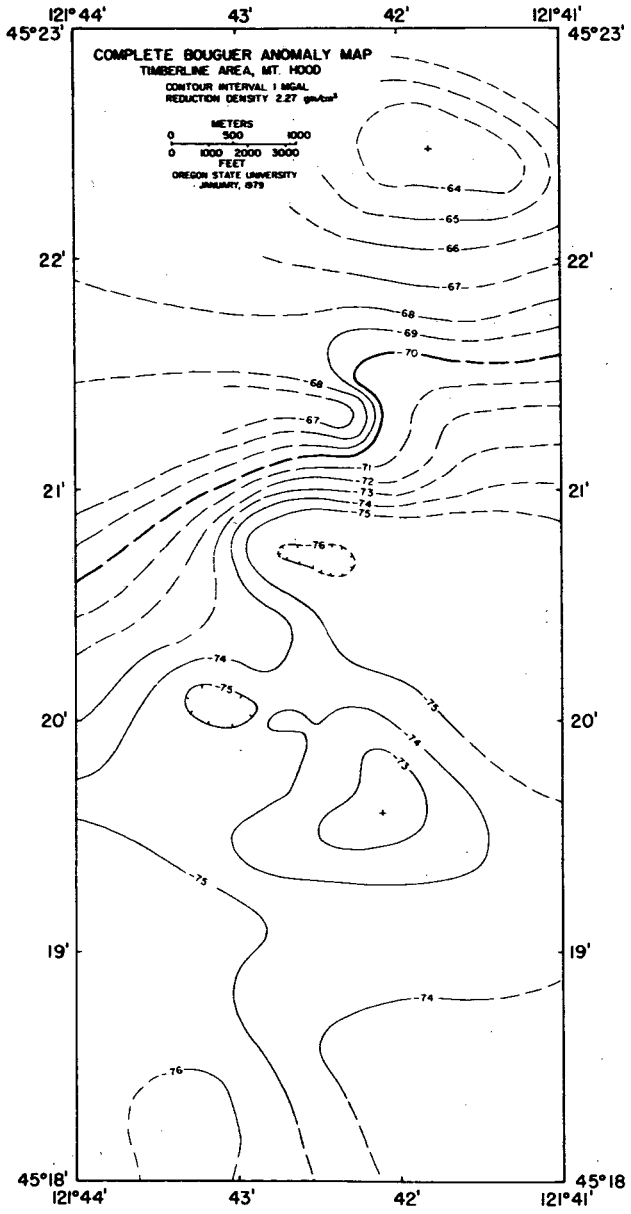

Figure 7b

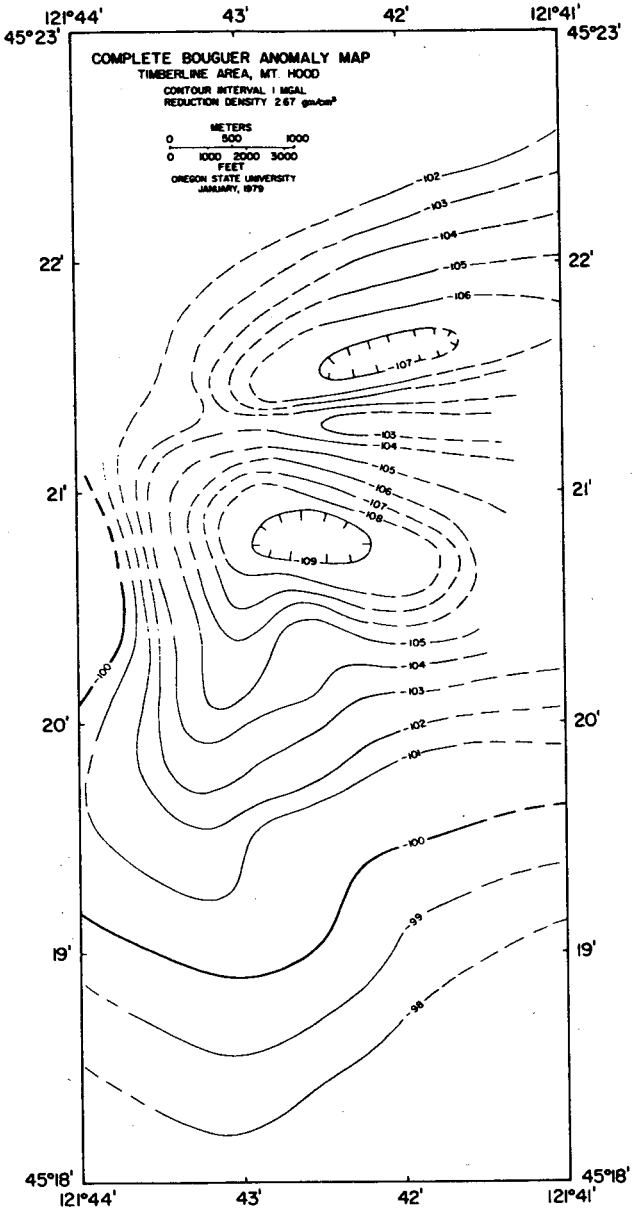

Figure 7a

lat. The anomaly is positive to the north and suggests that either a higher density layer (or flow) extends southward beneath the surface ash and cinder to approximately 45°21' or that a structural break (or fault) occurs in the subsurface layers with the southside down about one mile north of the drill site. Other interpretations are also possible, however, the gravity measurements do not indicate any marked lateral variations in structure or density in the immediate vicinity of the drill site.

Regional Gravity Anomalies

Spectral separation of the short and long wavelength components of the complete Bouguer anomalies of the Mount Hood area yields "regional gravity anomalies" and "residual gravity anomalies". Estimates of the frequency at which the spectral separation should occur were based initially on the wavelengths of the topography of the region. The authors postulated that, because of a relatively high density contrast, the long wavelength gravity anomalies more likely would be associated with the pre-Pliocene rocks of the region such as the Columbia River Basalts and the short wavelength anomalies would reflect shallow sources caused by lateral and vertical variations in the Pliocene and Holocene rock and ash which form Mount Hood and the surrounding mountains of the High Cascades. The initial spatial frequency separating the long and short wavelength parts of the gravity anomaly spectrum was 5 cycles per 65 kilometers or 13 km per cycle. Later iterations based on attempts to determine a "surface" for the Columbia River Basalts from the gravity

measurements as described below indicated a better separation of the anomaly wavelengths occurred at 8 cycles per 65 km or 8.1 km/cycle. Subsequently regional and residual anomalies separated spectrally at 8.1 km/cycle, were recomputed from the complete Bouguer anomalies shown in Figure 6.

Figure 8 shows a map of the regional gravity anomaly of the Mount Hood area with wavelengths longer than 13 km. The map shows gravity highs which trend generally north-south on the east and west sides of the map. Between the gravity highs a north-south trending gravity low suggests a depression or graben-like structure in the upper crustal rocks beneath the post-Miocene rocks of the High Cascades. A gravity high oriented approximately east-west transects the large north-south gravity low. The center of Mount Hood is located approximately on the east-west gravity high and the mountain's "core" may contribute to the positive anomaly.

Figure 9 shows a map of the residual gravity anomalies of the Mount Hood area shorter than 13 km. The map shows a large number of closed gravity highs and lows. These anomalies suggest density variations in the post-Miocene rocks of the area and may relate to individual flows or intrusions. No attempt was made to correlate these anomalies with the surface or near-surface geology.

Figure 10 shows a map of the regional gravity anomaly of the Mount Hood area with wavelengths longer than 8.1 km. The map includes shorter wavelength components than the map shown in Figure 8 and therefore shows more irregularity or character in the anomaly contours and steeper anomaly gradients.

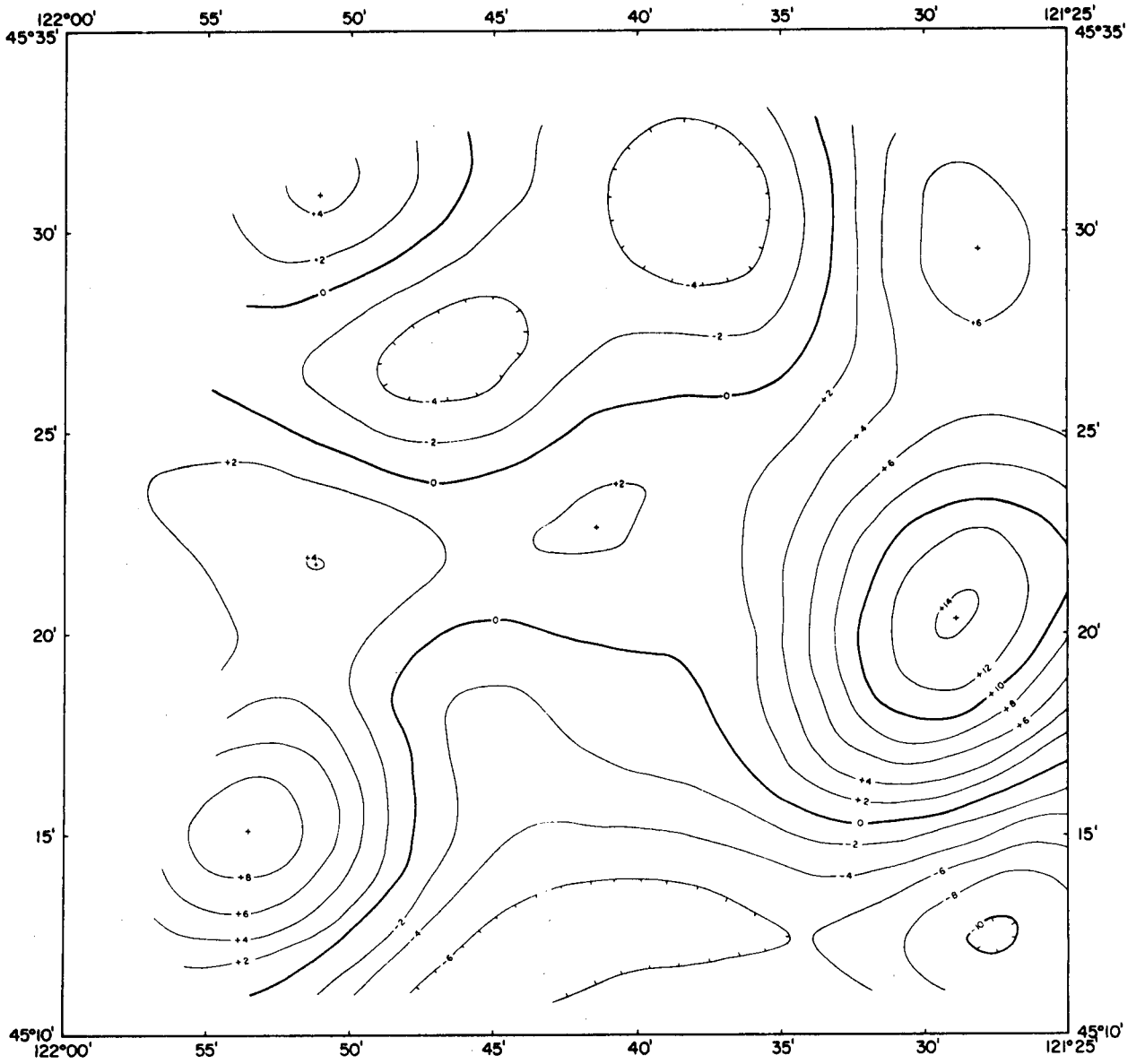

REGIONAL GRAVITY MAP
MOUNT HOOD AREA, OREGON

AREA OF THIS MAP

CONTOUR INTERVAL 2 MGALS

KILOMETERS
0 2 4 6 8
0 1 2 3 4 5
MILES

UNIVERSAL TRANSVERSE MERCATOR PROJECTION

OREGON STATE UNIVERSITY
DECEMBER, 1978

Figure 8

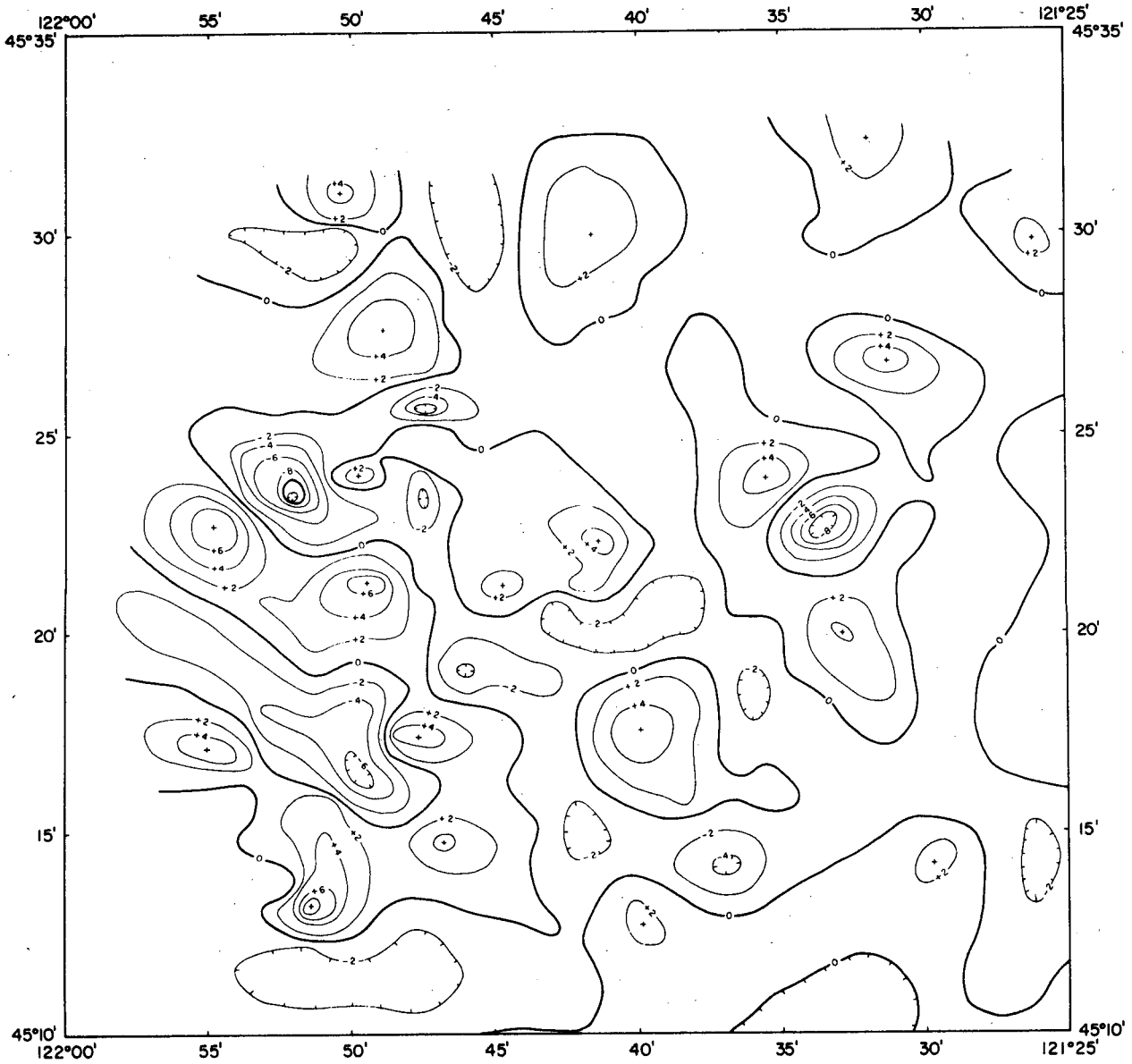

RESIDUAL GRAVITY MAP
MOUNT HOOD AREA, OREGON

AREA OF THIS MAP

CONTOUR INTERVAL 2 MGALS

KILOMETERS
0 2 4 6 8
0 1 2 3 4 5
MILES

UNIVERSAL TRANSVERSE MERCATOR PROJECTION

OREGON STATE UNIVERSITY
DECEMBER, 1978

Figure 9

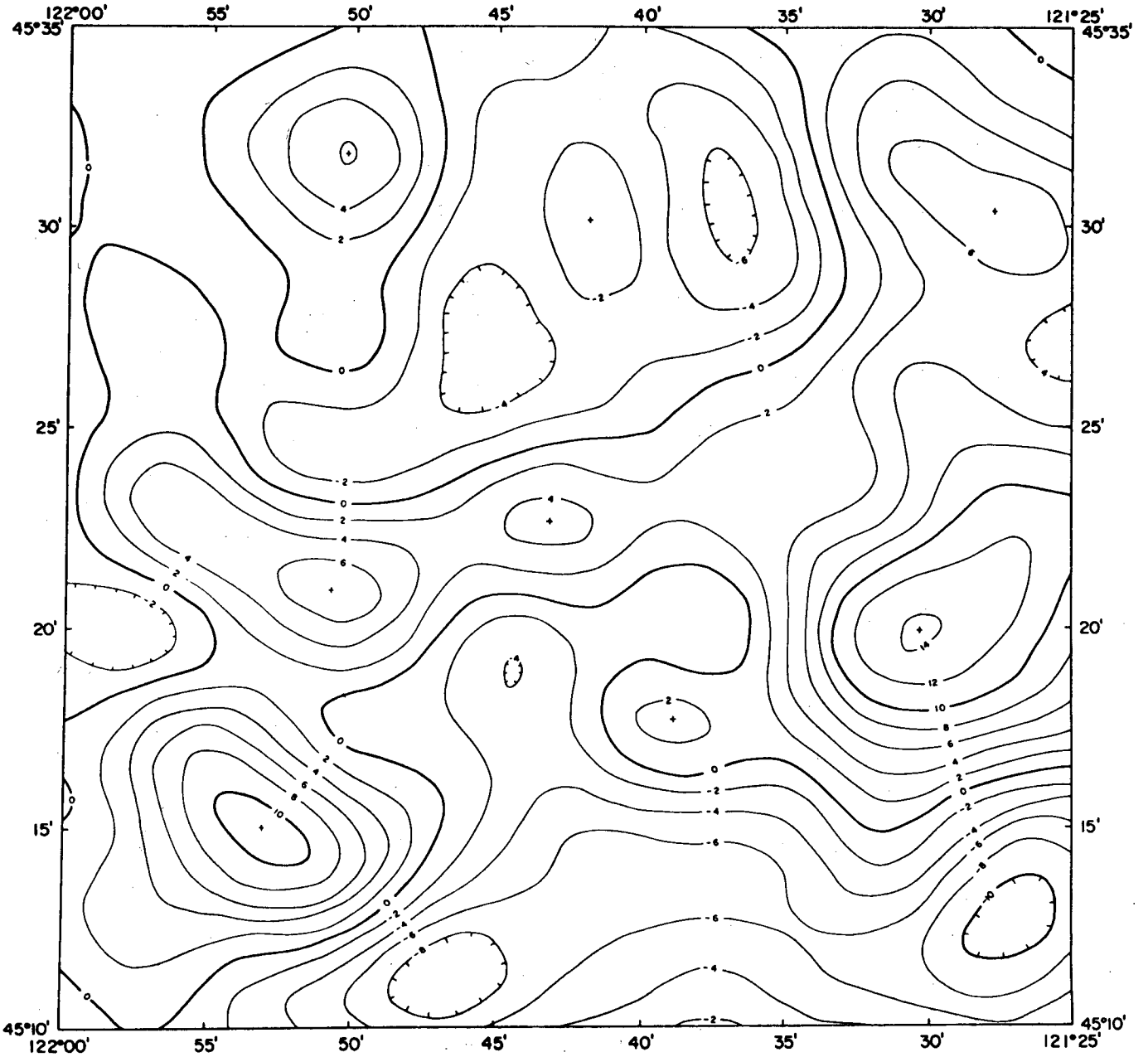

REGIONAL GRAVITY ANOMALY MAP
MOUNT HOOD AREA, OREGON

CONTOUR INTERVAL 2 MGALS

KILOMETERS
0 2 4 6 8
0 1 2 3 4 5
MILES

UNIVERSAL TRANSVERSE MERCATOR PROJECTION

OREGON STATE UNIVERSITY
FEBRUARY, 1979

Figure 10

Contiguous gravity highs, aligned north and south, occur east and northeast as well as west and southwest of Mount Hood. These highs together with a high northwest of Mount Hood flank a north-south oriented low. A relatively narrow high oriented approximately N75E, connects the highs on the western side with the highs on the eastern side and suggests a linear structure or an offset in structure beneath Mount Hood. A gravity low, south of Mount Hood, approximately parallels the N75E gravity high and intersects or truncates the north-south oriented highs east and west of Mount Hood. Hence two dominant anomaly lineations are evident; approximately north-south and approximately N75E. The north-south lineations suggest a graben-like structure in which Mount Hood is located and the east-northeast lineations that suggest folds and/or faults which cross the graben-like structure. The anomalies are relatively long wavelengths and are likely associated with the more dense pre-Pliocene rocks beneath Mount Hood and the surrounding mountains.

Figure 11 shows a map of the residual gravity anomalies of the Mount Hood area shorter than 8.1 km. The map shows a large number of closed gravity highs and lows of small areal extent. These anomalies suggest local density variations in the post-Miocene rocks of the area and may relate to individual flows or intrusions or relatively thick ash deposits. The station location density and the smoothing inherent in the computations and subsequent contouring of the data limit the resolution of the individual anomalies and consequently the anomaly causing bodies. No attempt was made to correlate

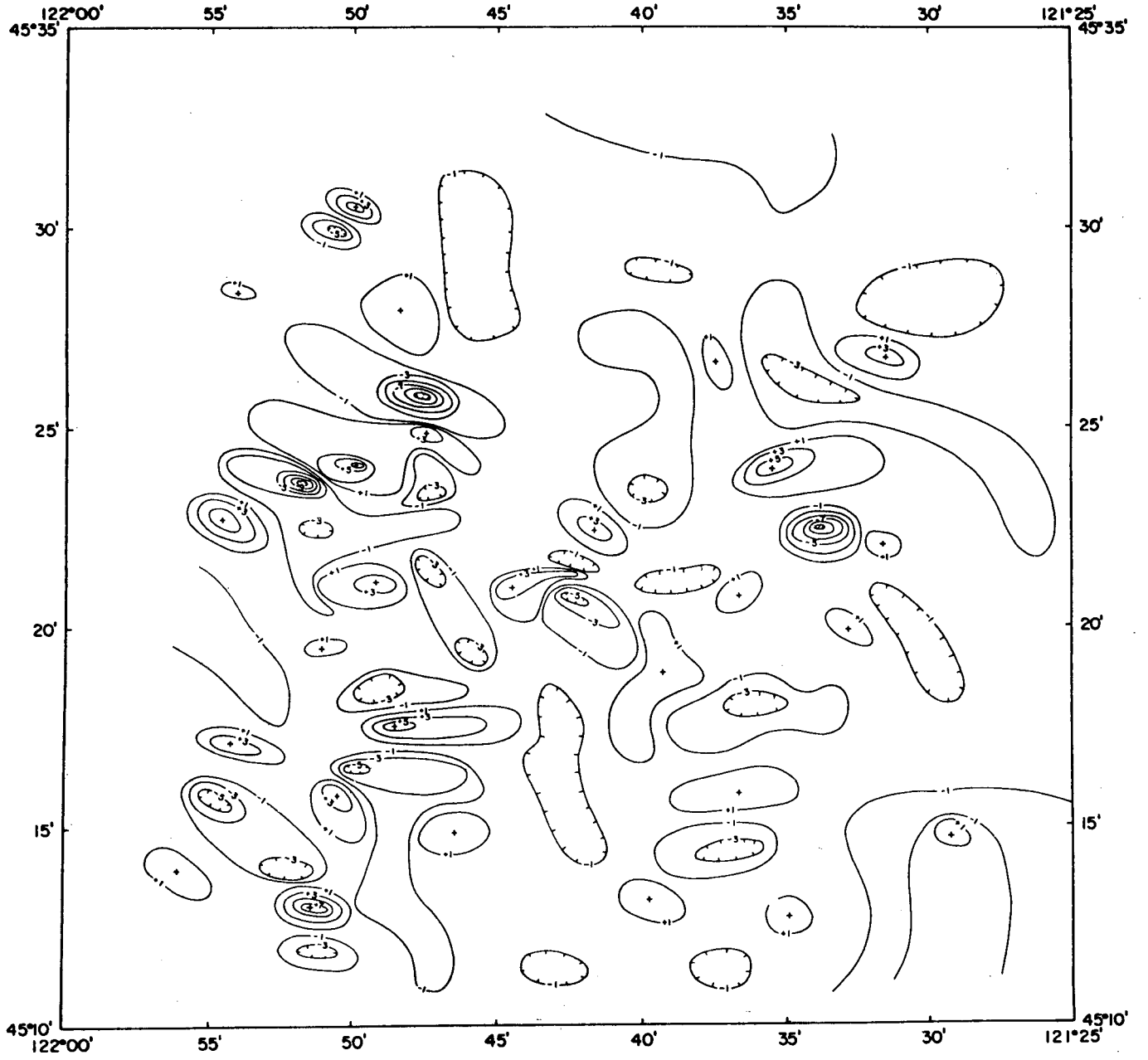

RESIDUAL GRAVITY ANOMALY MAP

MOUNT HOOD AREA, OREGON

AREA OF THIS MAP

CONTOUR INTERVAL 2 MGALS

KILOMETERS

0 2 4 6 8

0 1 2 3 4 5

MILES

UNIVERSAL TRANSVERSE MERCATOR PROJECTION

OREGON STATE UNIVERSITY

FEBRUARY, 1979

Figure 11

these anomalies with the surface or near-surface geology.

MODELS OF MOUNT HOOD

A large number of geological, geophysical, and geochemical studies contemporary with the gravity study described in this report will provide data with which to constrain future models of the internal and substructure of Mount Hood. Simple models, based on only a few gravity values, are offered and described below which may suggest limits or directions to other investigators studying Mount Hood. Topographic elevations, a Bouguer gravity anomaly based on a measurement on the summit of Mount Hood of 7.6 mgls, and an anomaly wavelength based on gravity measurements on the flanks of Mount Hood constrain the simple models.

Figure 12 shows a sphere model of Mount Hood that agrees with the observed Bouguer gravity anomaly and anomaly wavelength. The model assumes a density contrast, $\Delta \rho$, of 0.6 gm/cm^3 between mountain and "core". Because the average density associated with the topography of the region is approximately 2.3 gm/cm^3 the density of the spherical core would be approximately 2.9 gm/cm^3. A density of 2.9 gm/cm^3 would be near the maximum density expected for a volcanic core particularly if it were warm, altered and/or fractured. The size of core required to satisfy the observations and assumptions suggests the model is unrealistic.

Figure 13 shows a graph of a family of curves which describe the height and radius of a cylinderical core which satisfies the observed gravity anomaly on the summit of Mount Hood. The heavy curve which crosses the family of curves of different

SPHERE MODEL FOR MT. HOOD

Based on Peak Gravity Anomaly
and Anomaly Half-Width

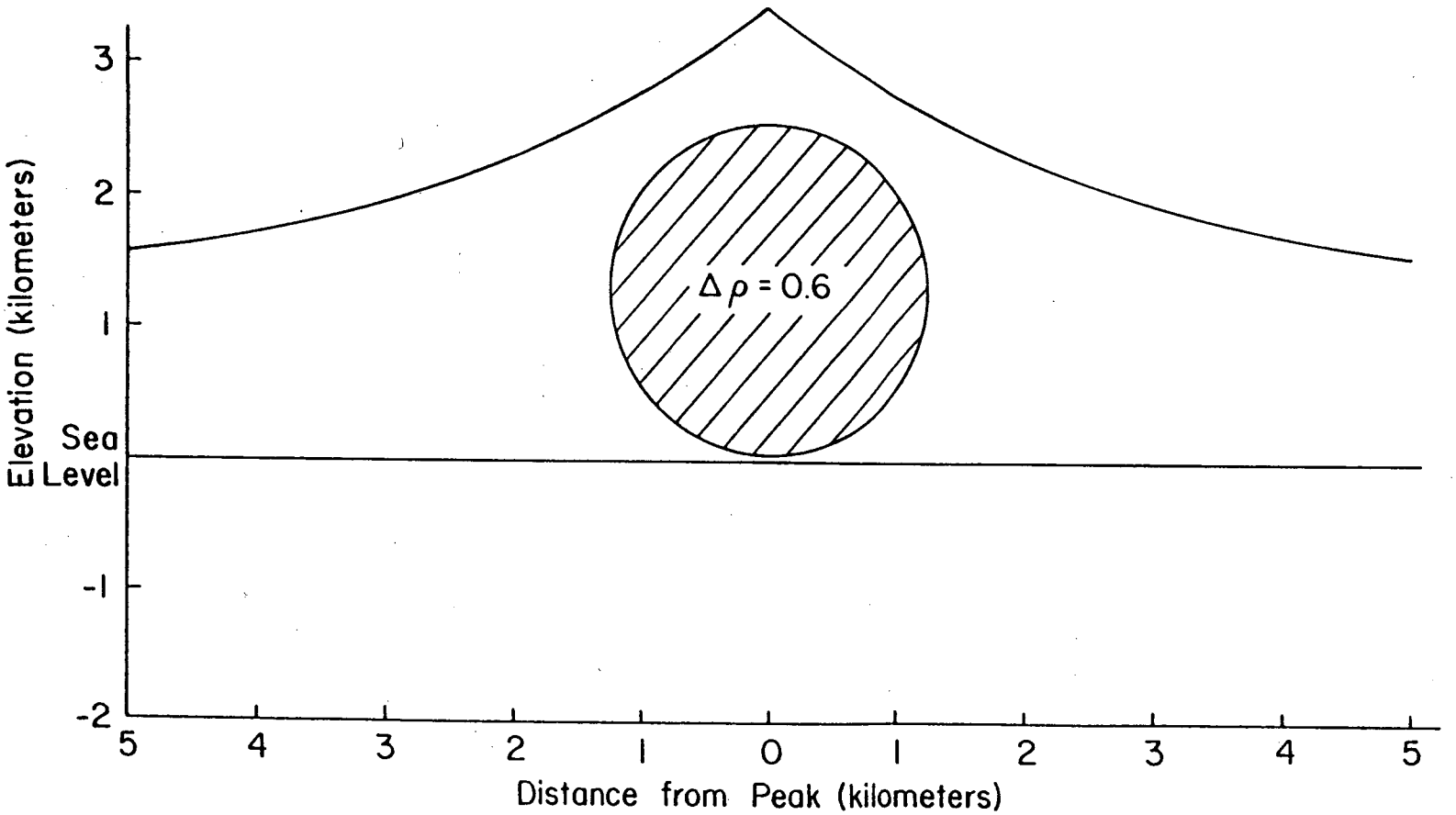

Figure 12

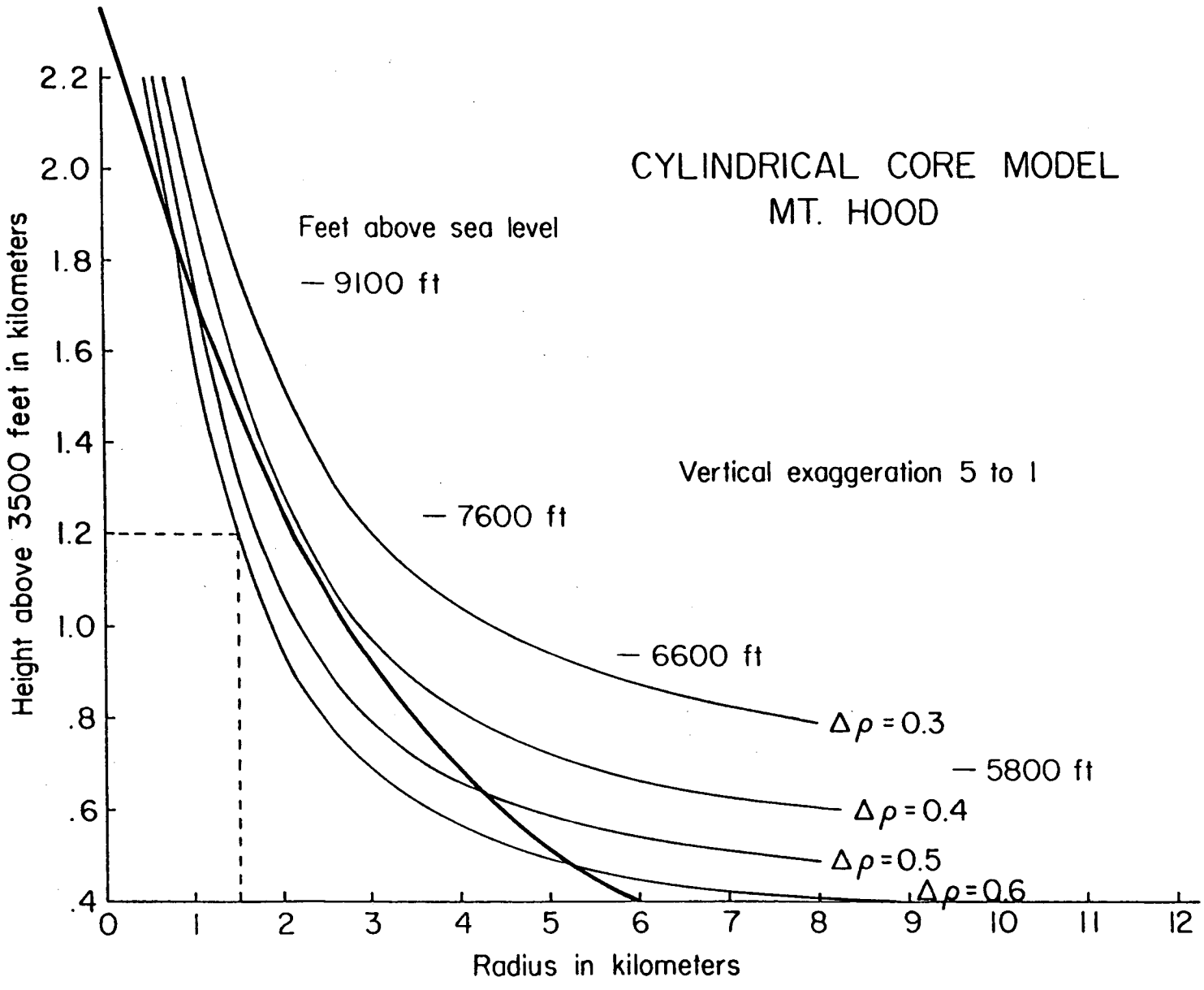
CYLINDRICAL CORE MODEL
MT. HOOD
Feet above sea level
— 9100 ft
— 7600 ft
— 6600 ft
— 5800 ft
Vertical exaggeration 5 to 1
Δρ = 0.3
Δρ = 0.4
Δρ = 0.5
Δρ = 0.6
Height above 3500 feet in kilometers
Radius in kilometers
2.2
2.0
1.8
1.6
1.4
1.2
1.0
.8
.6
.4
0
1
2
3
4
5
6
7
8
9
10
11
12

Figure 13

density contrasts is the smoothed topography of Mount Hood; therefore, any cylinderical model postulated is limited in radius and/or height by the topography. The dotted line illustrates one possible model: the cylinder has a radius of 1.5 km, a height of 1.2 km (above an assumed base for Mount Hood of 3500 ft), and a density contrast of 0.6 gm/cm^3. Smaller density contrasts yield larger cylinders but the minimum density contrast, limited by the topography, is slightly greater than 0.4 gm/cm^3.

Figure 14 shows a cylinder plus cone model of Mount Hood which satisfies the observed gravity anomaly, and topography. This model implies that the higher density rock of the volcanic core extends to the surface at the summit of the mountain. This is consistent with the resistant rocks which are visible near the summit and which are probably more dense than most of the rock on the flanks of the mountain. Figure 12 illustrates the size of the core when a density contrast of 0.5 gm/cm^3 is assumed. In this model the base of the cylindrical core rests on Columbia River Basalt at an elevation of 3500 ft; however, it could extend much deeper without significantly altering the gravitational effect of the model. Changes in the dimensions of the model near the summit cause the larger changes in the gravitational attraction of the cylinder and cone model. Figure 15 shows a graph of the changes in radius of the cylinder and core models versus the density contrast between the cylinder and core and the surrounding mountain. The curve assumes the density of the surrounding rock is 2.27 gm/cm^3 and the observed Complete Bouguer anomaly is 7.6 mgls. A large

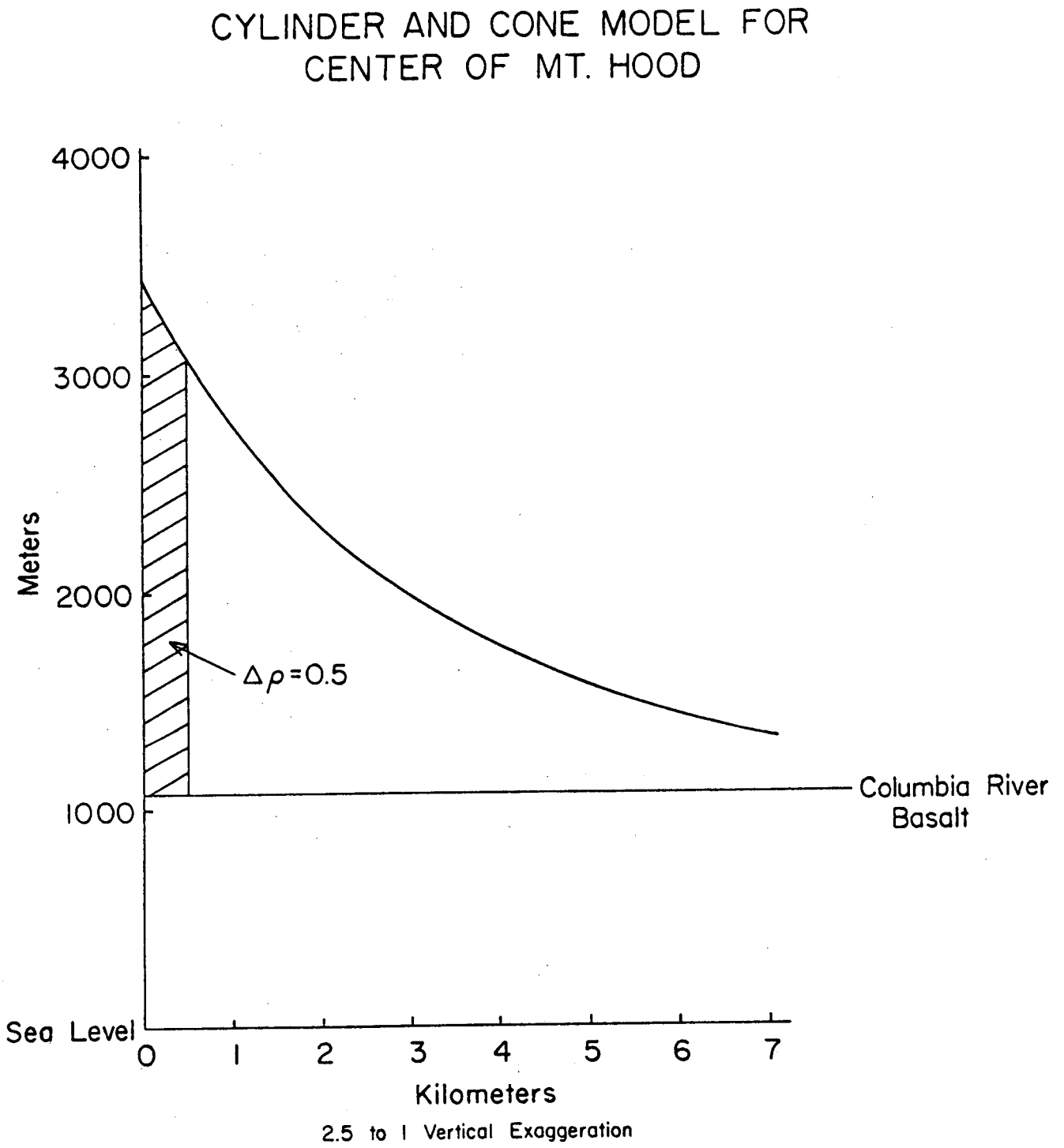
CYLINDER AND CONE MODEL FOR
CENTER OF MT. HOOD
4000
3000
2000
1000
Meters
Δρ=0.5
Columbia River
Basalt
Sea Level
0
1
2
3
4
5
6
7
Kilometers
2.5 to 1 Vertical Exaggeration

Figure 14

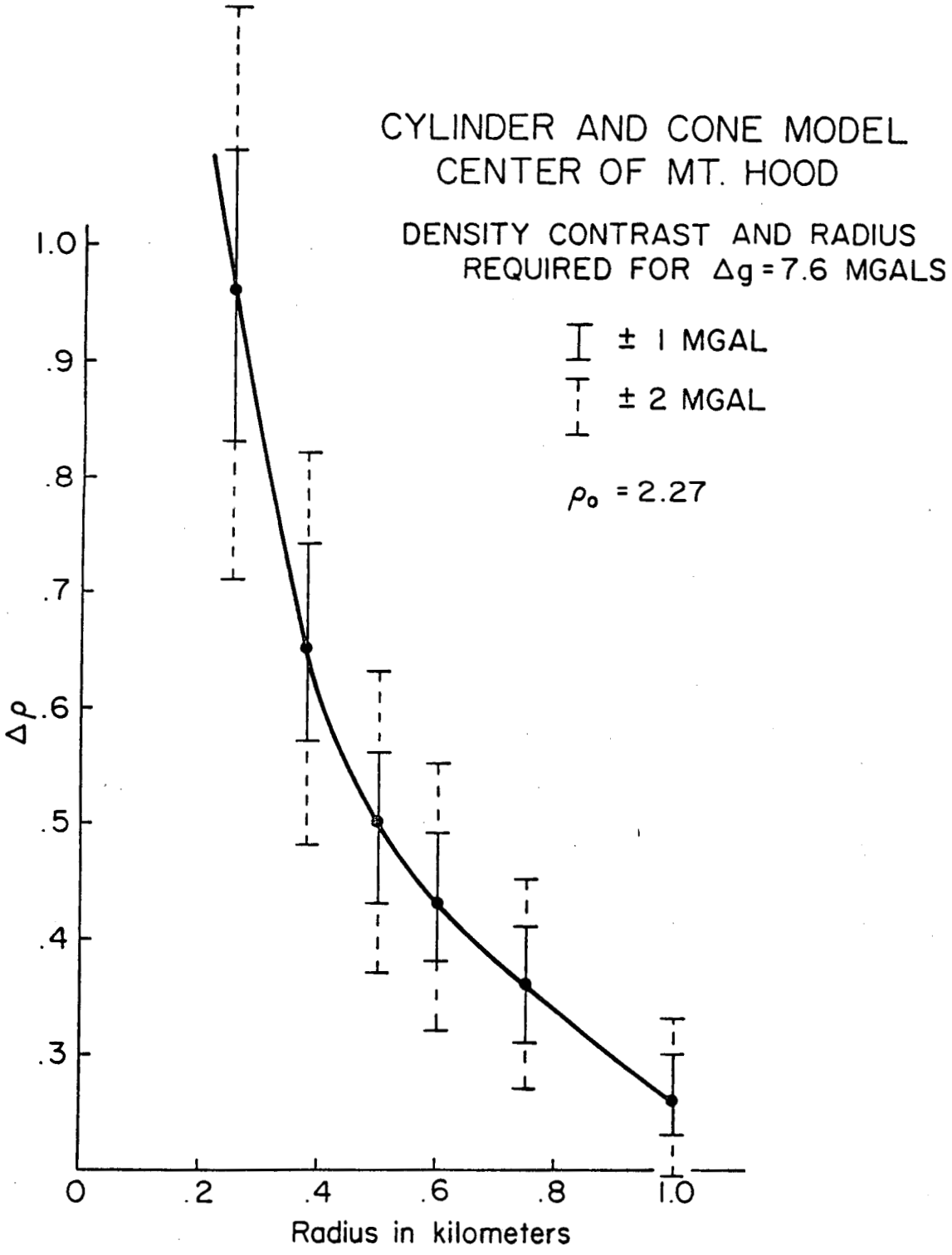
CYLINDER AND CONE MODEL
CENTER OF MT. HOOD
DENSITY CONTRAST AND RADIUS
REQUIRED FOR Δg = 7.6 MGALS
± 1 MGAL
± 2 MGAL
ρo = 2.27
Δρ
1.0
.9
.8
.7
.6
.5
.4
.3
0
.2
.4
.6
.8
1.0
Radius in kilometers

Figure 15

uncertainty is associated with the terrain correction of the summit anomaly on Mount Hood; hence, error bars of $\pm$ and $\pm$ 2 mgls are shown on the curve to indicate the uncertainties in the resulting models.

ELEVATION OF THE COLUMBIA RIVER BASALT

The 2.27 gm/cm^3 density of the rocks which form the topography of and about Mount Hood is considerably less dense than the density of 2.7 to 2.9 gm/cm^3 generally associated with the Columbia River Basalts. Therefore, the gravity anomalies of the area contain information on the structure or the shape of the interface between the Columbia River Basalts and the overlying rocks. To estimate the elevation of the Columbia River Basalt (Yakima Basalt) the complete Bouguer gravity anomalies, computed with a reduction density of 2.27 gm/cm^3, were spectrally separated into regional and residual components. The regional components that represent the anomaly field caused by the Columbia River Basalts were determined, after several interactions, to be best approximated by anomaly wavelengths longer than 8.1 km. The geologic map of the area indicates the Columbia River Basalts outcrop in several areas about Mount Hood. The elevations of the outcrops and the corresponding gravity anomalies provide a reference point for computations of the elevation of the Columbia River Basalt. The reference point selected was an elevation of 1040 meters and a gravity anomaly of +4 mgls. The equation to compute the elevation at other gravity stations was then

$$H = \left(\frac{RCBA_{2.27} - 4}{41.92\,\Delta\rho}\right) 1000 + 1040$$

where

H = is the elevation in meters of the Columbia River Basalt above sea level

$RCBA_{2.27}$ = is the complete regional Bouguer anomaly at a reduction density of 2.27 gm/cm^3

= is the assumed density contrast between the Columbia River Basalt and the overlying flows and pyroclastics.

Elevations were computed for density contrasts of 0.4 and 0.6 gm/cm^3. A density contrast of 0.6 gm/cm^3 yields the best fit to the mapped outcrops of the Columbia River Basalt. Figure 16 shows the estimated elevations of the top of the Columbia River Basalt (Yakima Basalt) based on computations that used a regional gravity field with spatial anomaly wavelengths greater than 8.1 km. The contour interval is 100 m with heavy contours shown at an elevation of 1000 m. Undulations in the surface range from less than 500 to greater than 1400 m above sea level. The highest elevations occur on the east, northeast and southwest sides of Mount Hood. The axis of Mount Hood is located approximately on an elevated ridge, oriented approximately N75E, that extends from the high elevations of the Columbia River Basalts on the east side of Mount Hood to the high on the southwest side.

Elevation estimates of the Columbia River Basalt is based on gravity measurements, an assumed density contrast between the Columbia River Basalts and the post-Miocene pyroclastics and flows of the High Cascade Mountains, and a reference elevation and gravity anomaly on an outcrop of the Columbia River Basalts in the study area. Inherent in these estimates are limits on the resolution of the surface configuration and elevation imposed by the position and spacing of the primary data grid and the continuity or smoothness of potential fields. Further, the elevations are computed independently for each station. Because of the limitations inherent in the method of

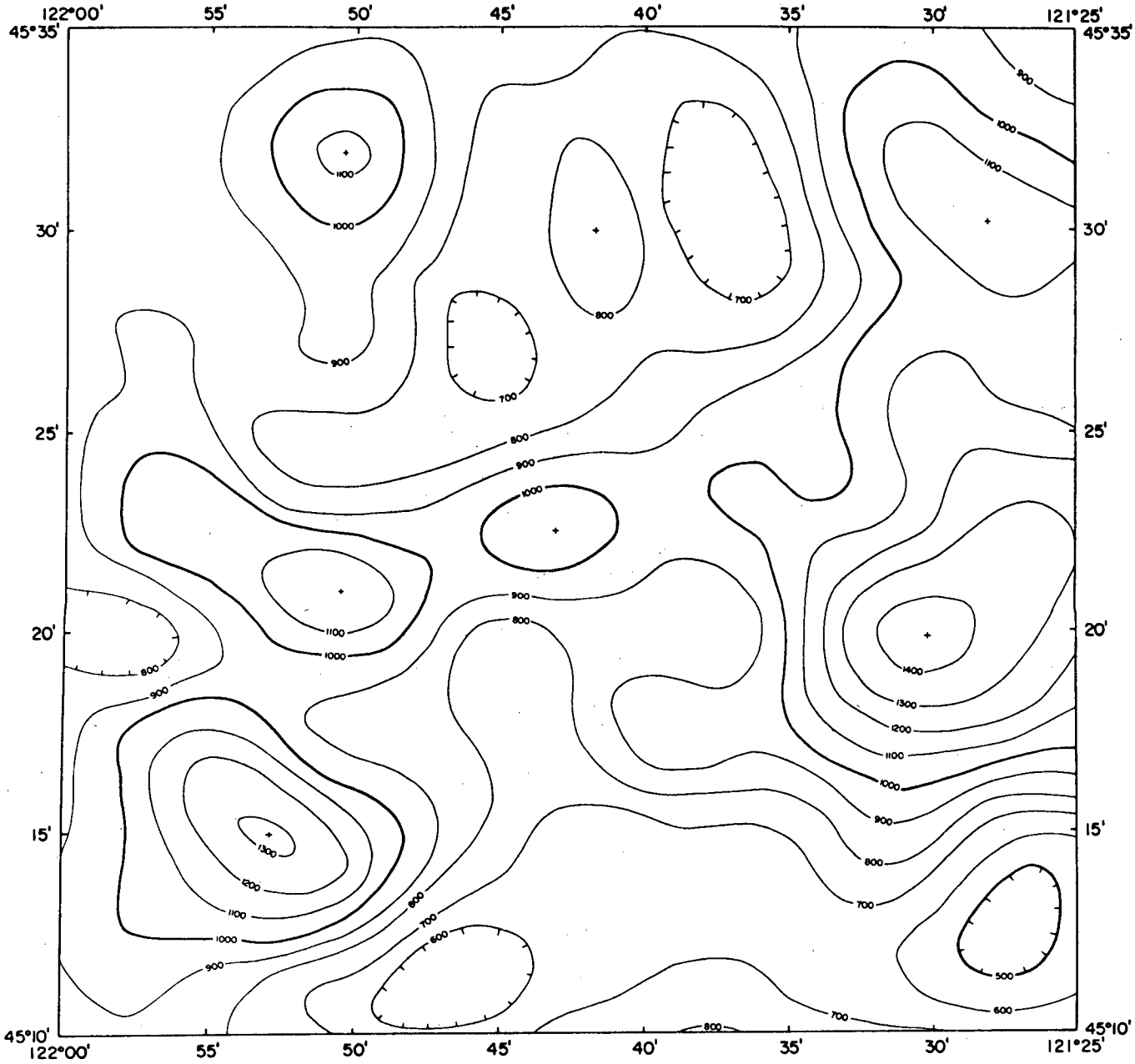

ESTIMATED ELEVATION OF THE COLUMBIA RIVER BASALTS
MOUNT HOOD AREA, OREGON

CONTOUR INTERVAL 100 METERS

KILOMETERS
0 2 4 6 8
0 1 2 3 4 5
MILES

UNIVERSAL TRANSVERSE MERCATOR PROJECTION

OREGON STATE UNIVERSITY
FEBRUARY, 1979

Figure 16

estimating the elevations many features cannot be resolved. For example, features with edges, such as faults or lava flows, are smoothed and included in the undulations of the estimated topography. The method also cannot differentiate between flows or changes in the Columbia River Basalt and other high density flows in the area, hence their surface is mapped as Columbia River Basalt. High density intrusions in the material above the Columbia River Basalt may be reflected or included in the undulations of the basalt.

To assess the effectiveness of the elevation estimates the computed elevations were compared to topographic elevations to generate a map of the "computed outcrops" of the Columbia River Basalts. Figure 17 shows a map of both the observed and computed outcrops of the Columbia River Basalts. The agreement between computation and observation is reasonable but generally more Columbia River Basalt is expected to outcrop than is actually observed. This discrepancy may be caused by a wrong reference elevation for the computations, erosion of the basalt in the area of expected outcrops, insufficient geologic mapping, or broadening of the surface during computation and contouring. West of Mount Hood relatively high density rocks are associated with Pliocene volcanism.

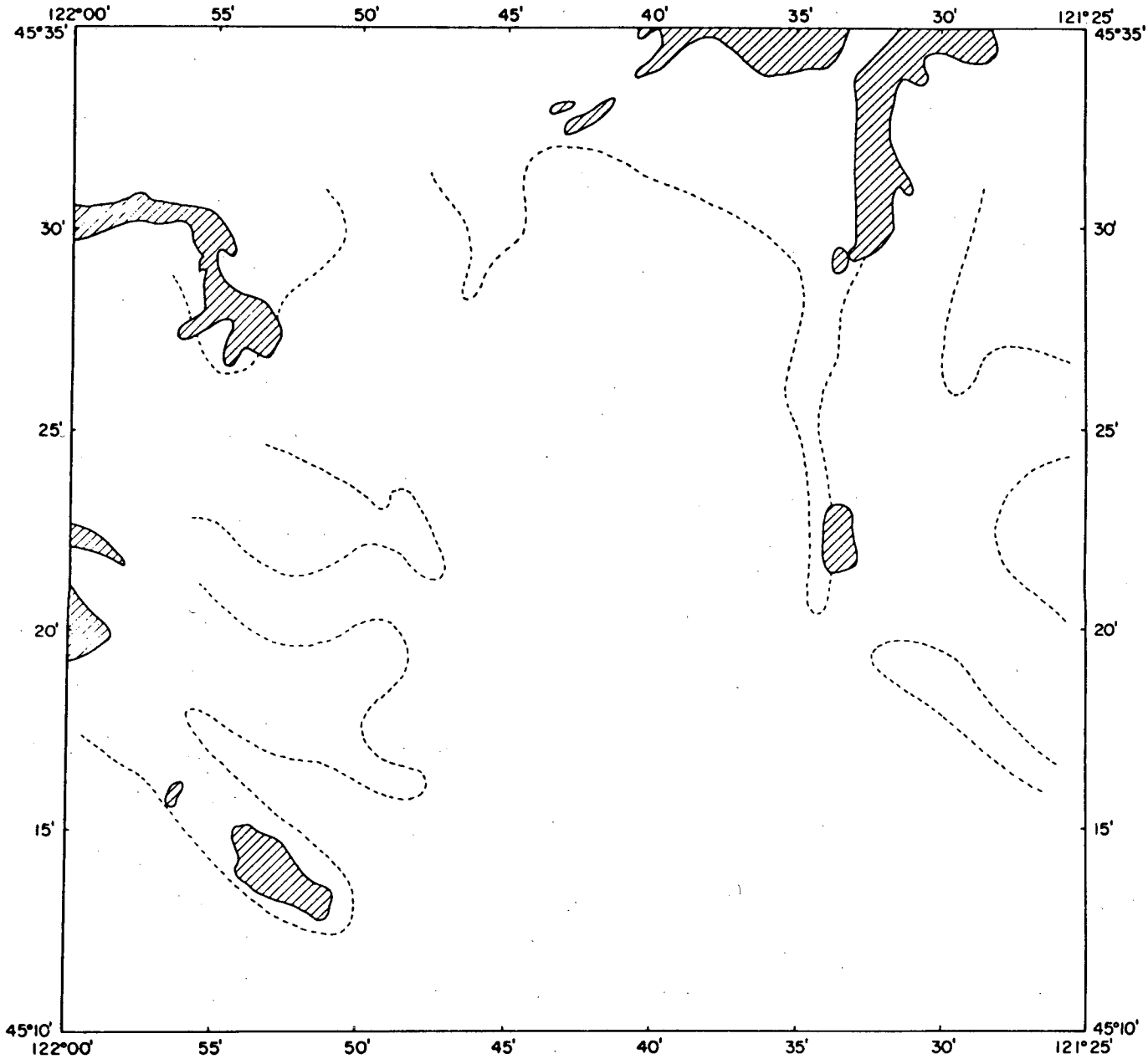

TOPOGRAPHIC SURFACE OF PRE-PLIOCENE ROCKS
MOUNT HOOD AREA, OREGON

COLUMBIA RIVER BASALT
OBSERVED OUTCROP
COMPUTED OUTCROP

KILOMETERS
0 2 4 6 8
0 1 2 3 4 5
MILES

UNIVERSAL TRANSVERSE MERCATOR PROJECTION

OREGON STATE UNIVERSITY
FEBRUARY, 1979

Figure 17

POROSITY ESTIMATES

Laboratory measurements on rocks from Mount Hood by Dr. N. Christianson (University of Washington, personal communication, 1978) show porosities of 6 to 7 percent in samples of fresh massive andesite. The measured samples have densities and p-wave velocities listed in Table 2.

TABLE 2

Sample	Density (gm/cm^3)	Velocity (km/sec)
1	2.56	4.49
2	2.58	4.52
3	2.60	4.65
4	2.62	4.52
5	2.62	4.97
6	2.59	4.84

The average density of the samples is 2.60 gm/cm^3 and the average velocity is 4.67 km/sec. If $p_{2.6}$ is the density of andesite at 7 percent porosity, then p_{max}, the density at 0 percent porosity is 2.80 gm/cm^3. Recognizing that the rocks which form Mount Hood are believed to be more than 90 percent andesite (Wise, 1969) the value, p_{max}, provides a reference point to compute average porosities for the rocks of Mount Hood above the Columbia River Basalts. The elevation difference, h, between the estimated elevation of the Columbia River Basalt and the topographic surface, the residual gravity anomalies (RGA), obtained as the difference between the complete Bouguer anomalies and the regional anomalies and the reduction density $p_{2.27}$, provide the parameters used to compute an average density

for the mass column between the Columbia River Basalts and the topographic surface. The equation is,

$$p_{avg} = p_{2.27} + \frac{RGA}{2\pi\sigma h}$$

where σ is the gravitational constant. The estimated porosity is given by the equation:

$$\text{Porosity (\%)} = 100 \left(\frac{2.8 - p_{avg}}{2.8}\right)$$

Because the rocks are porous they can contain water, consequently the equation above yields a porosity for dry rocks. The equation for 100 percent water saturated rocks is:

$$\text{Porosity (\%)} = 100 \left(\frac{2.8 - p_{avg}}{1.8}\right)$$

Figure 18 shows a map of the estimated average porosities of the rocks in the Mount Hood area above the Columbia River Basalts based on the assumption that the rocks are water saturated. Because the computed values have large inherent uncertainties and show a large scatter or range in values they result in numerous "one-point" anomalies. Consequently, the computed values were smoothed and the contours only separate areas of porosities greater than or less than the average porosity, 30 percent, of water saturated rocks. The map shows an area east of Mount Hood with porosities less than 30 percent that corresponds reasonably well to the area where the complete Bouguer anomalies suggest the presence of higher density rocks. These observations of course, are not independent. A contour line that separates porosities of greater than 30 percent on the east side from porosities of less than 30 percent on the west side crosses the summit of Mount Hood from approximately south southwest to north northeast. The difference in the

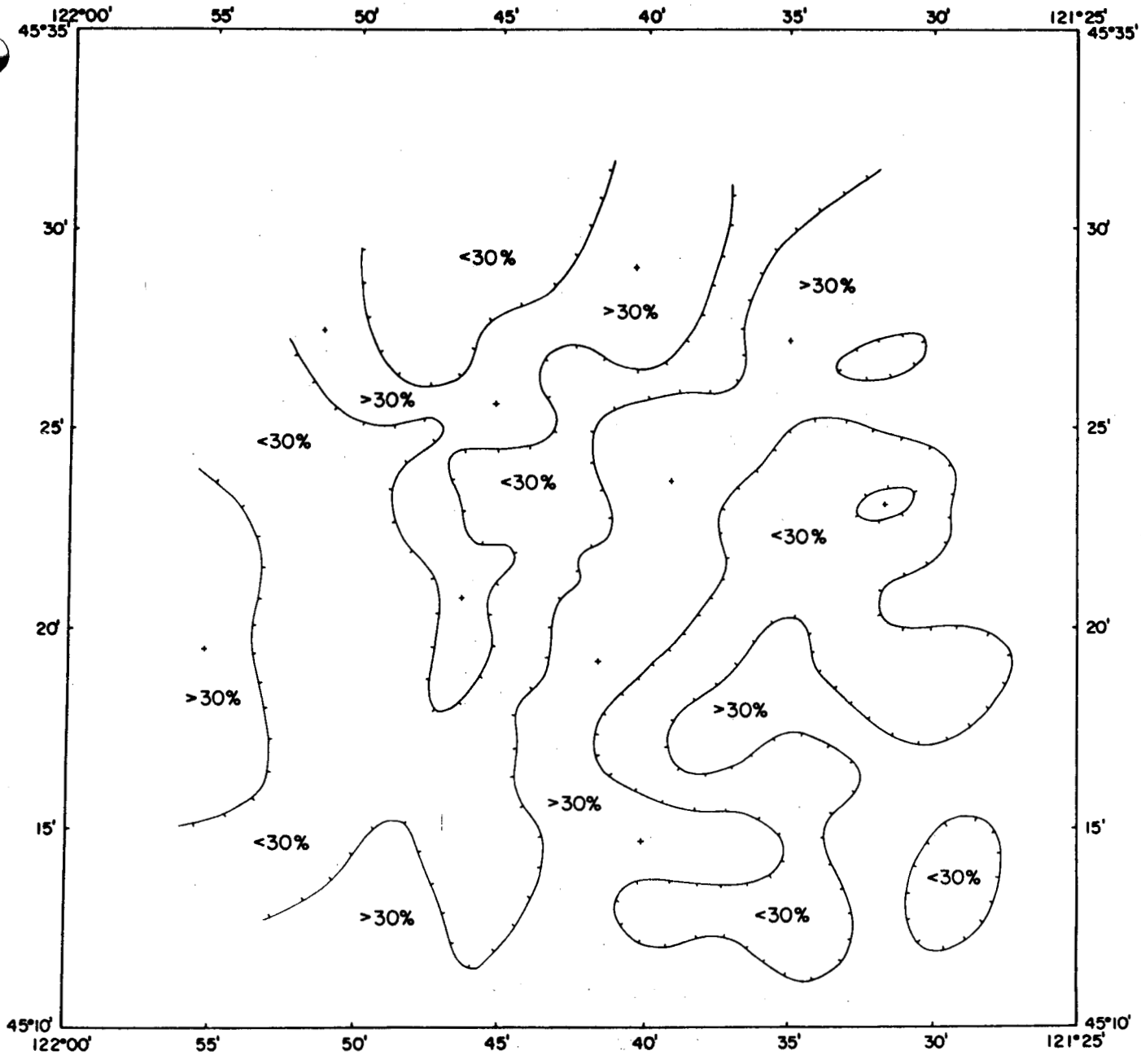

ESTIMATED REGIONAL POROSITY
MOUNT HOOD AREA, OREGON

AREA OF THIS MAP

KILOMETERS
0 2 4 6 8
0 1 2 3 4 5
MILES

UNIVERSAL TRANSVERSE MERCATOR PROJECTION

OREGON STATE UNIVERSITY
FEBRUARY, 1979

Figure 18

porosities indicated by the map suggests an asymmetry in the average rock, a composite of flows and pyroclastics, that forms Mount Hood. Alternatively, the average porosity of the rock materials may be the same about the summit and flanks of Mount Hood but the porous rocks may contain more water on the west side than on the east side.

TRAVEL TIME RESIDUALS

Empirical relations between rock density and compressional wave velocity (Ludwig, Nafe, and Drake, 1970) provide a means to estimate p-wave travel time residuals for the Mount Hood area based on gravity measurements. The empirical curves of Ludwig and others (1970) indicate a compressional wave velocity of approximately 3.3 km/sec for rock of density 2.27 gm/cm^3. Recognizing that the average complete Bouguer anomaly for the Mount Hood area is -71.7 mgl then the approximate travel time vertically through the material above sea level is given by the equation:

$$\Delta T = \frac{h}{1.45\ (2.27 + \Delta \rho)}$$

where h is the elevation in kilometers and

$$\Delta \rho = \frac{CBA + 71.7}{2 \pi \gamma h}$$

Figure 19 shows estimated travel time residuals for the Mount Hood area. The travel time residuals are the time of travel from sea level to the surface and the differences are caused by variations in topographic elevation and rock density along the ray path. The computed travel time residuals are estimates only and do not allow for irregular travel paths caused by refraction and diffraction of the seismic waves. The map does indicate, however, that significant travel time differences caused by near-surface effects can be expected.

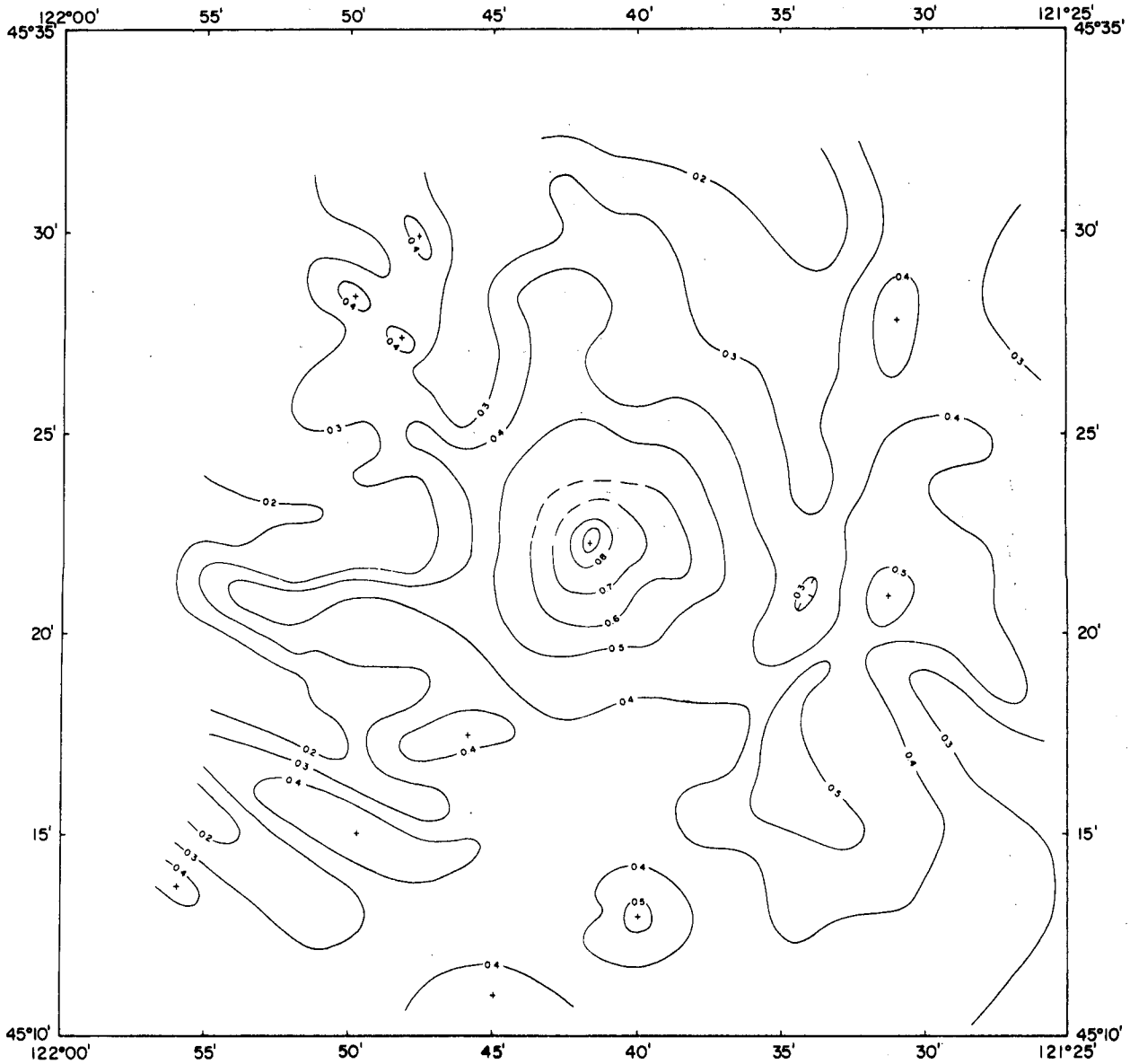

ESTIMATED TRAVEL-TIME RESIDUALS
MOUNT HOOD AREA, OREGON

CONTOUR INTERVAL 0.1 SEC

KILOMETERS
0 2 4 6 8
0 1 2 3 4 5
MILES

UNIVERSAL TRANSVERSE MERCATOR PROJECTION

OREGON STATE UNIVERSITY
JANUARY, 1979

Figure 19

ACKNOWLEDGEMENTS

Messuers. K. Keeling, T. Jones, W. Plant, G. Ness, M. Brown, and J. Bowers made the gravity measurements in the Mount Hood area. S. Pitts, K. Keeling, D. Braman, J. Cook, G. Axelsson and W. Avera assisted in the data reduction. P. Pitts, B. Priest, D. Burt, and S. Troseth prepared the maps and illustrations, J. Brenneman and N. Kneisel helped prepare the report. This work was supported by the Oregon State Department of Geology and Mineral Industries through a grant from the U. S. Department of Energy.

REFERENCES

Hammer, Sigmond, 1939, Terrain Corrections for Gravimeter Stations, Geophysics, v. 4, p. 184-194.

Longman, I. M., 1959, Formulas for computing the tidal accelerations due to the moon and the sun: J. of Geophys. Res., v. 64, n. 12, p. 2351-2355.

Ludwig, W., Nafe, J. E., and Drake, C. L., 1970, Seismic refraction, In: The Sea, A. E. Maxwell (editor), vol. 4, Part I, New York, Wiley-Interscience, p. 53-84.

Oliver, H. W., 1973, Principal facts, plots, and reduction for 1753 gravity stations in the Southern Sierra Nevada and Vicinity, California: NTIS pub #PB 231 185, U. S. Dept. of Commerce, Washington, D. C.

Oliver, H. W., Griscom, A., Robbins, S. L., Hanna, W. F., 1969, U. S. Geological Survey Gravity data in California, part IV: U. S. Geol. Survey, Internal report, Menlo Park, California.

Plouff, D., 1977a, Preliminary documentation for a FORTRAN program to compute gravity terrain corrections based on topography digitized on a geographic grid: U. S. Geol. Survey, Open-file report, no. 77-535, U. S. Govt. Printing Office, Washington, D. C.

Plouff, D., 1977b, Gravity observations near McDermitt, Nevada during 1976: U. S. Geol. Survey, open-file report, no. 77-536, 13 p., U. S. Govt. Printing Office, Washington, D. C.

Scheibe, D. M., and Howard, H. W., 1964, Classical methods for reduction of gravity observation: U. S. Air Force, Aeronautical Chart and Information Center Ref., Pub. 12, 65 p.

Swick, C. H., 1942, Pendulum gravity measurements and isostatic reductions: U. S. Coast and Geod. Survey, Spec. Pub., no. 232, 82 p.

Thiruvathukal, J. T., 1968, Regional Gravity of Oregon: unpub. Ph.D. Dissertation, Oregon State University, Corvallis, Oregon, 92 p.

Wise, W. S., 1969, Geology and Petrology of the Mt. Hood Area: A study of High Cascade Volcanism, Geo. Soc. of Am. Bull., v. 80, p. 969-1006.

Woollard, G. P., Rose, J. C., 1963, International gravity measurements: Society of Exploration Geophysics, Tulsa, OK, 518 p.

APPENDIX

THEORETICAL GRAVITY . IUGG 1930 INTERNATIONAL GRAVITY FORMULA

EXPLANATION OF SYMBOLS: ID - STATION IDENTIFICATION, LAT - LATITUDE, LONG - LONGITUDE, ELEV - ELEVATION (FEET), OG - OBSERVED GRAVITY, THG - THEORETICAL GRAVITY, HTC - HAND TERRAIN CORRECTION, TTC - TOTAL TERRAIN CORRECTION, CC - CURVATURE CORRECTION, FAA - FREEAIR ANOMALY, CBA1, CBA2 - VARIABLE DENSITY COMPLETE BOUGUER ANOMALIES. GRAVITY DATA, ANOMALIES, AND CORRECTIONS IN MGALS. ESTIMATED UNCERTAINTIES, FAA +- 1.0 MGL, CBA +- 1.5 MGL.
CBA1 REDUCTION DENSITY = 2.67 GM / CC CBA2 REDUCTION DENSITY = 2.27 GM / CC

ID	LAT	LONG	ELEV	OG	THG	HTC	TTC	CC	FAA	CBA1	CBA2	ID
MHL 3	45 20.61	-121 56.46	1425.0	980489.14	980660.39	0.00	4.85	0.57	-37.25	-81.57	-74.93	MHL 3
MHL 6	45 18.28	-121 45.27	3880.0	980328.18	980656.89	0.00	3.39	1.24	36.89	-94.89	-74.59	MHL 6
MHL 7	45 18.58	-121 42.29	4980.0	980260.54	980657.22	0.00	6.64	1.48	63.99	-97.98	-73.64	MHL 7
MHL 8	45 19.87	-121 42.16	5950.0	980190.14	980659.28	0.00	12.46	1.49	90.19	-101.77	-73.01	MHL 8
MHS01	45 17.04	-121 42.53	3652.0	980339.79	980655.03	0.00	3.11	1.19	28.13	-94.51	-76.14	MHS01
MHS02	45 25.46	-121 34.69	3860.0	980393.11	980667.69	0.00	5.51	1.06	13.14	-86.77	-71.81	MHS02
MHS03	45 30.39	-121 35.14	1831.0	980476.90	980675.10	0.02	2.77	0.71	-26.83	-86.41	-77.37	MHS03
MHS05	45 32.90	-121 42.83	1279.0	980513.34	980678.88	0.00	8.12	0.52	-45.27	-81.29	-75.89	MHS05
MHS06	45 13.87	-121 41.69	3874.0	980316.61	980649.06	0.00	3.47	1.24	31.79	-98.11	-78.65	MHS06
MH 01	45 19.96	-121 54.87	1577.0	980478.54	980659.42	0.00	6.71	0.62	-32.59	-80.28	-73.14	MH 01
MH 02	45 19.57	-121 54.42	1672.0	980472.62	980658.84	0.01	6.48	0.65	-28.99	-80.19	-72.52	MH 02
MH 03	45 19.01	-121 53.93	1804.0	980463.43	980657.99	0.00	6.49	0.70	-24.92	-80.66	-72.31	MH 03
MH 04	45 18.55	-121 52.88	1990.0	980451.92	980657.29	0.00	6.34	0.76	-18.24	-80.53	-71.28	MH 04
MH 05	45 18.43	-121 51.15	2294.0	980433.50	980657.12	0.00	5.41	0.85	-7.91	-81.59	-70.56	MH 05
MH 06	45 18.70	-121 50.04	2547.0	980416.69	980657.52	0.00	5.25	0.92	-1.34	-83.80	-71.52	MH 06
MH 07	45 18.85	-121 47.70	3120.0	980376.58	980657.75	2.38	9.06	1.07	12.19	-86.24	-71.49	MH 07
MH 08	45 18.80	-121 48.91	2806.0	980397.83	980657.67	0.01	4.85	0.99	4.98	-87.85	-74.09	MH 08
MH 09	45 18.46	-121 46.95	3581.0	980347.95	980657.15	0.00	3.30	1.18	27.49	-92.52	-74.54	MH 09
MH 10	45 15.55	-121 42.71	3420.0	980350.56	980652.78	0.00	3.60	1.14	19.34	-94.85	-77.74	MH 10
MH 11	45 14.48	-121 42.23	3550.0	980338.63	980651.16	0.20	3.21	1.17	21.25	-97.79	-79.96	MH 11
MH 12	45 13.55	-121 41.86	3952.0	980312.85	980649.77	0.02	2.82	1.25	34.65	-98.57	-78.62	MH 12
MH 13	45 11.65	-121 41.45	3826.0	980319.63	980646.91	0.01	1.64	1.23	32.44	-97.64	-78.15	MH 13
MH 14	45 17.33	-121 46.91	5027.0	980248.31	980655.46	7.77	14.33	1.41	65.45	-93.08	-69.33	MH 14
MH 15	45 17.63	-121 44.91	4656.0	980269.59	980655.91	10.32	14.23	1.37	51.41	-94.52	-72.66	MH 15
MH 16	45 19.04	-121 44.02	3925.0	980323.23	980656.53	0.00	4.89	1.25	35.73	-95.29	-75.66	MH 16
MH 17	45 17.24	-121 43.67	3838.0	980329.37	980655.32	0.00	2.94	1.23	34.15	-94.77	-75.45	MH 17
MH 18	45 16.13	-121 44.15	3608.0	980342.11	980653.65	0.00	2.69	1.18	27.69	-93.86	-75.65	MH 18
MH 19	45 15.19	-121 44.21	4145.0	980305.66	980652.24	0.04	4.27	1.29	43.13	-95.26	-74.53	MH 19
MH 20	45 14.34	-121 48.79	4705.0	980270.47	980650.96	1.88	6.94	1.37	61.85	-93.05	-69.85	MH 20
MH 21	45 15.87	-121 50.48	5041.0	980243.93	980653.26	14.02	22.61	1.42	64.58	-86.16	-63.57	MH 21
MH 22	45 16.02	-121 53.06	4770.0	980265.45	980653.49	11.64	19.78	1.38	60.40	-83.89	-62.27	MH 22
MH 23	45 16.45	-121 53.49	4226.0	980307.14	980654.13	5.83	11.44	1.30	50.33	-83.66	-63.59	MH 23
MH 24	45 17.04	-121 54.33	4110.0	980317.37	980655.03	9.35	14.61	1.28	48.76	-78.09	-59.89	MH 24
MH 25	45 14.66	-121 50.30	4689.0	980276.16	980651.43	0.29	10.46	1.37	63.56	-85.28	-62.68	MH 25
MH 26	45 17.87	-121 53.85	1846.0	980458.28	980656.27	0.00	8.62	0.71	-24.48	-79.46	-71.21	MH 26

ID	LAT	LONG	ELEV	OG	THG	HTC	TTC	CC	FnA	CBA1	CBA2	ID
MH 27	45 17.11	-121 51.25	2114.0	980436.04	980655.13	9.35	14.18	0.80	-20.38	-79.02	-70.23	MH 27
MH 28	45 16.41	-121 50.23	2388.0	980412.29	980654.08	10.31	14.42	0.88	-18.00	-85.63	-75.50	MH 28
MH 29	45 16.04	-121 48.40	2893.0	980381.40	980653.51	9.69	12.76	1.82	-8.09	-87.02	-74.80	MH 29
MH 30	45 16.38	-121 46.46	3188.0	980366.54	980654.83	0.82	6.08	1.09	12.66	-91.08	-75.54	MH 30
MH 31	45 16.96	-121 44.80	3531.0	980348.86	980654.98	0.83	4.78	1.17	25.95	-98.94	-73.43	MH 31
MH 32	45 14.88	-121 47.17	4457.0	980290.84	980651.78	0.85	4.68	1.34	58.89	-98.66	-68.38	MH 32
MH 33	45 13.64	-121 46.21	3467.0	980349.19	980649.90	0.83	1.84	1.15	25.26	-92.30	-74.69	MH 33
MH 34	45 12.43	-121 41.86	4824.0	980306.68	980648.09	0.18	2.39	1.26	36.92	-99.19	-78.80	MH 34
MH 35	45 11.56	-121 42.97	3573.6	980333.20	980646.77	0.84	2.87	1.18	22.37	-97.80	-79.79	MH 35
MH36A	45 19.16	-121 41.15	4799.0	980266.89	980658.22	0.82	7.08	1.39	59.84	-98.14	-74.47	MH36A
MH 37	45 17.53	-121 48.63	4414.0	980296.28	980655.76	0.18	7.64	1.33	55.51	-88.73	-67.12	MH 37
MH 38	45 12.82	-121 44.12	3879.8	980314.55	980647.47	0.82	1.98	1.24	32.19	-99.37	-79.66	MH 38
MH 39	45 12.66	-121 43.17	3931.8	980311.77	980648.44	0.83	4.24	1.25	32.93	-98.15	-78.52	MH 39
MH 40	45 11.99	-121 46.87	3844.8	980316.91	980647.42	0.80	1.79	1.23	30.91	-99.64	-80.08	MH 40
MH 41	45 11.22	-121 47.44	3969.8	980305.82	980646.27	0.81	1.82	1.25	32.72	-182.09	-81.89	MH 41
MH 42	45 12.13	-121 49.75	3588.8	980337.61	980647.63	0.84	3.79	1.18	27.33	-92.44	-74.49	MH 42
MH 43	45 11.92	-121 51.26	3223.8	980359.28	980647.31	0.49	3.42	1.18	15.01	-92.59	-76.47	MH 43
MH 44	45 11.81	-121 54.54	4888.8	980308.14	980647.15	0.81	3.66	1.28	45.34	-91.78	-71.17	MH 44
MH 45	45 13.69	-121 56.81	4877.8	980246.39	980649.99	19.49	27.61	1.40	54.91	-85.22	-64.22	MH 45
MH 46	45 12.58	-121 47.54	3586.8	980335.48	980648.31	0.42	3.85	1.18	24.25	-96.18	-78.14	MH 46
MH 47	45 13.86	-121 49.51	3236.8	980366.97	980649.84	0.11	2.22	1.18	22.19	-87.86	-78.69	MH 47
MH 48	45 13.88	-121 51.31	2867.8	980403.41	980648.95	0.19	3.22	1.81	24.84	-71.54	-57.22	MH 48
MH 49	45 13.88	-121 52.26	2710.8	980405.18	980650.15	0.46	4.50	0.97	9.84	-79.85	-65.74	MH 49
MH 50	45 14.48	-121 52.63	2655.8	980411.78	980651.85	0.83	4.69	0.95	10.38	-76.52	-63.51	MH 50
MH 51	45 15.81	-121 53.85	2492.8	980424.18	980651.97	0.62	5.23	0.91	6.46	-74.22	-62.13	MH 51
MH 52	45 15.65	-121 54.93	1773.8	980461.83	980652.93	0.88	9.54	0.69	-24.38	-76.88	-68.27	MH 52
MH 53	45 13.83	-121 39.95	5294.8	980219.99	980648.99	0.81	11.68	1.44	68.59	-101.64	-76.12	MH 53
MH 54	45 17.84	-121 35.57	5724.8	980196.95	980655.82	11.33	19.71	1.48	88.83	-96.96	-78.45	MH 54
MH 55	45 18.18	-121 33.47	4465.8	980294.61	980656.73	0.88	7.87	1.34	57.66	-88.89	-66.94	MH 55
MH 56	45 18.17	-121 31.74	5125.8	980259.31	980656.73	0.81	6.13	1.42	84.39	-85.78	-68.22	MH 56
MH 57	45 15.79	-121 35.52	5600.8	980202.62	980653.15	10.26	18.55	1.47	75.92	-98.88	-71.94	MH 57
MH 58	45 14.58	-121 34.58	4865.8	980256.81	980651.23	0.81	4.98	1.39	62.18	-100.24	-75.91	MH 58
MH 59	45 12.77	-121 35.82	4342.8	980286.34	980648.59	0.88	5.66	1.32	45.97	-97.78	-76.24	MH 59
MH 60	45 11.48	-121 34.43	3705.8	980327.55	980646.53	0.88	2.41	1.28	29.36	-95.79	-77.84	MH 60
MH 61	45 11.13	-121 32.51	3326.8	980350.38	980646.13	0.81	1.73	1.12	16.97	-95.86	-78.96	MH 61
MH 62	45 11.93	-121 30.84	3782.8	980325.37	980647.34	0.84	2.69	1.28	26.18	-98.68	-79.98	MH 62
MH 63	45 12.48	-121 32.76	3849.8	980319.26	980648.85	0.81	2.25	1.23	33.18	-97.16	-77.65	MH 63
MH 64	45 13.79	-121 31.91	4584.8	980274.18	980650.13	0.81	4.36	1.36	54.94	-98.48	-75.43	MH 64
MH 65	45 15.15	-121 32.88	5385.8	980222.88	980652.17	0.81	9.53	1.45	76.87	-99.51	-73.21	MH 65
MH 66	45 16.35	-121 32.55	5279.8	980237.88	980653.98	0.88	7.55	1.44	79.38	-94.56	-68.58	MH 66
MH 67	45 12.66	-121 28.29	3333.8	980348.95	980648.44	0.83	2.84	1.12	13.89	-98.87	-81.97	MH 67
MH 68	45 13.86	-121 29.49	3611.8	980337.17	980650.23	0.82	2.94	1.18	26.45	-94.95	-76.77	MH 68
MH 69	45 14.78	-121 29.34	4011.8	980316.18	980651.62	0.82	3.39	1.26	41.67	-93.88	-72.83	MH 69

ID	LAT	LONG	ELEV	OG	THG	HTC	TTC	CC	FAA	CBA1	CBA2	ID
MH 70	45 14.97	-121 26.52	3803.0	980375.78	980651.91	0.01	2.29	1.04	6.23	-94.94	-79.79	MH 70
MH 71	45 13.66	-121 26.51	2905.0	980376.97	980649.94	0.01	1.88	1.02	0.18	-98.12	-83.39	MH 71
MH 72	45 11.40	-121 27.01	2783.0	980382.91	980646.55	0.01	1.37	0.99	-1.96	-96.49	-82.33	MH 72
MH 73	45 16.68	-121 41.57	4867.0	980315.79	980654.47	0.10	2.90	1.27	43.69	-93.39	-72.86	MH 73
MH 74	45 18.17	-121 40.35	4250.0	980309.57	980656.72	0.01	4.07	1.30	52.43	-89.76	-68.46	MH 74
MH 75	45 18.63	-121 38.51	4674.0	980282.32	980657.41	0.03	4.55	1.37	64.34	-91.90	-68.49	MH 75
MH 76	45 19.80	-121 35.08	3793.0	980340.42	980659.18	0.00	5.22	1.22	37.86	-87.50	-68.72	MH 76
MH 78	45 17.47	-121 38.55	3856.0	980332.19	980655.67	0.28	4.15	1.23	39.06	-89.54	-70.27	MH 78
MH 79	45 17.03	-121 36.97	3585.0	980344.10	980655.81	0.16	6.58	1.18	26.16	-98.71	-73.20	MH 79
MH 80	45 14.30	-121 36.79	3449.0	980342.58	980650.90	0.01	3.15	1.15	15.96	-99.67	-82.35	MH 80
MH 81	45 12.81	-121 36.78	2970.0	980373.34	980648.66	0.00	6.36	1.04	3.94	-92.03	-77.65	MH 81
MH 82	45 11.32	-121 37.18	3452.0	980344.27	980646.42	0.03	2.81	1.15	22.42	-94.46	-76.95	MH 82
MH 83	45 14.82	-121 39.37	3283.0	980356.31	980651.68	0.01	5.62	1.11	13.31	-94.15	-78.96	MH 83
MH 84	45 15.98	-121 40.31	3639.0	980339.89	980653.43	0.00	4.68	1.19	28.68	-92.02	-73.95	MH 84
MH 85	45 20.13	-121 42.69	6277.0	980166.97	980659.68	0.01	13.85	1.51	97.36	-104.39	-74.17	MH 85
MH 86	45 20.48	-121 42.67	6635.0	980148.19	980660.19	0.09	17.93	1.52	103.78	-106.19	-74.74	MH 86
MH 87	45 20.71	-121 42.64	6980.0	980114.93	980660.55	0.05	19.83	1.52	110.49	-109.26	-76.34	MH 87
MH 88	45 20.91	-121 42.53	7282.0	980093.72	980660.85	0.13	23.46	1.51	117.35	-109.86	-75.14	MH 88
MH 90	45 21.32	-121 42.36	8068.0	980043.72	980661.46	7.55	33.61	1.46	140.58	-102.45	-66.84	MH 90
MH 91	45 21.51	-121 42.28	8484.0	980007.86	980661.76	8.19	39.68	1.42	143.51	-107.68	-70.85	MH 91
MH 92	45 22.70	-121 54.50	1947.0	980474.22	980663.54	0.01	4.48	0.74	-6.24	-68.91	-59.52	MH 92
MH 93	45 23.02	-121 52.79	2055.0	980453.72	980664.02	0.08	7.68	0.78	-17.06	-80.33	-70.85	MH 93
MH 94	45 23.61	-121 51.90	2389.0	980419.59	980664.90	0.22	6.73	0.88	-20.67	-96.30	-84.97	MH 94
MH 95	45 24.49	-121 50.70	2657.0	980416.55	980666.23	0.27	5.35	0.95	0.15	-86.08	-73.16	MH 95
MH 96	45 25.24	-121 49.32	3118.0	980387.61	980667.37	0.13	3.49	1.07	13.41	-90.51	-74.94	MH 96
MH 97	45 25.80	-121 47.73	3225.0	980367.87	980668.20	0.09	4.45	1.10	2.90	-103.75	-87.77	MH 97
MH 98	45 22.60	-121 49.75	2592.0	980421.09	980663.39	0.03	5.23	0.93	0.48	-83.29	-70.74	MH 98
MH 99	45 24.19	-121 48.84	3811.0	980340.60	980665.77	0.02	7.45	1.22	33.14	-90.62	-72.08	MH 99
MH100	45 26.47	-121 47.52	2909.0	980401.24	980669.21	2.77	6.57	1.02	5.55	-88.11	-74.00	MH100
MH101	45 27.81	-121 46.60	2399.0	980434.24	980671.22	0.08	4.66	0.88	-11.48	-89.45	-77.75	MH101
MH102	45 29.10	-121 45.72	2156.0	980449.63	980673.16	0.06	6.28	0.81	-20.60	-80.66	-78.47	MH102
MH103	45 29.91	-121 44.61	2323.0	980444.34	980674.39	0.13	4.83	0.86	-11.62	-86.80	-75.61	MH103
MH105	45 20.55	-121 53.03	4460.0	980285.53	980660.30	14.19	22.29	1.34	45.29	-86.15	-66.46	MH105
MH106	45 21.86	-121 53.53	4564.0	980274.74	980661.07	16.79	27.42	1.35	42.76	-86.84	-67.42	MH106
MH107	45 19.67	-121 51.93	4017.0	980324.07	980650.99	8.84	8.80	1.26	42.76	-86.71	-67.31	MH107
MH108	45 19.50	-121 51.36	3306.0	980374.48	980658.73	8.84	4.12	1.12	26.59	-83.16	-66.72	MH108
MH109	45 20.34	-121 50.82	3753.0	980346.88	980659.99	0.07	4.74	1.21	39.75	-84.72	-66.07	MH109
MH110	45 20.63	-121 49.47	3995.0	980333.41	980660.42	0.86	5.54	1.26	48.59	-83.30	-63.61	MH110
MH111	45 21.82	-121 50.98	4877.0	980265.86	980661.81	9.86	18.92	1.40	63.35	-85.46	-63.17	MH111
MH112	45 21.05	-121 48.86	4971.0	980260.32	980661.85	11.88	19.84	1.41	66.60	-84.51	-61.87	MH112
MH113	45 20.29	-121 43.80	5744.0	980206.00	980659.92	8.85	11.41	1.48	86.06	-99.92	-72.85	MH113
MH114	45 20.98	-121 44.70	5764.0	980208.98	980660.95	0.88	14.45	1.48	89.81	-93.82	-66.31	MH114
MH115	45 21.69	-121 44.85	5686.0	980211.57	980662.82	8.14	14.73	1.48	84.88	-96.59	-69.53	MH115

ID	LAT	LONG	ELEV	OG	THC	HTC	TTC	CC	FAA	CBA1	CBA2	ID
MH116	45 22.87	-121 45.78	4451.0	980297.07	980662.59	0.22	10.20	1.34	52.94	-90.00	-68.59	MH116
MH117	45 22.77	-121 47.01	3299.0	980373.28	980663.64	0.06	7.09	1.11	19.75	-86.80	-70.84	MH117
MH118	45 23.48	-121 48.63	2739.0	980412.88	980664.71	0.01	5.17	0.98	5.71	-83.51	-70.14	MH118
MH119	45 19.28	-121 46.06	3806.0	980329.67	980658.27	0.02	4.48	1.22	29.24	-97.31	-70.35	MH119
MH120	45 19.30	-121 43.89	4997.0	980252.68	980658.43	0.09	7.26	1.41	64.03	-100.55	-75.90	MH120
MH121	45 26.47	-121 35.66	3169.0	980386.00	980669.22	0.02	4.13	1.08	14.75	-90.29	-74.56	MH121
MH122	45 27.57	-121 35.83	2787.0	980411.89	980670.87	0.01	3.68	0.99	3.07	-89.89	-75.96	MH122
MH123	45 28.16	-121 35.13	2510.0	980430.47	980671.76	0.01	2.79	0.91	-3.28	-89.01	-76.46	MH123
MH124	45 29.63	-121 35.12	2026.0	980464.33	980673.97	0.01	2.74	0.77	-19.13	-86.26	-76.20	MH124
MH125	45 32.18	-121 31.87	3779.0	980358.57	980677.79	4.75	10.66	1.22	36.08	-83.37	-65.47	MH125
MH126	45 30.32	-121 29.34	3954.0	980350.01	980675.00	0.00	3.96	1.25	46.76	-85.39	-65.60	MH126
MH127	45 29.88	-121 26.90	3370.0	980390.35	980674.34	0.04	3.68	1.13	32.06	-79.53	-62.69	MH127
MH128	45 29.66	-121 38.65	3986.0	980344.91	980674.01	0.00	4.34	1.26	45.66	-87.20	-67.30	MH128
MH129	45 27.87	-121 31.60	4444.0	980303.51	980671.31	0.53	11.87	1.33	50.81	-91.83	-70.50	MH129
MH130	45 25.24	-121 31.22	4316.0	980316.84	980667.35	0.00	3.74	1.31	55.26	-89.52	-67.83	MH130
MH131	45 24.55	-121 32.91	4230.0	980321.00	980666.32	0.02	4.07	1.30	53.18	-88.32	-67.12	MH131
MH132	45 27.77	-121 37.52	2845.0	980409.29	980671.17	0.00	3.43	1.00	5.63	-88.98	-74.80	MH132
MH133	45 26.05	-121 40.07	3589.0	980356.46	980668.58	0.26	8.04	1.18	25.33	-90.22	-72.91	MH133
MH134	45 27.01	-121 39.64	3590.0	980357.46	980670.02	0.22	5.18	1.18	24.97	-93.47	-75.72	MH134
MH135	45 26.85	-121 41.81	3670.0	980352.84	980669.78	0.01	4.46	1.20	28.11	-93.79	-75.53	MH135
MH136	45 26.56	-121 43.25	4747.0	980279.89	980669.35	0.30	8.47	1.38	56.82	-97.99	-74.80	MH136
MH137	45 26.79	-121 31.36	4912.0	980274.62	980669.69	9.21	16.58	1.40	66.72	-85.71	-62.87	MH137
MH138	45 26.65	-121 27.81	3632.0	980364.48	980669.47	0.01	2.75	1.19	36.49	-85.82	-67.50	MH138
MH139	45 26.34	-121 29.37	3449.0	980376.63	980669.81	0.08	4.79	1.15	31.98	-82.09	-65.82	MH139
MH140	45 27.77	-121 29.21	3448.0	980376.33	980671.16	0.03	2.81	1.15	29.36	-86.58	-69.21	MH140
MH141	45 28.83	-121 27.57	3030.0	980407.71	980672.77	0.07	2.95	1.05	19.84	-81.69	-66.41	MH141
MH142	45 27.20	-121 26.34	3258.0	980389.53	980670.31	0.02	2.03	1.11	25.55	-84.64	-68.13	MH142
MH143	45 24.63	-121 28.05	4627.0	980295.56	980666.44	0.02	6.37	1.36	64.12	-88.68	-65.79	MH143
MH144	45 23.81	-121 24.68	3475.0	980377.45	980665.21	0.01	2.10	1.15	38.97	-78.61	-60.99	MH144
MH145	45 22.79	-121 26.78	3683.0	980358.92	980663.67	0.03	3.04	1.20	41.53	-81.44	-63.02	MH145
MH146	45 23.15	-121 28.66	4561.0	980302.79	980664.22	0.04	4.51	1.35	67.38	-85.03	-62.19	MH146
MH147	45 21.04	-121 26.41	4309.0	980319.89	980661.03	0.01	4.02	1.31	63.17	-81.00	-59.47	MH147
MH148	45 19.08	-121 27.92	5651.0	980218.77	980658.09	6.85	16.73	1.47	91.91	-85.57	-58.98	MH148
MH149	45 20.31	-121 27.52	4753.0	980287.60	980659.94	0.28	5.92	1.38	74.51	-83.06	-59.45	MH149
MH150	45 21.54	-121 29.07	5217.0	980258.67	980661.80	0.02	6.22	1.43	87.33	-85.02	-59.80	MH150
MH151	45 28.56	-121 31.38	6525.0	980157.61	980660.31	9.41	23.33	1.51	110.66	-90.07	-60.00	MH151
MH152	45 22.92	-121 32.11	5143.0	980257.45	980663.87	0.01	6.98	1.43	77.08	-92.77	-67.33	MH152
MH153	45 25.43	-121 36.73	3982.0	980334.81	980667.64	0.10	4.88	1.26	41.56	-90.63	-70.83	MH153
MH154	45 25.47	-121 38.83	4588.0	980291.06	980667.70	0.05	7.40	1.36	54.70	-95.74	-73.20	MH154
MH155	45 24.93	-121 38.19	4811.0	980278.00	980666.89	0.02	7.31	1.39	63.41	-94.76	-71.86	MH155
MH156	45 24.00	-121 38.80	5718.0	980213.74	980665.49	0.01	10.92	1.48	85.78	-99.80	-72.80	MH156
MH157	45 31.66	-121 37.80	1660.0	980488.61	980677.03	0.09	2.98	0.65	-32.32	-86.69	-78.54	MH157
MH158	45 27.98	-121 39.77	3837.0	980341.12	980671.48	0.02	8.18	1.23	38.39	-93.52	-74.96	MH158

ID	LAT	LONG	ELEV	OG	THC	HTC	TTC	CC	FAA	CBA1	CBA2	ID
MH159	45 28.93	-121 39.39	3204.0	980385.83	980672.92	0.04	3.35	1.09	14.17	-92.85	-76.82	MH159
MH160	45 29.43	-121 38.18	2670.0	980420.87	980673.66	0.00	2.96	0.96	-1.74	-90.80	-77.46	MH160
MH161	45 30.09	-121 39.98	3212.0	980389.21	980674.65	0.00	3.19	1.09	16.57	-90.89	-74.79	MH161
MH162	45 29.56	-121 40.72	3726.0	980354.94	980673.86	0.00	4.88	1.21	31.40	-92.89	-73.59	MH162
MH163	45 27.93	-121 42.00	4450.0	980303.22	980671.40	0.01	6.61	1.34	50.19	-96.31	-74.36	MH163
MH164	45 29.51	-121 42.25	3636.0	980362.44	980673.79	0.05	3.64	1.19	30.51	-91.05	-72.84	MH164
MH165	45 28.52	-121 43.74	4378.0	980306.85	980672.30	0.03	9.14	1.32	46.15	-95.35	-74.15	MH165
MH166	45 30.87	-121 42.77	3778.0	980350.76	980675.83	0.26	9.96	1.22	30.14	-89.97	-71.98	MH166
MH167	45 27.66	-121 44.37	3975.0	980331.21	980671.00	0.21	6.05	1.26	33.94	-96.84	-77.25	MH167
MH168	45 26.44	-121 46.24	2615.0	980417.60	980669.16	0.01	6.60	0.94	-5.68	-89.21	-76.78	MH168
MH169	45 29.39	-121 36.31	2234.0	980449.04	980673.61	0.02	2.86	0.83	-14.58	-88.67	-77.56	MH169
MH170	45 24.15	-121 46.49	4591.0	980283.13	980665.73	11.38	17.14	1.36	49.83	-91.77	-78.68	MH170
MH171	45 24.91	-121 47.58	4534.0	980288.49	980666.87	10.78	16.48	1.35	47.89	-91.62	-78.72	MH171
MH172	45 28.91	-121 48.81	3148.0	980395.81	980672.89	0.01	3.03	1.08	18.91	-86.51	-78.71	MH172
MH173	45 28.17	-121 47.56	3818.0	980338.67	980671.77	14.18	17.81	1.22	25.11	-89.85	-71.94	MH173
MH174	45 30.85	-121 46.67	2651.0	980425.62	980675.79	0.01	3.91	0.95	-0.91	-88.37	-75.26	MH174
MH175	45 29.76	-121 47.68	4468.0	980296.43	980674.15	12.16	19.57	1.34	42.34	-91.82	-71.72	MH175
MH176	45 28.68	-121 36.89	5060.0	980256.98	980660.50	0.02	6.88	1.42	72.18	-95.73	-70.58	MH176
MH177	45 21.51	-121 36.21	4801.0	980276.48	980661.76	0.17	6.56	1.39	66.88	-92.57	-68.81	MH177
MH178	45 22.86	-121 35.67	4169.0	980320.62	980663.79	0.09	6.66	1.29	40.79	-88.03	-67.53	MH178
MH179	45 23.96	-121 35.49	3744.0	980354.68	980665.43	0.40	5.98	1.21	41.26	-81.66	-63.25	MH179
MH180	45 19.38	-121 38.80	4472.0	980292.79	980658.54	0.00	4.56	1.34	54.68	-94.62	-72.25	MH180
MH181	45 19.18	-121 33.59	5916.0	980195.45	980658.12	10.28	19.60	1.49	93.47	-90.19	-62.60	MH181
MH182	45 19.87	-121 31.47	3899.0	980341.48	980658.87	0.03	7.27	1.24	49.91	-77.04	-58.02	MH182
MH183	45 19.88	-121 30.30	3586.0	980358.75	980658.89	3.52	7.91	1.18	37.83	-77.75	-60.43	MH183
MH184	45 18.80	-121 29.96	3424.0	980368.88	980657.67	3.56	8.19	1.14	32.27	-77.47	-61.83	MH184
MH185	45 17.49	-121 28.88	3049.0	980386.84	980655.71	0.87	8.55	1.06	17.82	-78.68	-64.22	MH185
MH186	45 17.08	-121 27.95	2848.0	980397.48	980655.88	0.18	8.57	1.08	10.11	-79.46	-66.84	MH186
MH187	45 16.12	-121 26.36	2549.0	980409.29	980653.64	0.28	7.68	0.92	-4.67	-84.93	-72.91	MH187
MH188	45 16.37	-121 29.87	4370.0	980299.25	980654.82	8.37	4.24	1.32	56.08	-98.85	-68.16	MH188
MH189	45 15.44	-121 29.34	4261.0	980299.97	980652.62	0.02	3.93	1.31	47.96	-94.75	-73.37	MH189
MH190	45 19.97	-121 39.86	5358.0	980229.32	980659.44	0.01	8.81	1.45	73.59	-101.79	-75.52	MH190
MH191	45 21.83	-121 39.44	5558.0	980215.57	980661.83	0.28	12.91	1.47	76.29	-101.56	-74.91	MH191
MH192	45 21.14	-121 37.99	5656.0	980213.87	980661.19	0.85	8.57	1.47	83.59	-102.22	-74.39	MH192
MH193	45 21.56	-121 38.74	6633.0	980140.46	980661.82	9.97	22.82	1.52	102.15	-102.78	-72.88	MH193
MH194	45 22.43	-121 39.58	7360.0	980096.09	980663.13	8.39	22.73	1.51	124.78	-105.82	-70.60	MH194
MH195	45 23.41	-121 39.48	6658.0	980146.84	980664.60	0.12	16.72	1.52	107.34	-104.26	-72.56	MH195
MH196	45 31.43	-121 34.80	1649.0	980493.41	980676.60	0.00	3.41	0.65	-28.21	-81.68	-73.67	MH196
MH197	45 29.86	-121 33.68	1831.0	980478.63	980674.31	0.02	5.71	0.71	-23.51	-80.96	-72.35	MH197
MH198	45 27.89	-121 34.12	2157.0	980452.56	980671.34	0.03	6.23	0.81	-15.95	-84.10	-73.89	MH198
MH199	45 26.77	-121 34.67	2401.0	980434.28	980669.66	0.03	8.16	0.88	-9.61	-84.23	-73.85	MH199
MH200	45 23.78	-121 34.14	3075.0	980391.24	980665.84	0.06	9.03	1.06	15.33	-81.50	-67.86	MH200
MH201	45 22.45	-121 33.96	3305.0	980364.42	980663.16	0.02	7.46	1.12	12.01	-94.37	-78.44	MH201

ID	LAT	LONG	ELEV	OG	THG	HTC	TTC	CC	FAA	CBA1	CBA2	ID
MH202	45 20.37	-121 34.19	3559.0	980357.88	980660.04	0.01	7.85	1.17	32.37	-82.30	-65.12	MH202
MH203	45 31.19	-121 36.52	1704.0	980485.98	980676.32	0.01	2.43	0.67	-30.10	-86.46	-78.01	MH203
MH204	45 30.78	-121 40.99	2803.0	980416.45	980675.69	0.28	5.24	0.99	4.32	-87.04	-73.35	MH204
MH205	45 30.52	-121 50.08	4057.0	980334.62	980675.30	16.04	28.01	1.27	40.75	-78.08	-60.96	MH205
MH206	45 24.20	-121 39.90	5994.0	980192.35	980665.80	0.31	15.28	1.58	90.22	-100.43	-71.87	MH206
MH207	45 24.34	-121 41.45	5915.0	980198.93	980666.00	0.00	13.85	1.49	88.98	-100.40	-72.03	MH207
MH208	45 24.84	-121 41.87	5828.0	980203.62	980666.76	0.00	15.23	1.49	84.73	-100.38	-72.58	MH208
MH209	45 24.76	-121 43.81	5653.0	980217.43	980666.64	0.13	12.82	1.47	82.21	-99.25	-72.86	MH209
MH210	45 24.16	-121 43.89	5579.0	980221.75	980665.73	0.10	14.12	1.47	80.49	-97.14	-70.53	MH210
MH211	45 21.37	-121 51.86	3866.0	980389.96	980661.53	0.12	6.40	1.06	16.71	-82.52	-67.65	MH211
MH212	45 22.49	-121 51.49	2458.0	980427.46	980663.23	0.58	6.61	0.90	-5.40	-83.24	-71.58	MH212
MH213	45 23.53	-121 49.91	2895.0	980401.58	980664.79	0.05	4.85	1.02	9.00	-85.91	-71.69	MH213
MH214	45 24.81	-121 53.99	2571.0	980421.18	980665.51	0.20	4.81	0.93	-2.58	-87.19	-74.51	MH214
MH215	45 24.88	-121 52.53	2943.0	980399.69	980666.70	0.88	3.80	1.03	9.71	-87.90	-73.27	MH215
MH216	45 25.75	-121 51.35	3633.0	980357.57	980668.12	0.01	2.73	1.19	31.03	-91.34	-73.81	MH216
MH217	45 26.99	-121 53.86	2791.0	980414.86	980669.99	0.06	2.38	0.99	7.38	-86.58	-72.45	MH217
MH218	45 26.83	-121 52.80	3043.0	980396.86	980668.54	0.03	4.32	1.05	13.64	-86.88	-71.83	MH218
MH219	45 27.84	-121 52.38	2938.0	980404.65	980670.06	0.19	3.42	1.03	10.84	-86.98	-72.32	MH219
MH220	45 28.43	-121 54.16	2739.0	980421.70	980672.15	0.01	2.58	0.98	7.09	-84.72	-70.97	MH220
MH221	45 28.71	-121 52.73	2622.0	980427.01	980672.58	0.09	4.78	0.94	8.97	-84.62	-71.88	MH221
MH222	45 29.52	-121 54.06	2489.0	980437.07	980673.80	0.01	3.39	0.91	-2.70	-85.10	-72.76	MH222
MH223	45 27.65	-121 50.64	3166.0	980392.23	980670.98	0.09	2.94	1.08	18.93	-87.19	-71.38	MH223
MH224	45 26.17	-121 49.87	4112.0	980324.46	980668.76	0.09	5.48	1.28	42.38	-93.82	-73.43	MH224
MH225	45 27.23	-121 48.32	4565.0	980284.17	980670.35	15.68	22.36	1.35	43.88	-91.69	-71.51	MH225
MH226	45 27.94	-121 49.43	4338.0	980308.38	980671.43	9.66	14.79	1.32	44.88	-89.68	-69.54	MH226
MH227	45 28.38	-121 50.86	4566.0	980291.15	980672.08	10.74	16.84	1.35	48.34	-91.98	-70.89	MH227
MH228	45 25.12	-121 46.11	2999.0	980388.93	980667.18	0.88	8.79	1.04	3.74	-90.88	-76.64	MH228
MH230	45 29.91	-121 58.65	2935.0	980405.07	980674.38	0.00	5.88	1.03	6.65	-88.68	-74.33	MH230
MH231	45 28.82	-121 46.78	4185.0	980311.17	980659.58	0.00	5.14	1.29	45.13	-93.76	-72.95	MH231
MH232	45 22.48	-121 41.69	11235.0	979763.58	980663.09	42.52	125.87	0.87	156.25	-181.94	-63.26	MH232
GS 1	45 18.18	-121 49.23	2798.0	980394.20	980656.74	0.89	7.37	0.99	-0.20	-88.98	-75.68	GS 1
GS 2	45 18.28	-121 43.16	4380.0	980292.94	980656.89	0.03	4.57	1.32	47.85	-98.38	-76.40	GS 2
GS 3	45 15.73	-121 38.39	4515.0	980283.25	980653.85	0.18	5.69	1.35	54.68	-94.97	-72.55	GS 3
GS 4	45 17.15	-121 40.26	4081.0	980320.43	980655.19	0.01	3.83	1.27	48.93	-88.58	-67.91	GS 4
GS 5	45 18.14	-121 36.13	4195.0	980306.98	980656.68	0.19	4.45	1.29	44.71	-95.21	-74.25	GS 5
GS 6	45 26.38	-121 37.40	3685.0	980357.47	980669.07	0.01	4.57	1.28	34.86	-87.45	-69.12	GS 6
GS 7	45 24.75	-121 36.23	3920.0	980339.83	980666.62	0.85	5.88	1.24	40.96	-88.98	-69.44	GS 7
GS 8	45 23.78	-121 29.98	4577.0	980301.26	980665.84	0.88	3.98	1.35	66.53	-86.95	-63.96	GS 8
GS 9	45 25.66	-121 32.86	3923.0	980339.45	980667.99	0.03	3.83	1.25	48.29	-98.92	-71.26	GS 9
GS10	45 26.46	-121 32.51	3730.0	980357.77	980669.19	0.01	4.87	1.21	39.27	-85.88	-66.45	GS10
GS11	45 21.38	-121 33.99	3445.0	980366.99	980661.55	0.00	6.93	1.15	29.35	-82.37	-65.63	GS11
GS12	45 17.58	-121 34.83	5220.0	980242.74	980655.71	0.39	6.52	1.44	77.76	-95.19	-69.28	GS12
GS13	45 18.41	-121 34.28	5585.0	980219.18	980657.88	0.38	18.61	1.47	87.13	-94.21	-67.84	GS13

ID	LAT	LONG	ELEV	OG	THG	HTC	TTC	CC	FAA	CBA1	CBA2	ID
GS14	45 20.00	-121 32.86	5220.0	980256.40	980659.48	0.01	7.07	1.44	87.66	-84.74	-58.91	GS14
GS15	45 22.05	-121 31.75	5495.0	980238.42	980662.56	0.01	8.40	1.46	92.44	-88.04	-61.00	GS15
GS16	45 21.48	-121 30.45	5685.0	980225.79	980661.70	0.00	8.37	1.48	98.52	-88.48	-60.47	GS16
GS17	45 23.82	-121 51.76	2870.0	980453.61	980664.02	0.00	5.15	0.78	-15.76	-82.00	-72.07	GS17
GS18	45 23.13	-121 50.33	2330.0	980437.13	980664.10	0.00	5.09	0.86	-7.96	-83.20	-71.93	GS18
GS19	45 23.03	-121 49.20	2940.0	980397.01	980664.03	0.25	4.69	1.03	10.21	-86.40	-71.93	GS19
GS20	45 21.43	-121 47.63	3230.0	980374.11	980661.63	4.76	8.86	1.10	16.10	-86.22	-70.88	GS20
GS21	45 23.79	-121 50.91	2540.0	980427.30	980665.10	0.02	3.92	0.92	0.95	-82.60	-70.15	GS21
GS22	45 24.44	-121 49.45	2900.0	980400.79	980666.16	0.12	4.69	1.02	7.31	-87.93	-73.66	GS22
GS23	45 24.06	-121 49.85	3410.0	980372.07	980665.50	0.57	5.33	1.14	27.90	-04.21	-67.41	GS23
GS24	45 24.19	-121 47.57	3865.0	980334.34	980665.70	0.33	6.54	1.23	31.95	-94.57	-75.62	GS24
GS25	45 23.20	-121 47.55	3015.0	980388.62	980664.41	0.39	6.34	1.05	7.70	-89.04	-75.23	GS25
GS26	45 23.75	-121 47.91	2820.0	980403.54	980665.12	0.00	5.00	1.00	3.50	-87.00	-74.11	GS26
GS27	45 23.43	-121 48.46	2750.0	980410.61	980664.63	0.00	5.31	0.98	4.55	-84.91	-71.51	GS27
GS28	45 19.11	-121 42.83	5220.0	980238.10	980658.14	0.38	7.94	1.44	70.70	-100.75	-75.05	GS28
GS29	45 18.79	-121 43.17	4920.0	980258.02	980657.65	0.01	6.59	1.40	62.91	-99.70	-75.34	GS29
GS30	45 16.82	-121 43.94	3620.0	980342.43	980654.69	0.00	2.54	1.19	28.10	-94.01	-75.72	GS30
GS31	45 17.91	-121 42.97	4192.0	980306.00	980656.33	0.03	3.94	1.29	43.07	-96.46	-75.43	GS31
GS32	45 17.63	-121 43.21	4040.0	980315.20	980655.91	0.05	3.56	1.27	39.13	-96.37	-76.07	GS32
N 1	45 19.05	-121 42.54	5910.0	980192.75	980659.25	0.01	11.35	1.49	89.00	-102.63	-73.91	N 1
N 2	45 19.90	-121 42.56	5949.0	980190.03	980659.32	0.04	11.66	1.49	89.95	-102.79	-73.91	N 2
N 3	45 19.94	-121 42.59	6004.0	980186.02	980659.30	0.04	12.17	1.50	91.04	-103.06	-73.90	N 3
N 4	45 19.99	-121 42.62	6041.0	980183.54	980659.46	0.05	12.50	1.50	91.97	-103.07	-73.85	N 4
N 5	45 20.03	-121 42.62	6101.0	980179.21	980659.52	0.16	12.89	1.50	93.22	-103.40	-74.01	N 5
N 6	45 20.07	-121 42.66	6148.0	980175.80	980659.50	0.00	13.07	1.50	94.24	-103.80	-74.20	N 6
N 7	45 20.11	-121 42.67	6190.0	980173.00	980659.65	0.11	13.24	1.50	95.24	-104.15	-74.20	N 7
N 8	45 20.15	-121 42.67	6229.0	980170.41	980659.71	0.07	13.38	1.51	96.25	-104.33	-74.20	N 8
N 9	45 20.20	-121 42.68	6274.0	980167.30	980659.70	0.11	13.72	1.51	97.30	-104.47	-74.24	N 9
N10	45 20.24	-121 42.68	6315.0	980164.54	980659.84	0.04	13.99	1.51	98.33	-104.57	-74.17	N10
N11	45 20.29	-121 42.70	6357.0	980161.59	980659.90	0.07	14.40	1.51	99.26	-104.50	-74.04	N11
N12	45 20.32	-121 42.70	6412.0	980157.52	980659.95	0.10	15.21	1.51	100.31	-104.60	-73.97	N12
N13	45 20.35	-121 42.71	6460.0	980153.95	980660.01	0.10	15.89	1.51	101.20	-104.75	-73.90	N13
N14	45 20.30	-121 42.72	6504.0	980150.69	980660.05	0.07	16.54	1.51	102.03	-104.77	-73.79	N14
N15	45 20.42	-121 42.74	6553.0	980147.00	980660.11	0.07	17.20	1.51	102.89	-104.85	-73.73	N15
N16	45 20.45	-121 42.77	6605.0	980142.95	980660.15	0.12	18.09	1.52	103.68	-105.02	-73.76	N16
N17	45 20.48	-121 42.78	6646.0	980139.80	980660.19	0.06	18.42	1.52	104.34	-105.43	-74.00	N17
N18	45 20.52	-121 42.76	6691.0	980136.50	980660.26	0.06	18.17	1.52	105.28	-106.20	-74.50	N18
N19	45 20.56	-121 42.76	6741.0	980132.90	980660.31	0.10	18.38	1.52	106.24	-106.81	-74.89	N19
N20	45 20.58	-121 42.76	6784.0	980129.68	980660.35	0.10	18.59	1.52	107.03	-107.20	-75.18	N20
N21	45 20.63	-121 42.75	6838.0	980124.62	980660.43	0.10	18.98	1.52	108.04	-107.60	-75.17	N21
S 1	45 19.86	-121 42.67	5932.0	980190.92	980659.27	0.04	11.65	1.49	89.30	-102.87	-74.00	S 1
S 2	45 19.82	-121 42.68	5886.0	980194.21	980659.21	0.04	11.19	1.49	88.32	-102.73	-74.10	S 2
S 3	45 19.79	-121 42.68	5854.0	980196.40	980659.16	0.05	10.90	1.49	87.56	-102.69	-74.19	S 3

ID	LAT	LONG	ELEV	OG	THG	HTC	TTC	CC	FAA	CBA1	CBA2	ID
S 4	45 19.75	-121 42.69	5804.0	980199.95	980659.89	0.06	10.51	1.48	86.47	-102.46	-74.15	S 4
S 5	45 19.70	-121 42.70	5759.0	980202.99	980659.83	0.06	10.26	1.48	85.35	-102.30	-74.18	S 5
S 6	45 19.66	-121 42.71	5696.0	980207.48	980658.96	0.07	10.04	1.48	83.99	-101.72	-73.98	S 6
S 7	45 19.62	-121 42.71	5640.0	980211.36	980658.90	0.07	9.95	1.47	82.67	-101.22	-73.67	S 7
S 8	45 19.57	-121 42.71	5582.0	980215.50	980658.83	0.05	9.93	1.47	81.43	-100.49	-73.24	S 8
S 9	45 19.52	-121 42.72	5541.0	980218.19	980658.75	0.07	9.86	1.46	80.34	-100.25	-73.19	S 9
S10	45 19.47	-121 42.73	5452.0	980223.92	980658.68	0.17	9.39	1.46	77.78	-100.24	-73.57	S10
S11	45 19.42	-121 42.73	5411.0	980226.70	980658.61	0.23	9.02	1.45	76.78	-100.20	-73.69	S11
S12	45 19.38	-121 42.74	5387.0	980228.33	980658.54	0.19	8.72	1.45	76.22	-100.24	-73.80	S12
S13	45 19.33	-121 42.76	5346.0	980231.06	980658.46	0.21	8.37	1.45	75.18	-100.24	-73.96	S13
S14	45 19.27	-121 42.76	5349.0	980230.50	980658.37	0.01	8.16	1.45	74.99	-100.74	-74.41	S14
E 1	45 19.99	-121 42.57	6022.0	980185.01	980659.47	0.05	12.19	1.50	91.64	-103.05	-73.88	E 1
E 2	45 19.98	-121 42.51	6019.0	980185.07	980659.45	0.05	12.12	1.50	91.44	-103.22	-74.06	E 2
E 3	45 20.01	-121 42.42	5998.0	980187.31	980659.49	0.15	12.15	1.50	90.91	-102.73	-73.72	E 3
E 4	45 20.03	-121 42.33	5977.0	980188.86	980659.52	0.50	12.76	1.49	90.41	-102.18	-73.33	E 4
E 5	45 20.01	-121 42.26	5951.0	980189.68	980659.50	0.01	12.30	1.49	89.61	-102.55	-73.76	E 5
E 6	45 20.02	-121 42.18	5939.0	980190.38	980659.50	0.03	12.23	1.49	89.18	-102.64	-73.91	E 6
W 1	45 19.98	-121 42.65	6058.0	980182.17	980659.44	0.05	12.86	1.50	92.21	-103.04	-73.79	W 1
W 2	45 19.99	-121 42.70	6071.0	980181.14	980659.46	0.05	13.04	1.50	92.38	-103.14	-73.85	W 2
W 3	45 20.00	-121 42.76	6083.0	980180.15	980659.47	0.05	13.21	1.50	92.51	-103.25	-73.92	W 3
W 4	45 20.01	-121 42.80	6072.0	980181.05	980659.50	0.05	12.87	1.50	92.35	-103.37	-74.05	W 4
W 5	45 20.03	-121 42.84	6067.0	980181.43	980659.52	0.11	12.83	1.50	92.23	-103.36	-74.06	W 5
W 6	45 20.04	-121 42.89	6044.0	980182.81	980659.53	0.12	12.62	1.50	90.65	-104.37	-75.15	W 6
W 7	45 20.04	-121 42.89	6045.0	980182.73	980659.54	0.05	12.56	1.50	91.45	-103.66	-74.43	W 7
W 8	45 20.05	-121 43.02	6057.0	980181.17	980659.55	0.05	12.55	1.50	91.01	-104.52	-75.23	W 8
W 9	45 20.06	-121 43.10	6033.0	980182.41	980659.57	0.22	12.61	1.50	89.98	-104.68	-75.51	W 9
W10	45 20.06	-121 43.16	6032.0	980182.13	980659.57	0.05	12.52	1.50	89.60	-105.11	-75.94	W10
CS33	45 19.71	-121 42.68	5776.0	980202.29	980659.04	0.12	10.37	1.48	86.23	-101.88	-73.70	CS33

HEAT FLOW MODELING OF THE MOUNT HOOD VOLCANO, OREGON

By

DAVID D. BLACKWELL
and
JOHN L. STEELE

Department of Geological Sciences

Southern Methodist University

Dallas, Texas 75275

June 1979

Final report of work carried out under Grant SMU #86-09 from the Oregon Department of Geology and Mineral Industries; July 1977 through March 1979.

TABLE OF CONTENTS

Page

INTRODUCTION..... 195

THERMAL MODELS OF MAGMA CHAMBERS WITH SPECIFIC APPLICATIONS TO STRATOCONE VOLCANOES..... 200

Introduction..... 200

Basic Model Shapes..... 201

Plane Surface Instantaneous Magma Chamber Models..... 206

More Realistic Models..... 211

Shallow Magma Chamber Models..... 212

Continuous Neck Magma Chamber Model..... 219

Discussion..... 221

REGIONAL HEAT FLOW IN THE NORTHERN CASCADE RANGE IN OREGON..... 225

Regional Heat Flow Setting..... 225

Northern Oregon Cascade Range Heat Flow..... 233

Interpretation of Heat Flow Transition Zone..... 243

Heat Flow Along the Eastern Boundary of the High Cascade Range..... 248

GEOTHERMAL STUDIES ASSOCIATED WITH MT. HOOD..... 250

Mt. Hood Regional Heat Flow Studies..... 250

Old Maid Flat Drill Holes #1/2 and #3..... 254

Timberline Lodge Drill Holes #1 and #2..... 261

REFERENCES..... 263

LIST OF FIGURES

		Page
1	LOCATION MAP OF CASCADE STRATOCONE VOLCANOES	198
2	TOPOGRAPHIC CROSS-SECTION OF MT. HOOD	202
3	BASIC MODEL SHAPES FOR TWO-DIMENSIONAL MAGMA CHAMBER MODELS	204
4	MAGMA CHAMBER MODEL SIZES IN RELATION TO SURFACE HALF-SPACE	207
5	SURFACE HEAT FLOW-VERSUS-DISTANCE CURVES FOR PLANE SURFACE INSTANTANEOUS MODELS	210
6	SURFACE HEAT FLOW-VERSUS-DISTANCE CURVES FOR SHALLOW MAGMA CHAMBER MODEL	213
7	HEAT FLOW-VERSUS-TIME CURVES FOR THE SHALLOW CYLINDRICAL CONTINUOUS MODEL	216
8	ISOTHERMAL CROSS-SECTION MAP OF THE VOLCANIC EDIFICE FOR THE SHALLOW MAGMA CHAMBER MODEL	218
9	HEAT FLOW-VERSUS-TIME CURVES FOR THE CYLINDRICAL INSTANTANEOUS AND CONTINUOUS NECK MODELS	220
10	GENERALIZED HEAT FLOW MAP OF OREGON	232
11	HEAT FLOW MAP OF THE NORTHERN CASCADE RANGE AREA OF OREGON	234
12	HEAT FLOW HISTOGRAMS FOR THE NORTHERN CASCADE RANGE PROVINCE BOUNDARIES	236
13	TYPICAL TEMPERATURE-DEPTH CURVES FOR THE WESTERN CASCADE RANGE-WILLAMETTE VALLEY PROVINCE BOUNDARY	237
14	TYPICAL TEMPERATURE-DEPTH CURVES FOR THE WESTERN CASCADE RANGE-HIGH CASCADE RANGE PROVINCE BOUNDARY	239
15	A AND B. HEAT FLOW CROSS-SECTIONS OF THE WILLAMETTE VALLEY-WESTERN CASCADE RANGE-HIGH CASCADE RANGE PROVINCE BOUNDARIES	240
16	A AND B. HEAT FLOW-GRAVITY TRANSITION ZONE MODELS	244
17	TYPICAL TEMPERATURE-DEPTH CURVES FOR THE EASTERN HIGH CASCADE RANGE PROVINCE BOUNDARY	249
18	TEMPERATURE-DEPTH CURVES FOR 1978 MT. HOOD DATA	251
19	HEAT FLOW PROFILE OF MT. HOOD	253

LIST OF FIGURES (Con't.)

Page

20 TEMPERATURE-DEPTH CURVES FOR THE OLD MAID FLAT HOLE #1/2..... 255

21 TEMPERATURE-DEPTH CURVES FOR THE OLD MAID FLAT HOLE #3 AND THE TIMBERLINE LODGE HOLES #1 AND #2..... 260

LIST OF TABLES

Page

1 VALUES OF PARAMETERS FOR THERMAL MODELS OF MAGMA CHAMBERS..... 209

2 THERMAL AND LOCATION DATA IN THE NORTHERN CASCADE RANGE OF OREGON..... 226-231

INTRODUCTION

Most of the currently active volcanoes are associated with volcanic arcs which form over subducting slabs of lithosphere in plate collision areas. Large stratocone volcanoes of generally andesitic composition are typically associated with these active volcanic arcs, although extrusions of basaltic composition are probably more volumetrically important. Along the western Pacific there is an almost continuous string of volcanic arcs associated with subducting slabs of lithosphere. Along the western margin of the North American Continent the subduction is more fragmented than in the western Pacific; however, there are several distinct regions where volcanic arcs are developed. These regions are the Aleutian arc of Alaska, the Cascade Range of the northwestern United States, the trans-Mexico volcanic belt in Mexico, and the Central American volcanic arc. Active subduction is definitely occurring at the first and last of these areas, as evidenced by large numbers of intermediate and deep focus earthquakes generated within the cold sinking block of lithosphere. Along southwestern Mexico there are numerous earthquakes of intermediate focal depth which generally line up to indicate a slab with a very shallow dip.

On the other hand, in the Pacific Northwest, there are no intermediate or deep focus earthquakes, so direct seismic evidence for the existence of a subducting slab does not exist. However, the deepest earthquakes in the conterminous United States (60 km) are associated with the Puget Sound area of

northwestern Washington, and so apparently the tectonic situation must be different in some way from the remainder of the western United States. Moreover, based on the evidence of abundant volcanism in the Cascade Range, and the present-day existence of many large stratocone volcanoes which would be rapidly removed by erosion, it is apparent that subduction has been active in the Pacific Northwest within the past few thousand years. Subduction may be continuing, but at a low level or with the block too hot to generate earthquakes.

Although extrusive rocks of basaltic composition often are volumetrically dominant in the volcanic arcs associated with subduction zones, the associated intrusive rocks are dominantly of granitic composition. Thus, it is felt that geothermal systems are more likely to be associated with volcanic rocks of andesitic to rhyolitic composition where the magmas are more viscous and more likely to solidify as intrusive rocks rather than proceed to the surface and be extruded (see Smith and Shaw, 1975). By cooling below the surface, more thermal energy is transferred into the shallow crust and hydrothermal convection systems are more likely to be formed. In fact, epizonal plutons probably cool dominantly, if not completely, by hydrothermal convection rather than conduction.

Around the world, many geothermal systems are associated with andesite volcanoes. In particular, several of the geothermal systems in Japan, such as Matzukawa and Otaki, are associated with stratocone volcanoes. In Central America, the geothermal fields at Ahuachapán, El Sálvador; Mombotambo, Nicaragua; and in Costa Rica are also associated with stratocone

volcanoes and are currently producing or will soon produce electrical power. Therefore, the Cascade Range of the Pacific Northwest represents an obvious focus for geothermal exploration. However, in spite of the abundant evidence of voluminous volcanism of variable composition in the Cascade Range, thermal manifestations are much more subdued than those typically associated with the island arcs. The only thermal manifestations which appear major from their surface evidence are associated with Mt. Lassen, in northern California. The remainder of the andesite volcanoes in the Cascade Range display only weak evidence of hydrothermal activity, although most of the volcanoes have vent fumaroles and have been historically active.

The overall thrust of this project was to investigate the geothermal potential of the Mt. Hood volcano as a guide to estimating the geothermal potential of other stratocone volcanoes in the Cascades. The assumption was made, therefore, that Mt. Hood represents a typical stratocone volcano and that the information obtained in the study of Mt. Hood could be transferred to other stratocone volcanoes in the western United States. A location map showing the Cascade stratovolcanoes is given in Figure 1. In view of the generality of the approach, part of the research carried out in the project was a more generally-oriented study of thermal effects of magma chamber systems associated with stratocone volcanoes and of regional heat flow in the Cascades.

The report is essentially divided into three sections. In the first section, some examples of simple cooling models of different shapes of magma chambers that might be associated

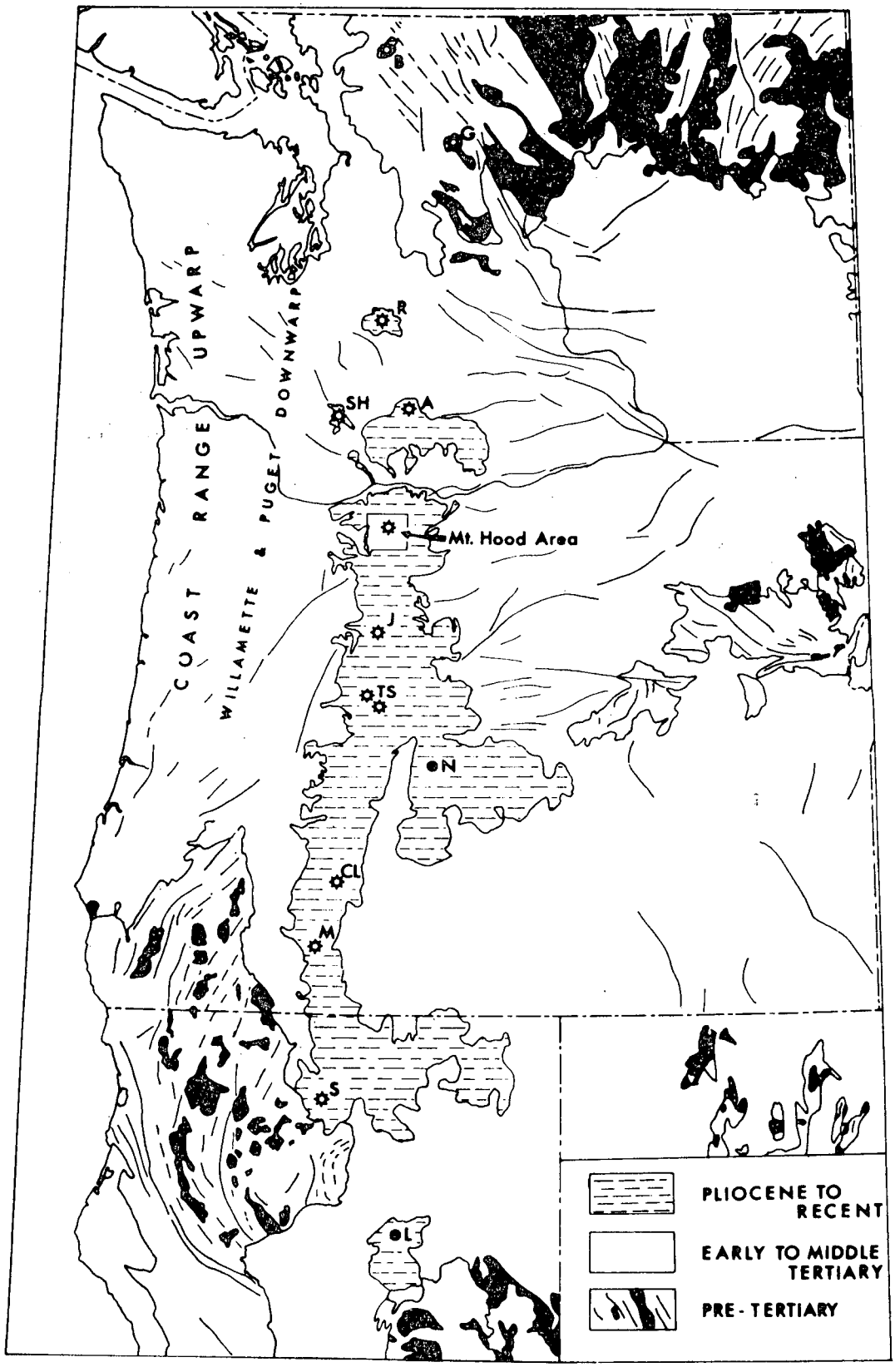

Figure 1. Location map of Cascade stratocone volcanoes (from Wise, 1969).

with stratocone volcanoes are discussed. These simple models are calculated in order to investigate the effects of different geometry on the total heat transfer of the system, rate of cooling, and volcanic recurrence times necessary to keep the crust hot.

In the second section, a description of a detailed study of the Western Cascade-High Cascade boundary in the Western Cascade province is discussed along with the results of heat flow studies along the eastern boundary of the Northern Cascade Range of Oregon. These studies are presented here for completeness and for comparison with the data obtained in the Mt. Hood region.

The final section is a discussion of the heat flow in the vicinity of Mt. Hood, including near-regional exploration holes, and deep exploration holes at Timberline Lodge and at Old Maid Flat at the foot of the Mt. Hood volcano.

THERMAL MODELS OF MAGMA CHAMBERS WITH SPECIFIC APPLICATIONS TO STRATOCONE VOLCANOES

Introduction

A number of different models for the cooling of magma chambers have been discussed in the literature. Most of the models have included discussion of the cooling of a magma emplaced instantaneously at constant temperature, with subsequent cooling from this constant initial temperature (Jaeger, 1963, 1964; Blackwell and Baag, 1974; Lachenbruch and others, 1976). In these models, the magma is assumed to cool conductively once it is in place, and no modifications are included to allow for possible convection in the magma during cooling, permeation of water through the cooling country rock or solidified intrusive rock, or any complexities that might be involved with emplacement of a major magma chamber. In the simplest form, the model predicts that the country rock temperature in contact with the magma chambers never reaches a temperature greater than 0.5 T_m,, where T_m is the melt temperature. This model is referred to as the instantaneous model.

Another simple conduction model for magma chamber evolution assumes emplacement of the magma at some time and its subsequent maintenance as a magma chamber over a long period of time. In this case, the rock in contact with the magma will eventually be heated up to the magma temperature. This model, the continuous mode, would be more appropriate for a long-lived magma chamber into which batches of magma were repeatedly emplaced or, for moderate times at least, a very large convecting

magma chamber. Of course, at some time such a chamber must eventually begin to cool off, but there is geological evidence that many magma chambers are resupplied by magma and thus can maintain a liquid zone over a long period of time relative to the cooling period of the instantaneous model.

If the magma chamber is maintained for an extreme period of time, the thermal effects eventually reach a steady-state. Ultimately, of course, the magma must start to cool off. Yuhara (1974) has presented some steady-state models of a linear volcano with a plane (vertical) source magma chamber. He illustrates the temperature for such a model for different depths to the plane source.

In general, the geological evidence indicates that most, if not all, magma chambers emplaced in the epizonal region of a crust (1-5 km) actually cool dominantly by convection of heated ground water through the cooling rock in a hydrothermal system. Very seldom is it likely that a large magma chamber would cool conductively. However, analysis of the rate of heat transfer in typical geothermal systems suggests that typical efficiency of convective cooling is not particularly great; the heat transferred by a convection system being on the order of two to ten times the rate of heat loss by conductive cooling alone. So the average heat loss for convective cooling as contrasted with conductive cooling of an active magma chamber might be estimated to be on the order of five.

Basic Model Shapes

Figure 2 shows a topographic cross-section along an

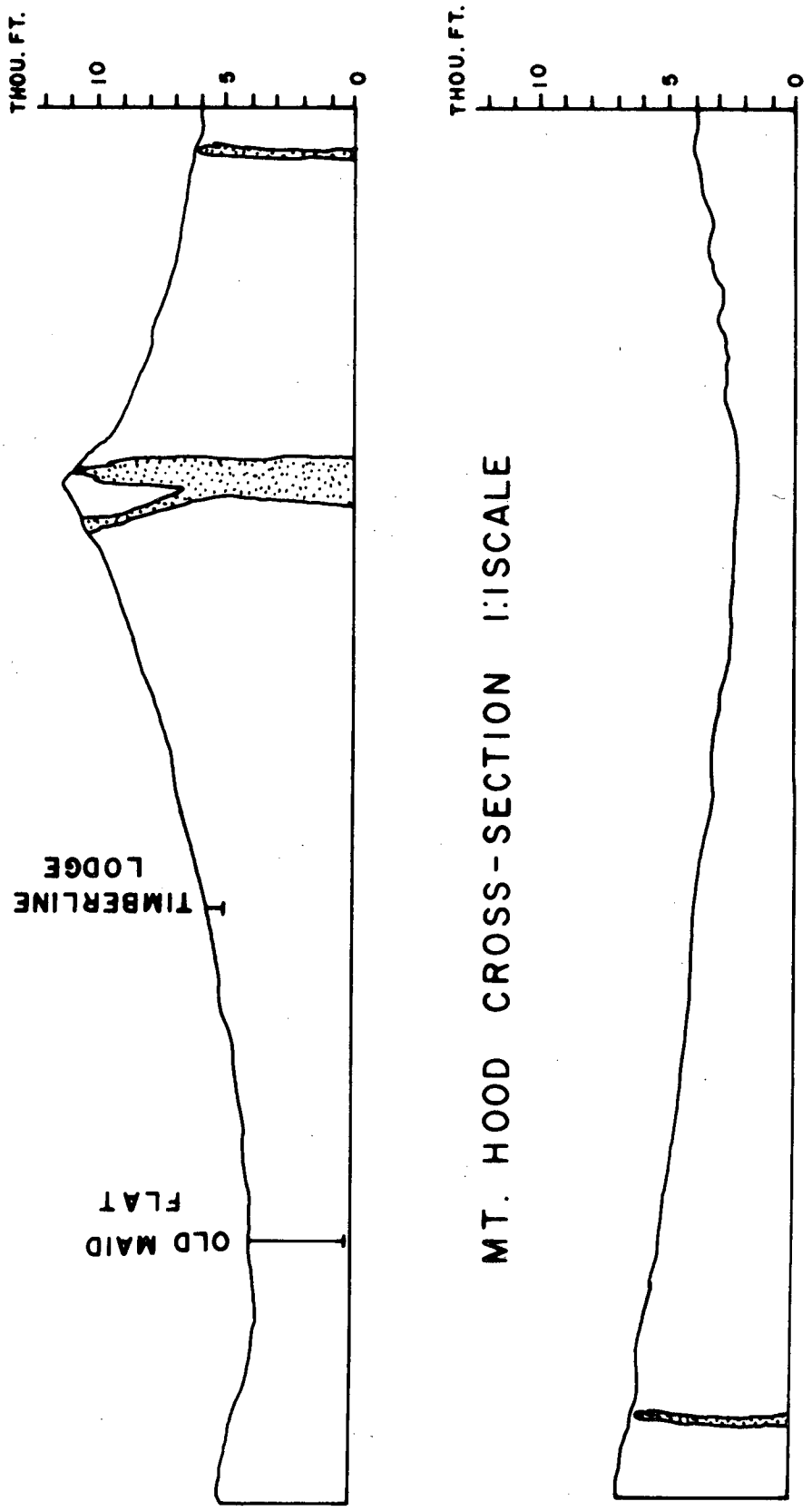

Figure 2. Topographic cross-section of Mt. Hood: east-west profile at a scale of 1:1. Locations and drilled depths of two major heat flow holes are shown.

approximately east-west line through Mt. Hood. This cross-section has equal horizontal and vertical scales. Also shown on the volcano are the locations and scaled depths of two relatively deep exploratory holes which have been drilled for geothermal studies.

Mt. Hood is a typical stratocone volcano. It has a relief of about 1.5 km and a radius of 5 km, giving an approximate surface area of 80 km^2 and a volume of 40 km^3. The geology of the volcano has been discussed by Wise (1968). Most of the volcano was formed in late Pleistocene, and a major eruption which formed most of the south flank of the volcano occurred about 1,600 years ago. The most recent major activity has been dated at about 220 years ago (Crandell and Rubin, 1977). The volcano was in minor eruption between 1848 and 1865, according to newspaper accounts. There is an active fumarolic system near the top of the volcano, but only a "single" thermal spring with several orifices is associated with the volcano (Swim Spring). The spring is along the southern edge of Mt. Hood.

In the discussion of the conductive cooling of magma chambers, two basic shapes will be considered (Figure 3). The first is a parallelepiped with infinite extent in the Y direction, a width equal to 2A, and a thickness equal to L, emplaced at a constant initial temperature (T_o), and at a depth D below the surface. This particular model might apply to a linear magma chamber, such as might exist if several stratocone volcanoes coalesced, or to a dike or sheet-like magma chamber. This sort of model might apply if there is a large regional magma chamber associated with the entire Cascade Range,

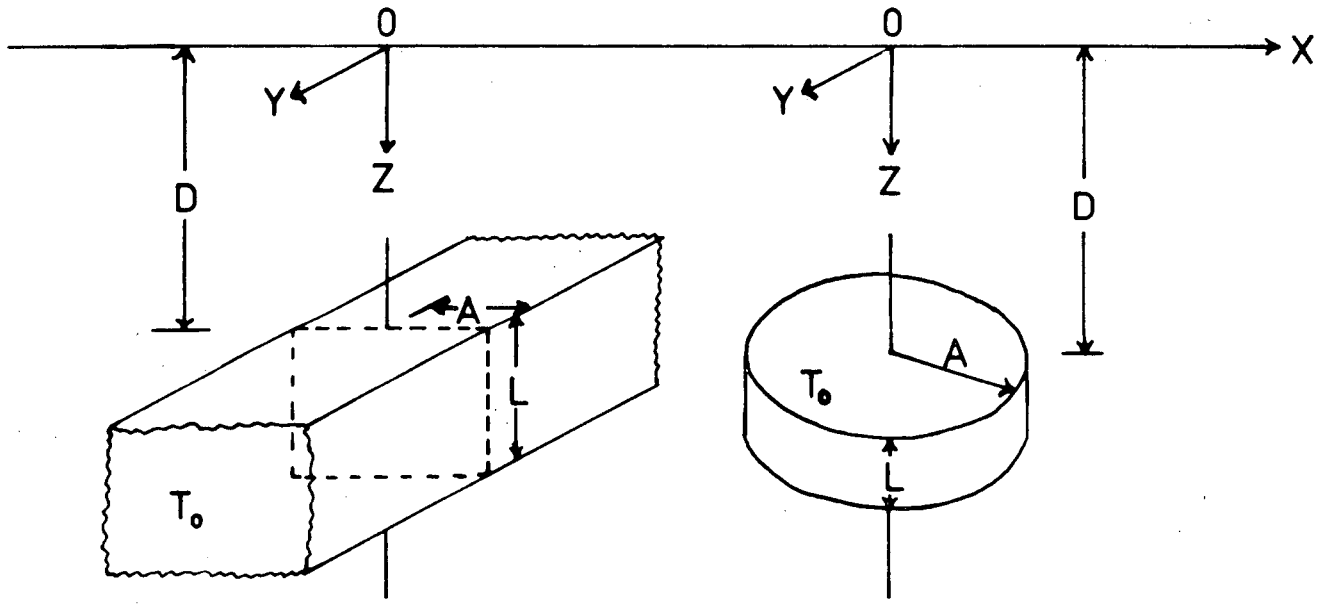

Figure 3. Basic model shapes for two-dimensional magma chamber models. A = half-width or radius; L = thickness; D = depth from surface to top of body; T_o = initial emplacement temperature.

rather than individual magma chambers associated with each stratocone volcano.

The other basic shape investigated is a cylinder that is considered to be buried at a depth D, to have a radius A, and a thickness L. This model would be more typical of a single magma chamber associated with a volcano, a volcanic pipe, or a very large circular magma chamber which might underlie several adjacent volcanoes. For example, it has been suggested by LaFehr (1965) that a single magma chamber may underlie the Medicine Lake Highland and Mt. Shasta area in California.

Comparing the two geometries, A is the half-width of the slab, or the radius of the cylinder; L is the thickness of the body; D is the depth of the top of the body from the surface; T_o is the initial temperature (assumed constant) of the body. In all the solutions, the medium is assumed to be homogeneous and to have constant thermal conductivity not dependent on temperature. In the solution, the magma is assumed to have the same thermal conductivity as the country rock. Intrinsically, although both are two-dimensional, a slab will have a larger heat content than a cylinder for equal values of A and D, and therefore will tend to cool more slowly.

In addition to the two types of geometry, two different models of magma chamber behaviors were calculated. The first of these is the instantaneous model discussed above, where emplacement of the magma at a given temperature takes place at a certain time and conductive cooling occurs subsequent to this emplacement. For the second set of models, the continuous

models, the magma is assumed to be emplaced at a constant temperature, and the boundary of the magma chamber is assumed to remain at this temperature for subsequent time so that the whole half-space is heated by the magma chamber.

In certain of the cases, a plane boundary above the magma chamber has been assumed so that a half-space solution applies. In several of the solutions for the cylinder, the effect of topography has been included so that the effect of the topographic edifice of the volcano on top of the magma chamber can be examined. In these models, the results have been illustrated for certain characteristic locations along the surface such as the apex of the volcano (A), the center of the slope (S), the toe (T), and the plane surface (F), as illustrated in Figure 4.

Plane Surface Instantaneous Magma Chamber Models

The plane surface instantaneous models are the simplest of the solutions and in the rectangular case have been discussed by many authors (Carslaw and Jaeger, 1959; Simmons, 1967; Blackwell and Baag, 1974; Lachenbruch and others, 1976). Some results for a spherical source and for a cylindrical source have been discussed in the literature (Carslaw and Jaeger, 1959; Rititaki, 1959; Blackwell and Baag, 1974). The object of this set of models is to show the relationship between heat flow, depth of burial, and cooling time. All solutions in this section can be calculated analytically from the results given by Carslaw and Jaeger (1959).

Throughout all these models, for consistency, certain shape parameters have been assumed to be constant. These have been

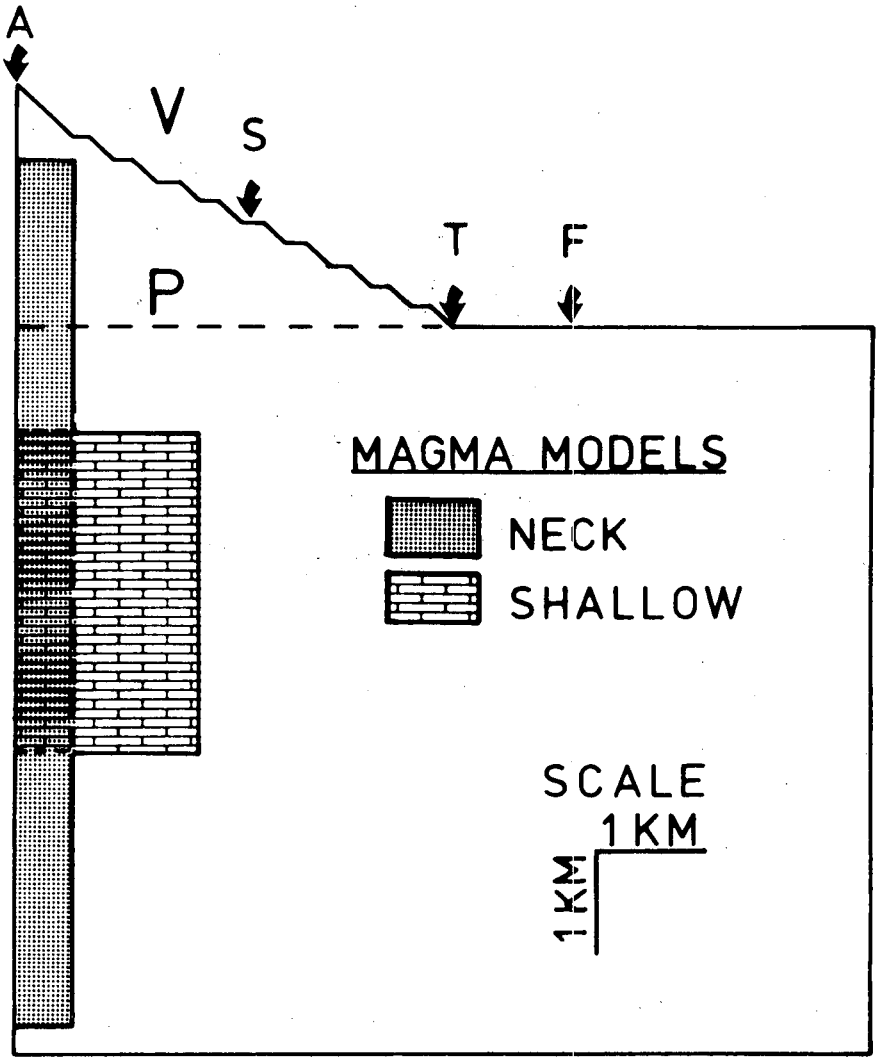

Figure 4. Magma chamber model sizes in relation to surface half-space. P = plane surface half-space boundary; V = volcano half-space boundary. Locations of detailed studies are indicated by A (apex), S (slope), T (toe), and F (flat) of the volcano.

given the dimensions of kilometers, but they can be scaled by the conduction length parameter (Lachenbruch and others, 1976). The assumed values of the parameters are shown in Table 1. Some sample results for the instantaneous models are shown in Figure 5. In all of these models the heat flow at the time of maximum surface heat flow over the apex of the magma chamber is illustrated. Results for both the rectangular and the cylindrical models are shown. The distance is measured from the center line or center point of the body.

The assumed emplacement temperature for these models is 800°C. This temperature is approximately typical of rhyolitic magmas. The actual temperature associated with an andesitic magma might be somewhat higher (1000°C), particularly if the effect of latent heat were included. It is a simple matter to scale the heat flow to any assumed T_o, however, as it is merely a matter of multiplying the heat flow shown on the ordinate by the ratio of the assumed T_o to 800°C.

Some points of interest from these solutions are that in the case of the neck model, where the magma chamber approaches within 100 m of the surface, there is a significant difference between the heat flow associated with the cylindrical neck model and the rectangular neck model. This difference is primarily because of the much larger volume associated with the rectangular chamber. It is also apparent that these anomalies are quite limited in lateral extent. The width of both bodies is assumed to be 500 m and their depth of burial is assumed to be 100 m. The time of maximum heat flow associated with the bodies is approximately 2,000 years in both cases.

TABLE 1

VALUES OF PARAMETERS FOR

THERMAL MODELS OF MAGMA CHAMBERS

		Magma Chamber Type		
		Neck	Shallow	Deep
Radius	(A)	0.25 km	1.5 km	25.0 km
Thickness	(L)	10.0 km	3.0 km	10.0 km
Depth	(D)	0.10 km	1.0 km	10.0 km

Thermal conductivity = 5 mcal/cm-sec-°C

Thermal diffusivity = 0.01 cm^2/sec

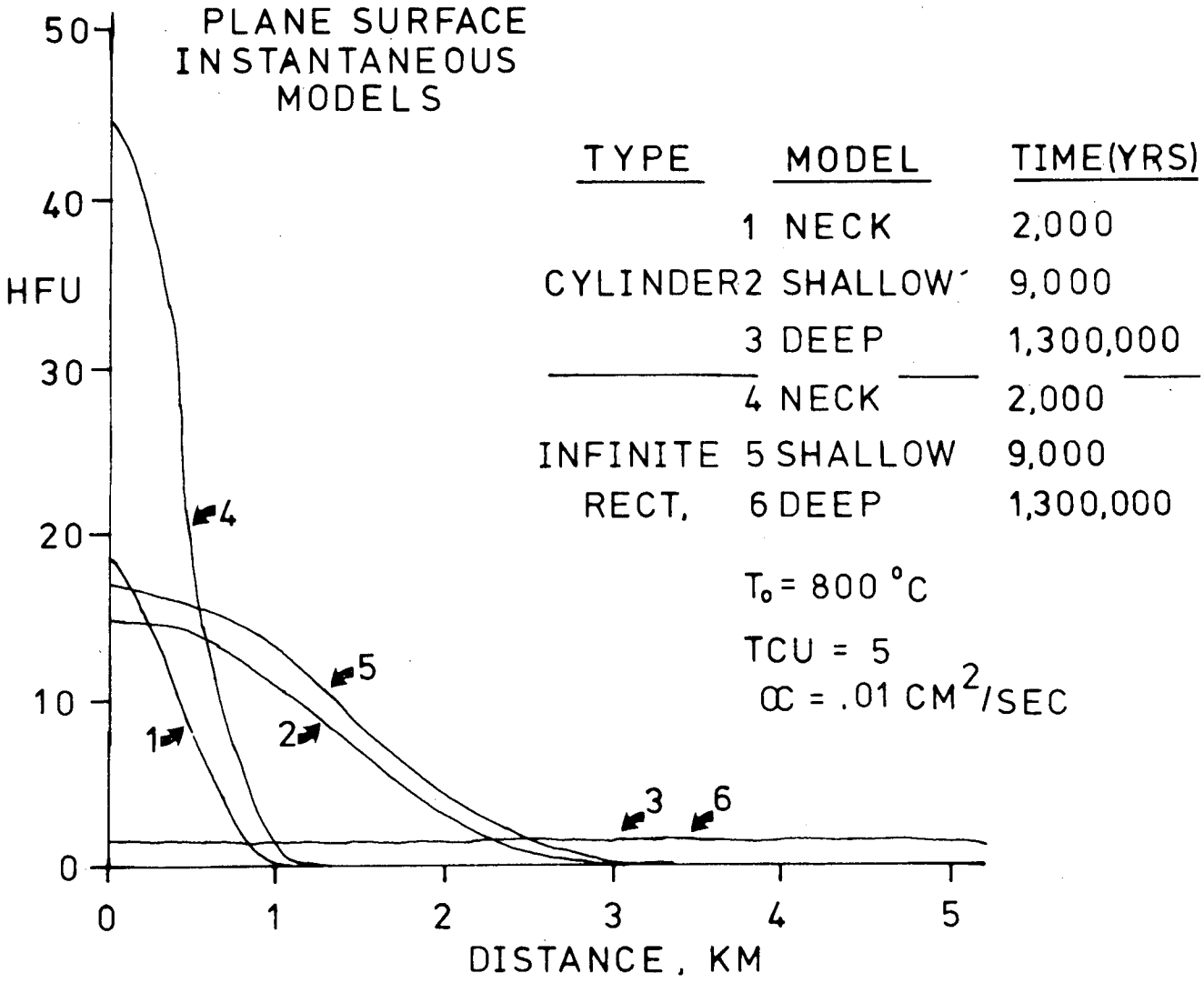

Figure 5. Surface heat flow-versus-distance curves for plane surface instantaneous models. Maximum surface heat flow over the apex of the volcano corresponds to time (yrs.) shown at right of figure; curves are labeled by number of respective models.

As the magma chamber becomes deeper and larger, the difference in heat flow, at the time of maximum heat flow, between the cylinder and the rectangular model chambers becomes less, until in the case of the largest magma chamber modeled (where the depth of burial is 10 km and the half-width, or radius, is 25 km) there is no significant difference between the two anomalies. Also illustrated is the dramatic effect of the depth of emplacement on the maximum heat flow value. Obviously, the cooling times are quite different; the cooling time for the large deep magma chamber is increased by a factor of over 100 compared to the shallow magma chamber, and over 500 compared to the neck model. In general, the cooling times are rather short geologically and, for deep chambers, the increase in heat flow is rather modest. For the rectangular plane surface model, a more complete set of heat flow-versus time curves are given by Lachenbruch and others (1976).

More Realistic Models

In order to obtain solutions for magma chamber models in addition to the simple analytical solutions available, a finite difference program was written for transient-radial heat conduction problems. Using this finite difference model, solutions were obtained that included a model surface shape based on the topographic profile of Mt. Hood (Figure 2 and Figure 4, boundary V). The heat flow effects were calculated at the surface for both instantaneous and continuous models for "neck" and "shallow" magma chambers under the apex of the volcano, of the characteristic dimensions shown in Table 1. A solution

was calculated for both cylindrical and rectangular coordinate geometry volcanoes and magma chambers, although the rectangular results are not discussed here. These types of solutions are illustrated schematically in Figure 6 for the "shallow" magma chamber model. The boundary labeled V in Figure 4 was used with the magma chambers placed below V according to the values of parameters given in Table 1.

Because the deepest magma chamber (Table 1) generates a more regional anomaly, rather than a local anomaly, discussion is focused in this and subsequent sections of this chapter on the two smaller magma chamber models calculated. The "shallow" model might correspond to a single magma chamber associated with an individual andesite volcano. The second solution ("neck" model) might be more characteristic of conditions associated with emplacement of a narrow neck or central magma chamber along the conduit of a volcano.

Shallow Magma Chamber

The dimensions of the magma chamber assumed in this discussion are given in Table 1. All models are assumed to be cylindrical, except for model 2 in Figure 6 (the slab model). The two contrasting types of heat conduction solutions, instantaneous and continuous, are shown for the shallow magma chamber model with both the volcano-surface and the plane-surface topography. The results for heat flow-versus-distance at the time of maximum surface heat flow for the models are shown in Figure 6. In Figure 6, the "plane" and "volcano" surface models refer to solutions using a cylindrical magma chamber.

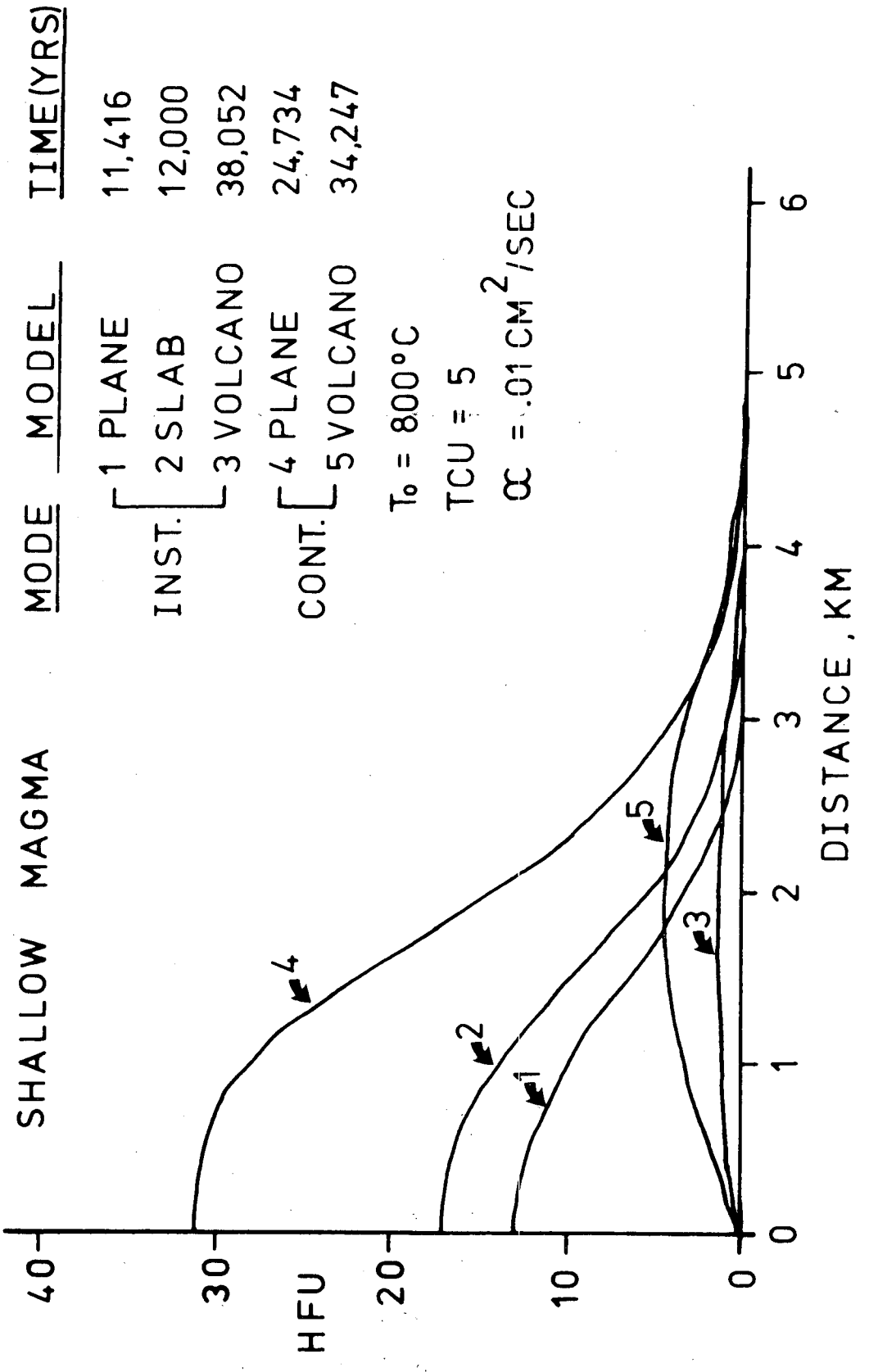

Figure 6. Surface heat flow-versus-distance curves for shallow magma chamber model. Maximum surface heat flow over the apex of the volcano corresponds to time (yrs) shown at right of figure; curves are labeled by number of respective models.

On the other hand, the slab model refers to a solution with a plane surface and an infinite rectangular magma chamber. The times indicated in the figure are the times of maximum surface heat flow associated with the instantaneous magma chamber and the maximum run time for the continuous magma chamber model. The horizontal distance shown in Figure 6 is measured from the apex of the volcano and/or the center of the magma chamber.

Curve 1 (Figure 6) is the maximum heat flow curve for the instantaneous plane magma chamber discussed previously, and curve 4 represents the heat flow for the continuous plane magma chamber at an age of 25,000 years. The continuous magma chamber has essentially reached its equilibrium heat flow in the center part of the anomaly, although the solution has still not reached equilibrium at distances of 2-4 km away from the center line. The maximum heat flow for the continuous (as opposed to the instantaneous) model differs by a factor of slightly over two. Similarly, the continuous plane solution has a much higher heat flow at any distance away from the magma chamber because of the continuous heat input of the replenished or convecting magma chamber. Thus, at any given period of time, the total heat output of the continuous magma chamber will exceed by a minimum of two times the maximum heat output of the instantaneous solution. Over the area of the magma chamber, this heat output might average a maximum of approximately 10 HFU for the instantaneous model, and 20-30 HFU for the continuous model illustrated.

The slab solution is essentially equivalent in dimensions to the instantaneous plane solution, except that the magma

chamber is assumed to be infinite in the Y axis direction instead of radially symmetrical. As noted previously, the heat flow is greater for the rectangular model due to the greater volume of magma involved. However, the characteristic cooling time and temperatures are not appreciably different for models 1 and 2 (Figure 6).

Very different results are obtained for the heat flow associated with conductive cooling of a magma chamber beneath a volcanic edifice. In this particular solution (curves 3 and 5, Figure 6) the times of maximum heat flow are much delayed because of the greater average distance between the magma chamber and the surface. Furthermore, the mean heat flow is decreased because of the much larger surface area over which the heat is dissipated in the volcano model, as opposed to the plane surface magma chamber. For these models, the maximum heat flow is associated with the edge of the volcanic edifice. Even for the continuous magma chamber, heat flow values are relatively modest compared to those associated with the cylindrical magma chamber beneath the plane surface. Part of this effect is due to the topographic effects of the volcano, and part is due to the greater effective depth of burial. Of course, if the magma chamber were larger or shallower than that assumed, then higher heat flow values would be associated with the volcanic edifice than with the areas at the toe of the volcano. There are many different solutions that might be developed, and the object is discussion of only a few typical examples.

Heat flow-versus-time curves are shown in Figure 7 for

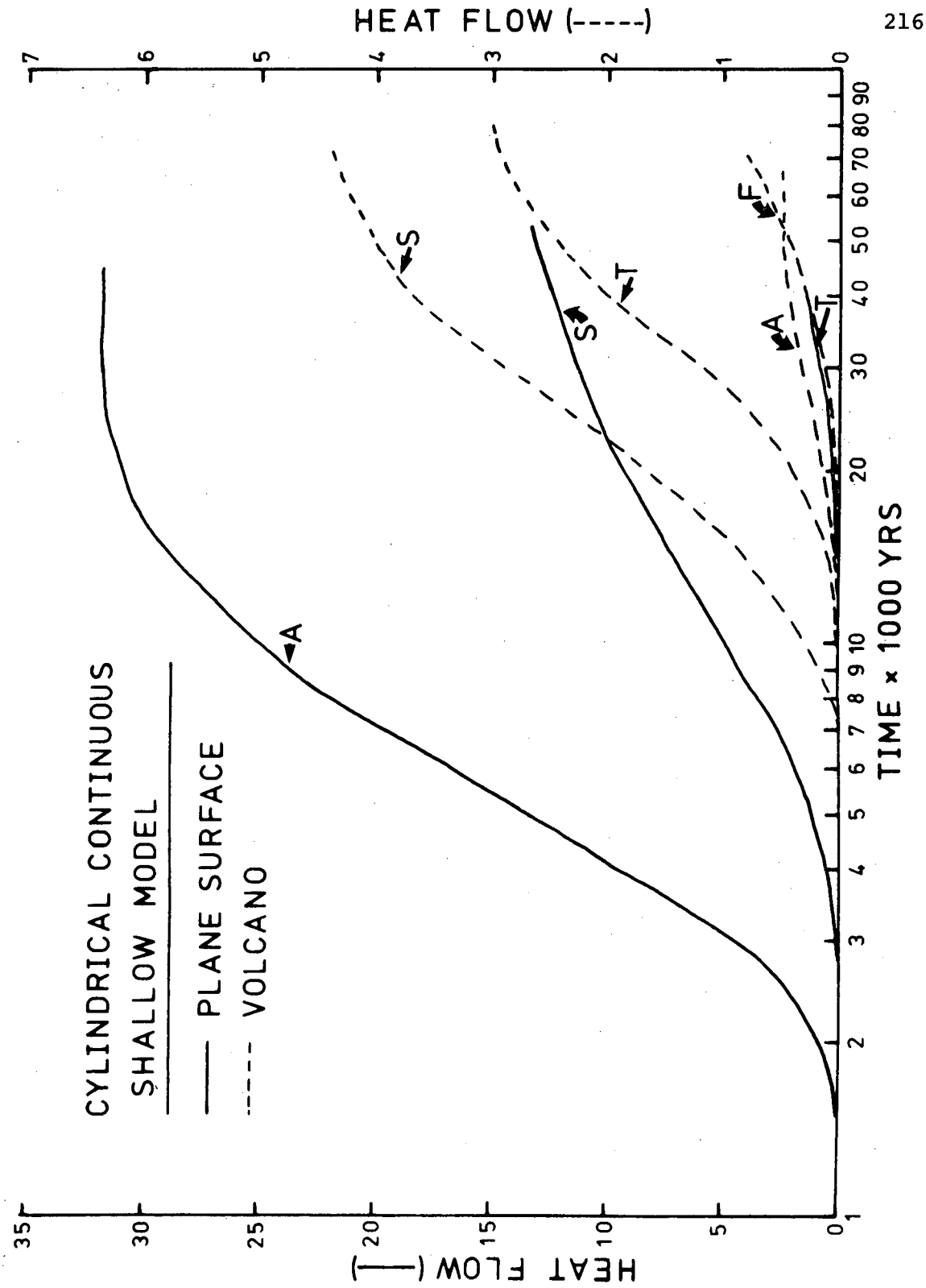

Figure 7. Heat flow-versus-time curves for the shallow cylindrical continuous model. The curves are shown for various positions along the surface of the volcano, keyed to the letters in Figure 4. The scale on the left side of the figure corresponds to the plane surface half-space, and the scale on the right side of the figure corresponds to the volcano surface half-space.

the continuous shallow cylindrical magma chamber model. Heat flow-versus-time curves are shown for various positions along the surface, keyed to the letters in Figure 4. In the case of the instantaneous model, the heat flow builds up rapidly and decays over a longer period of time. The times of maximum heat flow for the particular models described are given in Figure 6. In the case of the cylindrical continuous shallow magma chamber model (Figure 7), the heat flow builds rapidly over the first 10,000-50,000 years of the existence of the chamber to a maximum value (and constant heat flow) after the initial increase. The calculated heat flow continues to rise at larger distances from the volcano for 50,000-100,000 years, but the values are never particularly large.

These models indicate that if the heat transfer is primarily by conduction, then a period of some tens of thousands of years is required to heat up the volcano from a relatively local magma chamber below the volcano. The maximum heat flow values will be observed along the lower slopes of the volcano.

Figure 8 shows isotherms associated with the continuous and the instantaneous shallow cylindrical magma chambers after a period of approximately 38,000 years. The assumed thermal properties are shown in the figure. A comparison is made between the temperatures for the instantaneous cooling solution and the continuous solution. No regional background gradient has been added to these temperature data, so the actual temperature would be slightly higher in proportion to the depth and the background geothermal gradient. After this period of time, temperatures in the volcanic edifice have essentially

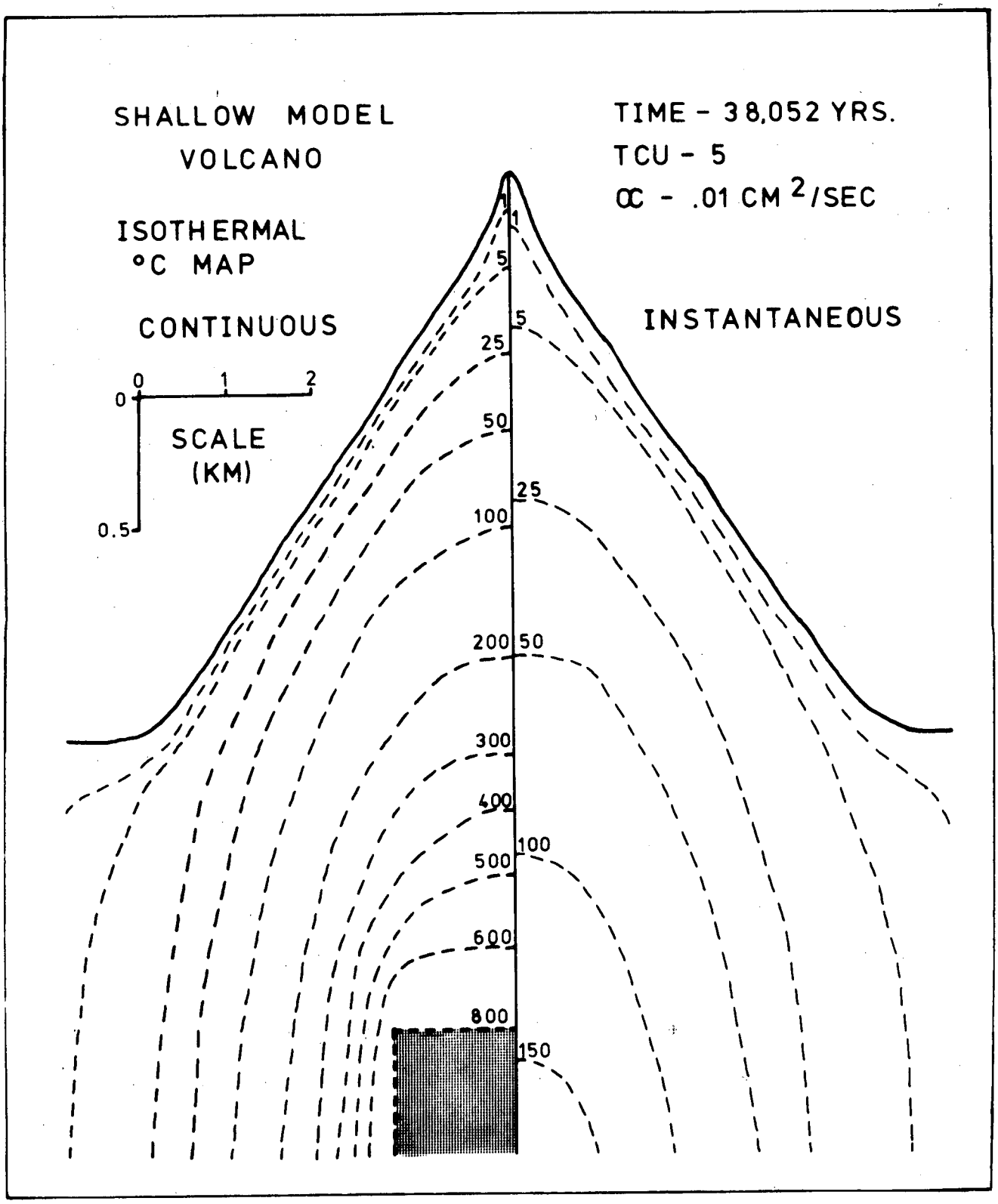

Figure 8. Isothermal cross-section map of the volcanic edifice for the shallow magma chamber model. The continuous model isotherms are on the left side of the volcano apex, and the instantaneous model isotherms are on the right side of the volcano apex. A portion of the shallow magma chamber is indicated by the shaded area at the bottom of the figure.

reached a steady-state for the continuous model; and for the instantaneous model, temperatures are well on their way to complete cooling, as indicated by the low temperatures.

Continuous Neck Magma Chamber Model

The final configuration discussed is the solution for a small neck type of magma chamber associated with a plane surface or with a volcano. The heat flow as a function of time at characteristic positions along the surface is shown in Figure 9. The solid lines are the heat flow values associated with the neck beneath a plane surface, while the dotted lines are the heat flow values associated with emplacement of the neck within a volcanic edifice (note difference in scales).

The spreading effect of the volcano surface is again apparent in the heat flow, as indicated by the factor of five difference in heat flow values associated with the magma chamber beneath the plane surface and the magma chamber beneath the volcano. Of course, the time to reach steady-state is relatively short for the magma chamber within the volcano, because of proximity to the surface. On the other hand, it takes some time for the effect to build up along the slope of the volcano. The heat flow never reaches significant values at the edge of the volcano. The instantaneous cooling of the plane surface and volcano magma chamber is also shown. In both cases, the heat flow anomaly has decayed significantly in a period of 2,000-3,000 years after emplacement. Significant heat flow is not seen along the slopes and flanks of the volcano.

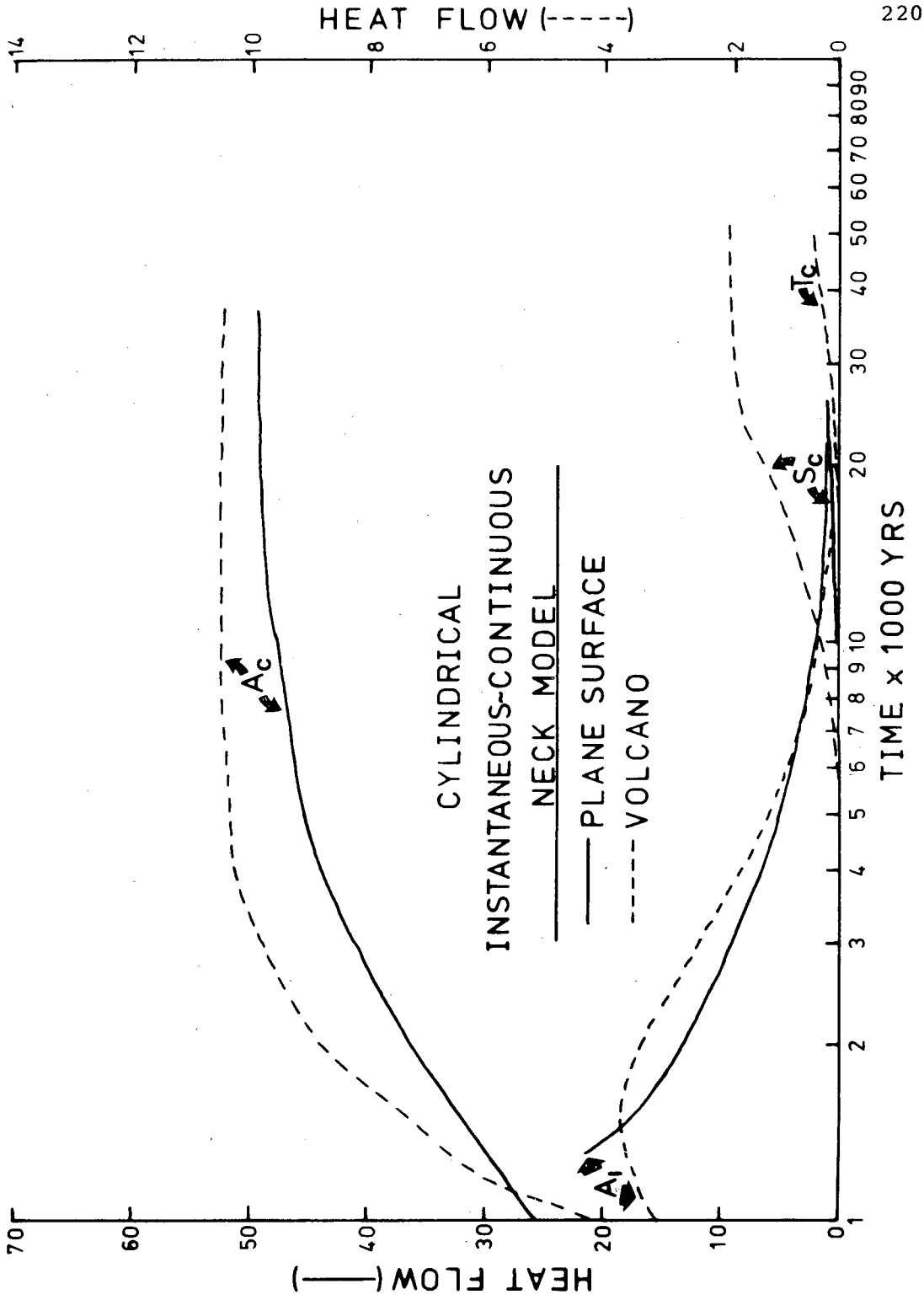

Figure 9. Heat flow-versus-time curves for the cylindrical instantaneous and continuous neck models. The curves are shown for various positions along the surface of the volcano, keyed to the letters in Figure 4. The scale on the left side of the figure corresponds to the plane surface half-space, and the scale on the right side of the figure corresponds to the volcano surface half-space. The subscript letters on the letters labeling the curves indicate the instantaneous (I) or the continuous (C) solutions.

The continuous neck model is reasonable only if the rate of occurrence of volcanism is rapid enough to cycle magma along the neck and thus to maintain a high temperature. Based on these solutions, it would appear that the recurrence of extrusive events would have to be less than 1,000-2,000 years if the axis of the volcano is to be kept at near-magma temperatures.

Discussion

The magma chamber models herein presented are highly idealized and the purpose of the following discussion is to briefly summarize their applications to the problem of geothermal resources associated with a stratocone volcano. In order to have a commercially attractive geothermal prospect, two things are needed: (1) high temperature, and (2) fuild flow sufficient to allow generation of economic amounts of power. The minimum heat loss that might be associated with an economic geothermal system is somewhere between 5×10^6 and 10×10^6 cal/sec. For a volcano such as Mt. Hood, with a radius of approximately 5 km and a total basal area of approximately 50 km^2, a mean heat flow, or thermal extraction rate, of 10-20 HFU would be required to maintain such a geothermal system. Furthermore, as discussed above, the rates of cooling of magma chambers associated with hydrothermal convection are probably greater by a factor of two to ten times than those associated with conductive cooling. Thus it is obvious that a single batch of magma, which might be approximated by the instantaneous conductive cooling model, would not be sufficient to

generate a very long-lived hydrothermal system, and the cooling of a magma chamber associated with a stratocone volcano (and of the same order of dimensions) would take place in less than a few thousand years.

It might appear that the application of the plane models to the stratocone volcano is somewhat questionable. However, one approach to modeling the cooling of a magma chamber associated with a stratocone volcano might be to assume that, for thermal purposes, the actual edifice of the volcano does not exist. Typically, the volcano edifice is composed of an alternating series of ashes and blocky flows, with a large horizontal permeability. Furthermore, these volcanoes are typically large topographic features and thus are subject to relatively high rainfall. Large amounts of meteoric water which are transferred into the subsurface along porous units tend to flow out at the edge of the volcano. Water flow may be so rapid as to prevent any appreciable heating of the volcanic edifice, or to confine heating to areas which have been hydrothermally altered where permeability has been significantly decreased. In a simple model, where the fluid flow is very high, the bottom of the aquifer could be treated as an upper boundary condition of constant temperature in the conductive solution, instead of treating the volcano surface itself as a constant temperature boundary. Therefore, the heat flow for the plane boundary model might approximate the amount of heat input from a magma chamber beneath the volcano into the circulating groundwater system.

It would appear, then, that if significant geothermal

systems are associated with andesite volcanoes, then either larger instantaneous magma chambers than those modeled are required, or volcanism must recur over a considerable period of time, so that the continuous solutions give a better estimate of potential heat transfer into the hydrothermal system.

While a neck type of magma chamber is capable of transmitting a large amount of heat into the volcanic edifice, it is relatively short-lived and a recurrence time of a few hundred years would be required for enough heat input from a neck type magma chamber to drive a hydrothermal system of any significance within the edifice of the volcano.

A somewhat more deeply buried magma chamber typical of the shallow magma chamber model could, if replenished over periods of a few thousands of years, easily impart the amount of heat required to drive significant geothermal systems. The presence of the volcano surface, as well as the probable flux of groundwater associated with the topographic features of the volcano, serve to indicate that whatever the shape of a magma chamber beneath a stratocone volcano, the maximum heat loss will probably be located along the lower slope of the volcano. Unless a magma chamber actually penetrates into the volcano itself, it is unlikely that significantly high temperatures will be associated with the upper part of the edifice. The general locations of thermal manifestations associated with stratocone volcanoes are usually near the outer edges of the volcanic carapace. The localization of the manifestations may be controlled by several different mechanisms, such as ring structures, etc. However, it appears that both the hydrologic

and the conductive heat loss models are consistent with such a localization, except in cases where the volcano has been active enough to thoroughly heat up its cone.

REGIONAL HEAT FLOW IN THE NORTHERN CASCADE RANGE OF OREGON

Regional Heat Flow Setting

The heat flow associated with the stratocone volcanoes in the Cascade Range can only be understood with respect to the regional background setting of heat flow in and around the Cascade Range itself. For several years DOGAMI and SMU have been involved in a systematic program of exploring the geothermal character of the Northern Cascade Range in Oregon. The studies have included location and logging of free holes in the Willamette Valley-Western Cascade Range areas during 1976; a drilling program involving 15 holes in the Western Cascade and High Cascade Range provinces during 1976; a free hole study of heat flow along the eastern margin of the High Cascade Range and the western portion of the Deschutes-Umatilla Plateau province in 1977; and regional investigation of heat flow around Mt. Hood in 1978. In addition, during 1977-79, a heat flow evaluation of deep holes drilled in the vicinity of, and on, Mt. Hood has been part of the program. In this section regional heat flow in the Northern Oregon Cascade Range, exclusive of the Mt. Hood region, will be discussed. Most of these data were obtained during 1976-77, but have not been summarized in any readily available report. Qualitative results have been discussed by Blackwell and others (1978).

A generalized heat flow map of Oregon based primarily on the data by Blackwell and others (1978), and updated using the data from Table 2, is shown in Figure 10. All of the heat flow

TABLE 2. Thermal and location data in the Northern Cascade Range of Oregon.

Location	N Latitude	W Longitude	Collar Elevation	Depth Interval	Avg. Thermal Conductivity [standard error]	N†	Corrected Gradient	Corrected Heat Flow	Quality
3N/12E-32cd	45°41.8'	121°20.7'	53.20 m	20.0 - 67.5	3.8		46.0	1.7	B
2N/12E- 6bb	45°41.4'	121°22.6'	85.10	10.0 - 80.0	3.8		28.0	1.1	B
2N/12E-16cba	45°39.5'	121°19.8'	380.00	100.0 - 185.0	3.8		34.0	1.3	A
2N/11E-20ab	45°38.8'	121°28.1'	629.30	60.0 - 120.0	2.8		37.0	1.0	B
2N/ 9E-29ad	45°37.8'	121°42.8'	1146.00		4.15 [0.92]	3		**	
2N/12E-30ad	45°37.7'	121°21.4'	457.30	20.0 - 120.0	3.8		39.0	1.5	A
2N/ 1W-32bb	45°37.2'	122°50.6'	282.70	0.0 - 200.0	3.8		25.0-32.0	1.1	B
2N/ 7E-31bd	45°36.8'	121°59.8'	536.70	50.0 - 150.0	3.79 [0.14]	5	42.2	1.6	A
2N/13E-31cd	45°36.7'	121°14.7'	279.70	90.0 - 175.0	3.8		52.0	2.0	B
1N/ 9E- 1ac	45°36.2'	121°38.1'	267.50	0.0 - 175.0	3.8		64.0	2.4	C
1N/ 2E-24da	45°33.3'	122°30.0'	4.60	60.0 - 95.0	4.8		27.0	1.3	B
1N/ 1W-25bc	45°32.6'	122°45.6'	326.80	70.0 - 150.0	3.8		23.0	0.9	B
1N/ 2E-29da	45°32.4'	122°34.9'	62.30	160.0 - 230.0	3.0	6	32.1	1.0	A
1N/ 3E-33ad	45°31.7'	122°26.0'	60.50	130.0 - 330.0	3.0	1	37.3	1.1	A
1N/ 6E-31cd	45°31.2'	122° 7.0'	743.70					**	
1S/10E- 9bc	45°29.8'	121°33.8'	560.00	10.0 - 25.0	3.70 [0.27]	5	256.0	9.5	C
1S/13E-20da	45°28.1'	121°11.8'	354.00	50.0 - 135.0	3.50		41.9	1.4	B
1S/10E-29ca	45°27.1'	121°34.8'	725.40		4.38 [0.20]	5			
2S/15E- 3bb	45°25.9'	120°55.5'	793.40	10.0 - 55.0	3.8		39.0	1.5	B

Location	N Latitude	W Longitude	Collar Elevation	Depth Interval	Avg. Thermal Conductivity [standard error]	N	Corrected Gradient	Corrected Heat Flow	Quality
2S/11E- 6aad	45°25.7'	121°27.7'	1161.00 m	95.0 - 150.0	3.80 [0.15]	5	30.4	1.15	A
2S/ 4E-18dda	45°23.5'	122°21.4'	196.60	50.0 - 225.0	2.8		34.0	0.95	A
2S/ 8E-15cd	45°23.5'	121°48.5'	777.40	1000.0 -1200.0	4.19 [0.14]	21	55.0	2.3	A
2S/ 8E-17cc	45°23.3'	121°51.6'	658.40	100.0 - 200.0	4.04 [0.32]	5	51.2	2.07	A
2S/ 4E-16cd	45°23.4'	122°19.3'	220.40	20.0 - 75.0	3.0		39.0-42.0	1.2	B
2S/ 2E-20bd	45°22.8'	122°35.4'	18.30	45.0 - 75.0	3.8		21.0	0.8	B
2S/ 6E-24ca	45°22.8'	122° 1.1'	359.70	70.0 - 150.0	4.33 [0.21]		42.7	1.85	A
2S/ 7E-34bb	45°21.5'	121°56.1'	442.10	35.0 - 85.0	4.30 [0.80]		47.0	2.0	A
2S/13E-36cd	45°20.9'	121° 8.0'	753.90	10.0 - 45.0	3.8		35.0	1.3	C
3S/ 6E- 3a	45°20.6'	121°55.4'	148.60					**	
3S/11E- 1aa	45°20.6'	121°21.6'	919.90	50.0 - 125.0	3.60 [0.30]	3	43.8	1.58	A
3S/ 9E- 6dd	45°19.9'	121°42.5'	1798.80		4.42 [0.16]	4		**	
3S/ 9E- 7ab	45°19.7'	121°42.6'	1761.70					**	
3S/14E- 7dc	45°19.0'	121° 5.9'	832.40	10.0 - 65.0	3.8		26.0	1.0	B
3S/ 8E-16cd	45°18.4'	121°49.9'	762.20	50.0 - 120.0	5.22 [0.15]	9	24.0	1.25	A
3S/ 8E-24bbd	45°18.1'	121°46.5'	1106.60	10.0 - 60.0	5.20		60.0	3.1	C
3S/8½E-25aa	45°17.2'	121°43.7'	1167.70		4.53 [0.26]	6		**	

Location	N Latitude	W Longitude	Collar Elevation	Depth Interval	Avg. Thermal Conductivity [standard error]	N	Corrected Gradient	Corrected Heat Flow	Quality
3S/ 8E-29ddc	45°16.6'	121°54.5'	722.40 m	80.0 - 140.0	6.32 [0.44]	5	28.2	1.78	C
4S/13E- 1ca	45°14.9'	121° 7.4'	340.50	10.0 - 75.0	2.8		77.0	2.2	B
4S/12E-10dd	45°13.8'	121"16.7'	530.50	20.0 - 90.0	3.8		36.0	1.4	B
4S/ 9E-28dd	45°11.3'	121°40.1'	1036.00					**	
4S/13E-32dc	45°10.5'	121°12.2'	547.20	20.0 - 145.0	3.0		60.0	1.8	B
4S/14E-33cb	45°10.5'	121° 4.1'	313.10	50.0 - 70.0	3.8		68.0	2.6	B
5S/16E-20cb	45° 7.1'	120°50.9'	755.40	10.0 - 80.0	3.8		34.0	1.3	B
5S/12E-31aa	45° 6.0'	121°20.5'	677.90	20.0 - 107.5	3.8		38.0	1.4	C
6S/15E- 5ba	45° 5.0'	120°57.9'	802.60	35.0 - 70.0	3.8		44.0	1.7	B
6S/ 7E- 4dc	45° 4.3'	121°57.6'	686.00					**	
6S/ 1E-13da	45° 2.9'	122°37.2'	326.10	95.0 - 140.0	3.9	1	39.0	1.4	A
6S/14E-13dd	45° 2.6'	120°59.8'	940.90	80.0 - 120.0	3.8		45.0	1.7	B
6S/ 7E-21cd	45° 1.8'	121°57.7'	603.70	10.0 - 40.0	3.52 [0.17]	4	168.1	5.91	C
6S/ 7E-30bb	45° 1.3'	122° 0.5'	512.10	50.0 - 130.0	3.95 [0.19]	9	203.5	8.04	C
6S/ 6E-34cd	44°60.0'	122°3.8'	487.80	10.0 - 50.0	3.91 [0.09]	9	65.7	2.57	A
7S/ 1E-11aca	44°58.8'	122°38.8'	214.00	0.0 -2379.0	3.50		26.0	0.9	B
7S/ 5E-22aa	44°57.1'	122°10.4'	655.50	20.0 - 90.0	3.48 [0.12]	7	66.1	2.3	A
8S/ 1E- 8db	44°53.3'	122°42.5'	303.30	95.0 - 215.0	4.1	1	28.0	1.1	A
8S/ 1E-17da	44°52.2'	122°42.3'	315.50	105.0 - 110.0	3.8		25.0	1.0	B
8S/ 2W-24bc	44°51.7'	122°53.0'	127.10	22.5 - 60.0	3.8		25.0	0.95	B

Location	N Latitude	W Longitude	Collar Elevation	Depth Interval	Avg. Thermal Conductivity [standard error]	N	Corrected Gradient	Corrected Heat Flow	Quality
8S/ 1W-32bb	44°50.3'	122°50.4'	115.80	30.0 - 80.0	3.8	1	34.0	1.3	A
8S/ 5E-31cc	44°49.9'	122°14.8'	705.30	35.0 - 345.0	4.30 [0.80]		28.0	1.2	A
9S/17E- 6cad	44°48.7'	120°44.0'	987.80	45.0 - 120.0	4.5		37.0	1.7	A
9S/ 3E-11ba	44°48.5'	122°24.5'	317.00	47.5 - 85.0	3.2	1	25.4	0.7	A
9S/ 3E-11cb	44°48.1'	122°24.8'	333.80	25.0 - 60.0	3.2	2	24.3	0.8	A
9S/ 6E-23bb	44°47.0'	122° 2.4'	550.00	30.0 - 105.0	3.84 [0.27]	7	54.1	2.08	A
9S/ 7E-21ad	44°46.7'	121°57.1'	725.40	70.0 - 150.0	3.67 [0.23]	12	81.5	2.38	A
9S/ 2E-21da	44°46.2'	122°33.6'	213.40	22.5 - 47.5	3.0	1	41.0	1.2	B
11S/ 1E- 7da	44°37.5'	122°43.3'	158.50	40.0 - 57.5	3.2	1	25.0	0.8	B
11S/ 1W-14dd	44°36.5'	122°45.9'	182.90	30.0 - 125.0	3.2	1	41.0	1.3	A
11S/15E-22cd	44°35.6'	120°55.1'	963.40	605.0 - 820.0	6.5	1	31.0	2.0	A
11S/ 1W-32bbb	44°34.6'	122°50.6'	108.20	0.0 -1345.0	3.8		19.0	0.7	B
12S/ 1W- 4dc	44°33.1'	122°48.7'	135.00	30.0 - 65.0	3.20 [0.30]	3	36.4	1.2	A
13S/ 2W- 3aa	44°28.3'	122°54.4'	317.00	40.0 - 95.0	3.2	1	31.0	1.0	A
13S/ 1W- 8db	44°27.1'	122°49.9'	329.20	15.0 - 195.0	3.8	1	21.0	0.8	A
13S/ 1W-10ca	44°27.1'	122°47.7'	149.40	27.5 - 62.5	3.2	1	23.0	0.75	B
13S/ 2W-18cb	44°26.2'	122°59.1'	378.00	95.0 - 190.0	3.8		26.0	1.0	B
13S/ 1E-20ba	44°25.9'	122°43.0'	402.90	90.0 - 130.0	3.2	1	40.0	1.3	B
13S/ 1E-35ab	44°24.1'	122°38.9'	310.90	90.0 - 150.0	3.2	1	40.1	1.3	A
14S/ 3W-24dc	44°20.0'	122°59.6'	207.30	10.0 - 47.5	3.2	1	25.0	0.8	B
15S/ 6E-11dc	44°16.1'	122° 3.2'	716.50					**	

Location	N Latitude	W Longitude	Collar Elevation	Depth Interval	Avg. Thermal Conductivity [standard error]	N	Corrected Gradient	Corrected Heat Flow	Quality
15S/ 7E-28aa	44°14.8'	121°58.4'	1143.30 m					**	
15S/15E-30ad	44°14.8'	120°58.0'	1002.80	40.0 - 65.0	>3		96.4	>2.9	B
15S/14E-36ac	44°13.2'	120°59.6'	1023.00	20.0 - 75.0	>3		123.5	>3.7	C
16S/ 6E- 2ca	44°12.1'	122° 3.0'	70.10	100.0 - 150.0	4.15 [0.06]	11	81.7	3.39	A
16S/14E-16daa	44°11.2'	121° 2.8'	1024.00	15.0 - 75.0	>3		181.8	>5.5	C
16S/ 4E-14dbb	44°10.1'	122°17.5'	457.20	12.5 - 45.0	4.30 [0.80]	2	38.0	1.6	B
16S/ 6E-27bb	44° 9.1'	122° 4.7'	573.00	30.0 - 150.0	3.75 [0.12]	12	73.8	2.77	A
17S/ 1W-26da	44° 3.7'	122°47.1'	327.70	20.0 - 145.0	3.8		27.3	1.0	A
17S/ 2W-36ca	44° 2.8'	122°52.7'	213.40	40.0 - 105.0	3.2	1	25.0	0.8	A
* 18S/12E- 5bbd	44° 2.8'	121°19.1'	1102.00					**	
18S/ 2W- 4ad	44° 2.2'	122°55.8'	175.30	45.0 - 125.0	3.2	1	33.0	1.1	A
* 18S/11E-25bd	43°59.4'	121°21.4'	1195.00					**	
18S/ 1W-32cc	43°57.3'	122°50.4'	192.10	70.0 - 215.0	3.8		37.0	1.4	A
19S/ 2W- 2ac	43°56.9'	122°53.7'	231.70	25.0 - 120.0	3.2	1	32.0	1.0	A
19S/ 2W-10ad	43°55.9'	122°54.6'	218.00	10.0 - 42.5	3.2		30.6	1.0	A
* 19S/16E-16dc	43°54.9'	120°49.1'	1376.00	25.0 - 300.0	3.6		51.1	1.8	B
* 19S/11E-25ba	43°54.4'	121°21.5'	1373.00					**	
* 20S/14E-25aa	43°48.8'	120°59.4'	1428.00	45.0 - 125.0	<4.4	4	34.4	1.5	B
20S/ 3E-26da	43°48.0'	122°25.0'	719.50	70.0 - 140.0	3.8		38.0	1.4	B
20S/ 3E-26cd	43°47.9'	122°25.2'	707.30	10.0 - 125.0	3.8		29.0	1.1	B
* 21S/17E- 1ad	43°47.0'	120°36.9'	1440.00	40.0 - 90.0	2.4	4	82.5	2.0	B

Location	N Latitude	W Longitude	Collar Elevation	Depth Interval	Avg. Thermal Conductivity [standard error]	N	Corrected Gradient	Corrected Heat Flow	Quality
21S/ 3E-10ad	43°45.6'	122°25.9'	548.80 m	22.5 - 100.0	7.6	1	35.0	1.3	B
* 21S/15E-16ab	43°45.2'	120°56.2'	1476.00	70.0 - 150.0	4.2	6	55.0	2.3	C
* 21S/11E-25bb	43°43.9'	121°21.7'	1515.00	27.5 - 35.0	3.6	2	65.3	2.4	C
21S/ 4E-28ad	43°43.2'	122°20.0'	533.50	10.0 - 150.0	4.54	13	58.0	3.0	A
* 22S/19E- 5cc	43°41.4'	120°28.7'	1450.00	10.0 - 37.5	2.4	1	83.0	2.0	B
22S/ 3E-10cd	43°40.3'	122°27.0'	490.70	20.0 - 90.0	3.76		39.4	1.48	B
22S/ 5E-26bc	43°38.2'	122°11.3'	975.40	30.0 - 150.0	4.72 [0.14]	13	53.0	2.7	A
* 22S/19E-32ad	43°37.6'	120°27.4'	1520.00	42.5 - 47.5	1.60	1	118.0	1.9	B
* 23S/19E- 5b	43°37.0'	120°28.4'	1550.00	70.0 - 150.0	3.90	1	50.9	2.0	A

† N is number of samples used to determine the average thermal conductivity. Where N is blank, value used is average estimate of type rock. Where standard error is blank when a value is given for N, this indicates value used is estimate from composite samples from drill hole.

* Hull et al., 1977.

** Considered unsuitable for heat flow calculations.

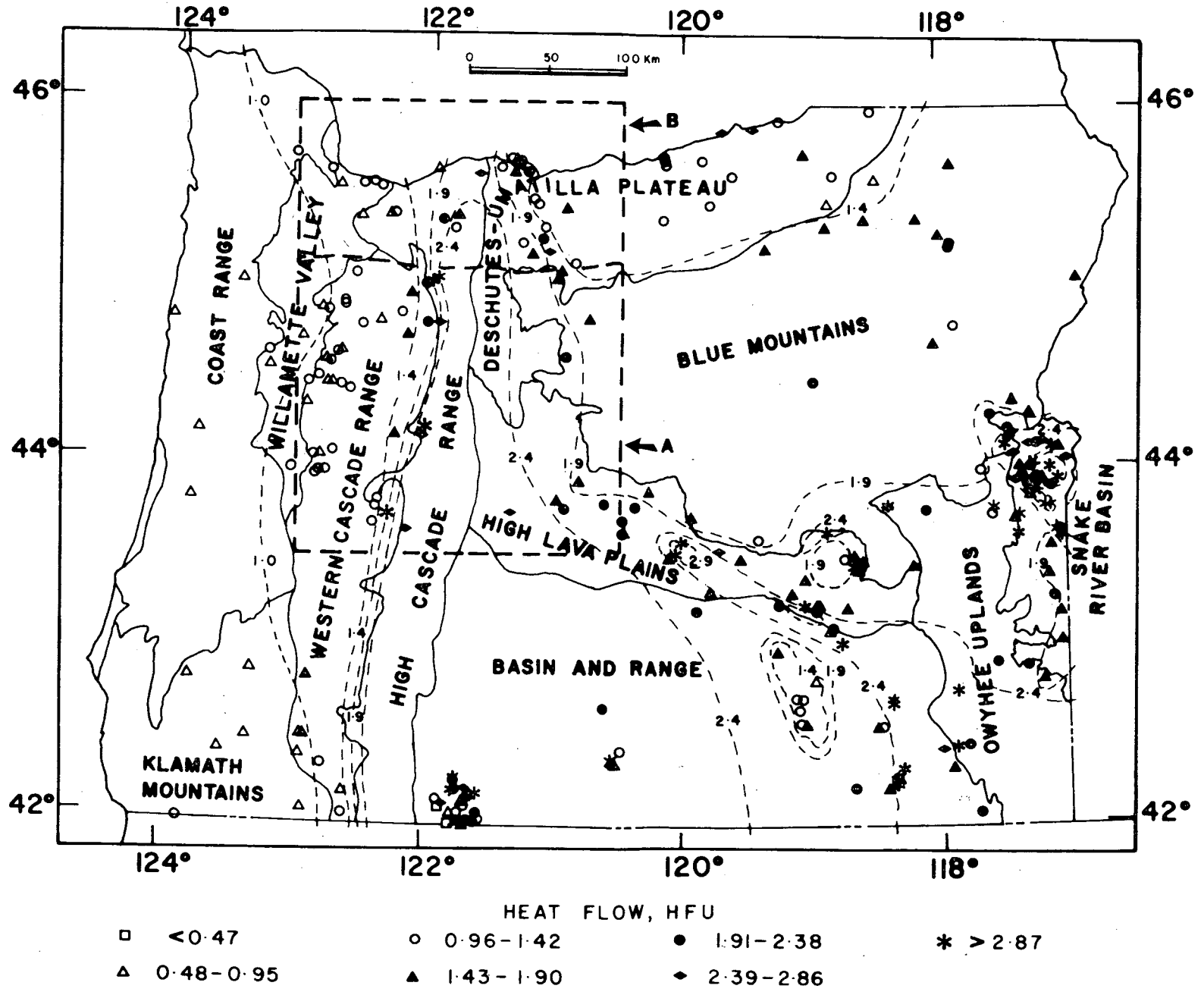

Figure 10. Generalized heat flow map of Oregon.

data discussed in this report are listed in Table 2. Included in this Table are all of the pertinent thermal and location data including latitude and longitude, township and range, elevation, interval of gradient calculation, average thermal conductivity, geothermal gradient and heat flow. All appropriate reductions have been performed to the data set, including terrain corrections. The data values are ranked by quality as discussed by Blackwell and others (1978), and Sass and others (1971).

It is apparent from Figure 10 that the northern part of the High Cascade Range in Oregon represents an area of higher heat flow than the Willamette Valley-Western Cascade Range provinces to the west and the Deschutes-Umatilla-Blue Mountains provinces to the east. The boundary between the High Cascade Range heat flow provinces is well-defined on the basis of the available data. The boundary between the High Cascade Range and the Deschutes-Umatilla-Blue Mountain provinces does not appear to be as well defined, and additional data are needed in order to completely delineate the location of the heat flow boundary and the magnitude of the heat flow contrast.

Northern Oregon Cascade Range Heat Flow

The heat flow data in the vicinity of the northern Cascade Range of Oregon are shown in greater detail in Figure 11. Available heat flow data from southern Washington (Schuster and others, 1978; Blackwell, unpublished) are also shown. Only the data south of Mt. Hood are discussed in the section (Box A, Figure 10).

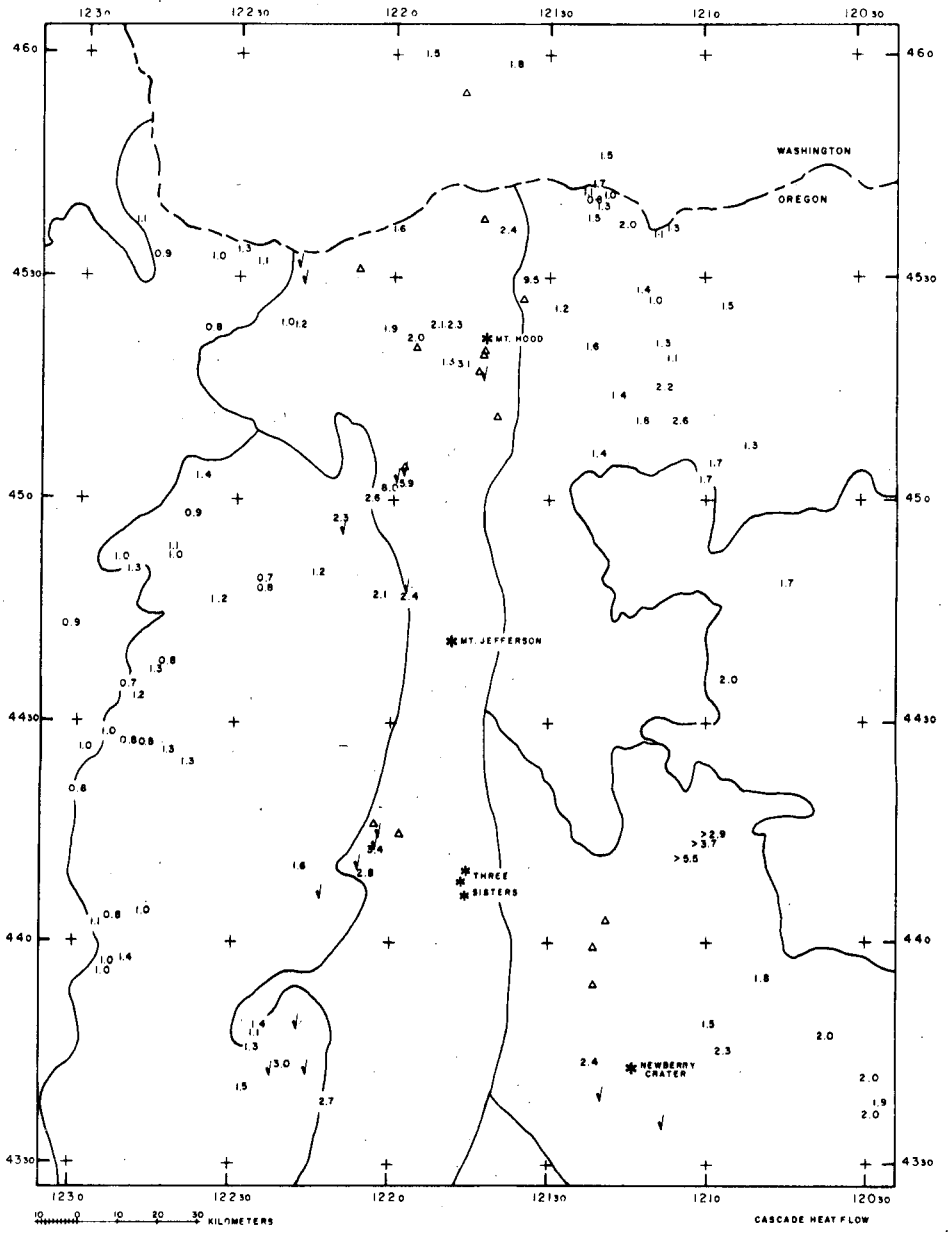

Figure 11. Heat flow map of the Northern Cascade Range area of Oregon (detail of area enclosed by heavy dashed lines in Figure 10). Heat flow values (in HFU) are plotted over their locations, with the decimal point of each value being the actual hole location. Holes drilled for heat flow studies, but considered unsuitable for heat flow calculations, are indicated by open triangles. Wells logged which are associated with regional aquifer disturbances are also shown by open triangles. Physiographic province boundaries are shown by solid lines. Locations of major volcanoes are indicated by the asterisks, and locations of major hot springs are indicated by √s.

The heat flow data in the Western Cascade Range west of the high heat flow boundary are very homogeneous. A histogram of the heat flow data from Figure 11 in the Western Cascade Range and Willamette Valley provinces is shown in Figure 12. Also shown in this figure is a histogram of the heat flow associated with the Western Cascade Range-High Cascade Range boundary south of 45°10'N as well as a histogram of heat flow values along the eastern boundary of the High Cascade Range.

The heat flow data in the Western Cascade Range-Willamette Valley average 1.1 HFU. Heat flow values along the Western Cascade Range-High Cascade Range boundary average 2.5 HFU, while heat flow values along the eastern boundary of the High Cascade Range average approximately 2.0 HFU, and the average has a large standard error. The average gradients associated with these heat flow values are 30°C/km, 60°C/km and 50°C/km respectively.

Typical temperature-depth curves observed in domestic water-supply wells in the Western Cascade Range-Willamette Valley provinces are shown in Figure 13. The holes are generally along major drainages where development is taking place. In general, the heat flow regime is completely conductive within the bedrock units of these two provinces with only occasional evidence of local water circulation and no evidence of regional water flow. The basic-to-intermediate composition volcanic and volcanoclastic rocks typical of these provinces seem to be pervasively altered to clay and zeolite minerals, resulting in relatively impermeable rocks. The staircase temperature-depth patterns, typical of water flow within drill

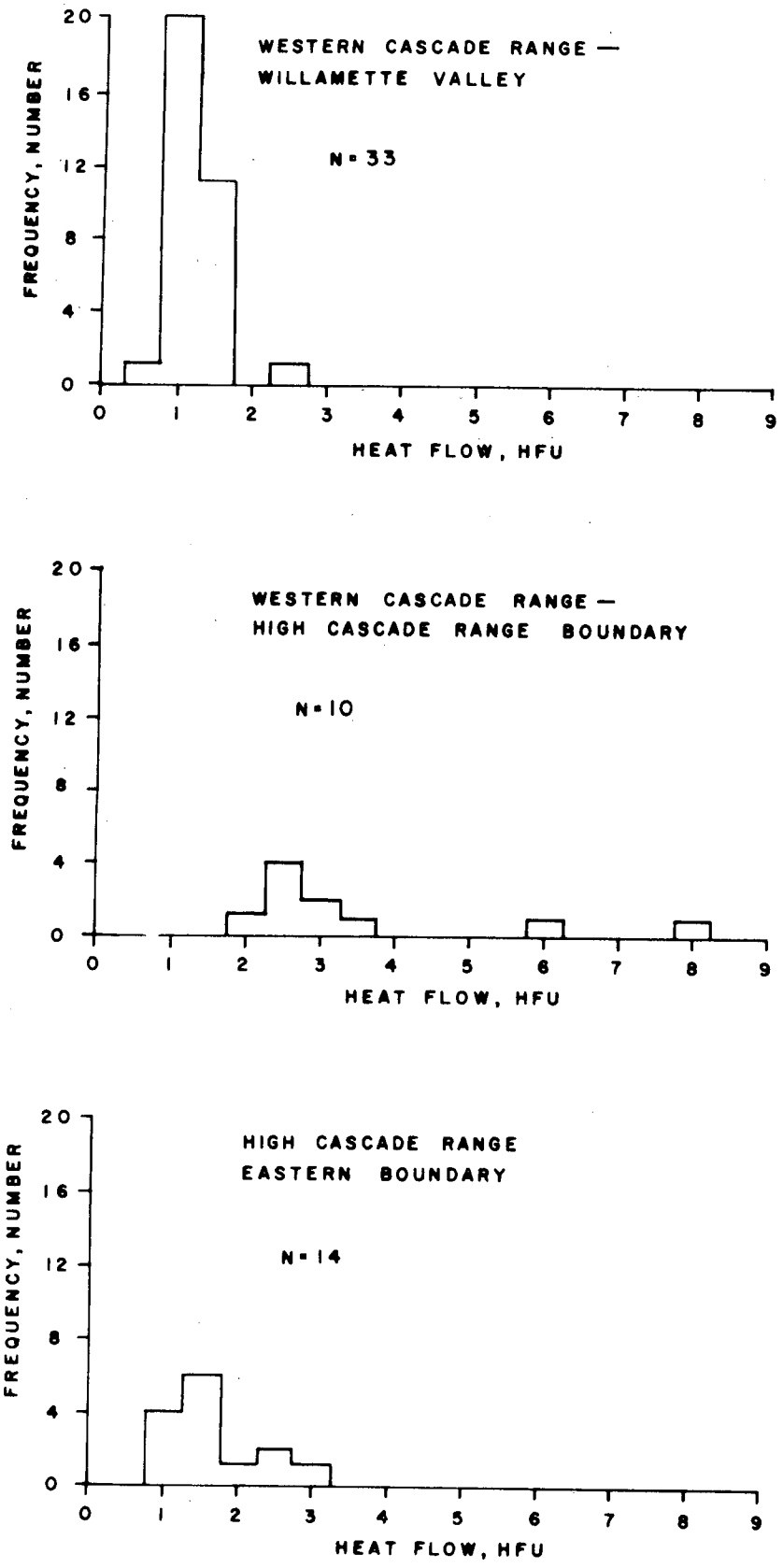

Figure 12. Heat flow histograms for the Northern Cascade Range province boundaries. Values for the histograms are shown in Figure 11.

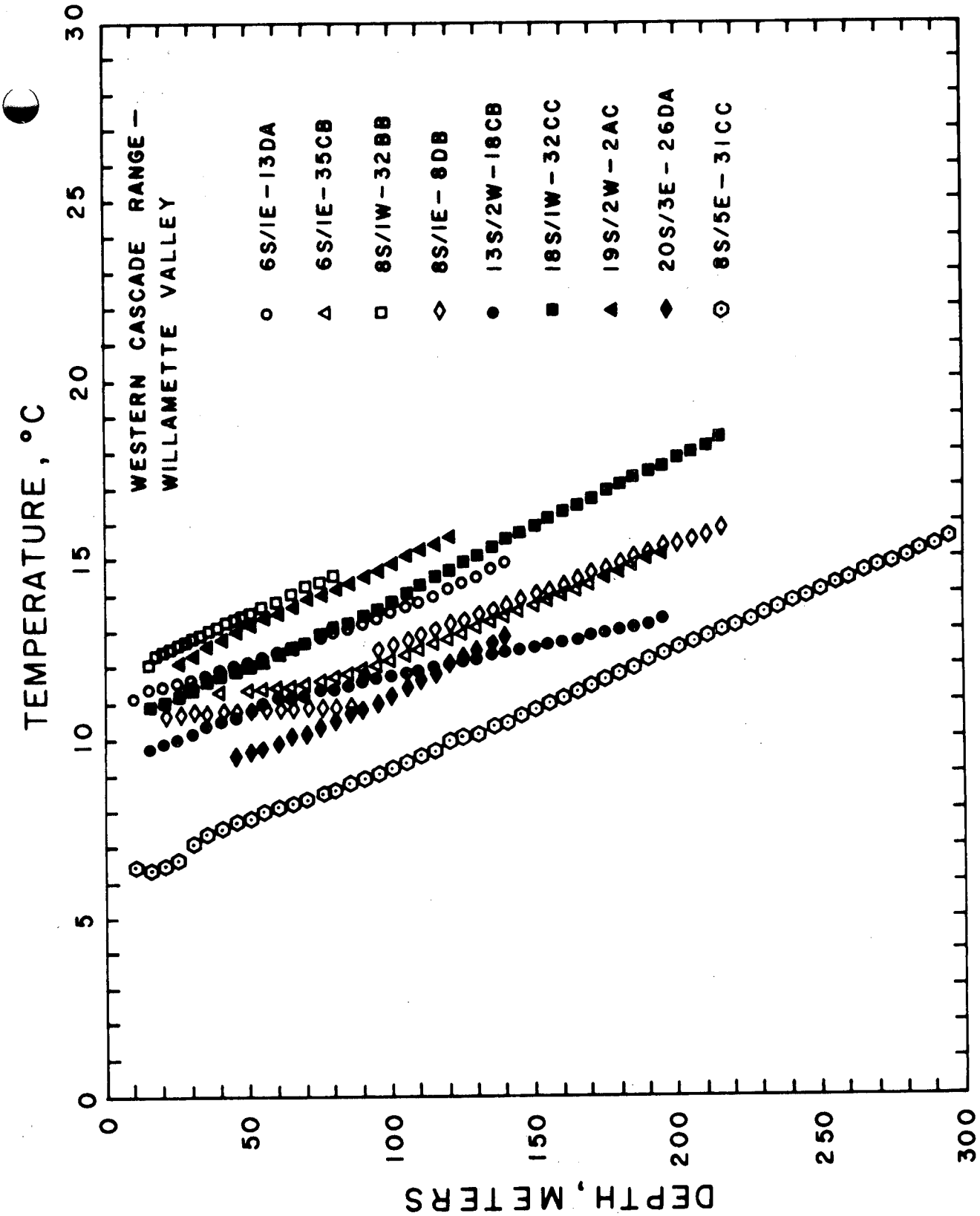

Figure 13. Typical temperature-depth curves for the Western Cascade Range-Willamette Valley province boundary. Locations of holes are given by township/range-section.

holes, which are typically noted in relatively high relief areas and in more brittle acidic rocks are seldom observed in the altered volcanic rocks of the Western Cascade Range-Willamette Valley regions.

Typical temperature-depth curves in the Western Cascade Range-High Cascade Range boundary region are shown in Figure 14. Most of the holes shown in this figure were drilled specifically for heat flow studies and were sited in the general vicinity of existing hot springs which are concentrated along the physiographic boundary between the Western Cascade Range-High Cascade Range provinces.

Detailed cross-sections of the heat flow results are shown in Figure 15 A-B. The cross-sections include corrected geothermal gradients and heat flow. From north to south, clusters of data are along the Clackamas River in the vicinity of Austin Hot Springs, along the Santiam River in the vicinity of Breitenbush Hot Springs, along the McKenzie River in the vicinity of Belknap and Foley Hot Springs, and along the Middle Fork of the Willamette River in the vicinity of McCredie Hot Springs. Each of the cross-sections also includes heat flow values derived from water wells in the western and central parts of the sections. The zero line for distance scale is the mean location of the physiographic boundary between the High Cascade Range and the Western Cascade Range (Figure 11).

Although many of the values plot within the High Cascade Range province (Figure 15 A-B), most of the holes were actually drilled in Western Cascade rocks. The province boundary is quite irregular with the High Cascade rocks generally lying at

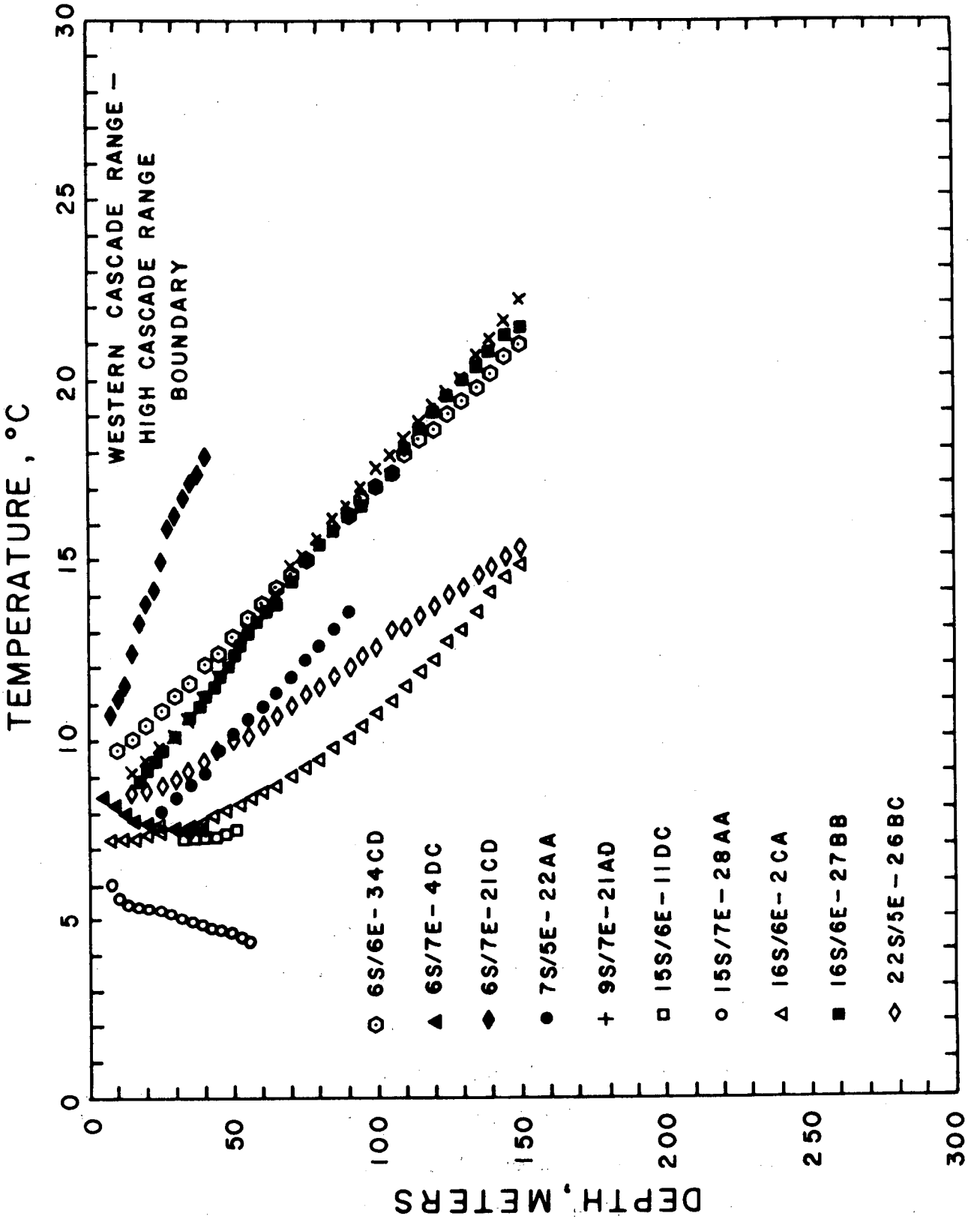

Figure 14. Typical temperature-depth curves for the Western Cascade Range-High Cascade Range province boundary. Locations of holes are given by township/range-section.

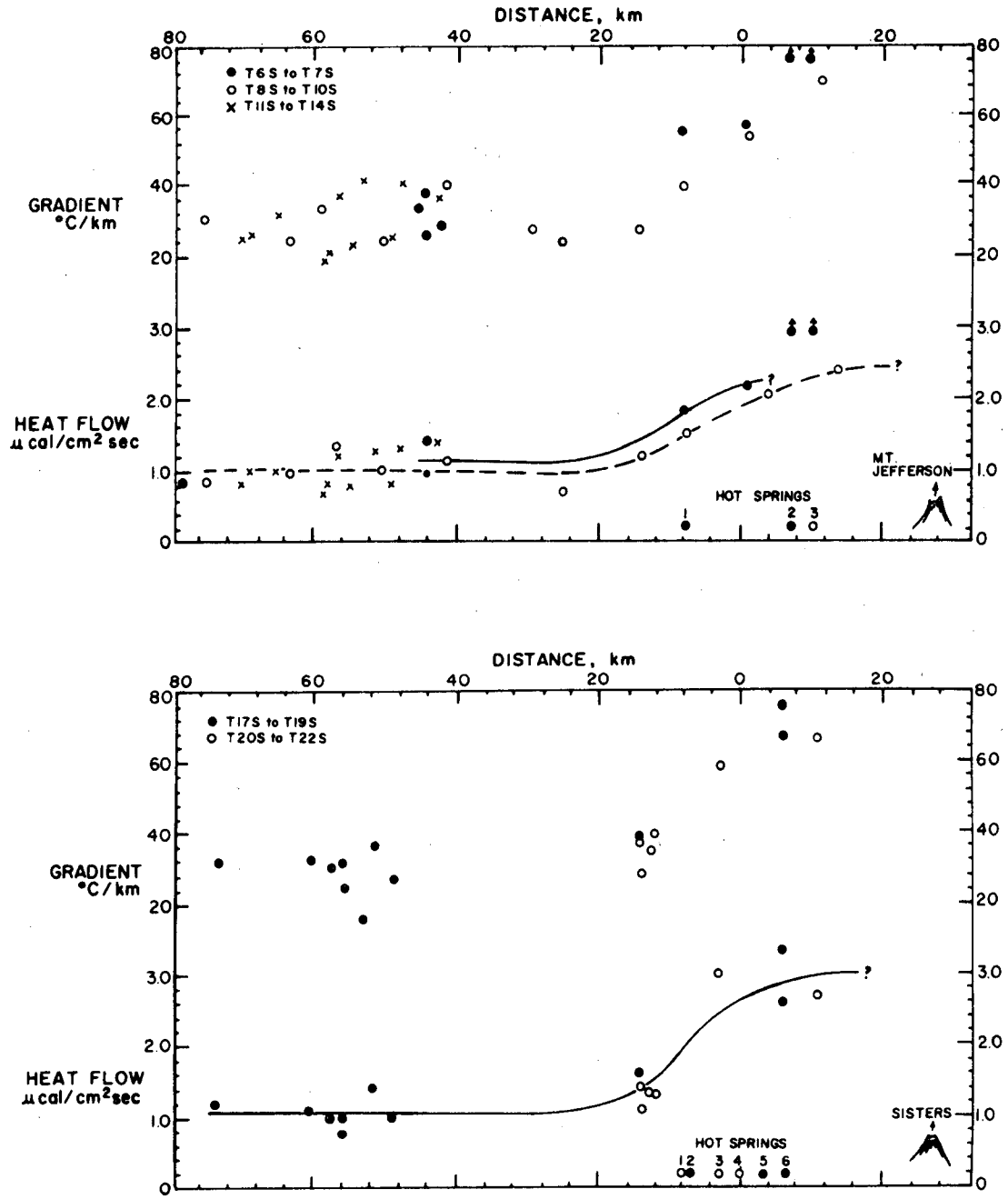

Figure 15 A-B. Heat flow cross-sections of the Willamette Valley-Western Cascade Range-High Cascade Range province boundaries. Heat flow and gradient values are grouped by townships as indicated. The hot springs near Mt. Jefferson (15-A) are (1) Bagby; (2) Austin; and (3) Breitenbush. The hot springs near Three Sisters (15-B) are (1) Cougar Reservoir; (2) Kitson; (3) Foley; (4) McCredie; (5) Wall Creek; and (6) Belknap.

higher elevations than the Western Cascade rocks, so that the latter tend to outcrop along the valleys while the former generally outcrop along the ridges. Three holes in the High Cascade rocks shown in Figure 14 were drilled in inter-canyon flow sequences that descend to lower elevations. All three holes have gradients typical of the downflow or lateral flow regime of an aquifer, although the gradients appear to be regional in the bottom of the drill holes. With these three exceptions, most of the holes have completely conductive gradients.

The data shown on the cross-sections in Figure 15 A-B is discussed in sequence from north to south. The northernmost data set includes the area of Townships 6S and 7S. At the High Cascade Range-Western Cascade Range boundary, the cross-section includes Austin Hot Springs and Bagby Hot Springs along the Clackamas River. A total of eight reliable heat flow values were obtained but the data are relatively widely spaced, one group being in the Willamette Valley and the second group being at the Western Cascade Range-High Cascade Range province boundary. Approximately 10 km west of the physiographic boundary, a heat flow value of 1.8 HFU was noted. The heat flow rises to approximately 2.2 HFU near the physiographic boundary. Two holes within 2 km to the east of Austin Hot Springs display heat flow values in excess of 5 HFU and indicate a relatively large geothermal system along the Clackamas River. This cross-section is the only one along which such high heat flow values, typical of hydrothermal circulation, were located during the drilling phase of the project, even though most of the holes drilled for heat flow values were within 5-10 km of hot springs.

The second set of data was obtained along a cross-section including the areas in Townships 8S and 10S. Eleven reliable heat flow measurements were obtained along this section. This cross-section is primarily along the Santiam River and crosses Breitenbush Hot Springs. The data show an almost constant heat flow of 0.9-1.1 HFU within the Western Cascade Range province. The heat flow rises gradually about 10 km west of the physiographic boundary and attains a value of 2.4 HFU approximately 15 km into the High Cascade Range province and at a distance of about 25 km from the easternmost low heat flow value.

No heat flow data were obtained along the heat flow boundary between Townships 11S and 14S; however, 11 heat flow measurements were obtained in the Western Cascade Range province. These heat flow values average 1 HFU, typical of those observed elsewhere in the province.

A third cross-section lies along the McKenzie River and includes data from Townships 16S to 19S. Holes were drilled just to the west of Belknap Hot Springs and Foley Hot Springs. Ten reliable heat flow measurements were obtained along this cross-section. Approximately 10 km east of the physiographic boundary, a heat flow value of 1.6 HFU was noted. Approximately 5 km east of the physiographic boundary, values of 2.0 HFU and 3.0 HFU were measured near Belknap Hot Springs and Foley Hot Springs, respectively. The distance between the high heat flow and the normal heat flow values is approximately 15 km.

The southernmost cross-section spans the area between Townships 20S and 22S. The holes were drilled in the vicinity of McCredie Hot Springs along the Middle Fork of the Willamette

River. Several free holes were also obtained in this area. These data show that the mean heat flow is 1.2 HFU approximately 8 km west of the physiographic boundary, whereas a value of 3.0 HFU is obtained only 5 km east of the boundary in a drill hole near McCredie Hot Springs. This value drops to 2.7 HFU about 10 km further to the east.

These data document clearly a systematic west-to-east increase in heat flow from 1 HFU to greater than 2.5 HFU over a lateral distance of 10 to 30 km and approximately coinciding with the mean physiographic boundary between the High Cascade Range and the Western Cascade Range provinces.

Interpretation of Heat Flow Transition Zone

All the profiles along the boundary between the Western Cascade Range and High Cascade Range provinces show the same characteristics: an almost constant heat flow with a mean value of 1 HFU in the High Cascade Range, and a mean heat flow of 2.6 HFU in holes drilled in Western Cascade rocks; an exceedingly abrupt transition zone between the two regions of heat flow, not exceeding 30 km in any location. The most remarkable aspect is the uniformity of the transition zone from north to south; although small variations may exist, the data suggest very similar conditions along the whole area under discussion.

In order to interpret the results, heat flow profiles representing several possible transition zones were constructed. These are shown in Figure 16 A-B. The different profiles represent different half-widths for the heat flow transition

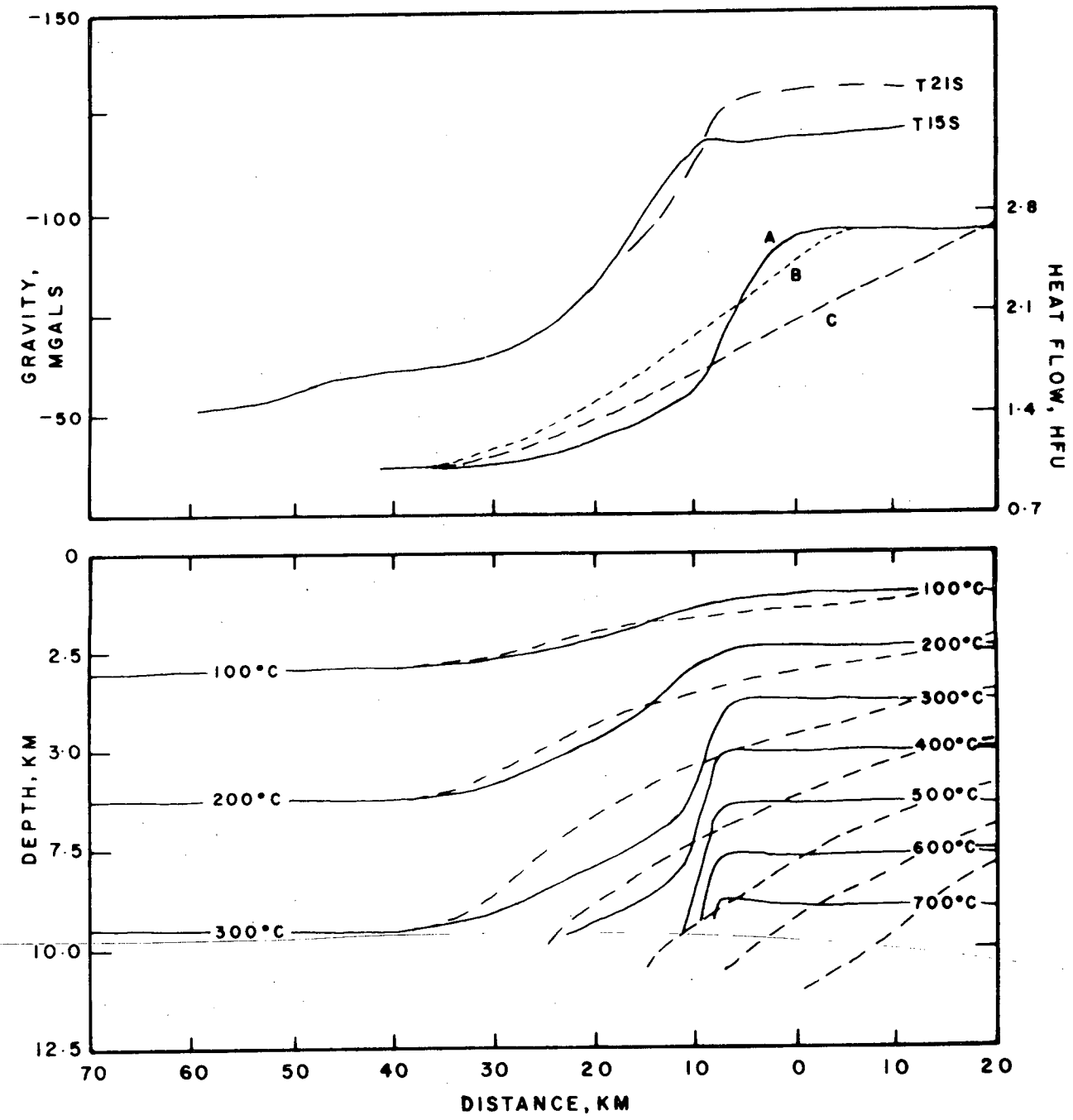

Figure 16 A-B. Heat flow-gravity transition zone models. In 16A, gravity curves are indicated by latitude, and heat flow curves are indicated by A, B, C. The heat flow curves are based on data from Figure 15: curve C, from the 6S-7S profile (15A); curve A, from the 20S-22S profile (15B). In 16B, steady-state isotherms corresponding to curve A are indicated by the solid lines, and those corresponding to curve C are indicated by the dashed lines.

based on the data in the 6S-7S profile (the largest half-width, curve C), the 20S-22S profile (the shortest half-width, curve A), and an intermediate half-width representing an average of the whole data set (see Blackwell and others, 1978).

Based on these heat flow transition zone profiles, temperature-depth cross-sections were calculated for two extreme cases of transition zones represented by curves A and C. The temperature values are based on a modification of the continuation of thermal data method discussed by Brott (1976). The more gradual transition zone has most of the heat flow difference occurring over a distance of 30 km, while the other shows a much sharper transition zone (over a distance of approximately 15 km). The isotherms were constructed for a steady-state and a transient model. In both models, homogeneous thermal conductivity was assumed. Because the geologic evidence indicates that greater than 6 m.y. BP the Western Cascade Range was the locus of intrusive activity, and because the heat flow now observed is low, there is strong evidence for a major temporal change in heat flow. The temperature sections were calculated assuming steady-state conditions, and assuming a uniform heat flow for the whole region of 2.5 HFU up to 6 m.y. ago with subsequent imposition of a constant strength heat sink beneath the Western Cascade Range which has resulted in the low heat flow values now observed. Over the scale of the area involved here, however, the steady-state and 6 m.y. temperatures do not differ significantly and so only the steady-state results are illustrated.

Both models imply very high temperature at relatively

shallow depth beneath the High Cascade Range and extending approximately 10 km into the Western Cascade Range. Any one of the isotherms shown could satisfy the heat flow anomaly so the source does not necessarily have to reach or exceed 700°C; however, the source does have to be relatively shallow and relatively intense. Because of the uniformity of the heat flow data from north to south, it seems unlikely that the boundary can be simply related to hydrology and therefore must be related to some regional crustal effect.

As discussed elsewhere, attempts to investigate the extension of the heat flow pattern further to the east toward the axis of the High Cascade Range have been unsuccessful. Volcanism has been most continuous during the Quaternary along the axis of the High Cascade Range and the cover of young volcanic rocks, with concomitant horizontal water circulation, effectively prevented successful heat flow determinations in this area at depth of 150 m or less.

Also shown in Figure 16A are two Bouguer gravity cross-sections, one at 44°15'N latitude and one at 43°45'N latitude. These profiles have been constructed from data discussed by Couch and Baker (1977). The profile for 44°15'N was extended west of the area based on the regional change in Bouguer areal gravity associated with (but opposite in sign to) the heat flow data. This gravity change is of major magnitude (over 50 milligals) and of relatively short half-width (10-15 km). The short half-width implies a crustal source for the density contrast which results in the gravity change. The coincidence of this gravity anomaly with the heat flow anomaly is additional

evidence that the heat flow data are related to regional crustal effects and not to upper crustal groundwater circulation.

Because of the close correspondence of the two sets of data, an interpretation of the gravity data was attempted based on the continuation model of crustal temperatures presented in Figure 16. In an attempt to model the gravity anomaly, a density contrast corresponding to the expansion of the rocks, based on the calculated temperatures, was assumed. These density contrast models did not generate a large enough gravity anomaly. Of course, in a complicated mountainous terrain with young volcanic rocks, density variations may be related to different factors. For example, in the High Cascade Range, shallow volcanic rocks may have a much lower density than the $2.67\ g/cm^3$ assumed in the reduction, whereas the density of the low-porosity rocks of the Western Cascade Range may be closer to the Bouguer reduction density.

The overall result of the interpretation is that a regional magma chamber or area of thermally anomalous crust exists under the High Cascade Range of Oregon. The width of the thermal anomaly is somewhat larger than the apparent width of the zone of volcanism and it extends at least 10 km west of the physiographic boundary of the province. Regional heat flow and gravity anomalies are associated with this disrupted crustal zone.

Most of the hot springs in the Cascade Range are located near the boundary of this region of high heat flow. This location may be related to a number of different effects such as the hydrologic conditions; location of faults, or fractures, along the boundary which focus the circulation of water;

outcrop of some horizontal unit that transmits water from higher elevations to the east; the location of permeable fractured acidic rocks at depth; and/or the possible location of a slightly more effective heat source.

Heat Flow Along the Eastern Boundary of the High Cascade Range

The heat flow data relating to the eastern boundary of the High Cascade Range geothermal anomaly are considerably less detailed and less consistent than those associated with the western boundary. The heat flow values in this area are shown in Figures 10 and 11. Typical temperature-depth curves are shown in Figure 17.

Around Bend, most of the holes are isothermal or show very irregular gradients to the maximum depth reached in each hole. To the north, generally conductive temperature-depth curves are obtained for holes in the older rocks immediately to the east of the High Cascade lavas. One hole (11S/15E-22cd) which was logged to a depth of over 800 m gives a heat flow of 2.0 HFU. A number of values are available further to the north. They are somewhat variable, ranging from average values for the Columbia Plateau (1.5 $\pm$ 0.3 HFU) to values greater than 2.0 HFU. On the basis of the data available at this time, no clear pattern has emerged and in fact, there may be considerable variations in the regional anomalies along the northeastern margin of the High Cascade Range.

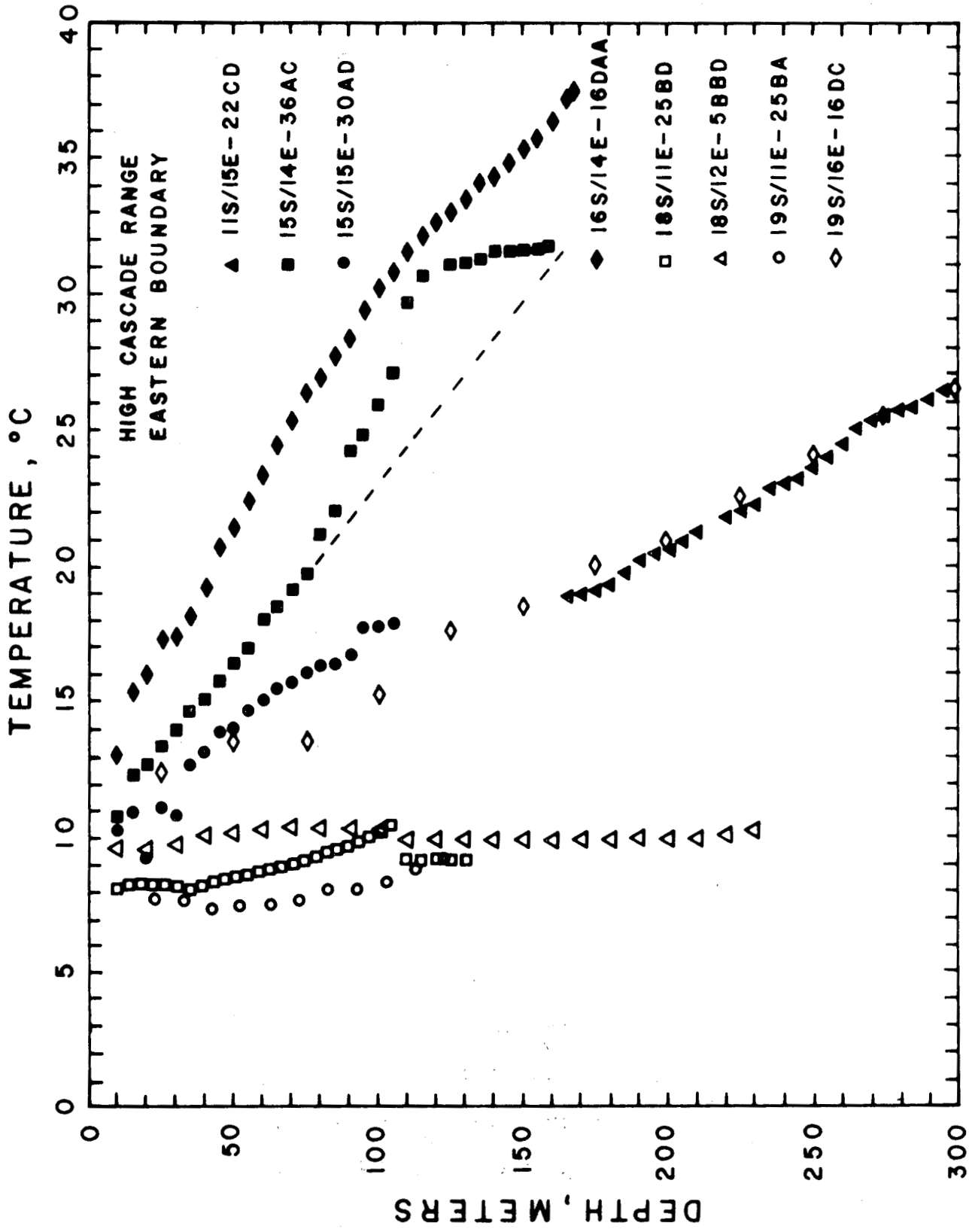

Figure 17. Typical temperature-depth curves for the eastern High Cascade Range province boundary. Locations of the holes are given by township/range-section.

GEOTHERMAL STUDIES ASSOCIATED WITH MT. HOOD

The main emphasis of this project was the analysis or theoretical study of magma chambers possibly associated with andesite volcanoes and a heat flow study of the Mt. Hood region. As part of the heat flow study of the Mt. Hood region, several holes were located during 1976 and 1977 in the Willamette Valley, along the eastern border of the High Cascade Range, and west of the Hood River Valley. In 1976, three holes were drilled specifically by DOGAMI for heat flow, one near Timberline Lodge, one near the southern margin of Mt. Hood, and one in the fine-grained plutonic rocks approximately 10 km southwest of Mt. Hood.

In 1977-78, two deep holes were drilled, one on the slope of Mt. Hood near Timberline Lodge, and one at Old Maid Flat along the Sandy River. In addition, eleven 150 m holes were drilled by DOGAMI for heat flow studies in the near-region of Mt. Hood in the fall of 1978. Temperature-depth curves for most of these holes are shown in Figure 18. The locations of all these drill holes and heat flow values (where appropriate) are shown in Figure 11.

Mt. Hood Regional Heat Flow Studies

The same dichotomy in heat flow regime is observed in the vicinity of Mt. Hood that is seen in holes drilled to the south. Drill holes that encounter rocks characteristic of the Western Cascade Range province, generally display conductive geothermal gradients. However, when the rocks drilled are of Pliocene or Pleistocene age, characteristic of the High Cascade

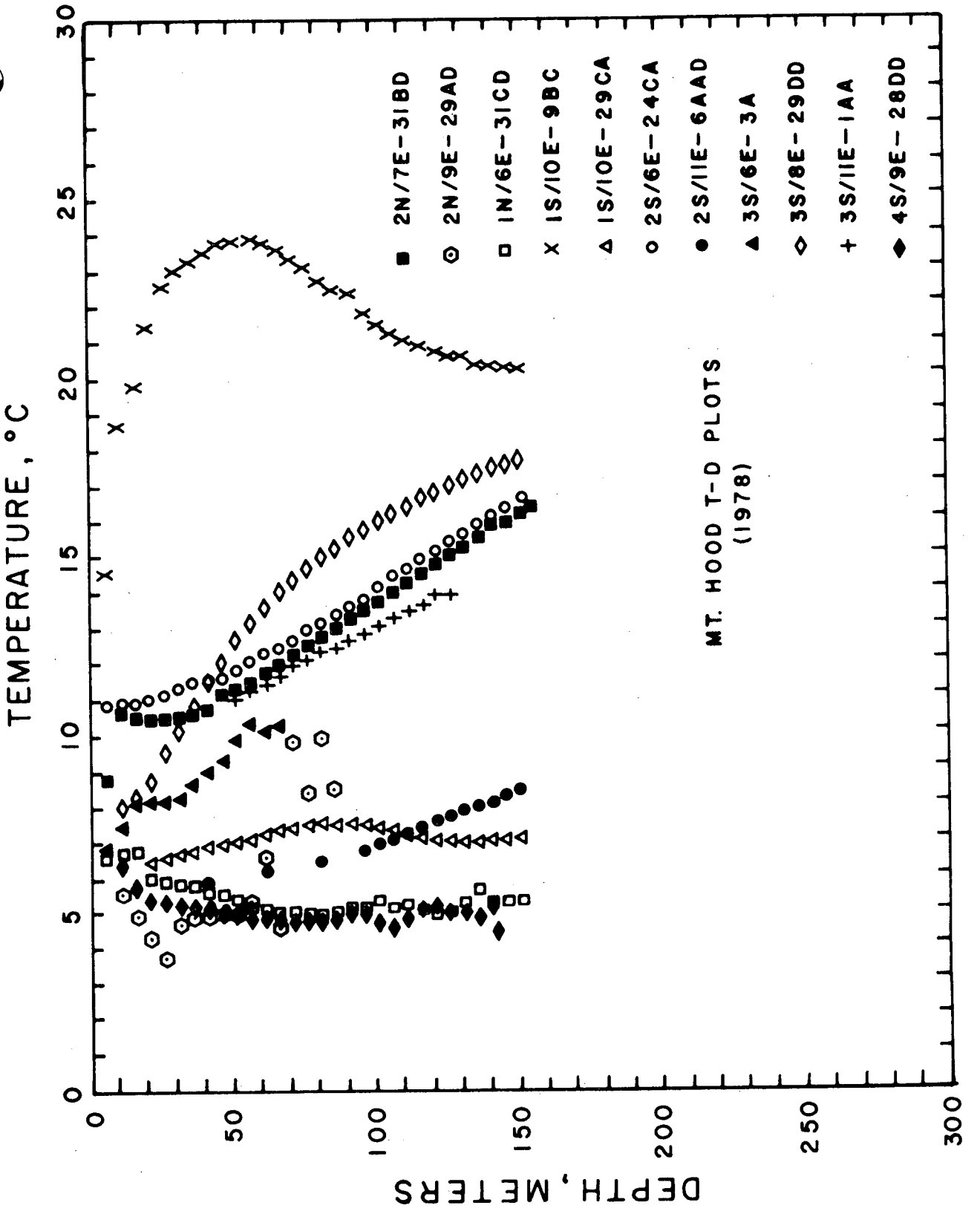

Figure 18. Temperature-depth curves for holes drilled by DOGAMI in 1978 in the Mt. Hood area. Locations of the holes are given by township/range-section.

Range, the holes do not yield useful geothermal gradient data. Most of the 150 m holes in these latter rocks gave isothermal temperature-depth curves.

The heat flow data are shown in Figure 19 projected onto a cross-section of the Cascade Range in the vicinity of Mt. Hood. The major transition zone observed to the south appears to exist in a somewhat subdued form at the latitude of Mt. Hood. Regional values of heat flow away from the volcanic edifice appear to be on the order of 1.5-1.8 HFU, as compared to values in excess of 2.5 HFU in locations to the south.

Only in the Old Maid Flat exploratory hole (2S/8E-15cd), at the toe of the volcano, is a value comparable to those to the south observed. Similarly, a gravity anomaly related to the heat flow transition also appears to be somewhat subdued compared to that further south (see Figure 16). The gravity data currently available are much less detailed than those used in the south. More detailed studies soon to be available (Couch, personal communication, 1979) will possibly allow better analysis of the relationship between gravity data and heat flow data at the latitude of Mt. Hood.

The continuation temperature model using these data shows lower temperatures (except in the immediate vicinity of Mt. Hood) than those shown in Figure 16. This model (not shown herein) is largely hypothetical due to the paucity of data in the immediate vicinity of the volcano and the large scatter of values, especially on the east side of the volcano.

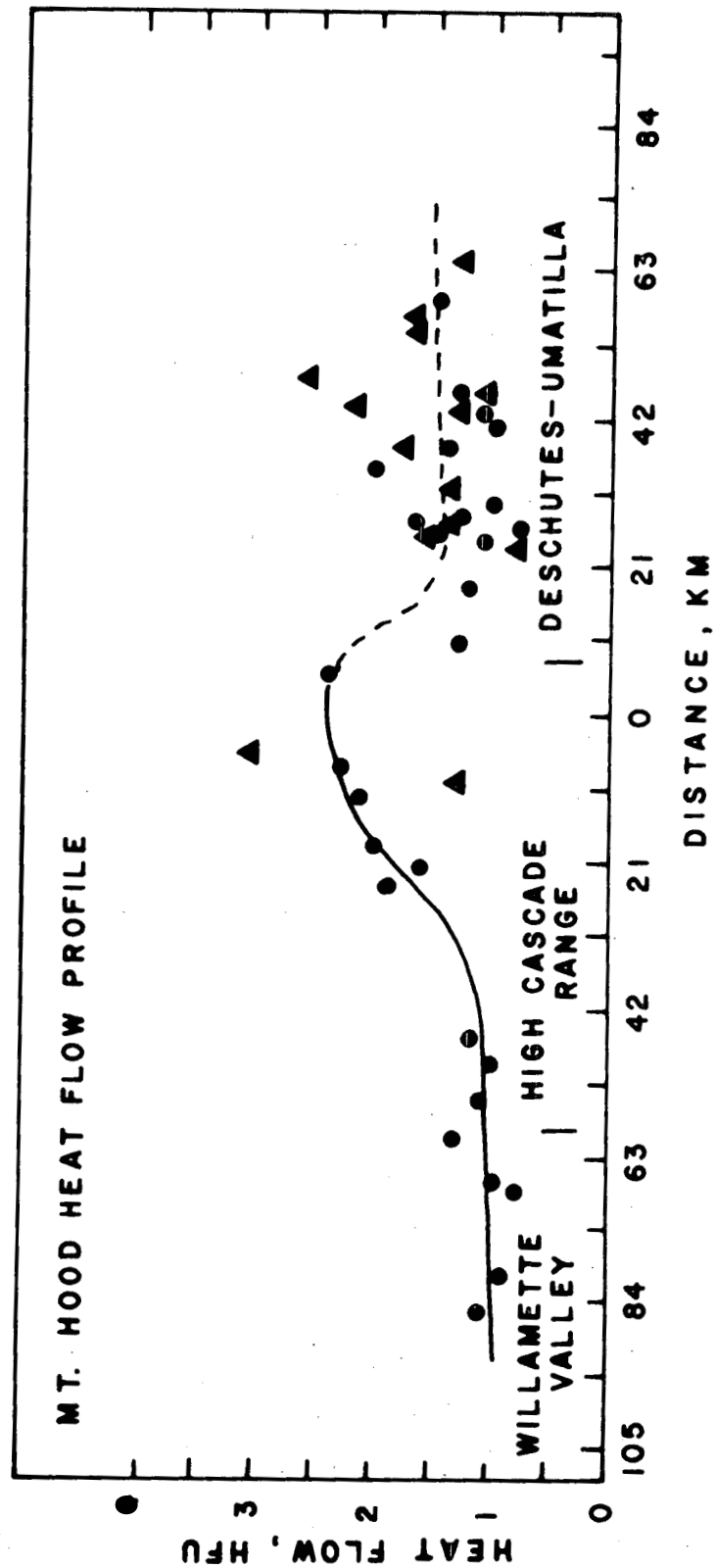

Figure 19. Heat flow profile of Mt. Hood. Baseline reference is through the profile of Mt. Hood. Heat flow values occurring south of Mt. Hood down to Latitude 45°N are represented by solid triangles, and heat flow values occurring north of Mt. Hood up to the Oregon-Washington border are represented by solid circles. All heat flow values are from Figure 11.

Old Maid Flat Holes #1/2 and #3

A major part of the project involved geothermal analysis by SMU and DOGAMI of a 1220.4 m deep geothermal test well drilled in the immediate vicinity of the Mt. Hood volcano. The hole is located at 2S/8E-15cd, along Old Maid Flat in the Sandy River valley, approximately 5 km from the apex of Mt. Hood, but almost 2 km lower in elevation.

The hole was initially drilled in the winter of 1977 to a total depth of 480 m, and designated Old Maid Flat #1. The drilling was done in two phases. A set of near-equilibrium temperature measurements was made during a pause in the drilling, for the purpose of setting casing, when the total depth was 230 m. This log (11/15/77) is shown in Figure 20. The gradient shows a disturbance in the uppermost 75 m of the hole. Below that, the gradient is linear, with a mean value of 67°C/km.

Upon completion of the hole (480 m), the temperature log (12/20/77) shows essentially equilibrium temperatures after completion of the second phase of the drilling. The log shows a somewhat higher temperature at the depths measured in the first log, with a uniform gradient of 67°C/km between 100-300 m. Below 300 m, the gradient decreases and then increases again with a value of approximately 65°C/km observed between 430-475 m. The absolute temperature values between 70-200 m in the 11/15/77 log and between 435-475 m in the 12/20/77 log are compared in Figure 20. At the time of the 12/20/77 log, there was a flow of about 10 ℓ/min from the collar of the drill hole. The nature of the temperature-depth curves indicates that a

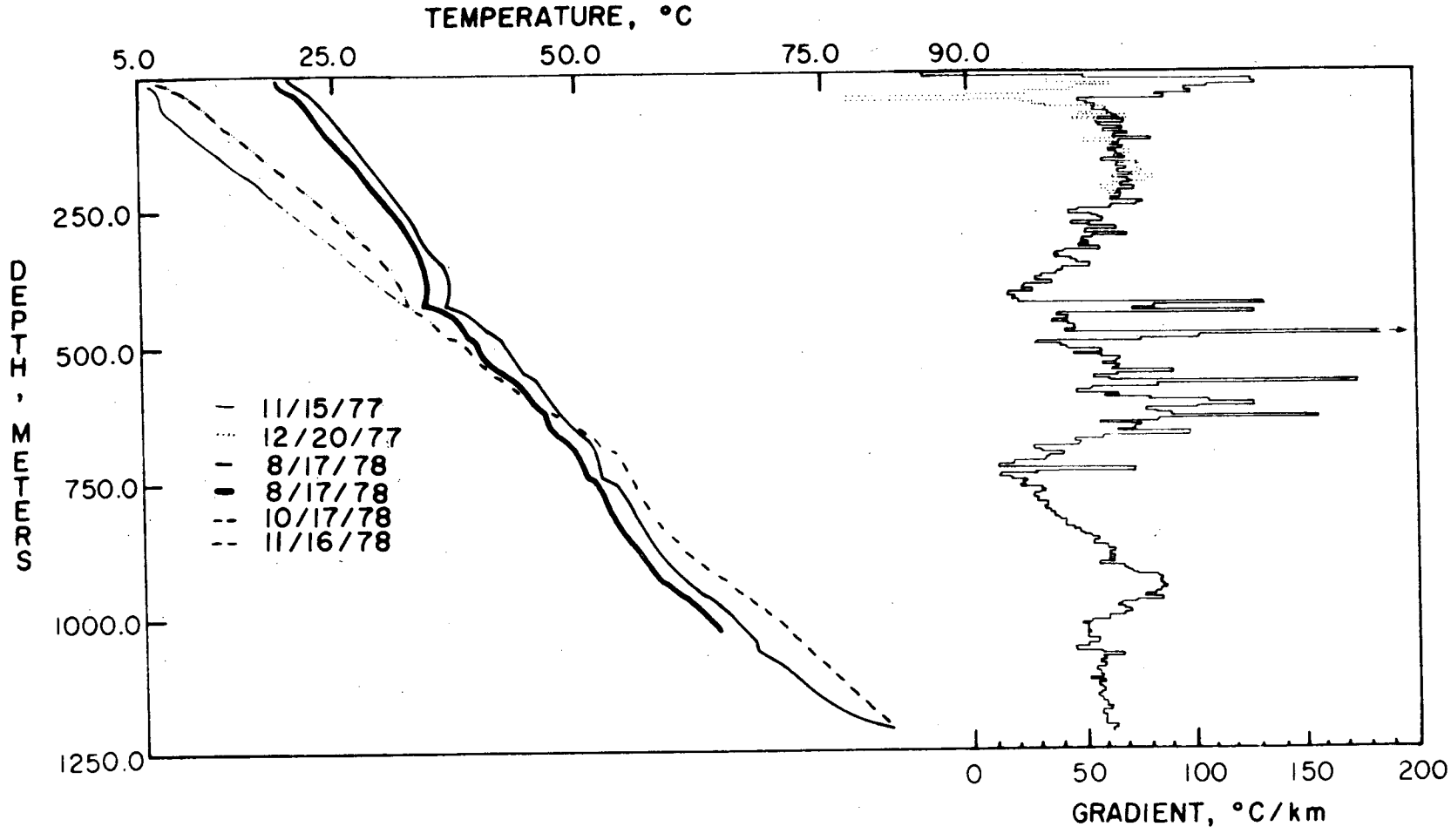

Figure 20. Temperature-depth curves for the Old Maid Flat Hole #1/2. Different dates of logging are represented by the symbols indicated. The bar graph at the right side of the figure is from the 11/16/78 data.

fracture zone with artesian fluid pressure was encountered at a depth of 430 m. At the time of the second logging, water was moving slowly up the borehole from that depth and out at the collar. The temperature of the water column is offset by about 4°C by this upflow in the borehole; thus, undisturbed temperatures in the borehole would agree approximately with the 11/15/77 log.

During the summer of 1978, the hole was deepened to a total depth of 1220.4 m and designated Old Maid Flat #2. Immediately after completion of the drilling, two temperature logs were made on 8/17/78. The lighter line on Figure 20 represents measurements by a commercial well-logging firm, while the heavier line represents measurements made with SMU's truck-mounted logging system, with a total depth capability of 1035 m. The shapes of the temperature-depth curves are essentially the same, but are offset by approximately 2°C. This could be due either to a calibration difference between the two sets of gear, or to differences in the actual temperature of the hole at the times of logging; however, the offset is probably due to a combination of causes.

The rapid return to equilibrium of temperatures in the artesian zone (around 435 m) is illustrated in the logs made immediately after the drilling. After completion, a 2" diameter observation pipe was set into the hole, but no attempt was made to grout the tubing as the hole is to be used to obtain fluid samples. Therefore, natural inter-formation flow in the annulus is not prevented by the completion technique.

After stabilization, the hole was logged on 10/17/78 by

SMU, to a total depth of 1035 m, and on 11/16/78 by USGS, to a total depth of 1214 m (John Sass, personal communication, 1978). Only the 11/16/78 USGS log is shown in detail, as the 10/17/78 SMU log is not significantly different. The temperature-depth curves observed at equilibrium are quite irregular. Even after the theoretical time needed for recovery of the temperatures, gradients in the middle part of the hole (between 300-1000 m) remained highly irregular, with significant changes which cannot be attributed to lithology. These changes are represented by the bar graph on the right side of Figure 20.

The only reasonable explanation for these gradients is a very large amount of borehole fluid communication. In fact, the only part of the hole which appears unaffected by intra-borehole fluid communication is that below 1,100 m. In this bottom portion of the hole, two distinct gradients are observed: a gradient of 52°C/km between 1010-1070 m, and a gradient of 61°C/km between 1170 m-total depth. The gradients in the central part of the hole appear to be due to fluid flow between fracture zones or flow contacts. There appears to be no instance of water flow from a single fracture zone all the way up or down the borehole, but merely localized effects. Each of the spikes of high gradient (Figure 20) corresponds to a fracture zone or flow contact. It appears that upflow is generally seen in the upper part of the hole, whereas downflow is typical of the bottom part of the hole.

If the hole had been grouted, this fluid flow would have been eliminated and a much simpler conductive gradient would be seen. Details of geothermal gradient cannot be deciphered

from the complexities of intra-borehole fluid flow. However, it is clear that the mean gradient over the entire borehole is relatively well-established, even if the detailed variations are not.

Thermal conductivity measurements were made on cuttings from between 580-1219 m. The measurements were made at intervals of approximately 30 m. Porosity values for the various depths were estimated from a neutron log. Most porosity values averaged between 1-10 percent, and these values were taken into account when calculating in situ conductivity. The mean thermal conductivity for all samples is 4.12 $\pm$ 0.14 mcal/cm-sec-°C. There are no systematic depth variations based on the bulk conductivity; however, if porosity is taken into account it would appear that slightly lower values of thermal conductivity (approximately 3.8 mcal/cm-sec-°C) occur between approximately 850-1000 m, with higher values (approximately 4.5 mcal/cm-sec-°C) above and below that zone.

The break in gradient at 1070 m, indicated in the temperature-depth curves, does not correspond with a change in thermal conductivity; however, on the commercial temperature log of 8/17/78 a "kink" in the curve was observed at that point, indicating the location of a possible fracture zone. Possibly there is some flow in the hole around this point, with the disturbed conditions only observed below 1070 m.

The mean gradient for the entire hole is 65°C/km, while that for the most undisturbed portion (below 1070 m) is 60°C/km. The gradients for the two apparently undisturbed sections of the upper part of the borehole (25-200 m and 430-475 m) are

60°C/km and 65°C/km, respectively. Taking all these data into consideration, the mean terrain-corrected heat flow for the Old Maid Flat hole is 2.4 HFU. The significance of this value with respect to the surrounding values has been discussed in the preceding section on regional heat flow in the vicinity of Mt. Hood.

Another hole, drilled to completion on 12/13/78 by Northwest Geothermal Corp., to a total depth of 400 m, was designated Old Maid Flat #3. This hole (2S/8E-17cc) is located about 3 km southwest of Old Maid Flat #1/2. The general lithology encountered in the hole is: recent mudflow debris, 0-35 m; pyroclastics with volcanic debris, 35-305 m; and an alternating sequence of Columbia River basalt and andesitic volcanic rock down to 400 m.

The first temperature-depth measurement by DOGAMI (Figure 21) was made on 12/5/78, when the hole was at a total depth of 152 m. The linear portion of the curve, from 75 m to total depth, appears undisturbed and yields a thermal gradient of 50°C/km. The disturbed upper portion of the temperature curve is probably due to fluid motion and drilling effects in the mudflow and upper pyroclastic sequence of rocks.

The hole was temperature-logged again by DOGAMI on 12/21/78 after being drilled to completion (Figure 21). The gap in the curve from 215-325 m is due to lost paperwork. However, from hand-plotted field results, the curve in this interval indicates a fluid disturbance originating around 275 m and affecting the entire missing interval. Excluding the data gap, the upper portion of the 12/21/78 log agrees in general with

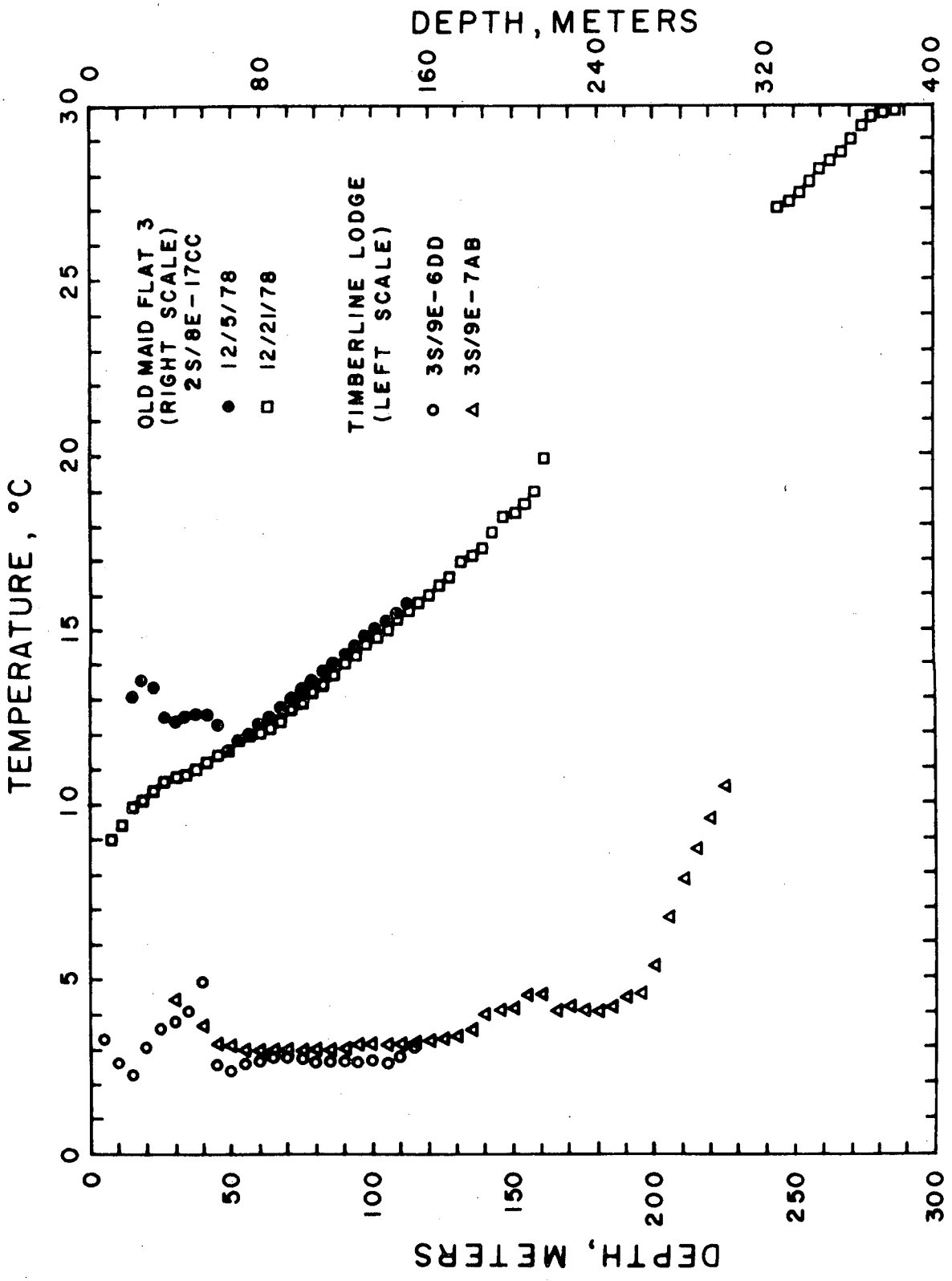

Figure 21. Temperature-depth curves for the Old Maid Flat hole #3 and the Timberline Lodge holes #1 and #2. The scale on the right side of the figure is for the Old Maid Flat hole #3 curve, and the scale on the left side of the figure is for the Timberline Lodge holes #1 and #2 data.

the 12/5/78 log; the lower portion of the 12/21/78 log gives a thermal gradient of 63°C/km.

Based on five measurements of the pyroclastic sequence of rocks, a thermal conductivity value of 4.04 ± 0.31 mcal/cm-sec-°C was obtained. A terrain-corrected thermal gradient of 51.2°C/km, with the above thermal conductivity, yields a corrected heat flow value of 2.1 HFU.

Timberline Lodge Drill Holes #1 and #2

On 9/8/76, a hole was completed to a total depth of 152 m on the carapace of Mt. Hood, about 0.2 km east of the Timberline Lodge Ski Resort. Timberline Lodge #1 (3S/9E-6dd) encountered mostly andesitic-type rocks, ranging from scoriaceous to basaltic andesite with fracture zones at 43 m, 91 m, and possibly at 122 m. The fracture at 43 m had an aquifer flow of about 19 ℓ/m.

The hole was temperature-logged on 9/8/76, 9/13/76, and 9/14/76. The 9/14/76 temperature curve (Figure 21) shows the effect of the aquifer at 43 m. The rest of the curve is essentially isothermal and not suitable for heat flow studies.

Two years later, another hole was drilled about 0.5 km south of the Lodge. Timberline #2 (3S/9E-7ab) encountered the same type of rocks as Timberline #1, to a total depth of 421 m. The resulting 12/13/78 temperature log (Figure 21) only reached 225 m, due to caving and drilling problems in the hole. Again, this hole shows fluid flow problems similar to Timberline Lodge #1, and over a similar depth interval. The linear gradient in the last 30 m of the hole appears to occur below

the aquifer zone, but has not yet approached the expected undisturbed gradient. The hole is currently considered unsuitable for heat flow studies.

REFERENCES

Blackwell, D. D., and Baag, C., 1973, Heat flow in a "blind" geothermal area near Marysville, Montana, Geophysics, 38, 941-956.

Blackwell, D. D., Hull, D. A., Bowen, R. G., and Steele, J. L., 1978, Heat flow in Oregon, Special Paper 4, Dept. of Geology and Mineral Industries, State of Oregon.

Brott, C. A., 1976, Heat flow and tectonics of the Snake River Plain, Idaho, Ph.D. thesis, Southern Methodist University, Dallas, Texas.

Carslaw, H. S., and Jaeger, J. C., 1959, Conduction of Heat in Solids, 2nd ed., University Press, Oxford, England.

Couch, R., and Baker, B., 1977, Geophysical investigations of the Cascade Range in Central Oregon, Final Report, U. S. Geological Survey, grant #14-08-0001-G-231.

Crandell, D. R., and Rubin, M., 1977, Late-glacial and post-glacial eruptions at Mt. Hood, Oregon (abstract), Geological Society of America, Abstracts With Programs, 9, p. 406.

Jaeger, J. C., 1964, Cooling and solidification of igneous rocks, in H. H. Hass and A. Poldervaart, eds., Basalts 2, Interscience, New York, p. 503-536.

Jaeger, J. C., 1964, Thermal effects of intrusions, Review of Geophysics, 2, p. 443-466.

Lachenbruch, A. H., Sass, J. H., Munroe, R. J., and Moses, T. H. Jr., 1976, Geothermal setting and simple heat conduction models for the Long Valley Caldera, Journal of Geophysical Research, 81, p. 769-784.

LaFehr, T. R., 1965, Gravity, isostasy, and crustal structure in the Southern Cascade Range, Journal of Geophysical Research, 70, p. 5581-5597.

Rikitaki, T., 1959, Studies of the thermal state of the earth, 2, Heat flow associated with magma intrusion, Bulletin of Earthquake Research Institute, Tokyo University, 37, p. 233-243.

Sass, J. H., Lachenbruch, A. H., Munroe, R. J., Green, G. W., and Moses, T. H. Jr., 1971, Heat flow in the western United States, Journal of Geophysical Research, 76, p. 6356-6431.

Schuster, J. E., Blackwell, D. D., Hammond, P. E., and Huntting, M. T., 1978, Heat flow studies in the Steamboat Mountain-Lemhi Rock area, Skamania County, Washington, Washington Division of Geology and Earth Resources, Information Circular 62.

REFERENCES (Con't.)

Simmons, G., 1967, Interpretation of heat flow anomalies, 2, Flux due to initial temperature of intrusives, Review of Geophysics, 5, p. 109-120.

Smith, R. L., and Shaw, H. R., 1975, Igneous-related geothermal systems, U. S. Geological Survey Circular 726, p. 58-83.

Thiruvathukal, J., 1968, Regional gravity of Oregon, Ph.D. thesis, Oregon State University, Corvallis, Oregon.

Wise, W. S., 1969, Geology and petrology of the Mt. Hood area: A study of High Cascade volcanism, Geological Society of America, Bulletin 80, p. 969-1006.

Yuhara, 1974, Morphological, hydrological and thermal characteristics of active volcanoes having no geothermal areas; and artificial hydrothermal systems for utilizing their latent internal heat: In Utilization of Volcano Energy; Colp, J. L. and Furnmato, A. S., eds., Sandia Labs Publ., Albuquerque, 23 pp.

OVERVIEW

Temperature Gradients

DOGAMI, in late 1978, successfully completed the drilling of eleven temperature gradient holes in the Mt. Hood area (Figure 1) to depths ranging from 76 to 152 m. Temperature gradients for the holes are shown in Figure 18 (Blackwell and Steele, 1979). Heat flow implications of these holes are discussed by the above authors. Those holes that were collared in the Columbia River Basalt or the Eagle Creek Formation were usable for heat flow determinations (1S/10E-9bc, 2S/6E-24ca, 3S/11E-1aa, and 2N/7E-31bd). The remainder of the holes that were collared in either andesite, alluvium, Pliocene volcanics, or plutonic rocks did not lend themselves to adequate heat flow analyses.

Based on the evaluation of the temperature-depth curves for the Mt. Hood area, it is apparent that holes collared in these materials need to be drilled much deeper than the heretofore depth of 152 m (500 ft). The quality of the data is affected by ubiquitous flows of water, lost circulation zones, indeterminate number of cinder and ash flows and/or soil or deeply weathered horizons. Thus, for holes not collared in the Columbia River Basalt or the Eagle Creek Formation, depth should be increased to at least a minimum of 305 m (1000 ft). The further upslope on the cone, the deeper the holes should be.

In order to better understand the heat flow regime of Mt. Hood, additional temperature gradient holes should be drilled

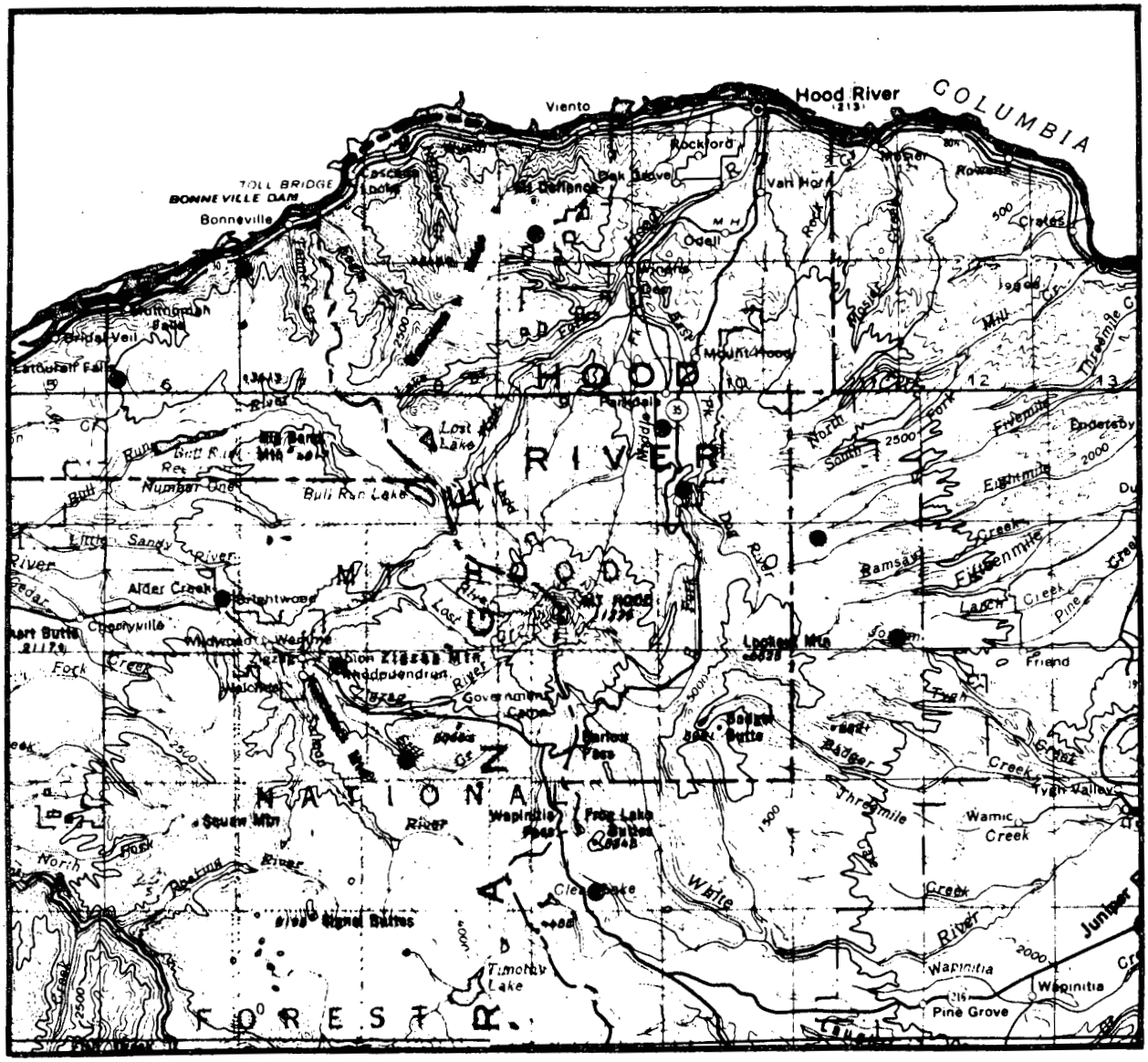

Figure 1. Location of temperature gradient holes, Mt. Hood area, Multnomah, Hood River, Clackamas and Wasco Counties. Scale - 1:500,000.

on the upper flanks of the cone and around the periphery or base of the volcano to fill in the gaps from the heat flow drilling recently completed. Northwest Geothermal Corp. has an ambitious drilling program with holes programmed to 500-2000 ft in depth for the southwesterly part of the Mt. Hood area. Further, the USGS plans to drill eight (8) hydrologic investigatory holes on or around Mt. Hood. Six holes are planned for the southern flank of the volcano; two holes on the northern flank. These holes, which are to be drilled to 500-2000 ft in depth, are to be equipped for temperature gradient measurements when the hydrologic studies are completed. It is entirely possible that the holes to be drilled by these two entities may suffice for the additional holes recommended.

The only geothermal anomaly discovered from the temperature gradient investigation was from a hole in Hood River Valley (1S/10E-9bc) northeast of Mt. Hood. The temperature-depth curve for this hole is shown in Figure 18 (Blackwell and Steele, 1979). This curve is characteristic of a shallow aquifer flow when the aquifer temperature is much above background temperature. Thus, water flowing in the aquifer heats the rock above and below the aquifer, resulting in the characteristic shape shown. Chemical analyses of the water from this hole suggest that the water may in fact be a geothermal fluid with a much higher geothermal temperature implied than is observed. This hole is immediately west of the Hood River fault northeast of the volcano and within a few kilometers east of a Holocene basaltic lava flow. Another temperature

gradient hole drilled approximately 3 miles to the south (1S/10E-29ca), also along the Hood River fault, did not display the same temperature relationship. Thus, it appears that the low-temperature water (24°C) is probably related to the intrusion that resulted in the lava flow. These results are of sufficient interest that additional geologic-geophysical studies should be carried out to investigate the geothermal implications of the anomaly. The proximity to major energy comsumption centers in Hood River Valley and The Dalles is also a favorable feature of the anomaly.

Temperature-depth relationships were also obtained from fifty (50) "free" holes, mostly water wells, as part of the Mt. Hood study. These holes were logged during 1977-79. The data were submitted to David Blackwell for heat flow modeling studies. Several anomalous temperature gradients were obtained from water wells near Powell Buttes, northeast of Bend, along the eastern margin of the High Cascade Range. For example, gradients in excess of 100°C/km were measured in two holes (16S/14E-16aa and 15S/14E-36aa) which are about 10 km apart. A bottom hole temperature of 37.5°C at 166.5 m and 31.7°C at 157 m were measured for the holes, respectively. According to Blackwell and Steele (1979), heat flow values for these two holes are in excess of 3.0 HFU. Additional studies including geologic mapping, spring sampling and associated water analyses as well as other "free" temperature gradient determinations, if available, should be initiated in order to more fully investigate the geothermal implications of this apparently anomalous area. In all probability,

drilling of temperature gradient holes would be required.

Old Maid Flat No. 1/2

The drilling history of this exploratory hole was made available to DOE by Northwest Geothermal Corporation and repetition is not warranted. The geology of this hole is discussed in the report by Beeson and Moran (1979) as well as by Blackwell and Steele (1979). Geophysical logs, including dual induction, compensated density, temperature, drift, fracture, and acoustic velocity, are available from the above company and from DOGAMI (Open File Report 0-78-6). Copies of these logs were previously forwarded to DOE.

According to Beeson and Moran (1979), the Columbia River Basalt has been ostensibly penetrated in this hole. This formation, which was the primary exploratory target, underlies the Old Maid Flat site at a depth interval from 618 m (2022 ft) to 991 m (3250 ft). Temperature in this interval ranges from about 46.5 to 79.4°C (Figure 2). Bottom hole temperature is approximately 82°C at 1220.4 m (4003 ft). Rocks in the interval from 991 m to total depth consist of andesitic volcanics which may be the equivalent of the John Day or Eagle Creek formations of lower Miocene to upper Oligocene age. However, it is also possible that this interval may represent the lower part of the Columbia River Basalt Group.

For a discussion of intra-hole fluid movement, see Blackwell and Steele (1979). To date, Northwest Geothermal Corp. has not undertaken any fluid sampling for geochemical analyses.

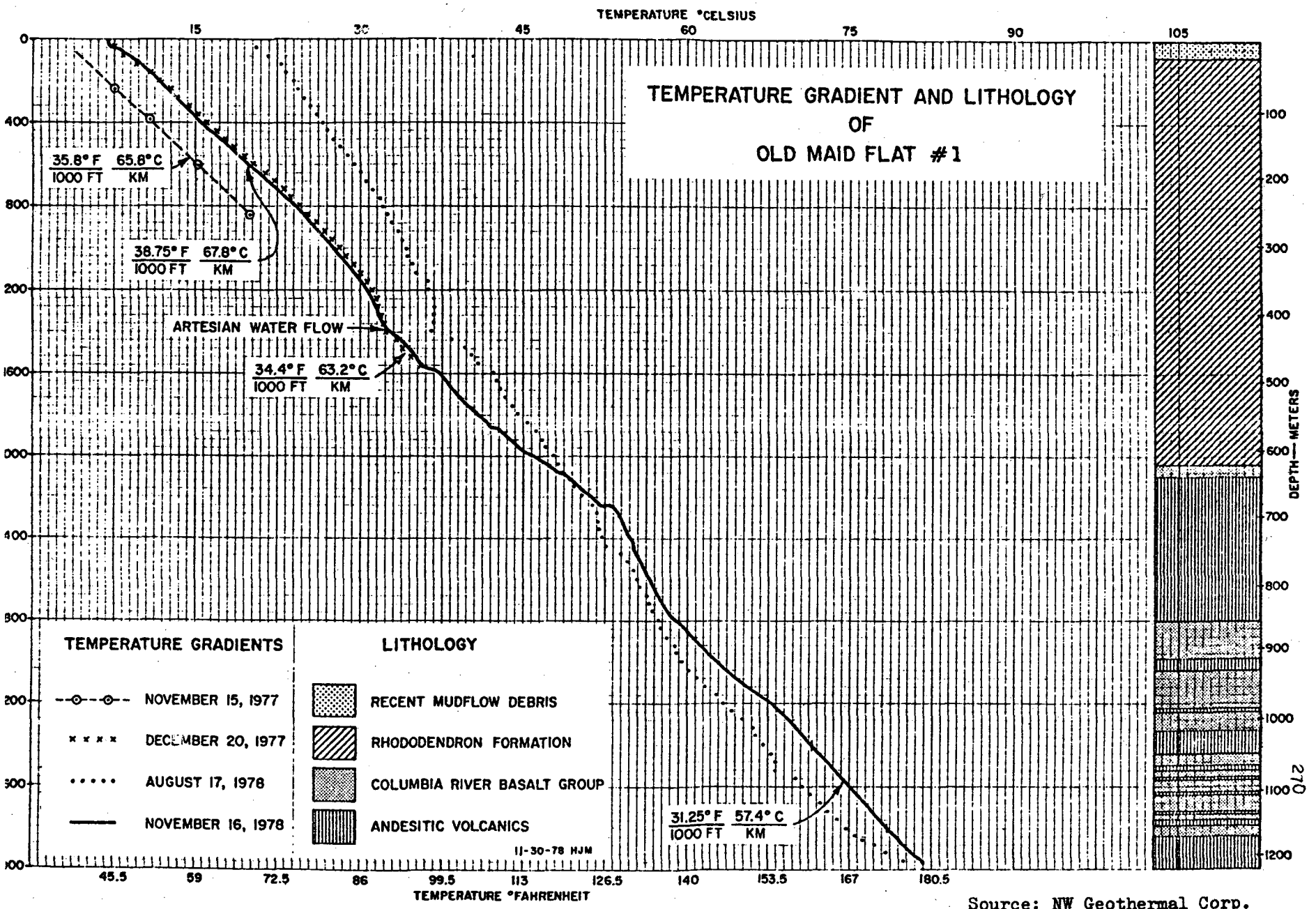

FIGURE 2

Source: NW Geothermal Corp.

Because of the heat flow implications (Blackwell and Steele, 1979) consideration should be given to the deepening of this hole to at least 1830 m (6000 ft). Northwest Geothermal Corp. should be encouraged to do the necessary fluid sampling as well as flow-testing either prior to or subsequent to the recommended deepening.

Timberline No. 2

The drilling history of this hole (3S/9E-7ab) was forwarded to DOE by others. The geology is discussed by White (1979) and the temperature-depth relationship is shown in Figure 21 (Blackwell and Steele, 1979). A subsequent temperature log of the hole by the USGS in late May 1979 indicates the temperature-depth relationship to be similar to that shown on the aforementioned figure.

This hole (target depth: 2000 ft) was originally drilled to 420.7 m (1380 ft) in depth and because of several re-drills due to either stuck drill pipe or twist-offs, the hole was completed at 226 m (741 ft). This hole represents the second attempt to drill at Timberline Lodge on Mt. Hood. The first, drilled in 1977, penetrated less than 100 ft of the planned 500-foot target depth.

One of the 2000 ft deep hydrologic holes to be drilled by the USGS this year (see above) is sited at Mt. Hood Meadows (3S/9E-3cc). This proposed hole is approximately the same distance from the center of the cone as is the Timberline hole and therefore should provide the data that would have been available if the Timberline hole had been drilled to the

target depth. Consideration should be given to drilling this hole to 3000 ft if conditions permit.

CONCLUSIONS

Notwithstanding the recommendation to deepen the Old Maid Flat hole, DOGAMI does not have sufficient data on hand to site a deep hole on or near Mt. Hood. Possibly when other data are made available from studies completed or in various stages of completion by the USGS and Lawrence Berkeley Laboratory that a firm recommendation can be made.

Provisions to carry out the several recommendations as indicated in the OVERVIEW should be engendered by DOE.

REFERENCES

Beeson, M. H., and Moran, M. R., 1979, Statigraphy and structure of the Columbia River Basalt Group in the Cascade Range, Oregon: PSU Grant No. 90-262-8126 from DOGAMI, unpublished report, 64 p.

Blackwell, D. D., and Steele, J. L., 1979, Heat flow modeling of the Mount Hood Volcano, Oregon: SMU Grant No. 86-09 from DOGAMI, unpublished report, 69 p.

White, G. M., 1979, Geology and geochemistry of Mt. Hood Volcano: OU Grant No. 50-262-8902 from DOGAMI, unpublished report, 54 p.

LBL-7092 and
State of Oregon DOGAMI
Open File Report 0-79-2

GEOCHEMICAL STUDIES OF ROCKS, WATER, AND GASES AT MT. HOOD, OREGON

Harold A. Wollenberg[1]
Richard E. Bowen[2]
Harry R. Bowman[1]
Beverly Strisower[1]

February 1979

1) Lawrence Berkeley Laboratory, Earth Sciences Division
2) Consultant to State of Oregon, Department of Geology and Mineral Industries

TABLE OF CONTENTS

		Page
	Abstract	275
	Acknowledgements	276
I.	INTRODUCTION	277
	A. Geologic Setting	280
	B. Hydrologic Setting	284
II.	SAMPLING AND ANALYSES	286
	A. Water	10
	B. Rocks	292
	C. Gases	294
III.	RESULTS	18
	A. Water Analyses	18
	1. Major and Trace Elements	18
	a. Swim Warm Springs	295
	b. Cold Springs and Wells	300
	c. Old Maid Flat Geothermal Test Hole	306
	d. Comparison of Water Chemistries	307
	e. Estimates of Subsurface Temperature	312
	f. Oxygen and Hydrogen Isotope Ratios	314
	B. Rock Analyses	316
	C. Gas Analyses	320
IV.	ORIGIN OF WARM WATERS AT SWIM SPRINGS	324
V.	CONCLUSIONS	326
VI.	CONTINUING ACTIVITIES	328
	Bibliography	329

ABSTRACT

Mt. Hood, a composite andesitic volcano, located near Portland, Oregon, is one of several large eruptive centers which dominate the Cascade Mountains of the western United States. As part of a program of geologic, geophysical and geochemical studies to examine Mt. Hood's geothermal resource potential, samples of warm-and cold-spring water, water from a geothermal test well in Old Maid Flat, fumarolic gases, and rocks were collected and analyzed for major chemical constituents and trace elements.

The only warm-spring area on Mt Hood is Swim Springs, located on the south flank. Orifices at Swim were sampled repeatedly with little overall change noted in water chemistry between summer and winter. Oxygen and hydrogen isotope data and mixing calculations based on analyses of Swim Springs and numerous cold springs, indicate that a large component of the warm water at Swim is from near-surface runoff. Chemical geothermometry suggests that temperatures at depth in the Swim Springs system are within the range 104-170°C; the temperature of unmixed hot water may exceed 200°C. Higher-than-background chloride contents and specific conductances of cold springs on the south flank of the mountain suggest that there is a small component of thermal water in these sources.

A geothermal model of Mt. Hood is proposed wherein snow- and glacier-melt water near the summit comes in close proximity to the hot central "neck" of the mountain, manifested by the summit-crater fumaroles. The hot water migrates down-slope, mixing with cold water along its path; a small portion of the mixed warm water surfaces at Swim Springs.

We were surprised to detect the platinum-group element, iridium in warm and cold spring waters and in a sample of altered andesite. Iridium is generally considered to be associated with basic to ultrabasic igneous rocks; its association with an andesite volcano is believed to be without precedent.

ACKNOWLEDGEMENTS

The authors wish to express their appreciation to the following people for their valuable assistance on this project:

- Personnel of the State of Oregon's Department of Environmental Quality for use of earlier chemical analyses of waters in the Mt. Hood region;
- Jerry Black and Joseph Riccio of the State of Oregon's Department of Geology and Mineral Industries for assistance in collecting water samples;
- James Robison of the U.S. Geological Survey for aid in collecting samples and guidance on the hydrologic setting of Mt. Hood;
- Alfred Truesdell and Nancy Nehring of the U.S. Geological Survey for isotope analyses and analyses of constituents of fumarolic gases;
- David Johnson of the U.S. Geological Survey for aid in sampling and analyses of fumarolic gases;
- Steven Flexser of Lawrence Berkeley Laboratory for assistance in X-ray fluorescence analyses and Alan Smith of Lawrence Berkeley Laboratory for gamma-ray spectrometric analyses of radioelements.
- To Orah Goldman, the authors' thanks for many careful typings of text and tables.

This work was done under the auspices of the U.S. Department of Energy.

I. INTRODUCTION

Large volcanoes together with numerous smaller eruptive centers along the Cascade Mountains from Northern California into British Columbia (Figure 1) are evidence of a tremendous release of thermal energy along this zone. The geologic history of the Cascade Range indicates that eruptions and mountain building have taken place over a long period, and continue into the present. Mount Hood, located 80 km east of Portland (Figure 2), has a volcanic history similar to many of the other Cascade volcanoes. It has high-temperature fumaroles near its summit and a warm spring area on the south flank. These recognized thermal manifestations along with the mountain's accessibility and proximity to Portland, Oregon's main energy consuming region, make it a desirable location for the study and development of geothermal energy.

Over the past two years, a multidisciplinary study of the geologic, geochemical and geophysical features of Mount Hood that relate to the location of geothermal energy has been under the direction of the Oregon Department of Geology and Mineral Industries (DOGAMI) with funding from the U.S. Department of Energy. Earlier studies (Wise, 1968, 1969) described the geologic and tectonic framework of the region. Detailed geochemical and geophysical investigations are being conducted in the same area. A separate but related program of potential volcanic hazards of Mount Hood is being conducted concurrently by the U.S. Geological Survey (USGS) under the direction of D. R. Crandell.

Technical support of the geochemical studies of Mount Hood is supplied by the Earth Sciences Division of Lawrence Berkeley Laboratory (LBL). Geophysical studies consist of gravity and aeromagnetic surveys by Oregon State University, aerial infrared surveys by the USGS, and electrical

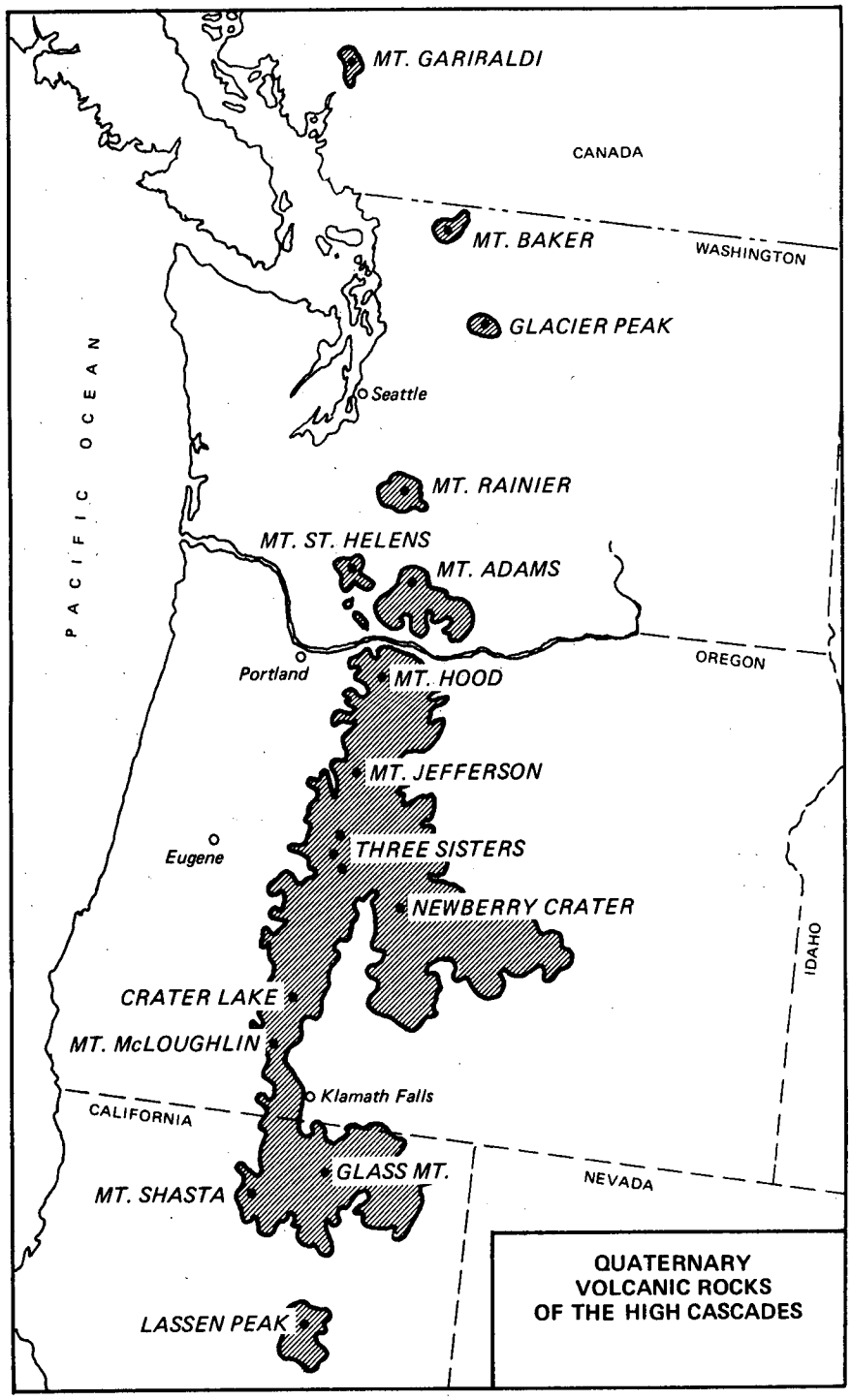

XBL 784-665

Figure 1. Regional geologic setting of Mt. Hood.

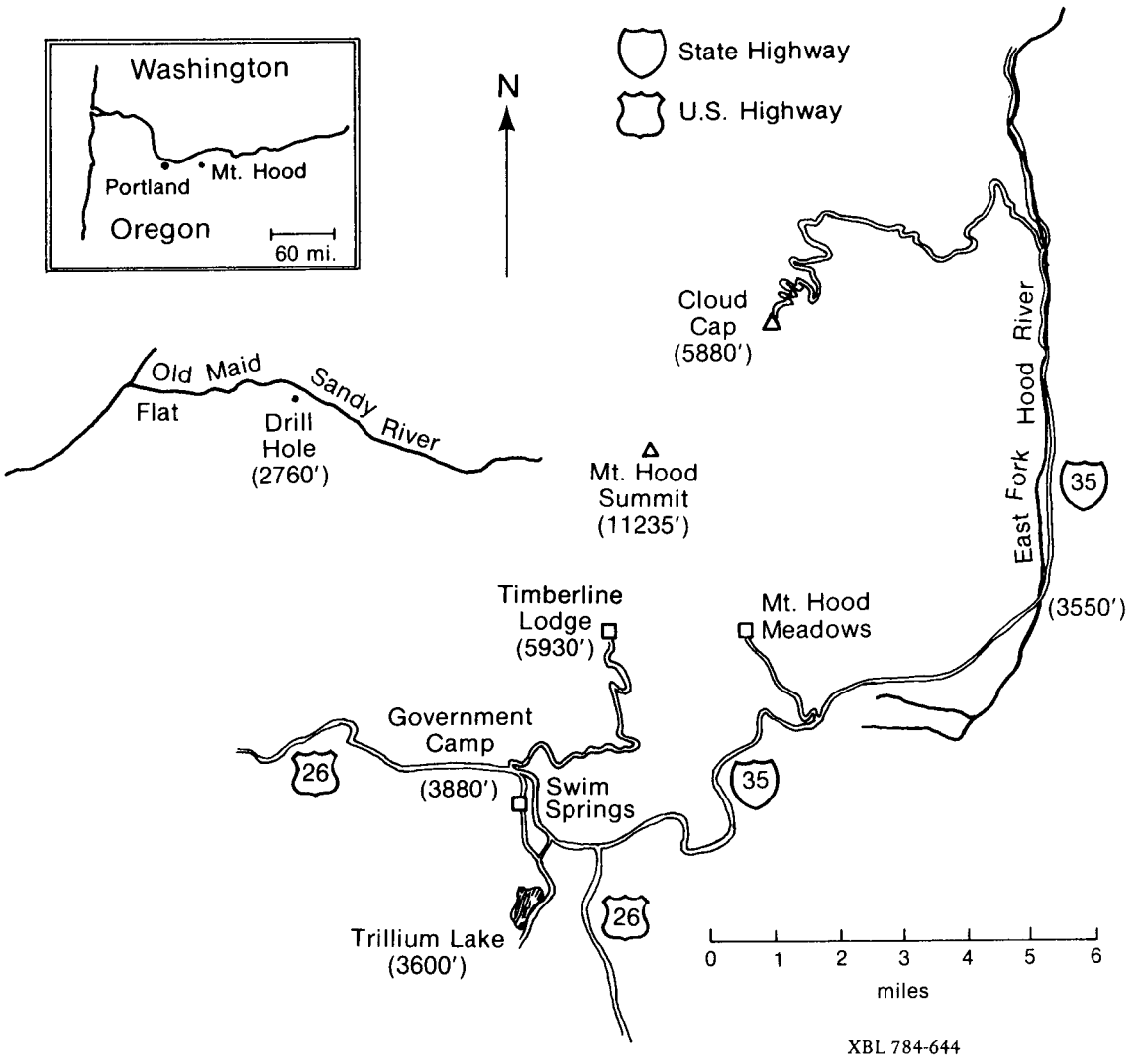

Figure 2. Location map, Mt. Hood area.

measurements by LBL (Goldstein and Mozley, 1978). Sampling and chemical analyses of rocks, gases, and ground waters in the area, including the fumaroles and the thermal and cold springs, has been a joint project between DOGAMI, USGS, and LBL. Suites of rocks typical of the area, both fresh and hydrothermally altered, have been analyzed to discern possible changes produced by the alteration. Selected water samples have been analyzed for oxygen and hydrogen isotope ratios to help determine the pathways water takes from its meteoric origin into and through the mountain's hydrologic system.

Analyses of waters from geothermal areas have proven to be very effective exploration tools. Truesdell (1975), in a comprehensive review, pointed out that several elements gave indications of minimum subsurface reservoir temperatures. The ratios between sodium, potassium, and calcium (Fournier and Truesdell, 1974) along with the silica content of warm-spring water may be definitive. A knowledge of silica contents and temperatures of cold and warm spring waters may be used to determine the amount of mixing of nonthermal waters and the reservoir temperatures before mixing.

This report emphasizes the presentation of analytical data obtained prior to October 1978. Since sampling and analyses have continued beyond that time, interpretative comments in this report are necessarily brief and should be considered as preliminary. A more detailed interpretation of the data awaits the results of continuing field sampling and laboratory analyses.

A. Geologic Setting

The regional setting of Mt. Hood is shown in Figure 1. Mt. Hood is a composite andesitic stratovolcano rising approximately 2500 meters above the surrounding terrain. It is largely Pleistocene in age with the main body of the cone constructed prior to the onset of Fraser Glaciation, about 20,000 years ago (Wise, 1968). Renewed volcanism took place about 12,000

years ago with the extrusion of several domes near the summit (Crandell and Rubin, 1977). Further episodes of extrusions near the summit about 1,600 years ago produced a series of hot avalanches that culminated in the collapse of the south rim of the crater which then topped the mountain. The collapse of the south crater wall resulted in a large debris fan that covers the south flank of the mountain (Wise, 1968). The most recent major eruption took place about 220 years ago from the Crater Rock area. At that time a series of hot avalanches cascaded down the east and west sides of the mountain, carrying incandescent debris several miles down the valleys (Crandell and Rubin, 1977). Historical eruptions were reported in 1859 and 1865 (Folsom, 1970).

Mount Hood is located along a linear trend with most of the other Cascade volcanoes of Oregon and Washington. Thayer (1937) and Callaghan (1933) have associated the lineation with a fault zone they recognized along the western edge of the High Cascades. Allen (1965) believes that the volcanoes are concentrated in a graben formed by the Hood River-Green Ridge faults on the east and the unnamed faults of Thayer and Callaghan on the west. The western fault has not been recognized in the Mount Hood area but recent drilling on the west side of Mount Hood at Old Maid Flat shows there is significant displacement of the Columbia River Basalt that may be caused by faulting.

The local geologic setting of Mount Hood is illustrated in Figure 3 (Wise, 1968). The predominant surficial material is clastic debris, of andesitic character. A plug dome of hornblende andesite, Crater Rock, was extruded about 2,000 years ago. The extensive lava flows which predated the clastic debris were predominantly hornblende andesite, while more recent extrusions on the north and northeast flanks were of olivine basalt and olivine andesite.

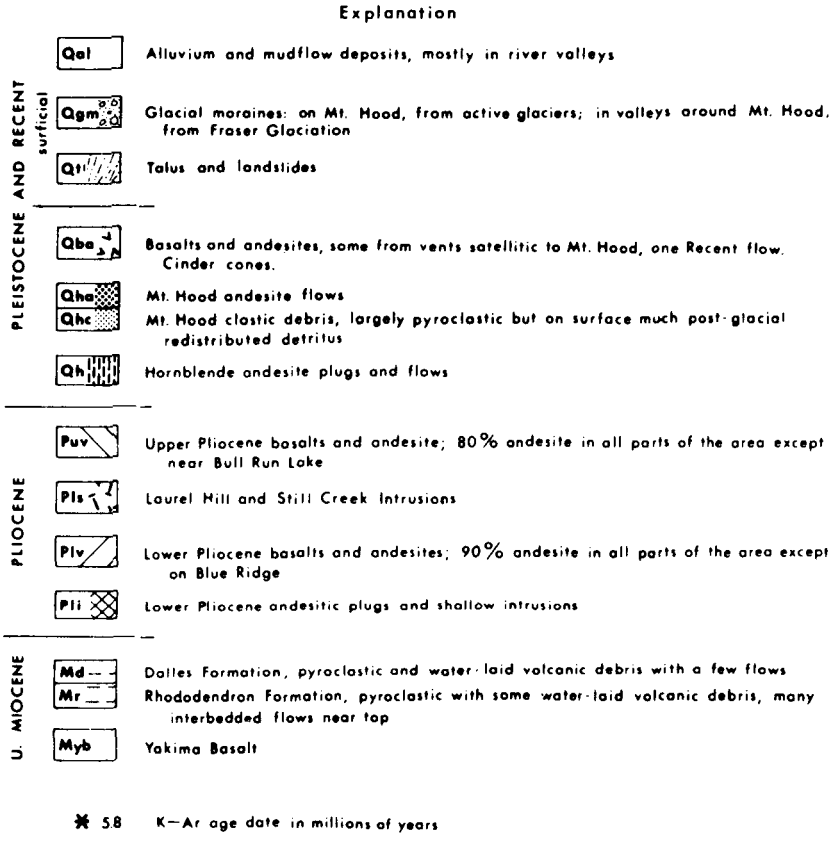

Surface water samples

Cold spring samples

Well samples

Warm spring samples

Rock samples

0 1 2 miles

0 1 2 3 kilometers

XBL 788-2661A

Figure 3. Local geologic setting of Mt. Hood (after Wise, 1968), showing locations of water and rock samples. XBL 788-2661

B. Hydrologic Setting*

Mt. Hood lies along the axis of the Cascade Range, and receives most of its precipitation during the fall and winter from storms that originate in the north Pacific and move southward and eastward across the range. The average annual precipitation is about 102 cm at Portland and increases to the east, to a maximum near the crest of the range. Records of the National Weather Service show that at Government Camp (Figure 2) the average is about 230 cm. Precipitation decreases rapidly to the east and is only 25 cm within 50 km of the crest.

Precipitation falling above an altitutde of about 1,500m on Mt. Hood is inferred to be within a recharge area, and ground water tends to move downward (Figure 4). The transition from recharge to discharge area is manifested by a band around the mountain where springs tend to discharge, and below which perennial streams are common. Above the band, many streams are intermittent; in smaller channels there is runoff only during spring, from melting snow.

At depths ranging to at least 250m in the vicinity of Timberline Lodge, ground water occurs in perched zones between or within andesite flows. The warm water emanating at Swim Springs may have circulated deeper than some of the perched zones, probably originating at elevations higher than Timberline Lodge. The water comes to the surface at Swim, where there is an abrupt flattening of the topographic slope (Figure 4); Mt. Hood andesite flows tend to dip down the mountain, and some permeable zones may intersect the land surface here. The Swim area also lies near a contact between Mt. Hood andesite flows or andesite debris and pre-Mt. Hood andesite and basalts (Wise, 1968); these older rocks are less permeable and may tend to direct ground water to the surface.

* Written in consultation with James Robison, U.S. Geological Survey, Menlo Park, California.

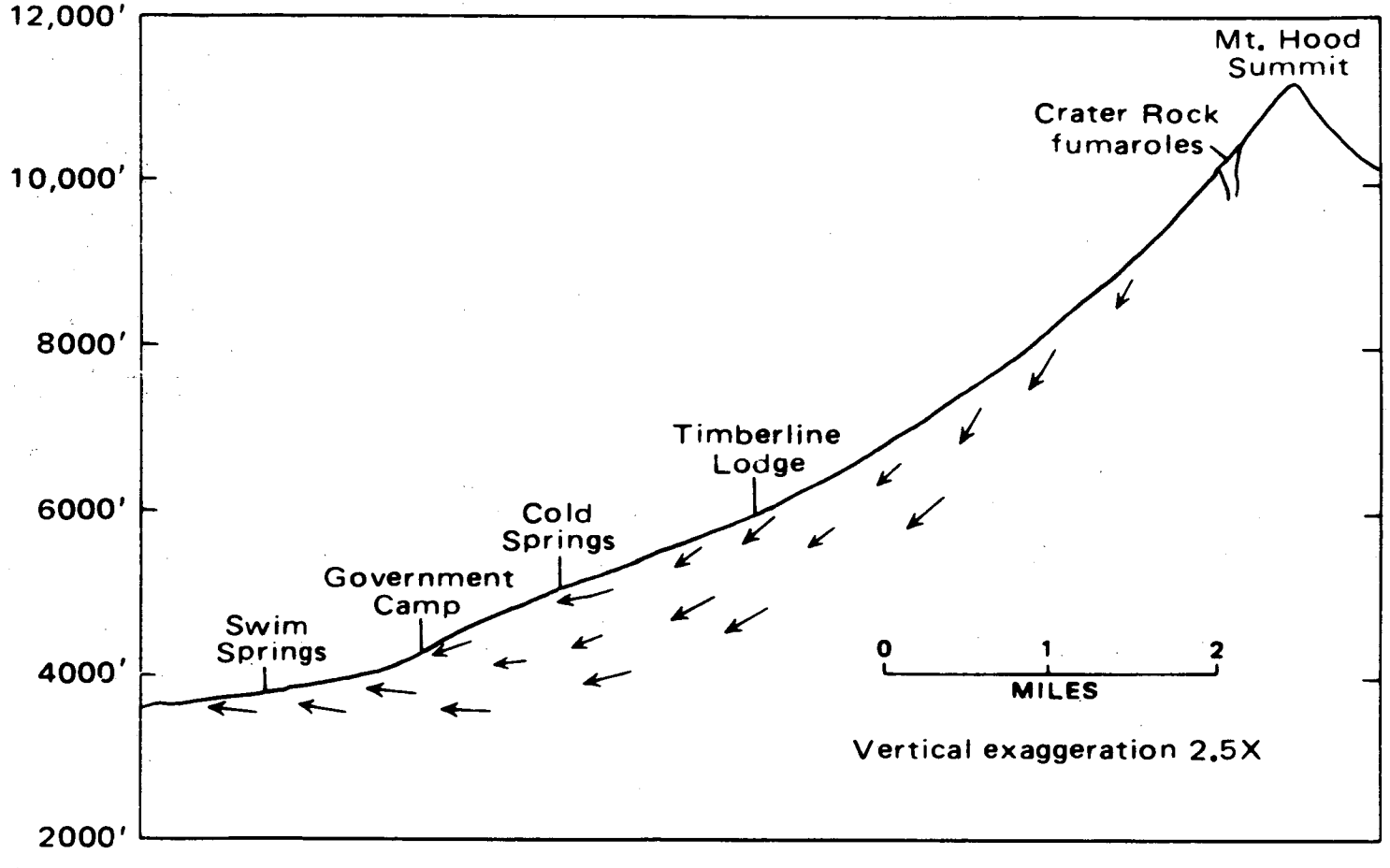

XBL 791-8145

Figure 4. Inferred ground water movement on Mt. Hood.

Distribution of runoff of streams draining Mt. Hood corresponds to that of precipitation. Records of a gauging station on Salmon River, 7 miles southeast of the summit of Mt. Hood (east of Trillium Lake near highway U.S. 26) show an average runoff of about 80 cm per year for the drainage area above the gauge. Sandy River has a runoff of 178 cm above a gauge 30 km west of the summit, and the West Fork of the Hood River has a runoff of 203 cm above a station 26 km northeast of the summit. The greatest runoff in the Mt. Hood area is reflected at a station on Bull Run River, 29 km northwest of the summit, where the average is more than 305 cm. The component of any deeply-circulating ground water in most of the springs is probably very small because the runoff is large.

II. SAMPLING AND ANALYSES

Techniques used by LBL to sample waters and rocks and to analyze them for major and trace elements have been detailed in papers by Bowman and others, (1975), Hebert and Bowman (1975), and Wollenberg (1975). In this section we shall briefly describe those techniques and the techniques to determine oxygen and hydrogen isotope ratios and constituents of fumarolic gases.

A. Water

Water samples were collected at the locations shown in Figure 3; locations are referenced by latitude and longitude in Table 1. Samples included waters from cold springs and wells, the Swim Warm Springs on the south flank of the mountain (the distribution of orifices at Swim is detailed in Figure 5), and the well drilled for geothermal water on the western flank of Mt. Hood in Old Maid Flat. Samples were collected for laboratory radiometry, X-ray fluorescence, neutron activation, and mass-spectrometric analyses. For analyses of major and trace elements, sampling was done by inserting a 1/4-inch diameter tygon tube into a spring. The water was drawn

Table 1

DESCRIPTION AND LOCATION OF WATER SAMPLES

MH-1	Still Creek, crossing with Timberline Road, 0.4 mi. N. of Highway 26 junction. 45°18.1′N, 121°43.8′W.
MH-2	Spring, White River outwash; streambed strongly iron-stained. 45°18.2′N, 121°40.4′W.
MH-3	Ski Bowl, artesian well head. 45°18.1′N, 121°46.0′W.
MH-4	Swim area, "Pipeline Spring." 45°18.0′N, 121°44.6′W.
MH-5	Swim area, "Screen Spring." 45°17.9′N, 121°44.5′W.
MH-6	Swim area, east side of old swimming pool. 45°17.9′N, 121°44.6′W.
MH-7	Swim area, cistern box upstream from pool. 45°17.9′N, 121°44.6′W.
MH-8	Spring, swim area, ~100m upstream from cistern box. 45°18.0′N, 121°44.6′W.
MH-9	Swim area, northernmost spring on west branch creek. 45°18.1′N, 121°44.7′W.
MH-10	Robin Hood Quarry, small spring in central bench. 45°20.1′N, 121°34.1′W.
MH-11	Spring, roadcut on north side of Highway 35. 45°18.6′N., 121°39.6′W.
MH-12	Spring, roadcut/quarry, north side of Highway 26, 1/3 mi. NW Trillium L. turnoff. 45°17.4′N, 121°44.0′W.
MH-13	Spring, roadcut on Highway 26, above Laurel Hill Quarry. 45°18.4′N, 121°49.6′W.
MH-14	Spring, Mt. Hood Meadows below Timberline Trail. 45°20.3′N, 121°40.1′W.
MH-15	Salmon River Canyon Springs. 45°19.9′N, 121°42.2′W.
MH-16	Spring, White River Canyon. 45°20.1′N, 121°41.9′W.
MH-17	Spring, from andesite flow. 45°20.1′N, 121°42.9′W.
MH-18	"Pipeline Spring." Same location as MH-4.
MH-19	Swim area, "Screen Spring." Same location as MH-5.
MH-20	Swim area, "East side of Pool." Same location as MH-6.

Table 1 (continued)

MH-21	"Iron Spring" near bridge over Clear Creek. 45°23.5′N, 121°51.5′W.
MH-22	Slightly artesian well, Clear Creek picnic ground. 45°21.4′N, 121°56.2′W.
MH-23	Spring area below Timberline Lodge. 45°18.9′N, 121°42.9′W.
MH-24	Spring at Camp Windy. 45°24.7′N, 121°32.8′W.
MH-25	Clinger Springs. 45°16.4′N, 121°45.9′W.
MH-28	Spring on Timberline Trail, 5700 feet elevation. 45°20.0′N, 121°39.6′W.
MH-29	Cold Spring. 45°21.7′N, 121°39.6′W.
MH-30	Runoff, small lake in crater area. 45°22.1′N, 121°41.9′W.
MH-31	Spring, base of lava flow, Zigzag Canyon. 45°20.9′N, 121°44.1′W.
MH-32	Spring, base of Mississippi Head. 45°21.2′N, 121°43.6′W.
MH-33A	Old Maid Flat, NWNG Co., test hole, artesian flow, 4 days after cessation of drilling. 45°23.4′N, 121°48.5′W.
MH-33B	Old Maid Flat, NWNG Co. test hole, artesian flow, second sampling, several days later. Same location as MH-33A.
MH-35	Old Maid Flat, NWNG Co., test hole, artesian flow, sample after well had been shut-in for ~1 week. Same location as MH-33A.
MH-36	Robin Hood Quarry, same spring as in MH-10 sample.
MH-37	Swim area, east side of large pool. Same location as MH-6.
MH-38	Swim area, "Screen Spring." Same location as MH-5.
MH-39	Swim area, "Pipeline Spring." Same location as MH-4.
MH-40	Old Maid Flat, NWNG Co., test hole, artesian flow for ~36 hours following MH-35 sampling. Same location as MH-33A.

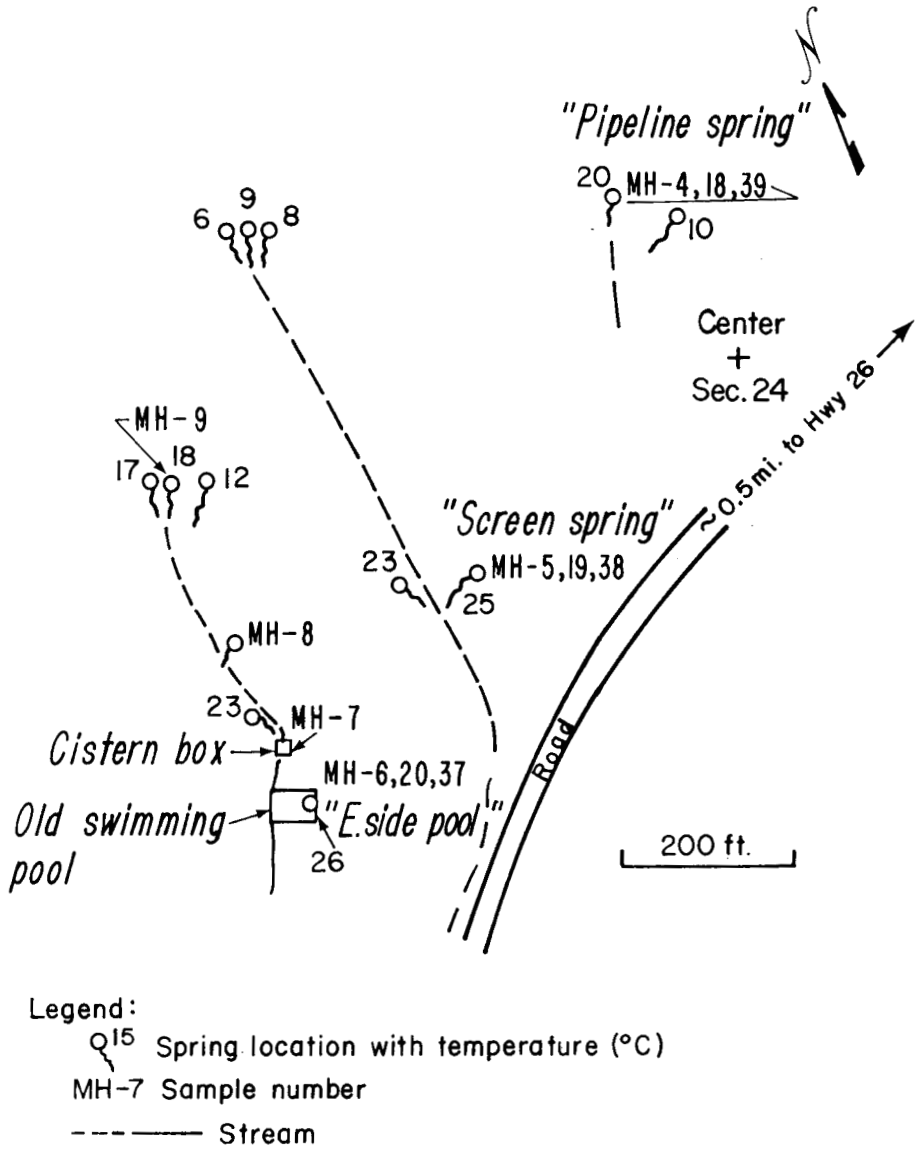

Location map, sampling sites and other springs in Swim Warm Springs area, (Sec.24, T3S., R. 8½ E.)

XBL 788-2660

Figure 5. The distribution of water sources at Swim Warm Springs.

through a 0.45 micron filter, using a hand-operated vacuum pump; the apparatus is shown in Figure 6. Most often, the water was introduced to the filter directly from the spring, but occasionally conditions required that samples be obtained in bottles and then filtered by pumping from the bottle in the field or laboratory. Generally, 500-ml "Nalgene" bottles were used to collect and store the samples. At the sampling site the pH of the water was measured using a color comparitor set and specific conductance measured by a portable electronic unit. Chloride contents were estimated on-site by immersing "Quantab" strips in spring or well waters.

In the laboratory the water samples were evaporated in the original collecting bottles at 80°C, and aliquots of each were taken for both neutron activation analysis and X-ray fluorescence analysis. In general, the X-ray fluorescence measurements determined the major element abundances, while neutron activation was used for the trace and minor elements. Some elements were determined by both methods so that cross-checks could be made.

For neutron activation, evaporates from water samples were made into pellets and irradiated, along with a composite standard pellet, in the TRIGA Research Reactor at the University of California, Berkeley. Nearly all elements in the samples have their counterparts in the standard, and the abundances are determined by comparing the gamma rays emitted from the unknowns with the gamma-ray spectra of the standards. This method is capable of quantitatively analyzing nearly 50 elements in a sample.

The X-ray fluorescence technique used in this study was developed by Hebert and Street (1974). In this method the evaporates were mixed with $LiBO_2$ and fused into glass discs. The major elemental abundances were determined by comparing these samples (indirectly) with USGS standard rock DTS, spiked with MgO, NaCl, $CaSO_4$ and K_2CO_3.

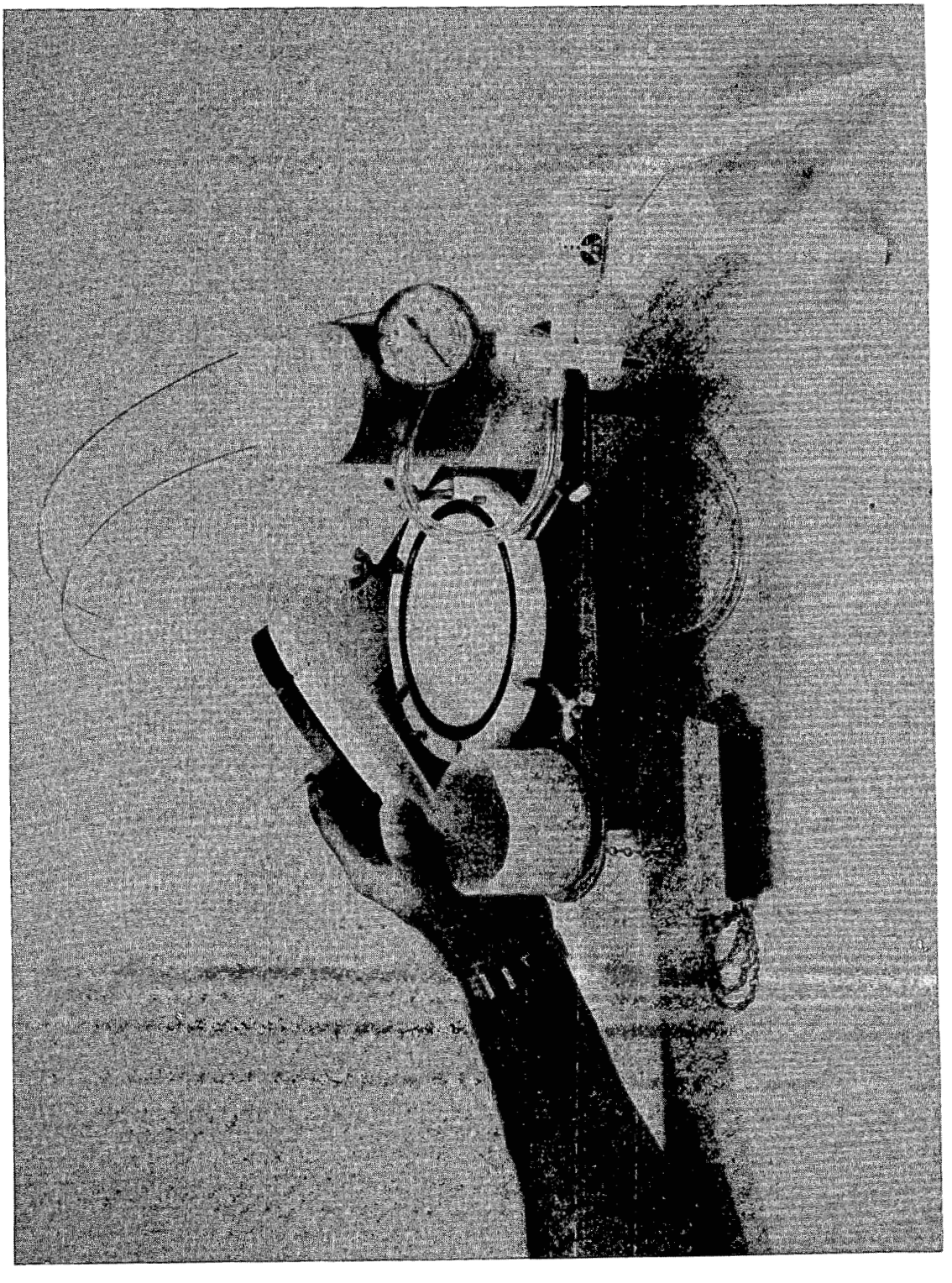

CBB 7410-7354

Figure 6. The filtering apparatus and hand pump used to collect samples in this study.

The precision of the neutron activation method depends mainly on the statistics of gamma-ray counting of the activated samples; for most elements analyzed precisions were of the order of a few percent of the abundance. Precisions and accuracies of X-ray fluorescence determinations of major elements were also a few percent of element abundances.

Samples for laboratory determination of ^{222}Rn were usually collected by filling "Nalgene" bottles with the spring water directly from the pools. This minimized radon loss which might occur if the water were drawn through the filter system. Bottles were immediately sealed, lids taped, and samples transported to the laboratory for gamma-ray pulse-height analyses. The time of sampling was noted to account for the radioactive decay of ^{222}Rn (3.8-day half-life) between sampling and gamma counting. With a reasonably short interval between sampling and counting, the sensitivity of this method is of the order of a few tens of pCi per liter of ^{222}Rn.

Samples for oxygen and hydrogen isotope determinations were obtained by filling 50 ml glass bottles directly with spring water. The bottles were tightly capped, taped, and sent via the U.S. Geological Survey, Menlo Park office, to the analytical laboratories at Saclay, France, where oxygen-16/oxygen-18 ratios and deuterium/hydrogen ratios were measured by mass spectrometry.

B. Rocks

Rock types sampled included altered and relatively fresh andesite and basalt from the flanks of Mt. Hood, a felsic dike in the Hood River Valley, and granodiorite and diorite from the Laurel Hill intrusive. Locations are shown in Figure 3, and listed in Table 2. Samples, each of the order of a kilogram, furnished adequate material for gamma spectrometric determination of uranium and thorium. At several locations gamma-ray counting rates were measured with a portable sodium-iodide crystal.

Table 2

DESCRIPTION OF ROCKS AND LOCATION OF SAMPLES

Mount Hood Rocks:

1. Felsic dike, Robin Hood Quarry
2. Basalt, Robin Hood Quarry
3. Altered Mt. Hood andesite breccia
4. Felsite dike, chloritized, with sulfide minerals
5. (pre?) Mt. Hood andesite
6. Platy Mt. Hood andesite
7. Granodiorite (?), Laurel Hill intrusive
8. Diorite (?), Laurel Hill intrusive

} Laurel Hill Quarry

9. Altered diorite (?), Laurel Hill intrusive
10. Pliocene hornblende andesite, Sandy River
11. Altered andesite, Sandy River
12. Microporphyritic olivine andesite, Cloud Cap
13. Pliocene hornblende andesite, Hood River Canyon (Polallie Campground)

Neutron activation and X-ray fluorescence techniques for analysis of rock samples have been described, respectively, by Perlman and Asaro (1969) and Hebert and Street (1974). Crushed rock samples were pulverized and powders pelletized for reactor irradiation, and fused with lithium borate into glass discs for X-ray fluorescence. With these techniques 25 to 30 elements were determined with precisions of less than 5%; a number were determined to better than 1%.

C. Gases

Gas samples were obtained from fumaroles in the summit crater area of Mt. Hood. Three fumaroles were sampled, one of which was most likely a fumarole sampled previously by Ayres and Creswell (1951). The samples were collected by inserting the end of an $\sim$1.5m-long stainless-steel tube into the fumaroles and allowing the gas to pass into evacuated 300 ml glass bottles containing $\sim$100 ml of 4N NaOH solution. The filled bottles were transported to the laboratory of Dr. A. H. Truesdell, U.S. Geological Survey, Menlo Park, California, where they were analyzed by wet chemical methods for CO_2 and H_2S and by gas chromatography for other constituents. Sampling and analytical procedures have been described in detail by Truesdell and Nehring (1978).

III. RESULTS

Analytical data on water, rock, and gas samples are presented and preliminary interpretations discussed.

A. Water Analyses

1. Major and Trace Elements

For the purposes of this discussion, results of analyses of element contents of water are divided into two groups: those from the Swim Warm

Springs and those from the predominantly cold-water sources elsewhere in the Mt. Hood region. Three analytical laboratories are represented in this study: the Lawrence Berkeley Laboratory, the Central Laboratory of the U.S. Geological Survey, Denver, and the State of Oregon's Division of Environmental Quality.

a. Swim Warm Springs

Results of chemical analyses from successive samplings of Swim Warm Springs are presented in Tables 3a and 3b. Locations of individual orifices are shown on the map, Figure 5. Spring temperatures and the abundance of major and trace elements generally follow a geographic distribution, with the southernmost spring, "East side of pool," being warmest and having the highest chemical contents. Element abundances and temperatures are progressively lower in the "Screen" and "Pipeline" springs, which are respectively up-slope from the "East side of pool" spring. The up-slope decrease of temperature and element content is repeated in the sample sequence MH6 through MH9, from orifices along the small stream entering the pool from the northwest. The successive decreases of temperature and element content suggest that the water at "East side of pool" is the least diluted by mixing with near-surface cold waters. This suggestion is supported by data shown in Figure 7, where major- and trace-element contents are plotted against sodium. In most cases there is a linear relationship between element abundances, with the warmer springs having higher contents. Least-squre linear regression coefficients exceed 0.96 for Na versus Rb, Cs, Cl, Br and K. The strong linear correlations indicate appreciable mixing between warm and near-surface cold waters. The geochemical mixing model, discussed more fully in section III-e, indicates that over 90% of the water emanating at Swim is near-surface cold water.

Table 3a

SWIM WARM SPRINGS

Spring	"PIPELINE"			"SCREEN"			"E. SIDE OF POOL"				Single Sampling		
	Successive Samplings												
Sample	MH-4	MH-18	MH-39	MH-5	MH-19	MH-38	MH-6	MH-20	USGS	MH-37	MH-7	MH-8	MH-9
Date	6/2/77	8/22/77	2/22/78	6/2/77	8/22/77	2/22/78	6/2/77	8/22/77	8/22/77*	2/22/78	6/2/77	6/2/77	6/2/77
pH	7.5	7.5	7.5, 7.5	7.5	7.4	7.5, 7.1	7.5	7.1	7.3	7.3	7.5	7.4	7.5
Temp. °C	22	21.8	21.6	25	23.5	25.5	26	24.1	26.5	26.2	20	21	19
Sp. Cond.			820			1000			1300	1160			
									*(Robison)				
					mg/ℓ								
B	2.0	1	0.5	1.0	3	0.5	3.0	2	0.15	0.5	1	2	0.2
Na	92	84	92	95	101	105	120	114	120	126	86	62	36
Mg	34	36	38	36	30	43	40	40	51	50	30	20	13
SiO_2	75	70	75	75	91	78	80	71	92	88	70	80	60
S	54	54	58	62	65	72	63	68	~80	74	52	48	26
Cl	110	110	102	120	125	135	140	140	170	154	95	80	25
K	7.5	6	7	8	7	8	9.2	7.2	12	9	7.2	6.4	3.6
Ca	50	52	53	55	62	60	60	58	64	64	42	41	19
					µg/ℓ								
Mn	<4	<0.7	3	<5	<4	<3	<7	<5	50	<3	<6	<?	<1
Fe	70	35	(50	27	50	<12	47	<50	220	<25	18	14	14)
Ba	15	26	21	27	28)	22	37	24		27)	17	21	11
Mo	4	<2	3	3	<1.6	<5	4	<4		<7	4	5	2
Rb	17	15	17	18	19	20	23	23		23	16	14	7
Cs	0.25	0.26	0.25	0.31	0.32	0.33	0.38	0.34		0.4	0.25	0.20	0.10
Co	<0.03	<0.03	-	<0.06	<0.03	-	<0.06	<0.03		-	<0.02	<0.02	<0.02
Sb	<0.05	<0.04	<0.06	<0.03	<0.03	<0.02	<0.03	<0.05		<0.1	<0.03	<0.06	<0.02
Cr	<0.7	<0.3	<0.5	<0.7	<0.5	<1	<0.7	<0.1		<5	<0.5	<0.5	<0.4
Zn	<10	1.5	2	<10	2	3	<10	4		3	<10	<5	<5
Ag	<0.06	<0.05	<0.2	<0.06	<0.14	<0.1	<1	<0.2		<0.1	<0.1	<0.06	<0.03
Ce	<0.6	-		<0.6	-			<0.9	-		<0.7	<0.6	<0.3
Sm	0.087	0.03	<0.06	≤0.047	0.06	<0.06	0.105	0.139		<0.06	0.09	0.075	0.03
Eu	<0.011	<0.004	<0.005	<0.013	<0.006	<0.005	<0.014	<0.006		<0.006	<0.012	<0.015	<0.005
U	0.87	0.8	1.1	1.2	0.8	1.2	1.4	1.6		1.3	0.45	0.6	0.2
Ir	<0.0013	<0.0001	<0.0010	≤0.0015	<0.0001	<0.0014	≤0.0012	<0.0001		0.007	≤0.0013	≤0.0012	<0.0003
As	<8	<2	<5	<8	<3	<5	<8	<36		<5	<8	<5	<3
Br	200	134	180	220	180	220	270	280		240	180	148	48
W	<2	<1	<2	<1.5	<1	<2	≤4	<7		<2	<1	<2	<1
Sc	0.02	<0.01	0.022	0.02	0.018	<0.009	0.03	<0.01		0.015	0.014	0.012	0.010
Hf	<0.10	<0.05	<0.006	<0.12	<0.03	<0.03	<0.9	<0.07		<0.03	<0.6	<0.06	<0.010
Th	<0.02	<0.02	<0.005	<0.02	<0.02	<0.015	<0.05	<0.04		<0.10	<0.012	<0.012	<0.010
^{222}Rn (picocuries/ℓ)	172						156			161		186	

Table 3b

SWIM WARM SPRINGS

(Analyses in milligrams per liter, by
State of Oregon, Department of Environmental Quality)

Location*	Pipeline	Screen	E. Side of Pool	E. side of Pool	W. side of stream 50'N of cistern
Date	12/2/76	12/2/76	8/13/76	12/2/76	11/4/75
pH	7.3	7.3	8.1	7.5	7.4
T (C°)	20	25	26.1	25.6	--
Conductance	871	1190	1265	1300	907
Alkalinity (total as $CaCO_3$)	116	157	74	179	121
Hardness (as $CaCO_3$)	253	310	357.0	357	258.2
B	0.28	0.40	0.32	0.32	0.34
Na	79.0	114.0	98.0	136.0	79.0
Mg	29.0	44.0	28.0	48.0	40.0
SiO_2	55.4	71.6	65.5	72.3	52.1
SO_4	149.0	193.0	227.0	205.0	181.1
Cl	103.0	139.0	160.0	161.0	90.0
K	6.0	10.0	10.2	11.7	9.2
Ca	42.0	57.0	27.0	60.0	46.0
Mn	<0.05	<0.05	<0.05	<0.05	0.10
Fe (total iron)	0.05	<0.05	0.2	<0.05	<0.05
As	<0.005	<0.005	<0.005	<0.005	0.04
F	0.15	0.23	0.27	0.23	0.20
PO_4 (soluble ortho.)	0.09	0.08	0.10	0.09	0.12
Al	<0.01	<0.02	<0.02	<0.02	<0.01
Nitrogen (NH_3)	0.06	0.09	<0.01	0.05	0.03
Nitrogen (nitrite)	<0.02	<0.02	<0.02	<0.02	<0.01
Nitrogen (nitrate)	0.04	0.04	<0.02	0.03	0.01
Li	0.08	0.12	0.12	0.13	0.09
HCO_3	141	191	90	218	148

* Refer to map, Figure 5.

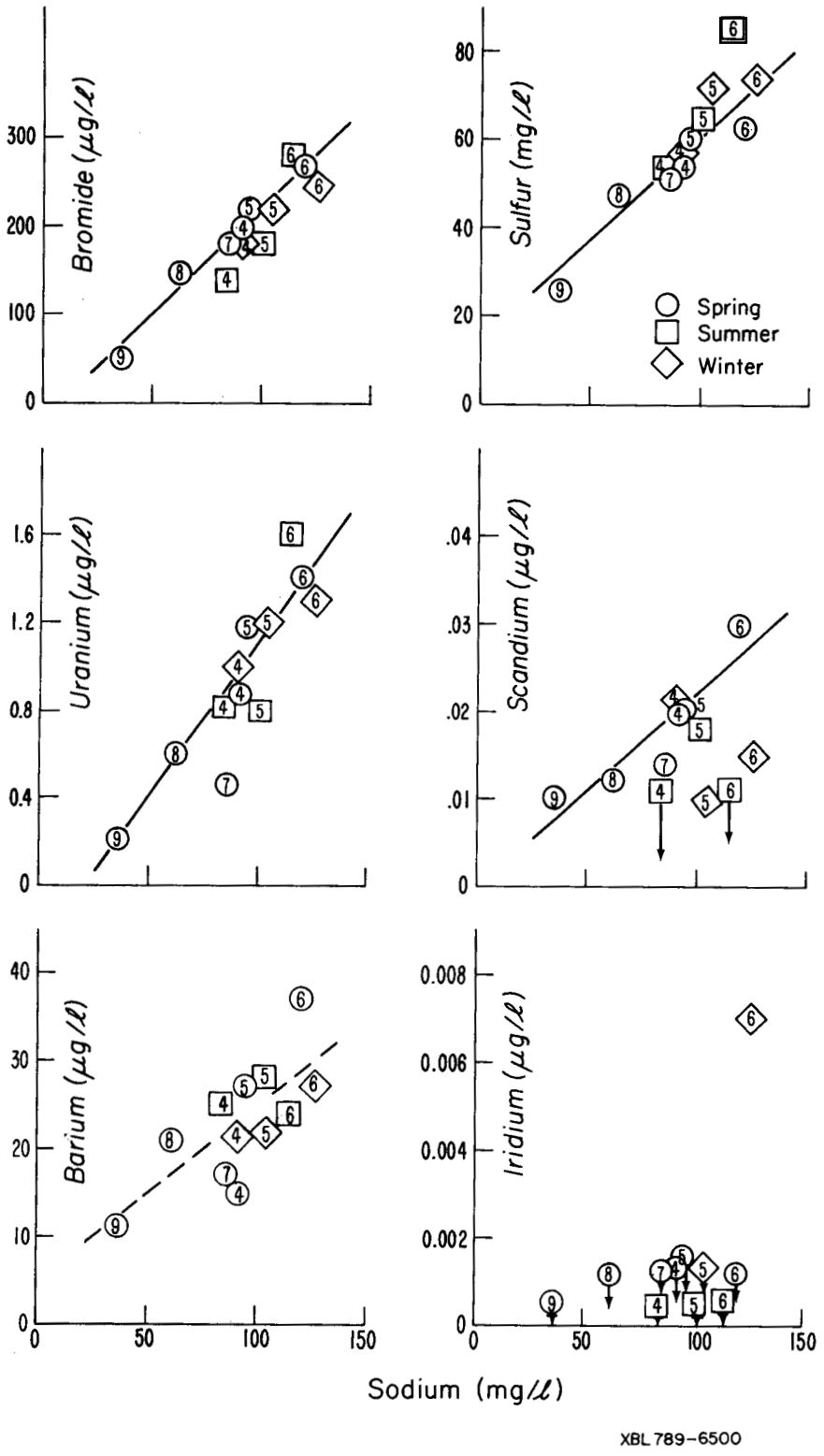

Figure 7a. Major- and trace-element contents of water from Swim Warm Springs, plotted against sodium.

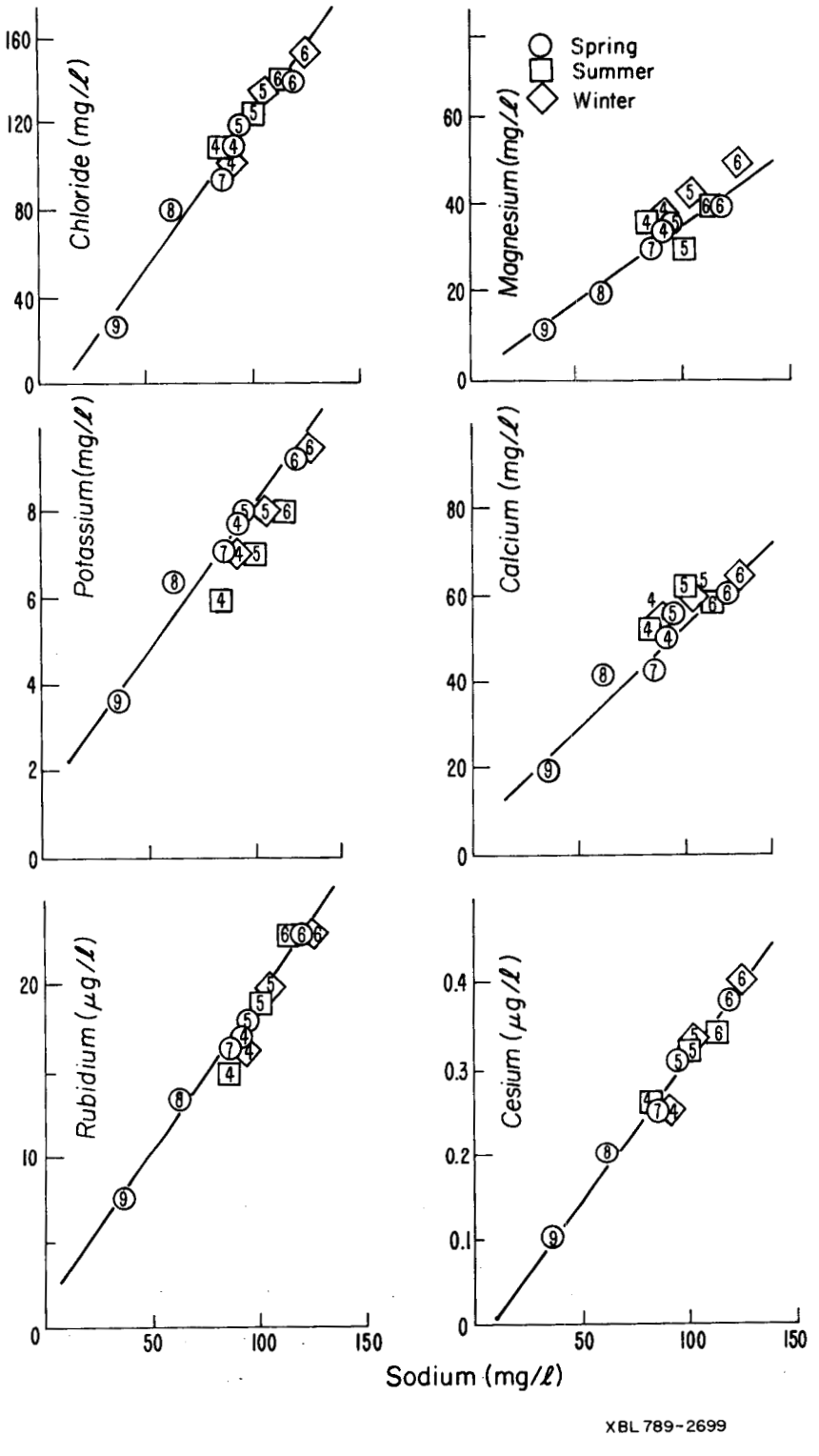

Figure 7b. Major- and trace-element contents of water from Swim Warm Springs, plotted against sodium.

The variation with time of element contents of three orifices at Swim is illustrated in Figure 8. Significant winter increases were observed in Mg and S at all three orifices, while Cl, Cl/B, Ca and Cs were greater in the winter at two of the orifices, and SiO_2, Na, Rb, and U were greater at one (but not necessarily the same) orifice. There were significant winter decreases in B at all three orifices, and in Cl, Ba, U and Br at one or another orifice. It was expected that winter samplings would yield higher contents because the surface runoff would be diminished. However, this was not substantiated because of the increase of some elements and decrease of others in the winter, with respect to the summer samplings.

The presence of the platinum-group element, iridium (0.007 µg/ℓ), in the winter sample from "East side of pool" is of interest, especially because it was not detected in the summer samples from that orifice. There were no other differences of this order in trace element abundances between summer and winter samplings. Iridium was also detected, in lower concentrations, in two cold-water sources: the iron-rich spring in White River Valley (MH 2), and the outflow of the small lake in the summit crater (MH 30). Silver is present along with iridium in these and other springs, and in the summit crater lake. A search of geochemical literature reveals that this is the first evidence of a platinum-group element being detected in geothermal or surface fresh waters.

b. Cold Springs and Wells

Results of specific conductance and chloride contents, measured in the field, are shown on Figure 9. Springs and surface waters sampled in the drainages of Still Creek, Salmon River, White River and the spring at Mt. Hood Meadows have greater abundance of Cl, and higher specific conductance than springs sampled to date on the north flank of Mt. Hood. Waters from 22 cold sources, 20 of them springs, were analyzed for major and trace elements; results of analyses, pH, and temperature measurements are listed in Table 4. With a few exceptions, the cold springs issue from andesite;

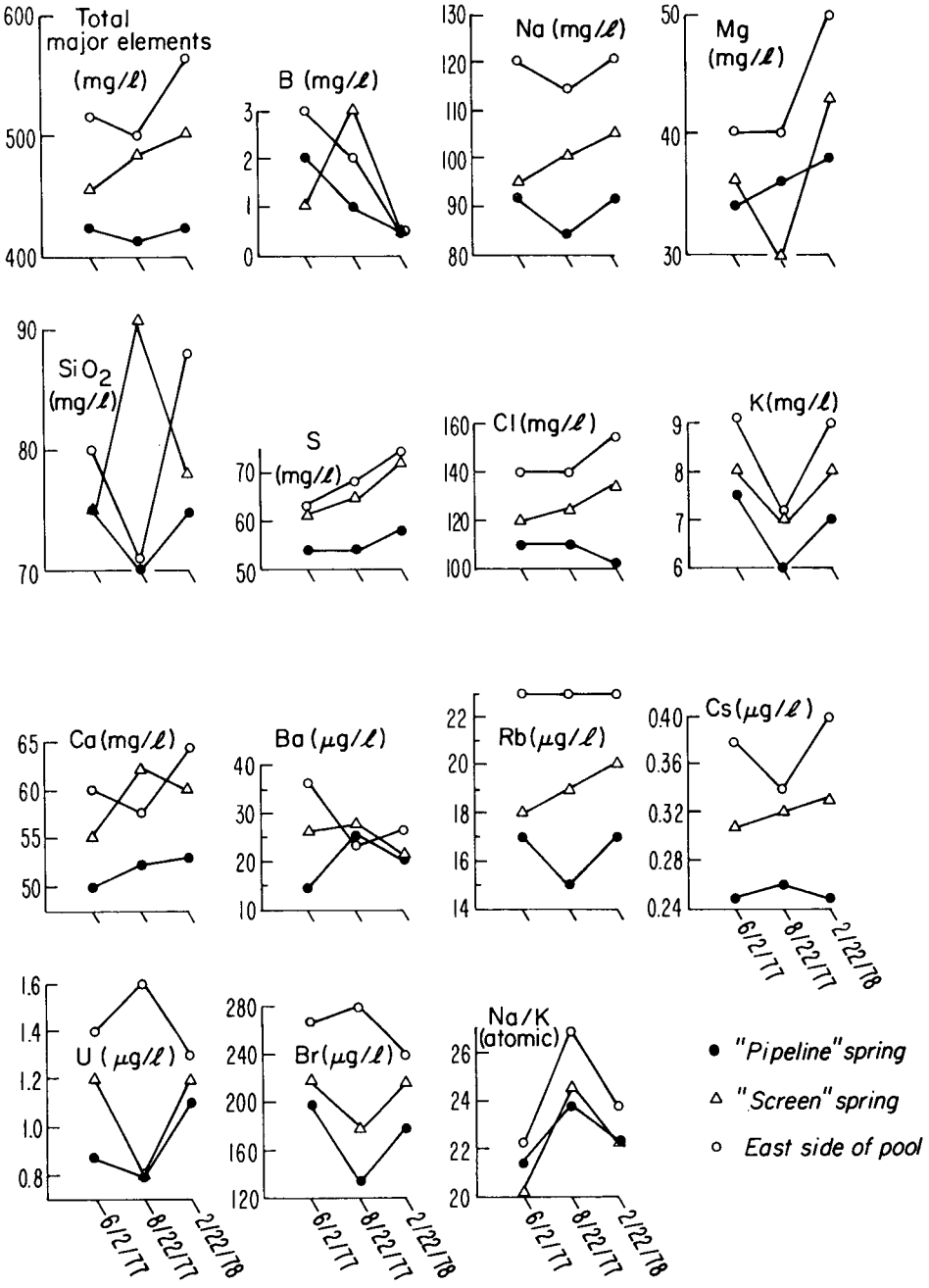

Variation in major and trace-element contents from successive samplings of three orifices at Swim Warm Springs 6/2 and 8/22/77, and 2/22/78.

XBL 789-6505

Figure 8. Element content variations with time at the three orifices at Swim Warm Springs.

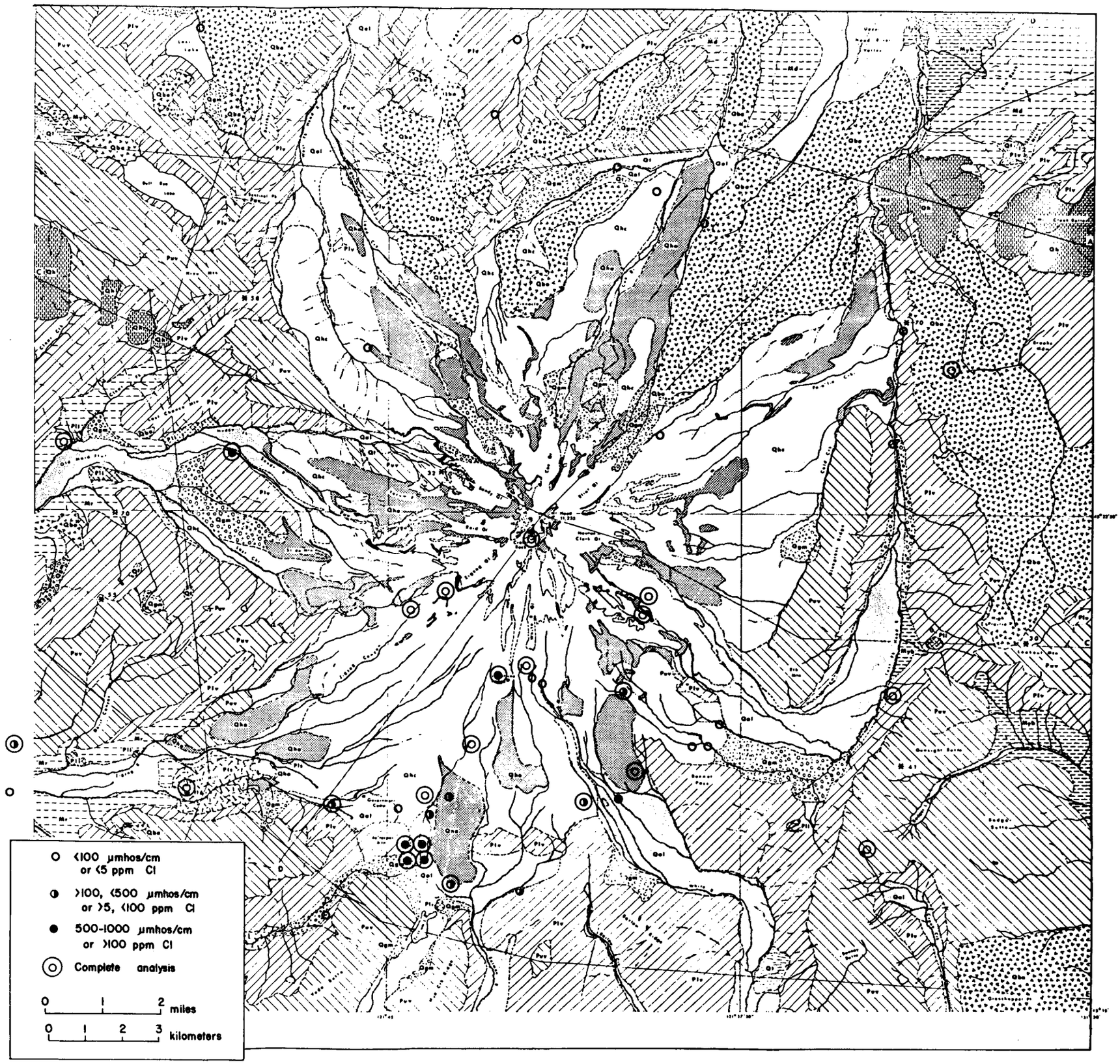

XBL 792-8468

Figure 9. Specific conductance and chloride content of waters plotted on the geologic map of Mt. Hood (after Wise, 1968).

Table 4a

Sample	MH-1	MH-2	MH-3	MH-10	MH-11	MH-12	MH-13
Date	6/1/77	6/1/77	6/2/77	6/3/77	6/4/77	6/4/77	6/4/77
pH	6.9	∿6.2	8.5	∿7.5	∿6.7	∿6.9	6.5
Temp. °C	4.5	3.5	7	7	3	5	10
			mg/ℓ				
B	3	0.5	0.2	0.5	0.3	0.2	0.5
Na	3	2.2	16	6	1.2	7	2
Mg	<0.5	<1	4	5	1	2	<0.6
SiO_2	-	-	-	-	-	30	-
S	-	-	-	-	-	3	-
Cl	1	1	2	<0.2	<0.1	5	<0.2
K	<0.7	1	2	<0.2	<0.4	1	<0.4
Ca	3	2	17	50	<0.01	0.11	0.15
			µg/ℓ				
Mn	0.7	27	2	<0.2	<0.1	1.5	4
Fe	30	2400	22		10	110	155
Ba	0.7	4	2.3	<2	5.6	3	1
Mo	0.37	0.2	3	13	≤0.06	0.02	<0.1
Rb	2.2	0.7	1.2	2	1	4	0.3
Cs	0.05	0.02	0.02	0.66	0.01	0.10	0.02
Co	0.02	0.36	<0.01	0.05	<0.02	0.05	<0.02
Sb	<0.03	0.01	0.11	2.4	<0.01	<0.01	0.02
Cr	<0.2	<0.2	<0.1	<0.3	<0.1	0.55	0.33
Zn	20	<5	120	<1	<1	8	3
Ag	<0.02	0.5	<0.03	<0.02	0.005	2.4	0.1
Ce	<0.04	0.17	< 0.2	<0.03	0.02	0.1	0.1
Sm	0.003	0.012	-	0.02	0.0018	0.012	0.009
Eu	<0.001	0.0019	<0.002	<0.004	0.0004	0.003	0.002
U	0.023	0.012	0.077	0.08	0.005	0.05	0.008
Ir	≤0.00005	0.00031	<0.00010	<0.0002	<0.0001	≤0.0002	<0.00001
As	<0.2	<4	1.4	12	<0.2	<1	<0.1
Br	2	1	3	<4	<2	6	7
W	<0.05	-	<0.2	<0.6	<0.07	<0.3	<0.1
Sc	0.031	0.023	<0.003	0.020	0.0027	0.030	0.05
Hf	<0.03	0.01	<0.03	<0.019	0.004	<0.009	<0.004
Th	<0.003	0.008	<0.005	≤0.008	≤0.0015	≤0.009	0.012

Table 4b

Sample	MH-14	MH-15	MH-16	MH-17	MH-21	MH-22	MH-23	MH-24
Date	6/5/77	7/29/77	7/29/77	7/29/77	8/2/77	8/2/77	8/3/77	8/3/77
pH	7.5	6.8	6.5	6.5	6.4	8.5	6.4	6.5
Temp. °C	8	4	10	9	4.5	10	1	3
				mg/ℓ				
B	0.5	0.5	1	0.5	0.5	3	0.5	0.5
Na	6.5	0.8	0.6	1.4	3	125	3	1.2
Mg	6	<0.3	<0.4	<0.3	2	20	1	<0.3
SiO_2	42	24	13	21	27	54	29	23
S					-			
Cl	6	0.2	0.3	0.8	1.5	25	1.3	0.5
K	3.5	0.3	0.3	0.6	<0.5	16	0.5	0.8
Ca	19	0.5	0.4	2	4	51	4	1.4
				µg/ℓ				
Mn	1.6	0.7	3	2	144	<7	0.5	2
Fe	90	38	180	100	5800	210	14	20
Ba	7	2.3	2.7	1.3	<3	10	<0.5	<1
Mo	<0.1	<0.1	<0.05	<0.04	0.13	5.5	≤0.1	<0.04
Rb	5	0.9	0.5	1.8	1.3	8	2	1.3
Cs	0.09	≤0.008	0.009	0.014	<0.04	0.06	0.06	0.01
Co	0.04	0.02	0.08	0.06	0.11	0.05	<0.01	0.03
Sb	0.01	0.01	<0.009	<0.02	0.04	0.05	0.02	<0.01
Cr	<0.4	0.23	0.45	0.23	0.7	<0.3	<0.1	0.2
Zn	1	0.8	2.5	0.8	3	4.6	<1	1
Ag	<0.07	≤0.02	≤0.6	<0.01	<0.06	<0.05	<0.04	<0.1
Ce	0.18	0.12	0.36	0.15	-	-	-	-
Sm	0.009	0.009	0.02	0.01	0.02	0.01	0.002	0.008
Eu	<0.001	<0.002	<0.004	<0.004	<0.004	<0.002	<0.001	<0.004
U	0.23	0.012	<0.02	<0.02	<0.01	0.04	0.02	<0.01
Ir	<0.0001	<0.0001	<0.0001	<0.0001	<0.0001	<0.0001	<0.0001	<0.0001
As	<0.5	<0.01	<0.1	<0.1	<0.2	<0.2	<0.2	-
Br	6	1	1	2	6	34	3	3
W	<0.1	<0.01	<0.02	<0.02	<0.05	<0.4	<0.03	<0.03
Sc	0.025	0.021	0.06	0.03	0.05	<0.01	<0.003	0.01
Hf	0.02	0.008	0.021	0.01	<0.02	<0.005	<0.001	0.007
Th	0.009	0.026	0.03	0.03	<0.01	<0.01	<0.001	0.02

Table 4c

MT. HOOD WATER SAMPLES

									Old Maid Flat Well		
	Sample	MH-25	MH-28	MH-29	MH-30	MH-31	MH-32	MH-36	MH-33B	MH-35	MH-40
	Date	8/3/77	8/24/77	8/25/77	2/30/77	9/7/77	9/7/77	2/22/78	12/19/77	2/21/78	2/22/78
	pH	6.5	7	7.4	∿4.7	6.5	6.5	7.8	10	10	10
	Temp. °C	9.5	9	6	2	10	4	4	9	6	11
						mg/ℓ					
B		0.5	0.5	0.3	0.1	1	1	0.5	10	7	7
Na		5	1.3	3.8	2.7	2	0.6	4	130	136	132
Mg		3	<0.5	<2	2.5	<1	<0.5	2	<1	<1	<1
SiO_2		47	16	61	14	28	24	10	40	34	31
S								15	23	23	25
Cl		1	<1	<1	<0.1	1	1.7	2	135	124	123
K		<0.3	<0.2	2	1	0.9	<0.2	0.1	<1	<0.2	<0.2
Ca		11	2.7	8.6	17	3	1	43	72	11	11
						µg/ℓ					
Mn		35	8	2.5	119	2	<0.1	10	<40	<8	<7
Fe		155	64	30	1200	103	25	120	200	21	<10
Ba		<3	3.5	2	<10	<1	<1	2.3	7	<4	<2
Mo		<0.05	0.15	0.17	0.4	0.3	0.2	4	<0.7	35	37
Rb		2	0.7	4.2	<0.6	1.1	0.5	1.5	1.0	1.3	1.3
Cs		<0.02	0.02	0.03	<0.03	0.02	<0.01	0.4	0.06	0.07	0.15
Co		0.14	0.10	0.035	3.3	0.06	0.02		0.08	<0.03	
Sb		0.11	<0.01	0.01	0.06	0.06	0.03	1	0.07	0.05	<0.01
Cr		0.2	0.87	0.04	1.2	0.23	0.20	<0.2	0.5	<0.5	<0.4
Zn		1	3.5	5	2400	13	0.8	7	4	2	<0.4
Ag		<0.05	-	-	0.79	0.06	0.10	<0.2	<0.2	≤0.1	<0.07
Ce		0.095	0.048	<0.04	2.4	0.2	<0.04				
Sm		0.013	0.005	0.0036	0.37	0.016	0.0026	<0.03	0.03	<0.04	<0.04
Eu		-	<0.002	≤0.0014	0.08	0.006	<0.004	<0.003	-	<0.003	<0.004
U		<0.01	<0.005	0.027	0.063	0.01	<0.004	0.05	0.15	0.12	0.14
Ir		<0.0001	<0.0001	<0.0001	0.0004	<0.0001	<0.0001	<0.0002	≤0.0008	<0.0004	<0.0010
As								4	<2	<15	<10
Br		5	1.5	4.8	<1	2.5	1	9	115	300	280
W		≤0.1	<0.1	<0.1	0.8	0.15	<0.06	<0.5	<0.4	12	13
Sc		0.013	0.011	0.013	0.11	0.026	0.007	0.053	0.06	0.013	0.011
Hf		<0.003	<0.005	<0.008				<0.05		<0.02	<0.015
Th		<0.002	<0.004	<0.005	0.03	0.013	<0.001	<0.007	<0.03	<0.015	<0.009
Ta					0.02						
Yb					0.15						

their element abundances are lower than those of the Swim Warm Springs. Exceptions are the iron-manganese-rich spring, MH 2, emanating from glacial debris in the White River Valley, the Ca-Mg-rich water of the spring from basalt in the Robin Hood Quarry (MH 10), and Fe-Mn-rich water from the outflow of a small pond in the strongly altered fumarolic area of the summit crater. In both the Fe-Mn waters of the summit crater and White River Valley spring there were identifiable contents of iridium, though in lower abundance than in the winter sample from "East side of pool" at Swim. (Fe and Mn were both below detection limits in the sample from Swim). Water from a cold well in the Government Camp area (MH 3) is similar in character, except for its high Zn content, to cold "andesite" waters. However, a cold well near Brightwood (MH 22), most likely producing from the Rhododendron Formation, has water low in Fe and Mn and relatively high in Na and Mg, in contrast to a nearby cold spring (MH 21).

c. Old Maid Flat Geothermal Test Hole

Water samples were obtained from the artesian-flowing geothermal test hole in Old Maid Flat in December 1977 and February 1978. It is expected that the water was flowing from a depth of 450m; total depth at that time was 550m. Since that time the hole has been deepened to 1200m. The initial sample, taken only a few days followng cessation of drilling, contained unusually high contents of SiO_2, Mn, Fe, Ba, and other constituents, indicating that the sample was contaminated by drilling fluid. A sample taken 16 days later (MH 33b) contained considerably lower amounts of these constituents but somewhat greater amounts of SiO_2, Cl, Ca, Fe, and Ba than samples obtained two months later (MH 35 and MH 40). It is possible that water from the Old Maid Flat well was still slightly contaminated by drilling fluid.

d. Comparison of Water Chemistries

To facilitate comparison between the chemistries of the various water sources, major- and trace-element contents were plotted generally in order of increasing abundance in Figures 10, 11, 12, and 13. The patterns on these figures afford qualitative assessment of significant differences or similarities between water types. Mean values and standard deviations of element contents of cold waters emanating from springs in andesite and of waters from Swim Warm Springs are plotted on Figures 10 and 11. In Figure 10, which compares major elements, there is a "high" in sulfur and sodium in the warm spring water, in contrast to the cold "andesite" water where SiO_2 is relatively prominent. In the comparison of mean values of trace-element contents in both water types (Figure 11), uranium is prominent with respect to its neighbors, Sm and Cs at Swim Warm Springs. Barium stands out among the trace elements in the cold-spring waters.

Plots of major-element contents in waters from the geothermal test well in Old Maid Flat (MH 40) and the cold spring in Robin Hood Quarry (MH 10) comprise Figure 12. Similar diagrams of trace-element contents in these two sources are shown in Figure 13. The major-element pattern of the Old Maid Flat well water has a Na-S "high," similar to but considerably more accentuated than, that of the Swim Warm Spring waters (Figure 10). The trace-element pattern of Old Maid Flat well water has a sharp "high" of Mo with respect to its neighbors on the plot, Cs and Rb; Br is also accentuated. The major element pattern of cold water emanating from basalt in Robin Hood Quarry accentuates S and Ca, in contrast to the cold "andesite" waters where SiO_2 predominates. The trace element pattern of the Robin Hood Quarry water has prominences of Mo and Ba; Ba is also relatively prominent in the cold "andesite" water. Barium and calcium contents are relatively high in a sample of basalt from Robin Hood Quarry (MHR-2, Table 2), and a sample of felsic dike rock from the quarry (MHR-1) also has a relatively high Ba content.

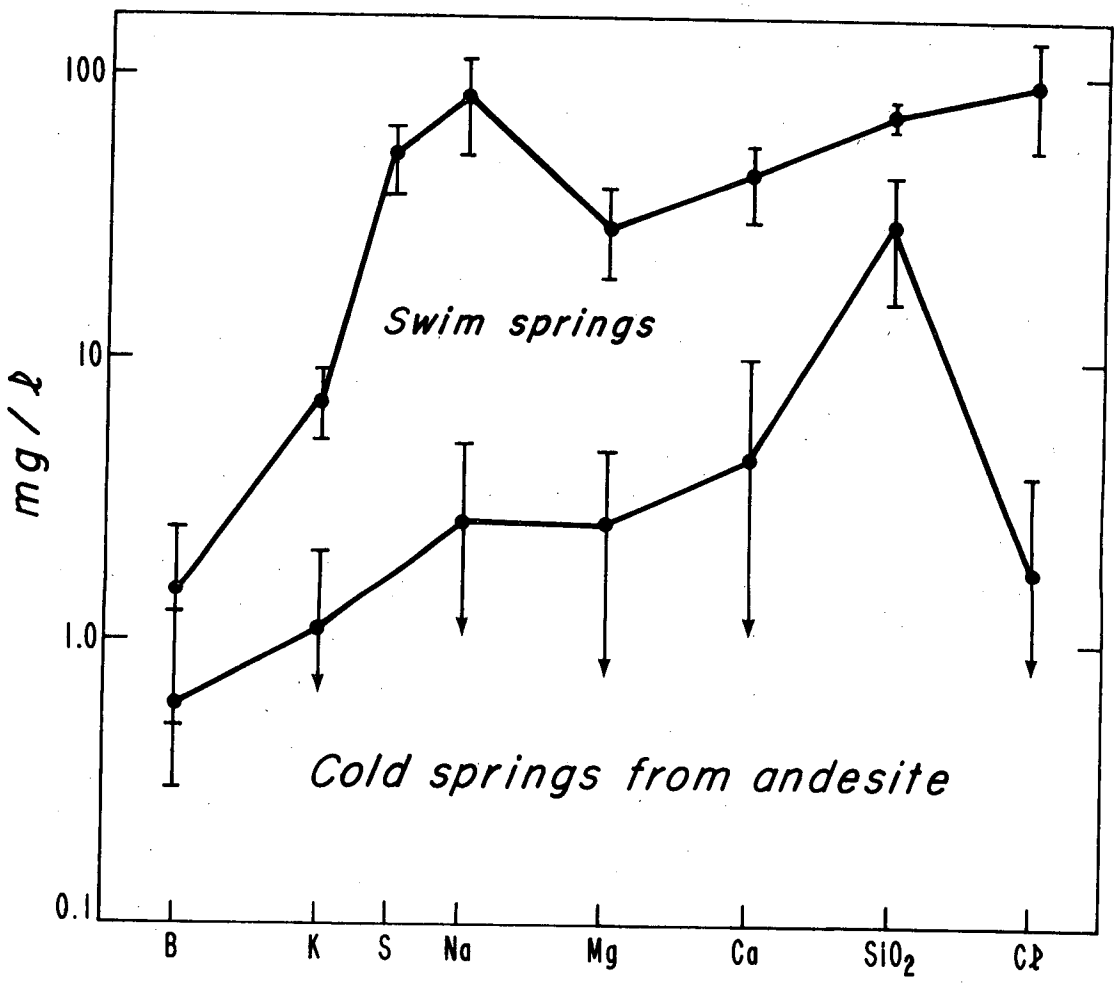

XBL 7811-2176

Figure 10. Major element contents of Swim Warm Springs and cold water from andesite.

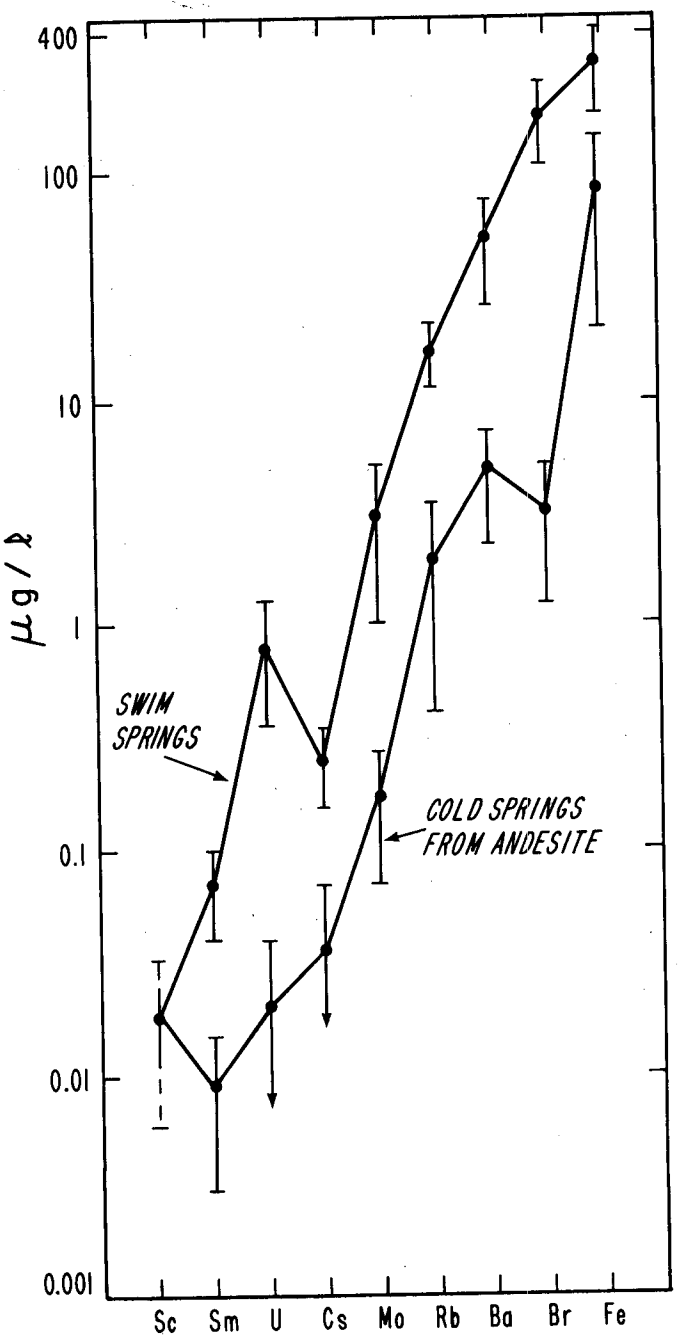

XBL 7811-2179

Figure 11. Trace-element contents of Swim Warm Springs and cold water from andesite.

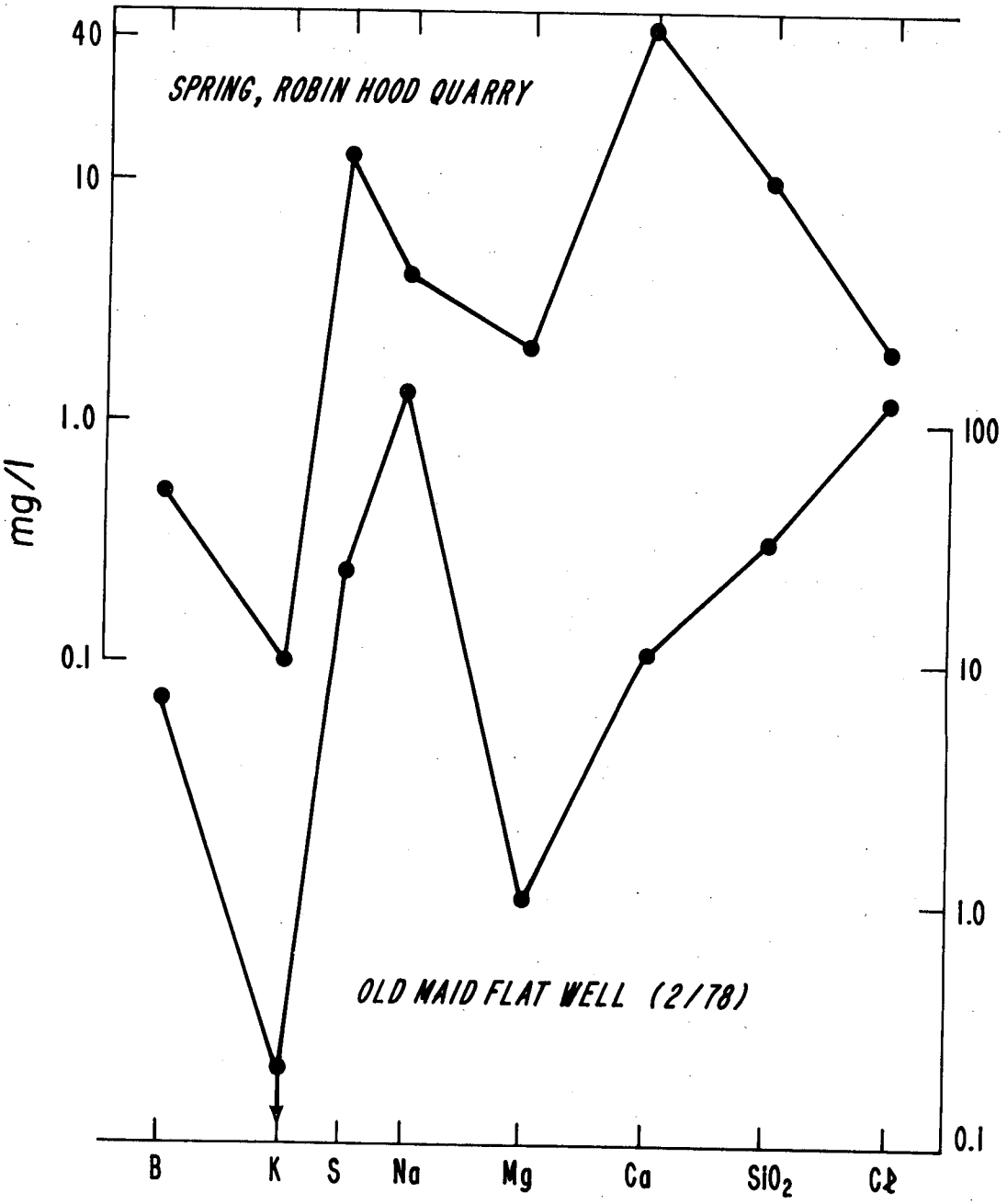

XBL 7811-2178

Figure 12. Major-element contents of the spring in Robin Hood Quarry and of water from the geothermal test well in Old Maid Flat.

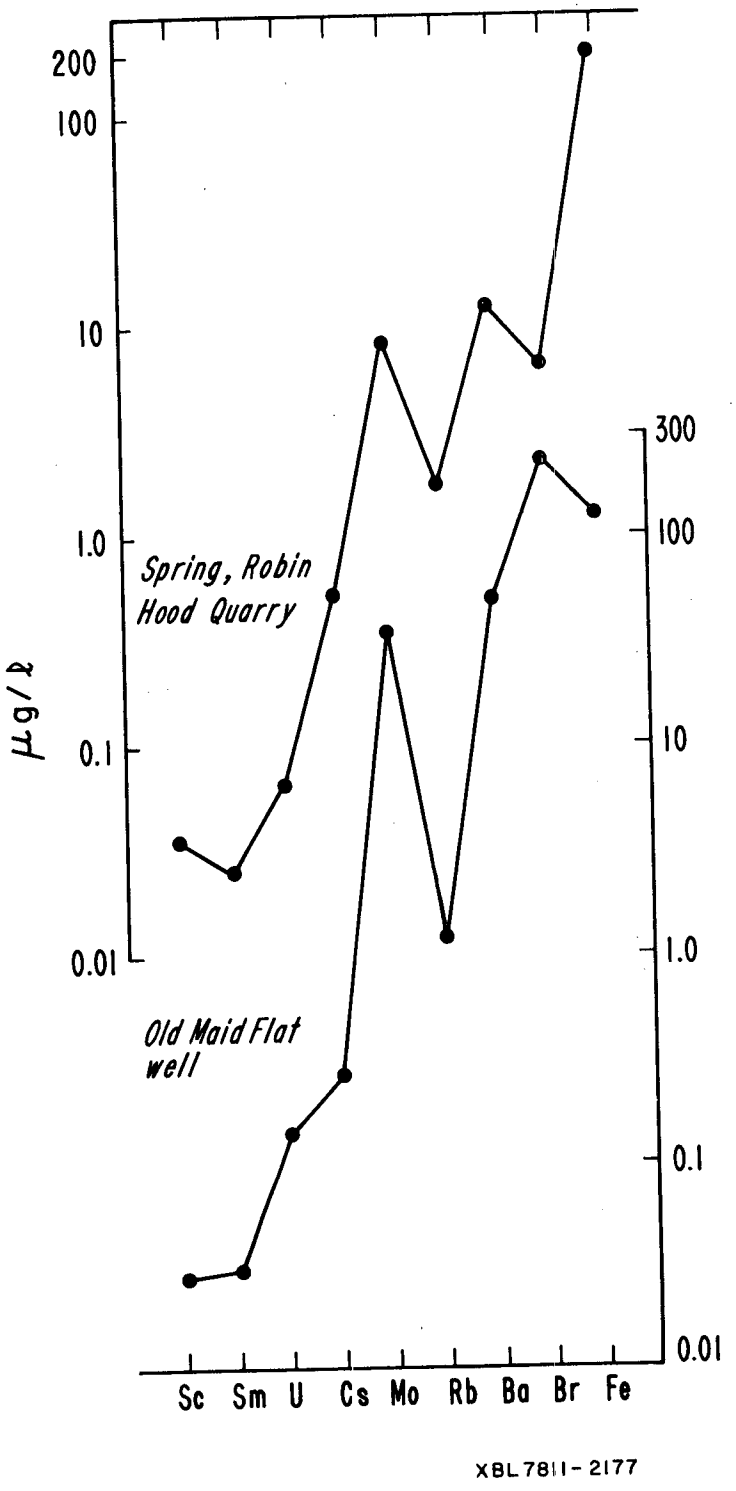

Figure 13. Trace-element content of the spring in Robin Hood Quarry and of water from the geothermal test well in Old Maid Flat.

e. Estimates of Subsurface Temperature

Major-element analyses were used to calculate the water temperature at depth within the Swim Warm Springs system. The calculations were based on chemical geothermometers afforded by the SiO_2 content of water and the ratio of Na to K, corrected for Ca (Fournier and Truesdell, 1973). The temperature of water at depth was also estimated by the ratio of oxygen isotopes in sulfate in the water (McKenzie and Truesdell, 1976), measured by N. Nehring and A. H. Truesdell at the U.S. Geological Survey, Menlo Park, California.

The temperature of hot water, unmixed with nearer-surface cold water, and the proportion of mixed cold water in Swim Warm Springs, were estimated by applying the mixing model of Fournier and Truesdell (1974). In this model simultaneous equations are employed, incorporating as factors the temperature of warm spring water, the SiO_2 content of the warm spring water, the temperature of the near-surface cold water, and the silica content of cold spring water.

The estimates of subsurface water temperature at Swim Warm Springs are summarized in Table 5. The temperatures estimated by the Na-K-Ca geothermometer and by the mixing model may be less reliable than those estimated by the silica and oxygen-isotope geothermometers, because surface flow at Swim is low. The Na-K-Ca and mixing-model temperatures should not be discounted, however, because the mixing model indicates the large proportion of near-surface cold water intuitively expected at Swim. Therefore, the agreement between the silica and oxygen-isotope temperatures indicate that the temperature at depth is, at least, within the range of 100-125°C, the temperature may be 150° to over 200°C.

The samples from the Old Maid Flat hole may contain some vestiges of drilling fluid. However, if we assume equilibrium conditions then the

Table 5

Summary of Estimated Subsurface Temperature
at Swim Warm Springs

Geothermometers	
SiO_2	100-125°C
Na-K-Ca (β = 1/3)	152-154°C
$\delta 18_O - SO_4$	108-110°C
Silica Mixing Model[a]	
Temperature of unmixed hot water	192-240°C[b]
Fraction of cold water	0.92

a) Fournier and Truesdell, 1974.
b) Questionable because it is a low-flowing system.

silica and alkali-element ratio geothermometers give consistent temperatures of 80-90°C. The temperature measured at 450m was 33°C; a measurement of bottom-hole temperature, following completion of the hole, was 81°C.

f. Oxygen and Hydrogen Isotope Ratios

A plot of isotope ratios of hydrogen and oxygen in cold and warm spring waters comprises Figure 14. The ratios are expressed in delta values, given in mils (°/oo), and defined as:

$$\delta \text{ in } {}^{o}/oo = \frac{R_{(sample)} \quad R_{(standard)}}{R(standard)} \times 1000 \qquad \text{(Hoefs, 1973),}$$

where R represents the isotope ratios of deuterium to hydrogen and $18_O/16_O$; the standard is "mean ocean water" (Craig, 1961). The points for warm and cold springs fall close to the line for meteoric waters, indicating that the warm waters are much diluted by near-surface runoff. The warm water points would be shifted to the right of the meteoric water line if a substantial component of the spring water had been in contact with rock at depth. However, the grouping of the warm water points at more negative values indicates that the source of the warm spring water is generally higher on the mountain than the sources of most of the cold springs sampled. Exceptions are the cold springs at Mt. Hood Meadows (MH 4) and a spring in Robin Hood Quarry (MH 10), which fall in the same range as the warm waters. The grouping of the points indicates that the cold waters have shorter pathways between their sources and the springs, while a component of the warm water may circulate deeply enough in the mountain to come in proximity to a hot central conduit system.

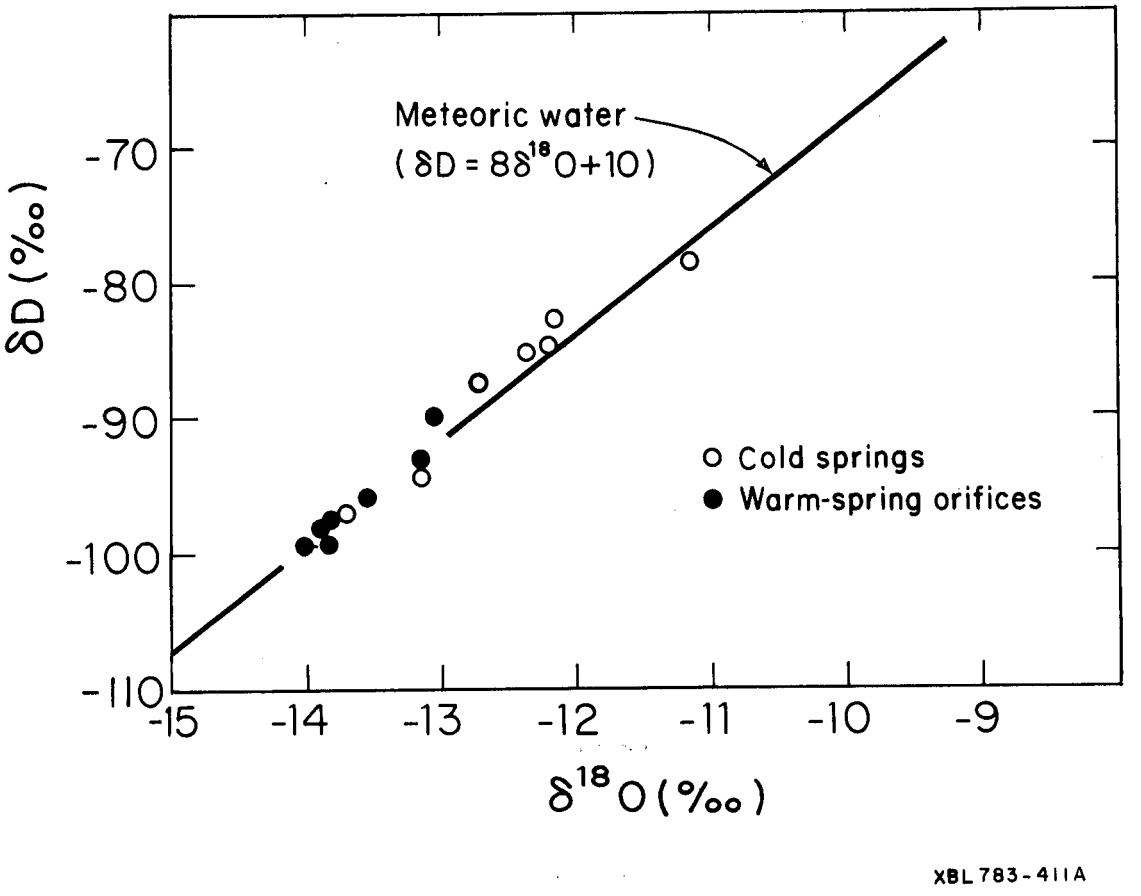

Figure 14. Isotope ratios of hydrogen and oxygen in cold and warm-spring water of Mt. Hood.

B. Rock Analyses

A limited number of samples of the igneous rock types in the Mt. Hood region were collected and analyzed. A more detailed investigation of the petrology, mineralogy, and geochemistry of Mt. Hood's extrusive rocks is presently being conducted by Craig White of the University of Oregon.

Results of major and trace-element analyses of 13 rock samples, together with brief sample descriptions, are listed in Table 6. Seven of the samples are andesite, two (MHR 3 and 11) are of appreciably altered rock. The major-element contents of the samples of relatively unaltered andesite are fairly uniform, with silica contents in the range 58-63%, Al_2O_3 17.4-17.7%, CaO 5.4-6.4%, Na_2O 3.7-4.3%, and K_2O 1.0-1.5%. There do not appear to be significant differences between chemistries of samples of Pliocene andesite from the west and east flanks of Mt. Hood (MHR 10 and 13), and the andesite of the more recent flows on the south flank of the mountain (MHR 5 and 6). This is supported by the small standard-deviations of mean values of rare-earth-element (REE) ratios (REE contents in sample/REE contents in standard chrondrite) of the unaltered andesite (Figure 15). The relatively higher Fe and Mg contents of the andesite from Cloud Cap (MHR 12) are in keeping with the presence of olivine in that rock, in comparison with other andesite samples where hornblende is the principal mafic mineral. The altered brecciated andesite sample (MHR 3) from the south flank of Mt. Hood is somewhat lower in MgO, but higher in K_2O than the fresher samples, while the strongly altered andesite (MHR 11) from the west flank of the mountain has considerably greater MgO and much less K_2O than a sample of nearby, relatively unaltered andesite (MHR 10). Both fresh and altered andesite samples from the MHR 10 and 11 localities have identifiable iridium contents, in contrast to other rock samples where the abundance of that element was well below detectability limits. It is surprising to find Ir in andesitic rocks; it is more normally associated with ultramafic rocks: peridotite, pyroxenite, and serpentinite.

Table 6a

MT. HOOD ROCK SAMPLES

Major Elements
(% by weight)

SAMPLE	1	2	3	4	5	6	7	8	9	10	11	12	13
Na_2O[(a)]	4.0	2.2	3.2	3.8	4.1	4.3	5.2	3.8	2.7	4.1	2.6	4.0	3.7
MgO[(a)]	0.3	4.0	1.6	1.2	3.1	2.9	3.7	3.3	2.4	1.7	6.5	3.1	2.8
Al_2O_3[(a)]	13.6	13.1	16.4	15.3	17.7	17.5	17.7	17.8	16.7	17.4	17.3	17.4	17.7
SiO_2[(a)]	71.7	50.3	59.3	64.9	60.4	61.5	58.1	58.0	62.3	62.8	54.8	58.3	59.8
K_2O[(a)]	3.7	1.2	2.4	3.0	1.5	1.3	1.2	0.9	1.3	1.3	0.3	1.0	1.3
CaO[(a)]	1.4	7.1	4.3	0.7	5.8	5.7	5.5	7.1	4.3	5.4	1.6	6.3	5.6
TiO_2	1.4	7.1	0.8	0.7	0.8	0.7	0.8	0.7	0.6	0.5	1.0	0.9	0.8
MnO	0.04	0.23	0.12	0.05	0.10	0.09	0.07	0.10	0.04	0.04	0.03	0.13	0.07
FeO	1.8	13.2	4.6	3.3	5.7	5.7	3.9	5.4	3.7	4.2	5.1	6.3	5.2
Cr_2O_3	0.00	0.04	0.02	0.01	0.03	0.03	0.02	0.02					
TOTAL	96.7	94.0	92.7	93.0	99.2	99.7	96.2	97.1	94.0	97.4	89.2	97.4	97.0

(a) Analyses by x-ray fluorescence.

Table 6b

MT. HOOD ROCK SAMPLES

Trace Elements
(ppm)

SAMPLE	1	2	3	4	5	6	7	8	9	10	11	12	13
Rb	120	190	40	65	20	20	30	20	40	18	<4	8	32
Cs	2	5	1	<1	<1	<1	<1	<1	2	5	0.5	<0.3	0.4
Ba	600	640	300	460	350	300	250	200	240	300	120	350	300
Hf	5.4	5.0	7.1	6.2	4.2	4.1	3.6	3.7	3.3	4.0	3.7	4.5	4.1
Cr	2	40	7	4	40	55	10	70	50	30	65	46	41
Co	3	37	7.6	5.8	19	19	16	21	13	12.8	21	21	19
Ni	<10	<30	<20	<10	30	30	<10	40	40	23	33	34	25
Sc	2.3	37.7	10.5	9.6	13.9	13.3	19.4	17.2	12.8	9.0	18	15	15
Th	15	4.5	6.6	6.2	3.7	2.4	2.4	2.4	2.3	3.0	2.2	2.1	3.6
Ta	1.3	0.84	1.1	1.0	0.57	0.54	0.54	0.51	0.54	0.65	0.51	0.62	0.59
La	25	23	25	24	19	15	10	18	13	16	13	17.5	16.2
Ce	56	52	58	53	45	33	29	44	27	36	29	40	35
Nd	15	27	26	26	15	17	15	20	14	16	16	20	18
Sm	2.6	6.3	4.8	5.2	3.6	3.2	2.8	3.9	3.0	3.1	4.0	4.3	3.4
Eu	0.66	2.2	1.5	1.3	1.4	1.3	0.83	1.3	1.1	1.1	1.0	1.4	1.1
Tb	0.41	1.0	0.71	0.76	0.49	0.46	0.52	0.47	0.45	0.45	0.60	0.55	0.47
Dy	2.5	7.9	4.9	4.9	3.2	2.9	3.7	3.3	3.3	2.5	4.4	3.8	3.0
Yb	1.7	3.7	2.7	2.6	1.6	1.5	2.1	1.8	1.6	0.95	2.1	1.9	1.4
Lu	0.22	0.54	0.35	0.32	0.19	0.18	0.24	0.27	0.21	0.14	0.27	0.25	0.19
U*	4.5	1.3	1.4	1.9	1.2	0.9	1.8	0.6	0.7	0.95**	0.76	0.61	1.05
Ir	≤0.02	≤0.003	<0.0010	<0.0010									

* By γ spectrometry
** By neutron activation

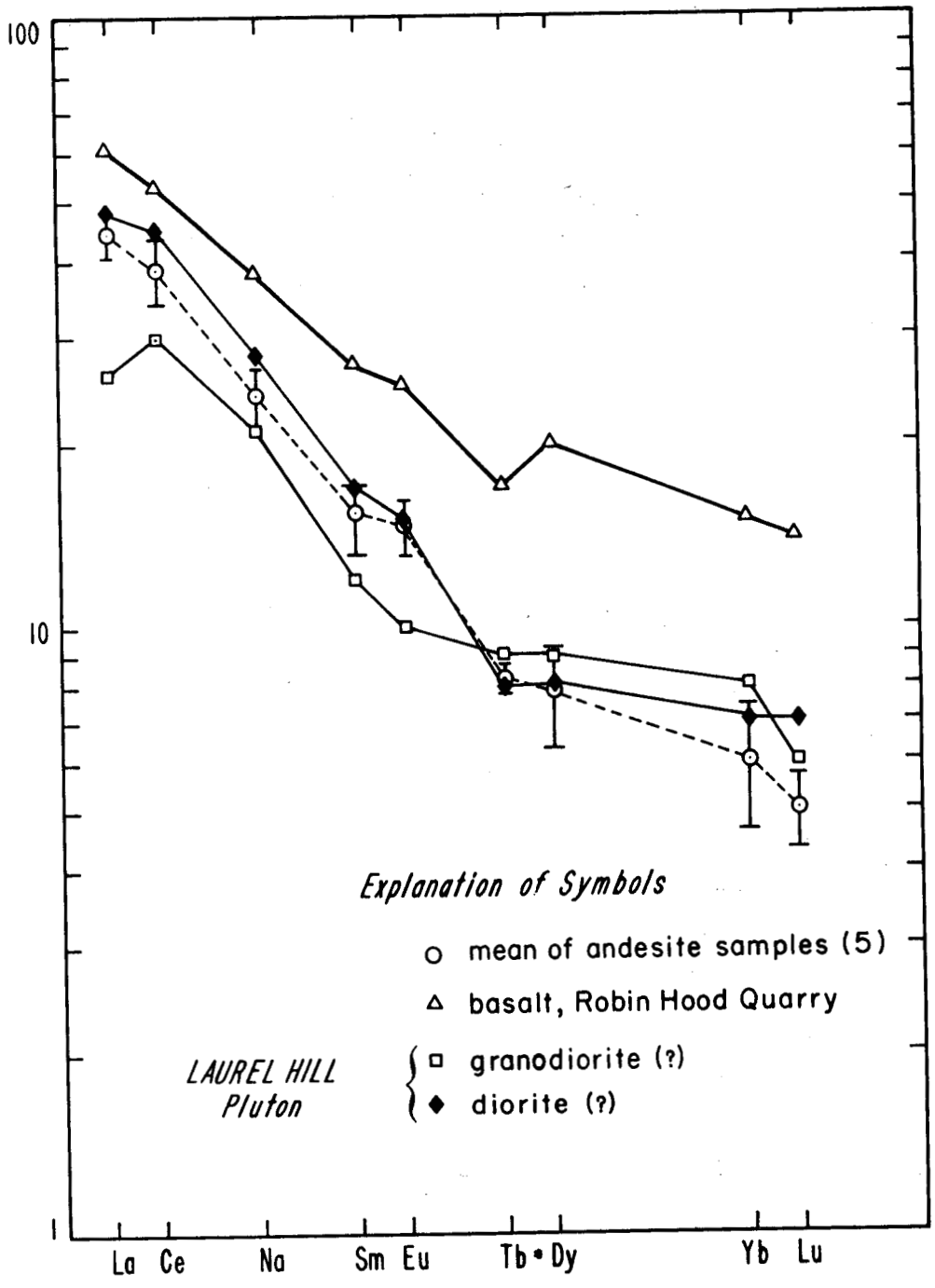

Figure 15. Rare-earth element ratios (sample/chrondrite) of rock samples from Mt. Hood.

The relatively high barium contents of the samples of felsic dike rock and basalt (MHR 1 and 2, respectively) from the Robin Hood Quarry, are reflected in the water sample from that locality (MH 10, Table 4a). The basalt has higher rare-earth-element ratios than those of the andesite or of the intrusive rocks. Comparison of major- and trace-element contents of the Robin Hood Quarry basalt with contents of Columbia River Basalt flows (Asaro and others, 1978) indicates strong similarities. An example is shown in Table 7, where sample MHR 2 is compared with basalt of the Roza flow of central Washington.

Major- and trace-element contents of the two samples of relatively unaltered intrusive rocks, diorite-granodiorite, from the Laurel Hill pluton (MHR 7 and 8), are similar to contents of the unaltered andesite samples. This is illustrated by the similarity between REE patterns of the andesite and intrusive rocks (Figure 15). A sample of altered intrusive rock from locality MHR 9 in the Laurel Hill pluton has markedly lower Na_2O, MgO and CaO, but higher SiO_2 than the unaltered samples. The similarity between the chemistries of the intrusive rocks and the andesites suggests that the intrusives may represent the roots of the Pliocene extrusive centers on the western flank of Mt. Hood. However, our sampling of andesites to date has not been extensive enough to support or deny the conclusions of Wise (1969) regarding the origin and character of the andesites of Mt. Hood.

C. Gas Analyses

Results of analyses of gases collected from two sites on Mt. Hood, Steel Cliffs and Crater Rock in the Summit Crater area, are listed in Table 8. These may be compared with analyses by Ayres and Creswell (1951) of gas samples collected in 1935 and 1951 from fumaroles near the Steel Cliffs. The bar graphs, Figure 16, permit this comparison and show that carbon dioxide predominates (88-97%) in the group of gases other than water vapor, with H_2S comprising 1 to 11% of this group. The Ayres and Creswell sample

Table 7

Major- and Trace-Element Contents of the
Robin Hood Quarry and Roza Flow basalts

	Robin Hood Quarry	Roza flow
	(%)	
SiO_2	50.3	50.3
Al_2O_3	13.1	13.6
FeO	12.9	14.3
MgO	4.0	4.4
CaO	7.1	8.2[5]
Na_2O	2.2	2.7
K_2O	1.2	1.2
TiO_2	2.5	2.6
	(ppm)	
Sc	37.7	39.0
Eu	2.2	2.67
Co	36.6	41.0
Ba	641	498
Cr	40.3	40.5

Table 8

Fumarolic Gas Analyses*

	Steel Cliffs	Crater Rock
Temperature	88-91°C	90°C
moles CO_2	0.1830	0.3056
moles H_2S	3.8368×10^{-3}	2.9228×10^{-3}
moles NH_3	1.8862×10^{-3}	1.72×10^{-3}
moles H_2O	1.1215	0
Gases other than H_2O (mole %)		
CO_2	96.85	98.43
H_2S	2.03	0.94
He	1.8×10^{-4}	4.3×10^{-3}
H_2	0.11	0.32
Ar	4.6×10^{-3}	2.0×10^{-3}
O_2	0	2.2×10^{-3}
N_2	0.87	0.25
CH_4**	1.0×10^{-3}	1.5×10^{-3}
NH_3	1.00	0.55

* Collected July 1977; analyzed by N. Nehring and A.H. Truesdell, U.S. Geological Survey, Menlo Park, California.

** Besides methane, chromatograms indicate the presence of ethene, ethane, propene, propane, 2-methyl-propane, 1-butene, n-butane, and n-pentane.

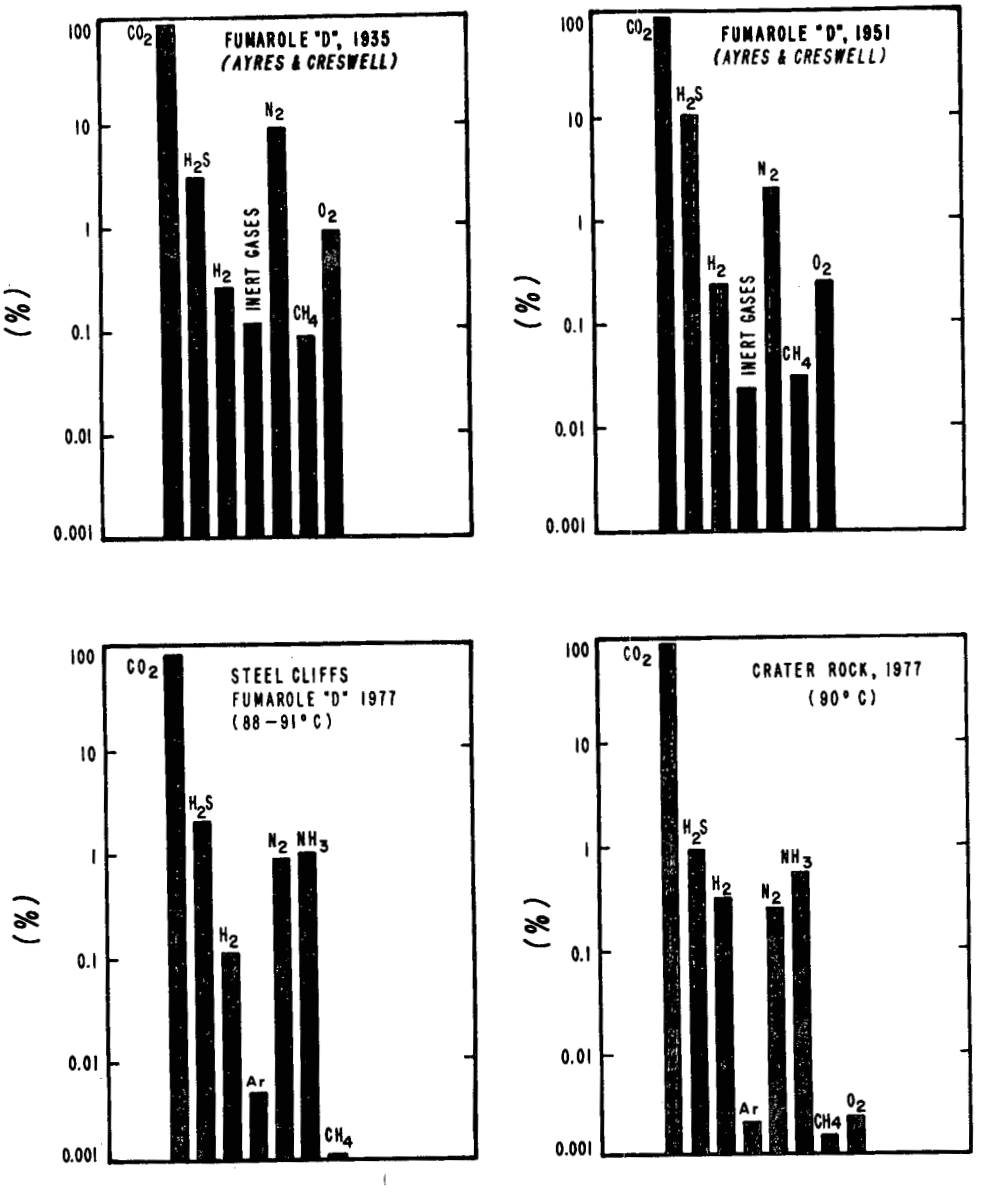

XBL 7811-2175

Figure 16. Bar graphs, showing abundances of constituents (other than water vapor) of fumarolic gases, Mt. Hood.

of 1951 differs from the 1935 sample in its relative contents of CO_2, H_2S, and other constituents. The difference between the 1951 sample and our 1977 sample is of the same order. The 1977 Steel Cliffs and Crater Rock samples have similar bar-graph patterns, with their H_2S contents substantially higher than H_2, N_2, and NH_3, which are in turn at least two orders of magnitude higher than argon.

A second set of gas samples was collected from fumaroles in the Summit Crater area in October 1978. It is expected that sufficient water vapor was collected at that time to permit analyses of stable isotope contents, providing comparison with isotope ratios in spring-water samples.

IV. ORIGIN OF WARM WATER AT SWIM SPRINGS

It is appropriate here to speculate briefly on the source of the warm water and the pathway it takes to reach Swim Springs. The most likely explanation for the occurrence of warm water at Swim is that the water has been heated higher on the mountain, has migrated downslope, mixing with cold water, and comes to the surface at Swim. Snow- and glacier-melt water near the summit may come in close proximity to the hot central neck of the mountain, manifested by the steam zone of the summit-crater fumaroles. Some of this heated water probably percolates downslope in the andesitic mud-and ash-flows, mixing with cold water along its path (Figure 17).

The oxygen-hydrogen isotope data (Figure 12) provide evidence for the high-elevation origin of the Swim water. Meteoric water deposited at higher elevations has a larger component of lighter isotopes than does water at lower elevations. This indicates that a significant proportion of the warm water originated at higher elevations than the cold spring water.

Field measurements and analyses of cold springs also suggest that there is a small thermal component in some of the cold-spring water on the south flank of Mt. Hood. Surface and spring waters in the Mt. Hood region

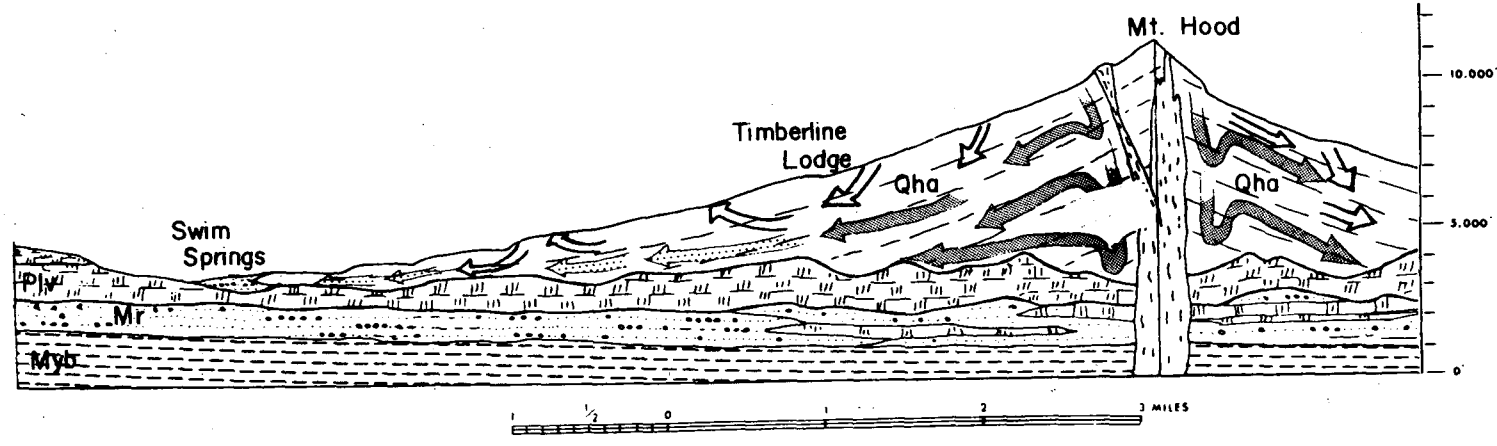

XBL 792-8469

Figure 17. North-south geologic cross section of Mt. Hood (after Wise, 1968) showing, schematically, the hypothesized circulation paths of hot water (dark arrows) heated near the volcano's central neck, mixed warm water (lighter arrows), and cold water (un-shaded arrows). The warm water emanating at Swim Springs is strongly mixed, and cold water in springs on the south flank of the mountain may contain a small component of the deeper-flowing hot water. Myb = Yakima Basalt; Mr = Rhododendron Formation; Plv = Lower Pliocene basalt and andesite; Qha = Mt. Hood andesite flows.

generally contain a few ppm of total dissolved solids, 1 to 3 ppm chloride, and have specific conductances of 30 to 70 μmohs/cm. In contrast, as is illusrated in Figure 9, several of the cold springs on the south flank, below the 6000 ft elevation, have chloride contents and/or specific conductances well in excess of these values. For comparison, undiluted geothermal waters may contain several hundred to several thousand ppm chloride and have specific conductances in the range from several hundred to several thousand μmohs/cm; at Swim, the values are ∿900 ppm total dissolved solids, ∿150 ppm chloride, and 1300 μmohs/cm specific conductance.

Another possible explanation for the presence of warm water at Swim Springs is deep circulation along a fault zone. An east-west oriented fault zone in the vicinity of Swim has been suggested from analyses of earthquake epicentral data (R. Couch, personal communication, 1977). However, to date, other geological and geophysical investigations have not confirmed the fault zone. If a fault zone were present and it contained permeable zones, these could serve as conduits for deep circulation of meteoric water. It is more likely that if a fault zone is present, it would serve as an impermeable barrier to warm water moving down-slope, causing some impoundment and the emanation at Swim Springs. That the highest temperature orifice at Swim is lowest in elevation (Figure 5) could be attributed to nearly vertical circulation associated with a fault zone. More plausible, however, is the explanation that the water emanating at the lower orifice is warm water moving down-slope from a deeper horizon in the andesite, and therefore less mixed with cold water than the water in the higher orifices. Neither the fault-zone nor the down-slope moving warm water mechanisms for Swim Springs are mutually exclusive; both could be operating.

V. CONCLUSIONS

Though this is not a final report, sufficient data have been obtained to provide some preliminary conclusions on the geochemical setting of Mt. Hood. Firmer conclusions on the usefulness of the geochemistry in evaluating the geothermal resource potential await results of analyses presently underway.

1. The warm water at Swim Springs on the south flank of Mt. Hood has a large component (~90%) of nearer-surface cold water. The flux of cold-water runoff nearly masks the surface indications of deeper-circulating hot water. The upper-slope orifices at Swim are the most diluted, those downslope are successively less diluted. The oxygen-hydrogen isotope data indicate that cold-spring waters have short pathways between their sources and the springs, while a component of the warm-spring water has its origin considerably higher on the mountain.

2. Chemical geothermometers and mixing-model calculations indicate that temperatures at depth in the Swim Springs system are within the range 104-170°C. The silica mixing model gives a range of 192-240°C for unmixed hot water.

3. The chloride contents and specific conductances of the water sources indicate that most of the cold spring waters are derived almost directly from snow melt. Relatively high chloride contents and specific conductances in some springs on the south flank of Mt. Hood indicate that these waters may circulate deeper or may mix with geothermal waters.

4. Water in the geothermal test hole in Old Maid Flat, in a sample most likely from the Rhododendron Formation, has a different chemical character from the water at Swim. Geothermometry is consistent with a temperature gradient of 60°C/km as measured in the Old Maid Flat well.

5. The Platinum-group element, iridium, is present in identifiable abundances at one orifice at Swim Warm Springs, a cold spring, and in the small lake in the summit crater area. Iridium also occurs in altered andesite at one location on the western flank of Mt. Hood. The association of Ir with an andesitic volcano is surprising; it is generally considered to be associated with basic to ultrabasic igneous rocks.

6. The similarity between major- and trace-element contents of Pliocene andesite on the west flank of the mountain and intermediate intrusive rocks of the Laurel Hill pluton in that area supports Wise's (1969) contention that the pluton represents the root zone of a center of extrusion of the andesite.

7. The basalt exposed in the Robin Hood Quarry in the Hood River Valley has major- and trace-element contents very similar to those of the Roza flow of central Washington. This supports the idea that the basalt on the east side of the valley is Columbia River Basalt, on the upward-thrown side of a north-south trending normal fault.

VI. CONTINUING ACTIVITIES

Activities underway include analyses of gas samples collected in October 1978 in the summit fumarolic area. In the sampling of 1977 we were not able to collect sufficient water vapor to permit determination of isotope ratios. The volume of water vapor collected in 1978 is sufficient for these analyses. This will afford comparison with the isotope ratios of cold- and warm-spring water reported here.

Water analyses still to be completed at the time of publication include a sample collected in October 1978 from the geothermal test hole drilled near Timberline Lodge and a set of samples collected at that time from the three orifices sampled periodically at Swim Springs. Deepening of the geothermal test hole in Old Maid Flat in the summer of 1978 may permit us to obtain a fluid sample from a deeper aquifer (most likely within the Columbia River Basalt) than the Rhododendron Formation sampled in 1977.

Samples of altered and unaltered andesite from the fumarolic area in the summit crater were collected in October 1978. These are being analyzed for major and trace elements and will indicate if iridium and silver are present in the strongly altered ground, coinciding with the presence of these elements in the runoff water from the small lake.

It is recommended that one or more geothermal test holes be drilled in the Swim Warm Springs area. These holes should be deep enough to obtain temperature measurements and fluid samples from below the zone of near-surface and shallow cold-water runoff, to permit major-, trace-element, and isotope analyses of relatively unmixed hot water. The holes should be located on the up hill gradient from the Swim system to test whether the water emanating from Swim is leakage from volcanic units higher on Mt. Hood, or whether it is from deeper circulation within a fault zone.

BIBLIOGRAPHY

Allen, J.E., 1966. The Cascade Range volcano-tectonic depression in Oregon, in Transactions of the Lunar Geologic Field Conference, Bend, Oregon, August 1965: Oregon Department Geology and Mineral Industries, 21-23, 2 figures.

Asaro, F., H.V. Michel and C.W. Myers, 1978. A statistical evaluation of some Columbia River Basalt chemical analyses, Rockwell International Report RHO-BWI-ST-3, 62 pp.

Ayers, F.D. and A.E. Creswell, 1951. The Mount Hood fumaroles, Mazama, 33(13), 33-39.

Bowman, H.R., A.J. Hebert, H.A. Wollenberg and F. Asaro, 1976. Trace, minor and major elements in geothermal waters and associated rock formations (north-central Nevada). Proc. 2nd U.N. Symposium Develop. Use Geothermal Res., San Francisco, 20-29 May 1975, 699-702.

Callaghan, E., 1933. Some features of the volcanic sequence in the Cascade Range in Oregon: Am. Geophys. Union Trans., 14th Annual Meeting, 243-249.

Craig, H., 1961. Standard for reporting concentrations of deuterium and oxygen-18 in natural waters: Science, 133, 1833.

Crandell, D.R. and M. Rubin, 1977. Late glacial and post-glacial eruptions at Mt. Hood, Oregon: Geol. Soc. Am. Abs. with Programs, 9(4), 406.

Folsom, M.M., 1970. Volcanic eruptions: The pioneer's attitudes on the Pacific Coast from 1800 to 1875: Ore Bin, 32(4), 61-71.

Fournier, R.O. and A.H. Truesdell, 1974. Geochemical indicators of subsurface temperature, Part II: Estimation of temperature and fraction of hot water mixed with cold water: U.S. Geol. Survey Journal. Res., 2(3), 263-270.

Fournier, R.O. and A.H. Truesdell, 1973. An empirical Na-K-Ca geothermometer for natural waters: Geoch. et Cosmoch. Acta, 37, 1255-1275.

Goldstein, N.E. and E. Mozley, 1978. A telluric-magnetotelluric survey at Mt. Hood, Oregon: A preliminary study. LBL-7050, 89 pp.

Hebert, A.J. and H.R. Bowman, 1976. Nondispersive soft X-ray fluorescence analyses of rocks and waters. Proc. 2nd U.N. Symposium Develop. Use Geothermal Res., San Francisco, 20-29 May 1975, 751-755.

Hebert, A.J. and K. Street, Jr., 1974. A nondispersive soft X-ray fluorescence spectrometer for quantitative analysis of the major elements in rocks and minerals. Anal. Chem., 46, 203.

Hoefs, J., 1973. Stable isotope geochemistry. Berlin: Springer Verlag.

McKenzie, W.F. and A.H. Truesdell, 1976. Geothermal reservoir temperatures estimated from the oxygen isotope compositions of dissolved sulfate and water from hot springs and shallow drill holes: Geothermics, 5(1-4), 51-61.

Perlman, I. and F. Asaro, 1969. Pottery analysis by neutron activation, Archaeometry, 11, 21-52.

Thayer, T.P., 1937. Petrology of the later tertiary and quaternary rocks of the north-central Cascade Mountains in Oregon, with notes on similar rocks in western Nevada. Geol. Soc. Am. Bull., 48, 1611-1652.

Truesdell, A.H. and R.O. Fournier, 1976. Calculation of deep temperatures in geothermal systems from the chemistry of boiling spring waters of mixed origin. Proc. 2nd U.N. Symposium Develop. Use Geothermal Res., San Francisco, 20-29 May 1975, 837-844.

Truesdell, A.H. and N.L. Nehring, 1978. Gases and water isotopes in a geochemical section across the Larderello, Italy, geothermal field. Pageoph., 117, 1-14.

Wise, W.S., 1968. Geology of the Mt. Hood volcano. Andesite Conference Guidebook, International Upper Mantle Project, Sci. Report. 16-S; also Oregon Dept. Geol. Mineral Ind. Bull., 62, 81-98.

Wise, W.S., 1969. Geology and petrology of the Mt. Hood area: A study of the High Cascade volcanism. Geol. Soc. Am. Bull., 80, 969-1006.

Wollenberg, H.A., 1975. Sampling hot springs for radioactive and trace elements: Proc. EPA Workshop on Sampling Geothermal Effluents, Las Vegas, Nevada, 20-21 October 1975, p. 24, and Lawrence Berkeley Laboratory Report, LBL-4422.

☆U.S. GOVERNMENT PRINTING OFFICE:1980 -640 -258/ 1781

GEOLOGIC MAP — BULL RUN WATERSHED AREA

R.5E. R.6E. R.7E. R.8E.

T.1N.

T.1S.

Geology by: B.F. VOGT

EXPLANATION

Qal

ALLUVIUM

Stratified silt, sand and gravel; undifferentiated. Mainly channel and bar gravel.

Qls

LANDSLIDE DEPOSITS

Random blocks of various formations in a matrix of finer material; some slump blocks retain stratigraphic relations of units involved.

Qtv

VOLCANIC ROCKS OF THE HIGH CASCADE RANGE AND BORING LAVA

Basaltic andesite, olivine basalt, and pyroxene andesite; mostly intercanyon flows.

Ts

SARDINE FORMATION

Pyroxene andesite, tuff, tuff breccia, lapilli tuff, and mudflows.

COLUMBIA RIVER BASALT GROUP
YAKIMA BASALT SUBGROUP
WANAPUM BASALT

Twpr

PRIEST RAPIDS MEMBER

Medium gray to dark gray medium to fine grained basalt containing rare plagioclase pheoncrysts; thin blocky to columnar joints in colonnade; thick hackly entablature; pillow palagonite breccia common at base.

Twfs

FRENCHMAN SPRINGS MEMBER

Medium gray to dark gray medium to fine grained basalt containing rare to abundant plagioclase phenocrysts; generally blocky to columnar jointed with platy jointing locally; often weathers to a characteristic pale red-brown.

GRANDE RONDE BASALT

Tgn2h

HIGH MgO GEOCHEMICAL TYPE

Dark gray fine-grained basalt, often diktytaxitic; jointing is irregular with poorly -formed narrow blocky columns predominating; vesicle sheets are common.

Tgn2l

LOW MgO GEOCHEMICAL TYPE

Dark gray very fine grained basalt with prominent thick hackly entablatures and thin blocky basal colonnades.

— — N_2/R_2 PALEOMAGNETIC HORIZON — —

Tpv

PRINEVILLE GEOCHEMICAL TYPE

Dark gray fine grained to very fine grained basalt; dominated by broad irregular columns or blocky jointing, with some platy jointing locally; weathers to a pale red-brown; anomalously large acicular apatite crystals.

Tgr2

LOW MgO GEOCHEMICAL TYPE

Dark gray very fine grained basalt physically resembling other low MgO flows.

— — N_1/R_2 PALEOMAGNETIC HORIZON — —

Tgn1

LOW MgO GEOCHEMICAL TYPE

Dark gray fine grained basalt physically resembling other low MgO flows.

Tybu

UNDIFFERENTIATED YAKIMA BASALT

Tlb

LITTLE BUTTE VOLCANIC SERIES

Dark-colored tuff, lapilli tuff, mudflows and less abundant andesite flows; some localized, stratified siltstone and silty sandstone.

N

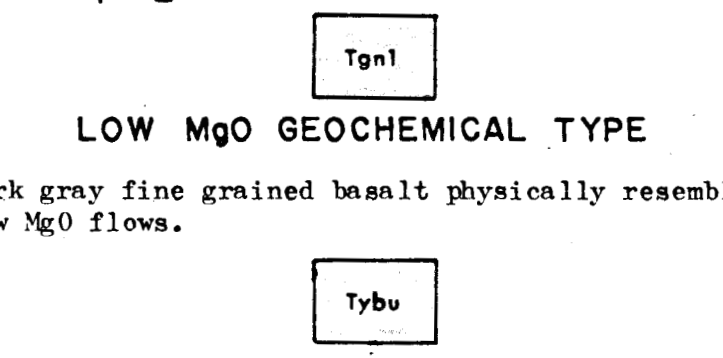

SCALE 1:62500

1 0 1 2 3 4 MILES

3000 0 3000 6000 9000 12000 15000 18000 21000 FEET

1 5 0 1 2 3 4 5 KILOMETERS

GEOLOGIC MAP—CLACKAMAS RIVER AREA

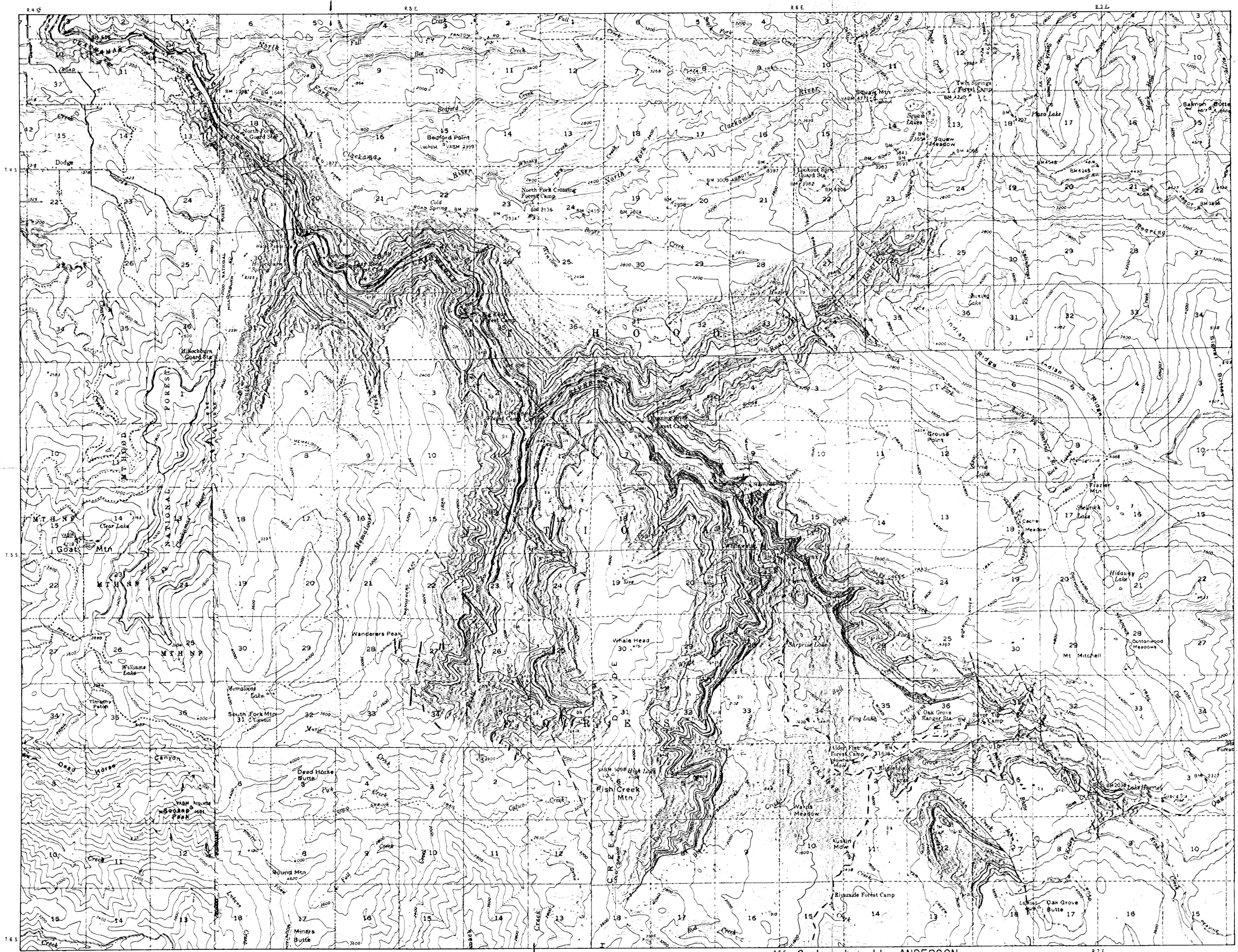

Geology by: J.L. ANDERSON

GEOLOGIC MAP—HOOD RIVER AREA

R.8E. R.9E. R.10E.

T.3N.

T.2N.

T.1N.

T.1S.

R8E R8½E R9E R9½E R10E

Geology by: S. TIMM

GEOLOGIC MAP—SALMON RIVER AREA

R.5E. R.6E. R.7E. R.8E.

T.2S.

T.3S.

T.4S.

Geology by: M.H. BEESON and M.R. MORAN

REGIONAL STRUCTURE of the COLUMBIA RIVER BASALT

(Exclusive of the Columbia River Gorge)

Distribution of Columbia River Basalt in the Cascade Range

Area of Subsidence

Faults — strike slip — normal (U / D) — thrust

Folds — anticline — syncline

CONTOUR INTERVAL 200 FEET
WITH SUPPLEMENTARY CONTOURS AT 100 FOOT INTERVALS

VANCOUVER
Orchards
Camas
PORTLAND
Troutdale
Gresham
Beaverton
Lake Oswego
Oak Grove
Oregon City
West Linn
Woodburn
BEACON ROCK STATE PARK
MOUNT HOOD NATIONAL FOREST
CASCADE RANGE FOREST
GIFFORD PINCHOT NATIONAL FOREST
MOUNT HOOD WILDERNESS
CONBOY LAKE NWR
WARM SPRINGS INDIAN RESERVATION
HOOD RIVER COUNTY
WASCO COUNTY
SKAMANIA CO
KLICKITAT CO

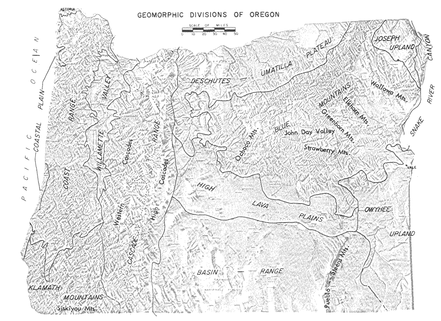

GMS-11

PRELIMINARY GEOTHERMAL RESOURCE MAP OF OREGON 1978

Compiled by Joseph F. Riccio

SCALE 1:500,000

Compiled by Joseph F. Riccio

LEGEND

GEOLOGIC UNITS

Intrusive volcanic rock, Pleistocene to Holocene age
These rocks, which represent feeders for Holocene and upper Pleistocene flows and pyroclastic ejecta, are composed primarily of andesite and dacite plugs, dikes, and vent breccia as well as rhyolitic and dacitic domal masses and small basaltic bodies. They do not include the mafic and silicic intrusive rocks of Pliocene-Pleistocene age of Peck and Wells (1961) or Walker (1977).

Extrusive volcanic rock, Pleistocene to Holocene age
These rocks include andesitic, basalt, rhyolitic, dacite, and obsidian flows and domes, flow breccia, and rhyolitic pumice cones. They do not include the basalt and andesite flows and flow breccia of Pliocene-Pleistocene age of Peck and Wells (1961) or Walker (1977).

Pyroclastic volcanic rock, Pleistocene to Holocene age
Semiconsolidated to unconsolidated subaerial deposits of basaltic and andesitic cinds, pumice, and ash. The pyroclastic rocks of Pliocene-Pleistocene age of the above authors are not included

Major volcanic centers and cones of late Tertiary to Quaternary age
Includes the large mafic and silicic units of Walker (1977) and those shown on the AAPG Geological Highway Map No. 6 (Brennan and others, 1962)

GEOTHERMAL DATA

Low-temperature geothermal resource areas
The numbered regions on the map represent areas greater than 20 km² in which geothermal fluids are believed to occur in aquifers within 3 km of the land surface. These areas were delineated on the basis of temperature measurements of thermal springs in excess of 30°C/min, and conductive heat flow measurements (heat flow is generally more than 1.5 HFU for the areas shown.) Limits of the area are approximate and subject to change pending further geothermal studies and evaluation. These areas may also contain hot-water hydrothermal convection systems that could range from 30 to 150°C. As more detailed geothermal studies are completed, other low-temperature resource areas may be identified.

1. BELKNAP-FOLEY HOT SPRINGS
2. WILLAMETTE PASS
3. UMATILLA PLAIN – COVE (LA GRANDE)
4. GLASS BUTTES
5. NORTHERN HARNEY BASIN
6. SOUTHERN HARNEY BASIN
7. ALVORD DESERT
8. LANGELL VALLEY
9. KLAMATH FALLS
10. WESTERN SNAKE RIVER PLAIN, IDAHO

N. McDERMITT, NEVADA
W. WALLA WALLA, WASHINGTON

Known Geothermal Resource Areas (KGRA)
Areas classified by the U.S. Geological Survey as Known Geothermal Resource Areas. Boundaries shown are those in existence in 1978 and are subject to change

I MT. HOOD
II VALE HOT SPRINGS
III BRETTENBUSH HOT SPRINGS
IV BELKNAP SPRINGS
V CRUMP GEYSER
VI LAKEVIEW
VII BELKNAP-FOLEY HOT SPRINGS
VIII KLAMATH FALLS
IX MACHEISE HOT SPRINGS
X BURNS BUTTE
XI VALE
XII SUMMER LAKE
XIII NEWBERRY CALDERA

Heat flow contours
A heat flow unit (HFU) = 10^{-6} cal cm^{-2} sec or 4.19×10^{-2} W m^{-2}

Thermal spring °C

Thermal Well °C

Geothermal exploratory well

BHT °C *(Bottom hole temperature)*
TDm *(Total depth in meters*

GEOLOGIC SYMBOLS

Faults, *based on published data; dashed where approximately located*

Lineaments
Based on unpublished data from preliminary interpretation of Earth Resource Technology Satellite (ERTS) imagery of Oregon.

Contact, approximate

Earthquake epicenters

Magnitude	
⋮	≤ 3.2
⋮	> 3.3
⋮	> 5.8
⋮	> 6.2
⋮	> 7.6

CULTURE

Urban area

National park or wildlife refuge

Indian reservation

SOURCES OF GEOLOGIC DATA

Bennison, A.P., Bentley, H.B., and Feray, D.E., 1962, Geologic highway map of the Pacific Northwest Region: American Association of Petroleum Geologists Map No. 6.

Blackwell, D.D., Hull, D.A., Bowen, R.G., and Steele, J.L., 1978, Heat flow of Oregon: Oregon Department of Geology and Mineral Industries Special Paper 4, 42 p.

Bowen, R.G., Peterson, N.V., and Riccio, J.F., 1978, Low- to intermediate-temperature thermal springs and wells in Oregon: Oregon Department of Geology and Mineral Industries Geological Map Series 10.

Gianella, Oregon Seismograph Station, 1978, Earthquake epicenters of Oregon and Washington: Oregon State University, [R. W. Couch, personal communication].

Lawrence, R.D., 1972, Lineament analysis, Oregon: Oregon Department of Geology and Mineral Industries unpublished report.

Walker, G. W., 1977, Geologic map of Oregon east of the 121st meridian: U. S. Geological Survey Miscellaneous Investigations Series Map I-902.

Wells, F.G., and Peck, D.L., 1961, Geologic map of Oregon west of the 121st meridian: U. S. Geological Survey Miscellaneous Geologic Investigations Map I-325.

GMS-11
PRELIMINARY
GEOTHERMAL RESOURCE
MAP OF OREGON
1978

STATE OF OREGON
DEPARTMENT OF GEOLOGY AND MINERAL INDUSTRIES
DONALD A. HULL, STATE GEOLOGIST